Seismology of the Solar Convection Zone

A thesis submitted to the
University of London for the
degree of Doctor of Philosophy

Mário João
Pires Fernandes Garcia Monteiro

Queen Mary and Westfield College
February 1996

Abstract

The thesis deals with the study of several problems associated with the solar convective envelope using seismic data. We start with a general introduction to the subject of solar seismology and convection with the basic physics being presented in the appendices. A general discussion on the seismic properties of solar models including asymptotic analysis are also reviewed having in mind their later use.

The detection of convective overshoot at the base of the solar convection zone is the first topic to be presented, starting with a discussion of the theoretically expected behaviour of the oscillations in the presence of overshooting. Using a variational principle for linear adiabatic nonradial oscillations an expression for the frequency changes due to overshoot at the base of the convection zone, modelled as predicted by several studies, is deduced. We then proceed to a detailed application to solar models. The implications of the assumptions present in the analysis are determined and their effect on the conclusions established. Finally, solar data are used to determine the extent and properties of the solar overshoot region using the calibration constructed with the solar models.

We then proceed to another application of the method developed in connection with overshoot, by investigating the possibility of determining the solar helium abundance. This is done by using the effect of the second ionization of helium in the solar structure and frequencies of oscillation. The main advantages and limitations of this method are investigated.

A qualitative and quantitative study of the importance of how we model low-efficiency convection on the seismic properties of a solar model is also discussed. We introduce a general parametrization that has as particular cases the standard mixing length theory and other recently proposed corrections to this description. Using such a parametrization it is shown how significant can be the shift in absolute value of the frequencies due to this extremely thin region at the top of the solar convective envelope. We then proceed to analyse why this is so and attempt to constrain the available theoretical descriptions of convective energy transport in the solar envelope. Other effects associated with convection and also contributing to the discrepancy in the observed frequencies are also reviewed. We analyse some of these using numerical simulations of convection.

The main results of the above topics are reviewed and discussed with the suggestion of some possible implications to be considered in future in the concluding Chapter of the thesis. Also included in the thesis are two appendices which review the basics physics and mathematics involved both in calculating solar models and their frequencies of oscillation.

Acknowledgments

My gratitude to Dr Michael J. Thompson, not only for all he taught me as my supervisor for the last few years, but also for making the learning process an interesting and pleasurable one. It has been a privilege to work with him. My thanks also for all the assistance he provided in the preparation of this thesis.

For the crucial contribution to my learning as a research student my thanks go also to Dr Jørgen Christensen-Dalsgaard who in so many ways was involved in my work. I am grateful for all the data and subroutines he kindly provided along the last few years. His hospitality in my visits to Aarhus is also warmly thanked.

My thanks go also to the Astronomy Unit, in the person of Prof Ian W. Roxburgh, for all the support that in many different ways has helped me during the time I spent there.

I am extremely grateful to Prof M. Teresa V.T. Lago who has contributed in so many ways to my career as an Astronomer; from the time I was an undergraduate student up to finishing this thesis.

The Centre for Astrophysics of the University of Porto has provided me with the conditions to write the thesis and look beyond it with hope. Life would have been much harder if it was not for the facilities being available to me for the last two years.

I am indebted to all my friends and colleagues, which I had the pleasure to meet and share a few years in London with, for the crucial contribution they had (and have) to the quality of my life. Specially, the Portuguese speaking ones; Bonifácio, Daniel, Graça and Teresa - o meu obrigado; and my office neighbours Gerardo, Othon, Silvia, Xochitl and Vasso. Back in Portugal I must also thank everyone at CAUP whose company I greatly enjoyed while writing the thesis.

Finally, big thanks go to my family for their support in every step in life that I take, and in particular to my parents for being the best parents in the world and my brothers for being themselves. Special thanks go to my other family in Porto; Antero, Guida, Ana e João, who are always available and have so much in so many ways helped me along the last ten years.

——

During the period I spent in London, I was a research assistant at the Department of Applied Mathematics of the Faculty of Sciences, University of Porto. The support for that period has been provided both by the University and from grants of *Programa* CIÊNCIA: BD-1274/91-RM, and *Programa* PRAXIS XXI: BD/3112/94, from *Junta Nacional de Investigação Científica e Tecnológica*, Lisbon.

Aos meus pais e avós

Contents

List of Tables

List of Figures

1. Solar Structure and Oscillations

A general introduction to the present state of modelling the solar structure and oscillations is presented here. The objective is to describe in general terms what we believe we know and most importantly what are the major difficulties we still have to overcome in understanding the physics that control the life of the Sun.

Some basic results in stellar structure and oscillations are also reviewed. We address briefly what goes into modelling the internal structure of the Sun, and how important each of the ingredients is to the answer we get in the end. Some basic characteristics of a "standard" solar model are presented and discussed. In particular the aspects that are more strongly affected by the assumptions used when modelling the internal structure.

The seismic properties of a star are the basic tool we use in this Thesis to study the solar interior. Therefore the basic equations for linear adiabatic non-radial oscillation of the Sun and some results from asymptotic analysis are reviewed. In particular, we consider the expression for the variational principle for the oscillations which is one of the results used in the following Chapters. We also discuss the properties of the structure that determine the frequencies of oscillation and characteristics of the corresponding eigenfunctions.

1.1 Introduction

One of the reasons the Sun is so important, other than providing us with the conditions that made/make our existence possible, is the potential it represents for learning in detail aspects of stellar physics not accessible in any other way. As an example we recall that it was the Sun that led to the necessity of ruling out gravitational energy as the main stellar source of energy, with the necessary introduction of nuclear reactions as the only other possibility. Or even the fact that stars may have significant magnetic activity. The fact that we now know that convection is present in stars is also a direct consequence of it being observed at the Sun's surface. It is the detailed observational information, and in particular the fact that unlike other stars for us the Sun is not only a point but can be resolved in all spatial dimensions that makes it an ideal laboratory for stellar physics.

For a long time that stars have been known to oscillate. In particular high amplitude

oscillators have been used as distance indicators. Only recently has it been recognized that all stars most probably pulsate even if only with very low amplitude oscillations. The Sun is such a case. These solar pulsations observed at the surface correspond to modes which are waves trapped between the surface layers and a lower region in which the waves undergo total internal reflection. The ones which are more clearly observed for the Sun are waves whose restoring force is pressure, i.e., acoustic waves. Each of these modes has an associated resonant cavity defined by these two reflecting boundaries, and therefore the characteristics of a mode, e.g. its frequency, will depend on the properties of the medium constituting the cavity. By using such a dependence, helioseismology has proved to be an excellent window on the interior of the Sun, providing otherwise inaccessible information about the physics of the solar interior.

The objective of this Chapter is not to report original work but to discuss with some detail two important aspects that go into the following Chapters, namely the calculation of static solar models and their oscillation frequencies. These provide the access to the interior of the Sun allowing us to confront the model internal properties with the real Sun. When studying the seismic properties of the Sun our objective is indeed to be able to understand how each physical aspect going into the modelling of the structure contributes to the oscillations frequencies. In doing so we hope to isolate each individual contribution and by comparison with the Sun to correct the assumptions and descriptions used in the modelling. Both calculations of the structure and the oscillations are described with some detail in Appendices A and B. There we address mainly the numerical task of calculating models and frequencies of oscillations. However, for later use we review here the basic aspects and some of the important characteristics of the calculated models which we shall be discussing in the following Chapters. We also present, together with some of the basic equations, asymptotic results for stellar oscillations which are frequently used to represent the approximate behaviour of the oscillations. These are essential to obtain some estimates on how the eigenfunctions are affected by some particular aspect of the structure. In this way we want to provide here all the theoretical tools we later need to relate the observed solar behaviour with the formulations we use to reproduce this behaviour.

1.1.1 Our understanding of the Sun

Our present knowledge of the Sun is what could be classified as “reasonably good”. The reason for this statement is that we can now construct numerically a solar model, which is able to reproduce the global properties that we measure in the real Sun to a reasonable degree. We believe we understand how the star produces the energy it radiates away, why it has the properties is does resulting intrinsically from the mass which establishes the

configuration a star must have to be in equilibrium.

However, we also know that many aspects of the solar structure that we do not understand are at play (see for example the reviews by Roxburgh 1985, and Pecker 1991). Most of these, like rotation, magnetic fields, convection and overshoot, diffusion of chemical elements or production of neutrinos, do not change radically the global properties of the Sun, but they are important physical aspects which must be understood, and the Sun can most certainly help us to achieve that. We have now come to a point where due to the rapid technological advances, a large amount of extremely accurate data is available and powerful computers can do very large calculations, that we can allow ourselves to be ambitious. Also possible, and in many cases already done, is the improvement of the available descriptions. Examples are the opacities and the equation of state describing the thermodynamic behaviour of the gas. In both, the use of seismic data and more powerful machines have led to a rapid evolution in testing and improving of these two extremely important aspects of stellar structure.

1.1.2 Uncertainties in modelling stellar structure

The Sun provides us with a laboratory for physics in the sense that our theories, descriptions or some times guesses can be tested by comparing the models that come out of our assumptions with the real Sun. As in everything else, when the opacities are calculated, for example, we need to use our knowledge from atomic physics, and the quality of what comes out reflects the quality of what was put in. By testing a solar model that results from using the calculated opacities we are testing the physics that we have used to calculate such values. It has been this association that has induced to a recalculation of the opacities leading to values that represent more closely the actual behaviour of variable stars, and have an important effect on stellar models in general (cf. Christensen-Dalsgaard et al. 1985).

Another example is convection. It is known, and observed in many different situations, that an inverse thermal stratification of a fluid with very low viscosity induces an instability that drives the fluid in order to move cooler portions towards the bottom and hotter portions up to the top in order to invert the negative gradient of the temperature. This is observed in the laboratory and in many other situations in nature, as the oceans and the earth's atmosphere (see Zahn 1991, and references therein). However, to model it theoretically is extremely difficult and to measure it, in the laboratory for the conditions within a star, is impossible. So, to try to understand how on average the fluid behaves in the star we must use for example numerical simulations that better represent what goes on. Such types of "observation" are essential to improve our insight of the phenomena in order

to improve the theories that model such a phenomena. This must then be complemented with whatever we may observe for real stars.

And more importantly is the possibility of studying aspects that even if they are not dominant in the Sun, they most certainly are for other stars, and so must be considered. The interaction of rotation and the magnetic field is a typical example. It is expected not to change drastically our present solar model, but it is known to be fundamental in understanding how young stellar objects evolve.

1.1.3 Using frequencies of oscillation

One of the reasons why it has been so difficult to improve the details in stellar structure and evolution comes from the fact that for all the stars the only information we have are their global properties. Mass, luminosity and effective temperature (value at the surface) are examples of these. There are a large set of solutions for the basic equations, each corresponding to a different combination/version of the relations involved in the set of differential equations. Therefore, as long as we only need a solution whose boundary conditions correspond to the observed global characteristics, it is always possible to find one if the physics used are adequately adjusted. Therefore the usual technique is for example to use statistics to restrict the possibilities available to reproduce the observable properties. To this we add what we know from other branches of physics, in order to progressively narrow the set of possible solutions. However, the observational constraints are still too few to be able to reduce the set of solutions to a reasonably small set in order to restrict the hypotheses going into modelling.

The importance of oscillations is precisely because these are not only a large number of observed values, but have the added advantage of being possible to associate observed behaviour to specific interior properties, increasing greatly the number of constraints available to select the possible valid solutions in the modelling of stellar structure. Also important is the fact that observed frequencies provide restrictions that can be traced to specific regions of the observed star, and so we may attempt to restrict selectively different aspects going into the modelling, contrary to constrain only the global solution.

Such a richness of information became available with the identification of normal modes of oscillations in the Sun back in the 1970's (Ulrich 1970, Leibacher & Stein 1971) after observations done in the previous decade (Leighton et al. 1962, see for example the review by Deubner & Gough 1984). These correspond to standing waves, which can be pressure or gravity supported, being trapped in resonance cavities which vary with the mode characteristics (eg. Unno et al. 1989). Acoustic modes, known as *p-modes* are the ones more easily observed since they are confined between some point in the interior

and the surface. Also observed are what we classify as *f-modes* which correspond to surface gravity waves. Up to a few millions have been observed and identified so far. The others, known as *g-modes* have not conclusively being identified because these being gravity supported can not propagate in convective unstable regions as happens for the outer 30% of the Sun. The value of such a large data set is the fact that different modes are associated with different regions of the Sun's interior, which provides a selective sampling of the interior.

Of course, the Sun is again a special case relative to other stars, since its proximity once again is crucial not only in the quality but also in the quantity of information about the interior that we may obtain. Some reviews on the subject of *helioseismology* - the study of the Sun using its modes of oscillation - with emphasis on the observational aspect, are presented for example by Deubner & Gough (1984) and Gough & Toomre (1991). See also the reviews on how the oscillations have been or can be used to study the solar structure by Libbrecht (1988), Gough (1991) or Christensen-Dalsgaard (1996).

1.1.4 Problems addressed in this thesis

In this work we shall be discussing what can be classified as three separate subjects. Two of them are related to the same physical problem. However, since they approach different aspects in different ways we shall present them as separate. Both deal with convection in stellar interiors. Observed at the solar surface, and known as granulation, the Sun displays what is believed to be evidence of a convective envelope. This region is estimated to occupy the outer 30% of the Sun. There, due to the high opacity of the material which makes the gas opaque to radiation, the fluid is unstable to small perturbations. The result is what is classified as convection corresponding to a highly turbulent regime where energy is carried around by the motions of the gas. The net effect of such a velocity field is to transport energy towards the surface where it is eventually released as radiation. How to model the average effect of such a phenomena is a very difficult task. From this difficulty arises some of the present problems of modelling convective energy transport in the solar envelope. One is the existence of overshoot at the borders of a convective unstable region. The problem is associated with the fact that the boundary of the unstable region is determined by a zero condition on the acceleration. However, as observed in other transition regions, the kinetic energy is non-zero there and therefore the motions go beyond this stability boundary. Qualitatively it is easy to describe, however without a full theory of convection it is very difficult to quantify this overshooting into the radiative regions.

The other problem associated with convection is a thin layer at the top the solar convective envelope where due to the low density the efficiency of convection becomes

extremely low. Therefore the equilibrium stratification that the fluid eventually has is a balance between what flux can be carried by convection and/or radiation. How this balance between the two is reached is very difficult to model and depends crucially on the formulation we may use to describe convective energy transport. However, because most of the convection zone is nearly adiabatic it is not really important for the global structure how this layer is modelled as far as the rest of the convection zone adapts in order to correspond to the same adiabat, and therefore to fit the structure of the radiative interior. This is the reason why traditionally a parameter has been used that implicitly does this adjusting of the solution and therefore the problem has been formally ignored in stellar structure. But it can only be done as long as we are comparing global properties, in particular the radius of our models with the observations. The problem is that in this way the observations can no longer be used directly to constrain the formulation of convection used. Fortunately, with the observation of the oscillations we have added information that, if selectively used, can indeed test a particular formulation. Our objective here is to quantify how significant the effect coming from this region of low convective efficiency is in the seismic properties of the star and how can it be used to improve our description of convection.

Finally, the third subject to be broached is the abundance of helium at the solar envelope. This is a subject we consider as one more example on how the method developed to study overshoot can be used to infer properties of the Sun associated to regions in its structure that correspond to localized effects. In this way we provide one more independent constraint for the study of the equation of state in solar interiors and more importantly construct a method do determine the solar envelope helium abundance. Such a value is essential for modelling the Sun.

1.2 Modelling the structure of the Sun

To fully model the present structure of the Sun, we must start by what is known as a zero-age main sequence star, and evolve it until it has the same characteristics as observed for the Sun at the present age. However, to do so demands a much larger effort. Since here we deal mainly with frequency or model differences it is only the differences in a particular aspects of our models that are important. Therefore, as long as other ingredients are the same for the models under comparison, the estimates obtained from model differences are representative of the physical aspect under study. In particular we avoid the difficult problem of evolving solar models by using a chemical profile of a present age solar model from a more detailed calculation to represent that evolution. Therefore, all calculations discussed in this work correspond to static solar models, determined using the simplest

set of basic assumptions for modelling the structure. These correspond to considering a time-independent spherically symmetric configuration for the Sun. With these we neglect rotation, magnetic fields, asphericity, meridional circulation, winds, etc.

The full details of the equations are given in Appendix A; here we discuss the main equations that are frequently referred to in the following Chapters. We also present some aspects of the models that are of interest for the topics presented later. In particular the characteristics of the models that determine their seismic properties are shown. The actual ingredients going into each individual model depends on what aspects we shall be analysing, therefore we leave to each Chapter the discussing of the physics that have been used for the models reported there. Here we only present one of the cases calculated to illustrate the type of properties and characteristics that are important for the subjects included in this work.

The models constructed with the code described in Appendix A, and whose results are discussed here, are used mainly to study the measurement of the helium abundance (Chapter 4) and the modelling of solar convection (Chapter 5). In Chapter 3, concerning overshoot, we have used instead models constructed with Christensen-Dalsgaard's code (Christensen-Dalsgaard 1982).

1.2.1 Basic equations

By assuming a time independent spherically symmetric structure, the differential equations describing the structure given the boundary conditions, are reduced to a set of four first order non-linear equations. These are associated with conservation of mass, hydrostatic equilibrium and conservation of energy. For the system to be solved, besides the boundary conditions, we also have to define some relations and dependences of quantities entering the differential equations. These relations and dependences correspond to what we call here the physics of the models. Among them we have the equation of state, energy production rates, convection and the opacity. In here we discuss mainly convection. In particular we address the problem of overshoot associated with the boundaries of convective unstable layers and the modelling of the convective flux in regions of low efficiency of convection.

The four basic equations for a static spherically symmetric fluid, of density ρ, pressure P and temperature T, are then written as (for a more detailed discussion see for example; Schwarzschild 1958, Cox & Giuli 1968, Kippenhahn & Weigert 1990, etc)

$$\begin{aligned} \frac{\mathrm{d}m_r}{\mathrm{d}r} &= 4\pi r^2 \rho(r) & \qquad \frac{\mathrm{d}P}{\mathrm{d}r} &= -\frac{G m_r(r)}{r^2}\,\rho(r) \\ \frac{\mathrm{d}L_r}{\mathrm{d}r} &= \frac{\mathrm{d}m_r}{\mathrm{d}r}\;\varepsilon(r) & \qquad \frac{\mathrm{d}T}{\mathrm{d}r} &= \frac{T(r)}{P(r)}\,\frac{\mathrm{d}P}{\mathrm{d}r}\;\nabla(r) \end{aligned} \tag{1.2.1}$$

Here, r is radius while m_r and L_r are, respectively, total mass within the sphere of radius r and energy crossing this sphere per unit time. The constant G is the gravitational constant (see Table A.1 for the value of this and other physical constants used here) while ε gives the energy produced per unit mass and time. Finally the temperature gradient $\nabla \equiv \partial \log T / \partial \log P$ depends on the dominant process at work for transporting the energy at each point. For a more detailed discussion on the construction of solar models see for example Christensen-Dalsgaard (1982), Turck-Chièze et al. (1993) or Turck-Chièze & Lopes (1993).

1.2.2 Physics needed

As discussed above to find a solution of these four differential equations we must have, besides the four boundary conditions, the physics that give ρ, ε and ∇ from the other dependent variables. For the first we use an equation of state and for the last a diffusive approximation if energy is carried by radiation or a convection theory if the gas is unstable to convection. For the energy generation rate, ε, we must have nuclear data that describe the fusion processes taking place in the interior. Implicit to these are the abundances of the elements that constitute the gas of the star. The abundances used here are a scaling of the values found for an evolved solar model at the estimated age for the Sun. In this way, we simulate the result of an evolution program, even if not consistently, with the problem being reduced to a much simpler form.

In our code we have implemented two equations of state. One is just a simple equation of state (seos) which describes a perfect gas with radiation pressure and ionization of hydrogen and helium described by the corresponding Saha equations. For the high pressure limit we use a transition to the fully ionized case in order to simulate pressure ionization. This equation of state is discussed with some detail in Appendix A. The other option also used is the ceff equation of state (Christensen-Dalsgaard & Däppen 1992) which uses the eff relations from Eggleton, Faulkner & Flannery (1973) with a Debye–Hückel approximation for the Coulomb term. The subroutines of this eos have been developed by Christensen-Dalsgaard. We also consider in the Thesis models calculated with the mhd equation of state (Hummer & Mihalas 1988, Mihalas, Däppen & Hummer 1988, Däppen et al. 1988).

For the transport of energy we have used, by default, the Mixing length Theory (Böhm-Vitense 1958). However in the Chapter concerning convection theories other options have also been implemented. The criterion for instability, in terms of the temperature gradient ∇, that we use in order to determined the location of the convection zones is the

Schwarzschild criterion. This is (Schwarzschild 1958),

$$\begin{cases} \nabla_{\rm r} \geq \nabla_{\rm a} & \rightarrow \qquad \text{Convection theory giving } \nabla{=}\nabla(\nabla_{\rm a}, \nabla_{\rm r}) \\ \nabla_{\rm r} < \nabla_{\rm a} & \rightarrow \qquad \nabla = \nabla_{\rm r} \end{cases} \tag{1.2.2}$$

Here, the two typical gradients are the adiabatic gradient $\nabla_{\rm a}$, corresponding to the logarithmic derivative at constant entropy, and the radiative gradient $\nabla_{\rm r}$, giving the temperature gradient necessary for all flux to be carried by radiation. This is the criterion used to find the two dotted lines in all figures included in the next Section. Also shown there is a plot with the gradients for an envelope model. For models discussed in Chapter 3 where convective overshoot has been included we also had to add an overshoot layer at the bottom of the convection zone, by including a specified behaviour for the gradient immediately below the boundary given by the above criterion.

Finally, the other important ingredient going into the modelling are the opacities. In general we have used the Cox & Tabor (1976) opacities. For more details see the discussion in Appendix A. Again, we also discuss other models which have been calculated using the more recent OPAL table of opacities (Iglesias & Rogers 1991).

Given all these ingredients and considering that the model has a specified radius, mass and surface luminosity (for the Sun, we have used the values listed in Table A.2) it is possible to find a solution for the four differential equations given above. The details on how this is done, and in particular how the boundary conditions are used, is described with some detail in Appendix A.

1.2.3 Some thermodynamic quantities

What comes out of the numerical calculation of a solar model is of course the run of the four dependent variables. In the case of using radius as the independent variable these are; mass, pressure, luminosity and temperature. Associated with these we also have other thermodynamic quantities which describe the properties of the gas like density, the adiabatic gradient, adiabatic exponent or the expansion coefficient.

Because we shall be using the seismic properties of the models as given by p-modes there are some basic thermodynamic quantities that determine the behaviour of the oscillations. Being standing acoustic waves, one of the thermodynamic quantities that is more strongly associated with the seismic properties of the Sun is the adiabatic sound speed. It is defined as

$$c \equiv \left(\frac{\Gamma_1 P}{\rho} \right)^{1/2} \tag{1.2.3}$$

where $\Gamma_1 \equiv (\partial \log P / \partial \log \rho)_S$ is the adiabatic exponent, with the derivative being taken at constant specific entropy S. The sound speed is plotted in Fig. 1.1 versus the logarithm of

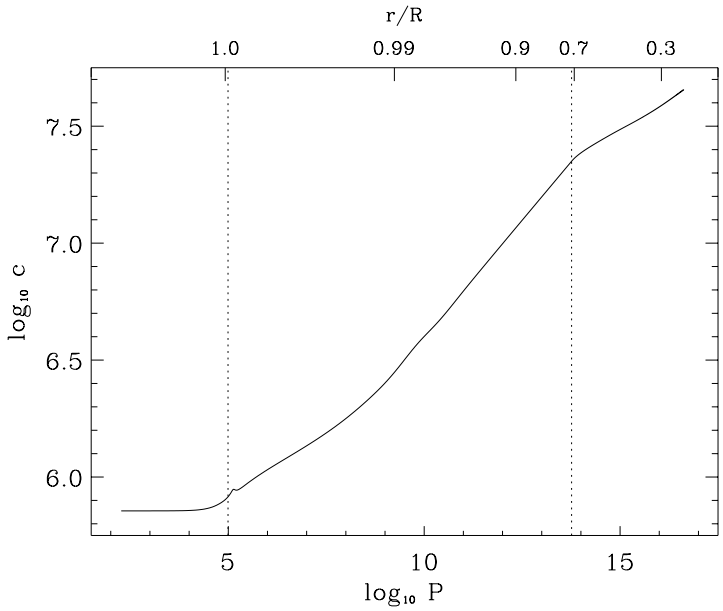

Fig. 1.1: Sound speed versus pressure for a solar envelope model. The dotted lines mark the boundaries of the convective envelope.

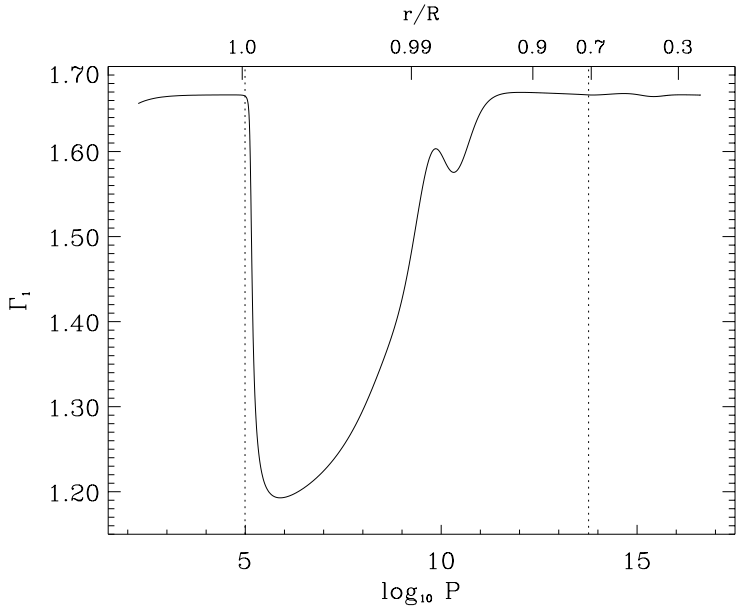

Fig. 1.2: Adiabatic exponent versus pressure for the same solar envelope model as in the previous figure. Again the dotted lines mark the boundaries of the convective envelope.

the pressure. The linear section, for $\log P$ between 10 and 14, corresponds to the deeper convection zone where the temperature is adiabatically stratified.

The adiabatic exponent is shown in Fig. 1.2. The big dip for $\log_{10} P$ between 5 and 10 is due to the ionization of hydrogen and to the first ionization of helium, while the second smaller dip at $\log_{10} P \sim 10.5$ results from the second ionization of helium. The

behaviour of this function is fundamental to understanding the small layer near the top of the convection zone. It is strongly dependent on the equation of state in this region and is therefore frequently used as a probe of the equation of state. We shall also use it when attempting to measure the envelope helium abundance from the signal in the frequencies created by the small depression in the adiabatic exponent associated with the second ionization of the helium. Note that this "bump" takes place over a very short distance, which results in a characteristic effect on the seismic properties of the model.

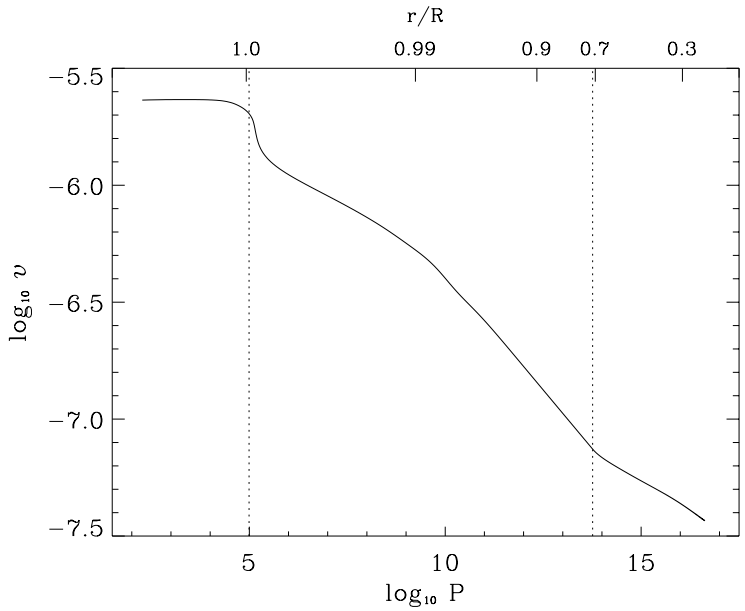

Fig. 1.3: Thermal time length $\upsilon = \Gamma_1/c$ versus pressure. Note the rapid variation at the top of the convection zone similar to the variation of the temperature, which makes this variable useful to describe model differences for variations of the convective theory in this region of low efficiency of convection.

Another variable which is also associated, but in a different way, to the three thermodynamic variables entering the definition of sound speed has been considered by, for example, Christensen-Dalsgaard & Thompson (1996). It is a very convenient quantity to relate frequency differences to model differences confined to the top layers of the model. The definition of this quantity is

$$\upsilon = \sqrt{\frac{\Gamma_1 \rho}{P}} \, . \tag{1.2.4}$$

As we discuss in Chapter 5 this is one of the most convenient variables to describe the changes in the model coming from changing the description of convection. It is shown in Fig. 1.3 for our standard model. Note the strong variation in the superadiabatic region where the ionization of hydrogen takes place. It is this strong variation that is associated with the reflection of acoustic waves near the surface. To first order υ is proportional to $g\omega_c$, where ω_c is an acoustic cutoff frequency (defined in the next Section) which describes

asymptotically the reflection of acoustic modes at the surface of the Sun. This has been the reason for the introduction of v.

1.2.4 Temperature stratification

One other aspect that will be under study in this work is our modelling of energy transport within the convective zone of the Sun. Most of the currently available formulations rely on typical lengths to describe the effects of convection on the average stratification for such regions. A commonly used process to write representative scales is to take the scales for the variation of thermodynamic quantities.

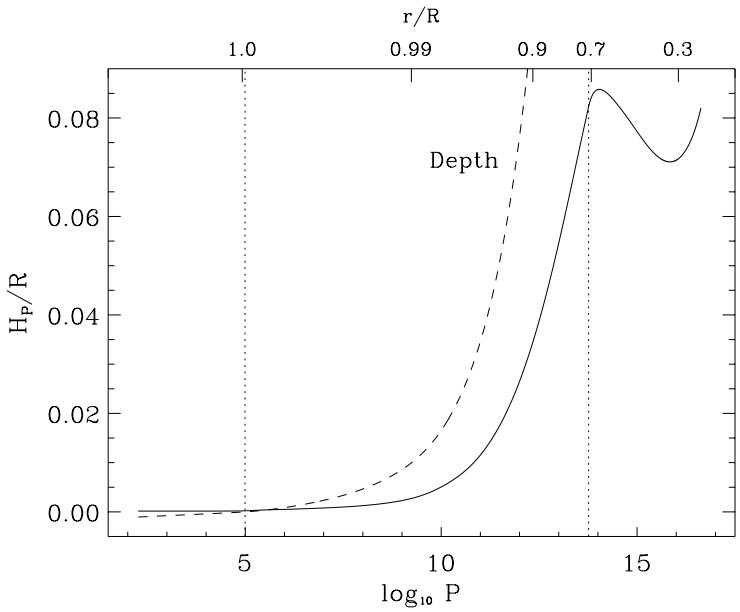

Fig. 1.4: Pressure scale height H_P versus pressure. For comparison we also plot depth $z=(r_u-r)/R$ from the top r_u of the convection zone as a dashed line. Note that the latter is smaller than H_P very near the top of the convection zone while being larger for the rest of the interior.

One of this is for example, the pressure scale height, H_P, defined as

$$H_P \equiv \frac{P}{\left|\frac{\mathrm{d}P}{\mathrm{d}r}\right|} \tag{1.2.5}$$

and used in phenomenal descriptions of convection (for example in Böhm-Vitense 1958). This function, together with depth from the top of the convection zone, is shown in Fig. 1.4. It is this scale that is usually taken as being representative of the typical size of convecting elements of fluid. We have included depth, z, because it is also used as a typical length scale of convection in Chapter 5, which has the added characteristic of introducing some

non-locality in the convection theory. Such character comes from the fact that contrary to the pressure scale length, the value at each point depends on the position of the upper boundary which is of course not local. One of the important features that we note here is that it has smaller values than H_P in the region where the temperature gradient ∇ reaches its maximum, at about $\log P \sim 5.2$.

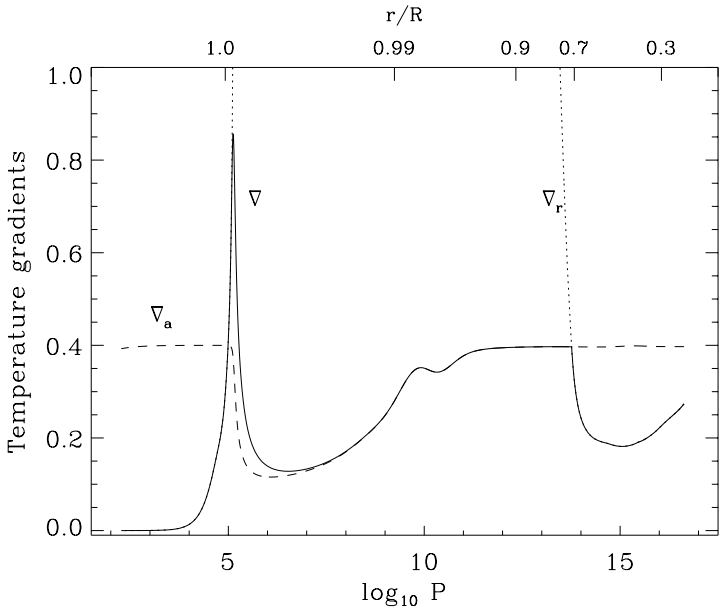

Fig. 1.5: Temperature gradients for a solar envelope. The actual gradient $\partial \log T / \partial \log P$ is the continuous line while the other two typical lengths are the adiabatic (dashed line) and the radiative (dotted line) gradients. The latter being the gradient necessary for all flux to be carried by radiation. According to the Schwarzschild criterion the convection zone corresponds to regions where $\nabla_r \geq \nabla_a$.

We also include a plot (Fig. 1.5) of the two gradients that determine the transport mechanism for carrying the flux. Also shown there as a continuous line is the result of a particular formulation for modelling convection, usually known as the Mixing Length Theory (*MLT*), first proposed by Böhm-Vitense (1958), and commonly used ever since. Note that as given by the criterion in (1.2.2), the dotted lines in the previous figures correspond to the points where $\nabla_a = \nabla_r$ in Fig. 1.5. The convection zone in the model is the region where ∇ is determined from a convection theory, and so corresponds to the zone where $\nabla_a \leq \nabla_r$.

1.2.5 Models as input for seismic studies

One of the objectives when using seismic data is to try to measure the properties in the interior of Sun that are associated with some aspects of these ingredients that we use in stellar structure and evolution. In doing so we attempt to validate or at least to

understand why the model does not reproduce the observed behaviour in order to improve the description used for modelling the internal structure. In here we shall be mainly concerned with two aspects. One is convection, which is associated with the process by which the star transports energy in regions of convective instability. Associated with convection is also the problem of modelling the boundaries of the convective regions where some kind of overshooting by the fluid into the stable layers is expected. The other aspect is the determination of the envelope helium abundance. Associated with this we have the equation of state which poses serious difficulties in such a determination.

1.3 Modelling linear adiabatic oscillations

The observed oscillations in the Sun have a very low amplitude. This, fortunately, allows us to treat theoretically those oscillations as linear perturbations to the equilibrium configuration reducing the problem of solving the hydrodynamic equations to a relatively simpler task. However, the task of observing them is unfortunately much harder because of these small amplitudes. In Appendix B we have included the full derivation from the basic hydrodynamic equations to the set of four linear first order differential equations. These are the equations we solve numerically to calculate the oscillations eigenvalues for a given equilibrium model for the star/Sun. The details of the numerical calculation are also presented there. Here we shall just give a summary of the main equations and discuss some of the numerical results.

Also important in helioseismology is to be able to estimate the approximate behaviour of the oscillations in order to determine how these are affected by some particular characteristic of the model. Such use of these estimates is frequently done along the next Chapters every time we need to describe the eigenfunction or eigenvalue in order to relate them with the property of the model under study. Therefore, we also present in this Section some analytical results and asymptotic expressions which are used latter.

Some examples of reviews in the theoretical interpretation of the solar oscillations, and used as references for this Section, are for example; Vorontsov & Zharkov (1989), Christensen-Dalsgaard & Berthomieu (1991), Gough (1991), and also Christensen-Dalsgaard (1996).

1.3.1 Basic equations

Starting from the basic hydrodynamic equations for a fluid of density ρ, pressure P, velocity $\vec{v}$ and gravitational potential Φ, we considered small perturbations to an equilibrium configuration which is time-independent and spherically symmetric. In this way we can linearize the equations reducing the system of equations to a relatively much simpler sys-

tem of linear differential equations. See Appendix B for the full derivation of the linearized differential equations obtained from the fluid equations. Also needed is a linearized energy equation. Considering the thermal time scale of the gas in the star and the typical period of the oscillations, the assumption of adiabatic fluctuations is used. In terms of the Lagrangian fluctuations, it is written as

$$\frac{\delta\rho}{\rho} = \left(\frac{\partial \log\rho}{\partial \log P}\right)_S \frac{\delta P}{P} \equiv \frac{1}{\Gamma_1}\ \frac{\delta P}{P}\ , \tag{1.3.1}$$

where the derivative is taken at constant entropy S.

Because of the spherical symmetry it is possible to decouple the horizontal dependence, corresponding to (θ,ϕ) in spherical coordinates, for the solutions. This is accounted for by spherical harmonics Y_l^m where (l,m) are two integers (l is positive and $|m|\leq l$) which describe the possible eigenfunctions associated with the horizontal dimensions. The first is called *degree of the mode* while m is the *azimuthal order*. Note that because of the spherical symmetry one of these is redundant since there is no preferred direction (which does not happen if rotation is included, defining the rotation axis as a special direction). After some algebra it can be shown that the general solutions for the Eulerian perturbations, with time dependence of the type $\mathrm{e}^{\mathrm{i}\omega t}$, can be written as

$$\begin{aligned}
P'(t,r,\theta,\phi) &= \tilde{P}(r)\ \ Y_l^m(\theta,\phi)\ \mathrm{e}^{\mathrm{i}\omega t}\\
\rho'(t,r,\theta,\phi) &= \tilde{\rho}(r)\ \ Y_l^m(\theta,\phi)\ \mathrm{e}^{\mathrm{i}\omega t}\\
\Phi'(t,r,\theta,\phi) &= \tilde{\Phi}(r)\ \ Y_l^m(\theta,\phi)\ \mathrm{e}^{\mathrm{i}\omega t}\\
\vec{\xi}(t,r,\theta,\phi) &= \left[\xi_r(r)\ \ Y_l^m(\theta,\phi),\ \xi_h(r)\ \frac{\partial Y_l^m}{\partial\theta},\ \frac{\xi_h(r)}{\sin\theta}\ \frac{\partial Y_l^m}{\partial\phi}\right]\ \ \mathrm{e}^{\mathrm{i}\omega t}\ .
\end{aligned} \tag{1.3.2}$$

Where the new tiled functions describe the dependence on radius r of the amplitude. The displacement vector $\vec{\xi}$ has a vertical component with amplitude ξ_r and an horizontal vector with amplitude ξ_h given by (Eq. (B.2.33)),

$$\xi_h(r) = \frac{1}{r\omega^2}\ \left(\frac{\tilde{P}}{\rho_0} - \tilde{\Phi}\right)\ . \tag{1.3.3}$$

The subscript "0" represents quantities of the equilibrium configuration. For the determination of the radial dependence of the amplitudes $\tilde{P}$, $\tilde{\rho}$, $\tilde{\Phi}$ and ξ_r we have the following differential equations

$$\begin{aligned}
&\left(1-\frac{S_l^2}{\omega^2}\right)\ \frac{\tilde{P}}{\rho_0} - \frac{1}{r^2}\ \left(g_0 - c_o^2\ \frac{\mathrm{d}}{\mathrm{d}r}\right)(r^2\xi_r) + \frac{S_l^2}{\omega^2}\ \tilde{\Phi} = 0\\
&\frac{1}{\rho_0}\left(\frac{g_0}{c_0^2} + \frac{\mathrm{d}}{\mathrm{d}r}\right)\ \tilde{P} - (\omega^2 - N^2)\ \xi_r - \frac{\mathrm{d}\tilde{\Phi}}{\mathrm{d}r} = 0\\
&\tilde{P} + \frac{\rho_0 c_0^2 N^2}{g_0}\ \xi_r - \frac{S_l^2}{4\pi G}\ \tilde{\Phi} + \frac{c_0^2}{4\pi G r^2}\ \frac{\mathrm{d}}{\mathrm{d}r}\left(r^2\frac{\mathrm{d}\tilde{\Phi}}{\mathrm{d}r}\right) = 0
\end{aligned} \tag{1.3.4}$$

These can be reduced to a system of four linear first order differential equations corresponding to an eigenvalue problem, when adequate boundary conditions are taken. It has an infinite number of solutions (eigenfunctions) associated with eigenvalues ω_{nl}. Each eigenvalue is given by a unique association of the numbers l and a number n, which is called the *mode order*, and measures the number of zeros in the radial direction of the amplitude functions ξ_r, $\tilde{P}$, etc.

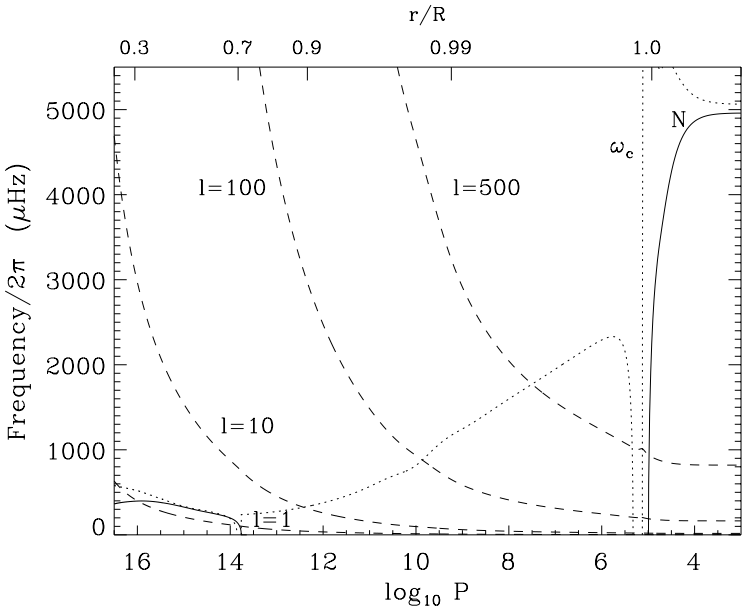

Fig. 1.6: Buoyancy frequency N (continuous line), acoustic cutoff frequency (dotted line) and Lamb frequency (dashed lines) for several values of l as indicated.

The typical frequencies of the equilibrium model appearing in the above system of differential equations are

$$\begin{aligned} \text{Lamb frequency} \quad & S_l^2 \equiv l(l+1)\,\frac{c_0^2}{r^2} \\ \text{Buoancy frequency} \quad & N^2 \equiv g_0 \left(\frac{1}{\Gamma_{1,0}} \frac{\mathrm{d}\log P_0}{\mathrm{d}r} - \frac{\mathrm{d}\log \rho_0}{\mathrm{d}r} \right) \end{aligned} \tag{1.3.5}$$

For completeness we also include here a third definition of a frequency that is responsible for the reflection of the waves at the surface. This is the acoustic cutoff frequency ω_c, given by

$$\omega_c^2 \equiv \frac{c_0^2}{4H_\rho^2} \left(1 - 2\,\frac{\mathrm{d}H_\rho}{\mathrm{d}r} \right) , \tag{1.3.6}$$

where $H_\rho \equiv |\mathrm{d}\log\rho/\mathrm{d}r|^{-1}$ is the density scale height. These characteristic frequencies are shown in Fig. 1.6.

Given the assumptions used here there are only two possible types of waves that can be supported in the star and described by Eqs. (1.3.4). One type is acoustic waves, using

pressure as the driving mechanism - the standing modes corresponding to these we call *p-modes*. The other driving mechanism is gravity, through the buoyancy of the gas - these type of standing modes we call *g-modes*. There is also a group of modes which have mixed characteristics known as *f-modes*. They correspond to surface gravity waves.

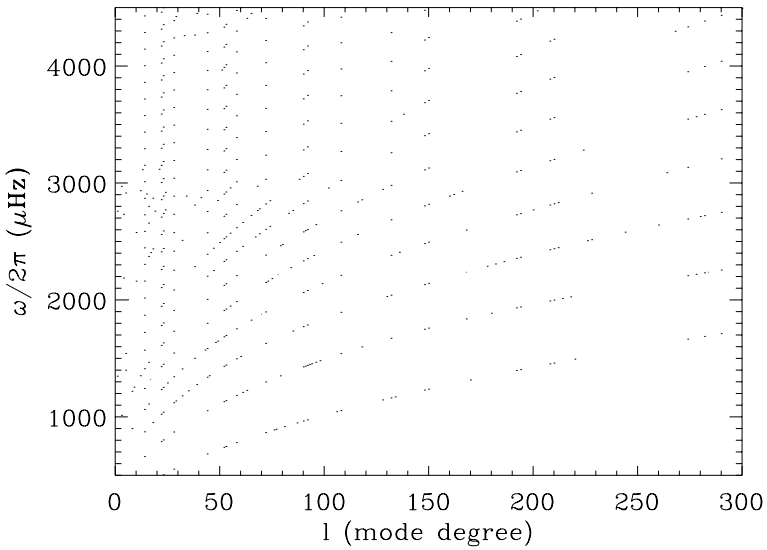

Fig. 1.7: Frequencies of oscillation for the solar envelope model used to obtain the plots shown in this Chapter. Only p and f-modes are shown. The region of g-modes is located in the bottom of the plot since these have frequencies below typically 500μHz.

Using Eqs. (1.3.4) and corresponding boundary conditions we can, given the structure of a particular equilibrium model, determine the frequencies of oscillation for that model. This calculation is described with some detail in Appendix B. To illustrate the results of such a calculation the frequencies of p-modes are shown in Fig. 1.7 for the envelope model described in the previous Section. These data can now be compared with observed solar oscillations in order to test the assumptions going into the construction of our model of the internal structure and its frequencies of oscillation.

1.3.2 Resonance cavity of p-modes

Instead of solving the full set of differential equations for a numerical model of the Sun in order to determine the seismic properties of our model/Sun, it is more intuitive to estimate the approximate behaviour. By using some simplifying assumptions it is indeed possible to find an analytical description of how the eigenfunctions behave, what are the eigenvalues, etc. The method is to find ways to simplify the full set of differential equations whose solution can only be found numerically, in order to have a simpler, but yet representative,

set of equations whose solution is known analytically.

One example, concerning p-modes, is to note that for high eigenvalues ω or/and high degree modes the fluctuations in the gravitational potential can be neglected. This reduces the system to two first order differential equations in the form

$$\begin{aligned} \frac{\mathrm{d}\xi_r}{\mathrm{d}r} &= -\left(\frac{2}{r}-\frac{g_0}{c_o^2}\right)\xi_r - \frac{r\omega^2}{c_o^2}\left(1-\frac{S_l^2}{\omega^2}\right)\xi_h \\ \frac{\mathrm{d}\xi_h}{\mathrm{d}r} &= \left(1-\frac{N^2}{\omega^2}\right)\frac{\xi_r}{r} - \left(1-\frac{rN^2}{g_0}\right)\frac{\xi_h}{r}\,. \end{aligned} \tag{1.3.7}$$

These are obtained from (1.3.4) by neglecting $\tilde{\Phi}$ and using (1.3.3). Introducing the function $\psi(r)$ according to

$$\psi(r)\; Y_l^m(\theta,\phi)\; \mathrm{e}^{\mathrm{i}\omega t} = c_0^2\rho_0^{1/2}\;\nabla\cdot\vec{\xi}\,, \tag{1.3.8}$$

which gives that

$$\psi(r) = c_0^2\rho_0^{1/2}\left[\frac{1}{r^2}\frac{\mathrm{d}}{\mathrm{d}r}\;\left(r^2\xi_r\right) - \frac{L^2\xi_h}{r}\right]\,, \tag{1.3.9}$$

and after neglecting derivatives of g_0 and r, the following equation for ψ can be obtained (Deubner & Gough 1984, Gough 1991),

$$\frac{\mathrm{d}^2\psi}{\mathrm{d}r^2} + \frac{\omega^2}{c_0^2}\left[1-\frac{\omega_c}{\omega^2} - \frac{S_l^2}{\omega^2}\left(1-\frac{N^2}{\omega^2}\right)\right]\;\psi = 0\,. \tag{1.3.10}$$

The characteristic frequency ω_c, called cutoff frequency, has been defined in (1.3.6). The coefficient in the second term corresponds to a squared wavenumber, which we here define as

$$\begin{aligned} k_l^2(r) &= \frac{\omega^2}{c_0^2}\left[1-\frac{\omega_c^2}{\omega^2} - \frac{S_l^2}{\omega^2}\left(1-\frac{N^2}{\omega^2}\right)\right] \\ &= \frac{\omega^2}{c_0^2}\left(1-\frac{\omega_{l,+}^2}{\omega^2}\right)\left(1-\frac{\omega_{l,-}^2}{\omega^2}\right) \end{aligned} \tag{1.3.11}$$

The equation in (1.3.10) is a simple wave equation with an oscillatory solution (physically valid) in regions where k_l^2 is positive and exponentially damped otherwise.

The zeros of the wavenumber k_l, as function of r, define two frequencies given by

$$\omega_{l,\pm}^2 = \frac{\omega_c^2+S_l^2}{2} \pm \left[\frac{(\omega_c^2+S_l^2)^2}{4} - S_l^2N^2\right]^{1/2}\,, \tag{1.3.12}$$

corresponding to the points where the transition between oscillating and decaying solutions takes place for that frequency. In the case of p-modes, when we neglect the buoyancy frequency N, the reflecting points correspond to have $\omega^2{\sim}\omega_c^2{+}S_l^2$. The oscillatory region is the zone of the model where $\omega^2{>}\omega_c^2{+}S_l^2$. As shown in Fig. 1.6, S_l increases towards the interior while ω_c is important very near the surface. This is the reason why p-modes are confined between some point in the interior and the surface. A plot of the larger

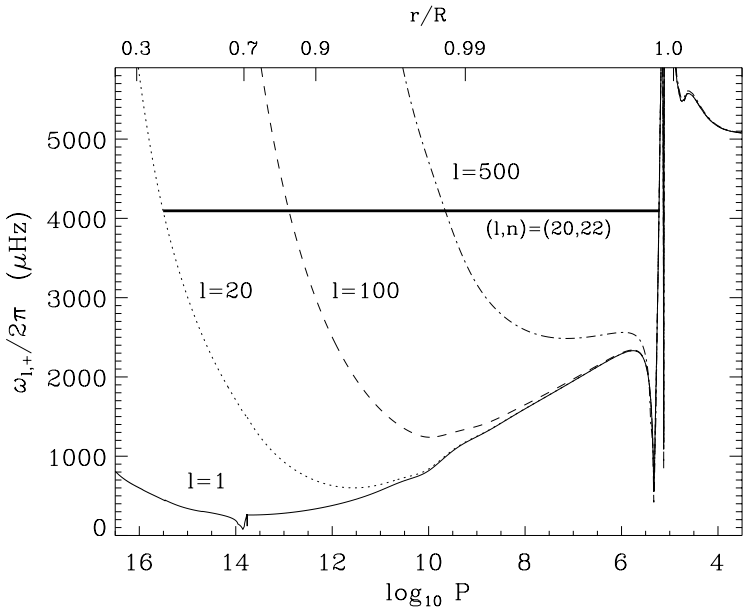

Fig. 1.8: Plot of the frequency $\omega_{l,+}$ (see text). An eigenfunction is oscillatory in the regions where its eigenvalue is above $\omega_{l,+}$ for a given degree. Not plotted here is the other root which corresponds to lower values of frequencies. Also shown as a thick line is the resonant cavity for a mode with degree 20 and order 22, having a cyclic frequency of 4095.56μHz.

root is shown in Fig. 1.8 for a solar model using different values of the degree. Note that since the other root has lower values, oscillatory behaviour is restricted (for p-modes) to regions where a given mode has a frequency above $\omega_{l,+}$. Therefore, for higher degree the mode is progressively confined to a smaller region close to the surface. Also shown is the cavity corresponding to a p-mode of degree 20 and mode order 22, with cyclic frequency of 4095.56μHz.

1.3.3 Asymptotic eigenfunctions and eigenfrequencies

Another process of solving the two differential equations in (1.3.7) is to use, instead of ψ, a new radial amplitude $\tilde{\xi}_r$ defined by

$$\xi_r = f^{1/2}\,\tilde{\xi}_r \qquad \text{with} \qquad f = \frac{\omega^2}{r^2\rho c^2}\left(1-\frac{S_l^2}{\omega^2}\right) . \tag{1.3.13}$$

After eliminating ξ_h and substitute ξ_r by this new variable we find a second order differential equation for $\tilde{\xi}_r$ in the form

$$\frac{\mathrm{d}^2\tilde{\xi}_r}{\mathrm{d}r^2} + \left(k_l^2+\tilde{h}\right)\tilde{\xi}_r = 0 , \tag{1.3.14}$$

where

$$\tilde{h} = \frac{\mathrm{d}h}{\mathrm{d}r} - h^2 - h\,\frac{\mathrm{d}\log f}{\mathrm{d}r} + \frac{1}{2}\,\frac{\mathrm{d}^2\log f}{\mathrm{d}r^2} - \frac{1}{4}\,\left(\frac{\mathrm{d}\log f}{\mathrm{d}r}\right)^2 \;, \qquad \text{for} \qquad h = \frac{2}{r} - \frac{g}{c_0^2}\;. \tag{1.3.15}$$

This equation is equivalent to Eq. (1.3.10) if the assumption that derivatives of g_0 and r can be neglected is used. Indeed in this approximation, the term in $\tilde{h}$ from Eq. (1.3.14) is removed, and the resulting second order differential equation can be solved approximately using JWKB. This implies neglecting variations of the equilibrium structure relatively to variations of the eigenfunction in order to find an approximate expression for the eigenfunctions within the oscillatory cavity. This is

$$\tilde{\xi}_r(r) \propto |k_l|^{-1/2}\;\cos\left(\int_r |k_l(r')|\;\mathrm{d}r' - \frac{\pi}{4}\right)\;, \tag{1.3.16}$$

valid in regions where $k_l^2{>}0$. The phase comes from fitting the oscillatory solution to the exponentially decaying functions in the regions where k_l^2 is negative. Using (1.3.13) and defining the two zeros of k_l as r_1 and r_2, we can write that

$$\xi_r(r) \propto \frac{1}{r\sqrt{\rho_0 c_o}}\;\left|\frac{1-S_l^2/\omega^2}{1-N^2/\omega^2}\right|^{1/4}\;\cos\left(\int_{r_1}^{r} k_l(r')\;\mathrm{d}r'\;-\frac{\pi}{4}\right)\;, \tag{1.3.17}$$

for r well within the interval limited by r_1 and r_2.

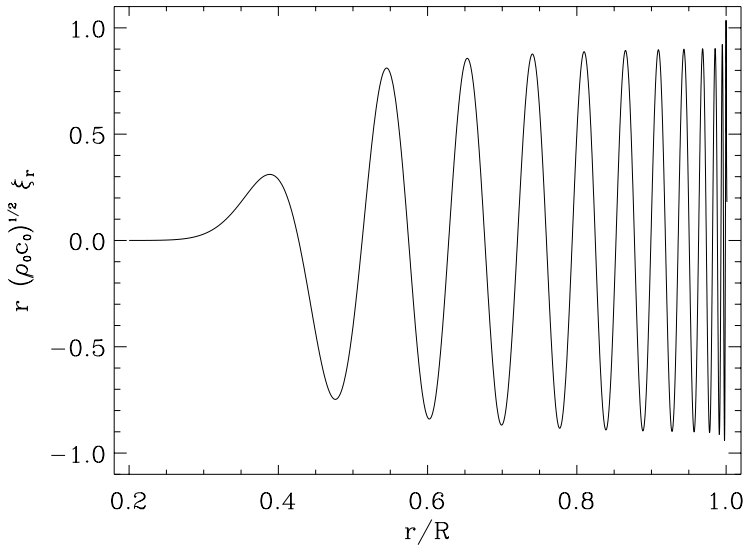

Fig. 1.9: Amplitude of the radial component ξ_r of the displacement vector $\vec{\xi}$, for the same mode shown as a thick line in the previous figure. It corresponds to a p-mode with $(l, n){=}(20, 22)$.

Note that if we introduce a normalized eigenfunction as

$$E_r^2 \equiv r^2 \rho_0 c_0 \; \xi_r^2 \; , \tag{1.3.18}$$

and noting that well inside the resonance cavity S_l and N are much smaller than ω, it follows that this normalized eigenfunction has approximately constant amplitude. An example is given in Fig. 1.9 for a (l,n)=$(20,22)$ mode of the envelope model considered before (we have also shown in the previous figure the resonance cavity for this mode). Note, that within the approximations in finding (1.3.17), we can also write that,

$$\frac{\mathrm{d}^2 E_r}{\mathrm{d}r^2} \sim -k_l^2 \; E_r \; , \tag{1.3.19}$$

valid again only in the interior of the oscillatory region. The expressions shown so far are valid for p-modes with a resonance cavity between some point in the interior and the surface. For most of this region, as can be seen in Fig. 1.6, the only important contribution to k_l comes from S_l, and therefore we can in general approximate this by

$$k_l^2 \sim \frac{\omega^2}{c_0^2} \; \left(1 - \frac{S_l^2}{\omega^2}\right) \; . \tag{1.3.20}$$

This is not, however, valid near the upper turning point where ω_c becomes dominant.

Finally, we can also use the JWKB analysis to obtain an approximate dispersion relation for the eigenvalues. We do so by noting the condition that if the eigenvalues correspond to standing waves then the oscillatory cavity has an integer number n of wavelengths in the radial direction. This is translated simply as

$$\int_{r_1}^{r_2} k_l(r) \; \mathrm{d}r \; \sim \; \pi(n+\epsilon) \; . \tag{1.3.21}$$

The integer number n, called mode order, and introduced before, measures the number of zeros in the radial direction of the amplitude function. The constant ϵ is included since the eigenfunctions are not zero at r_1 and r_2 but take the amplitude from the exponential solutions there. This is associate to the phase $(\pi/4)$ introduced in the asymptotic expression (1.3.17) for the eigenfunction. Replacing k_l, we have,

$$\omega \int_{r_1}^{r_2} \left[1 - \frac{\omega_c}{\omega^2} - \frac{S_l^2}{\omega^2}\left(1 - \frac{N^2}{\omega^2}\right)\right]^{1/2} \; \frac{\mathrm{d}r}{c_0} \; \sim \; \pi(n+\epsilon) \; . \tag{1.3.22}$$

By approximating further the argument of the integral, using (1.3.20), and adding the effect of doing so to ϵ, this expression can be reduced to the simpler form, known as the *Duvall law* (from Duvall 1982),

$$\omega \int_{r_t}^{R} \left(1 - \frac{S_l^2}{\omega^2}\right)^{1/2} \frac{\mathrm{d}r}{c_0} \; \sim \; \pi(n+\alpha) \; . \tag{1.3.23}$$

Note that we have also replaced the limits of the integrand by their approximate values. In the interior, by r_t, corresponding to the solution of the equation $S_l(r_t)=\omega$, and at the surface by the total radius of the star. In doing so, and also because of the approximate expression used for k_l, the constant ε has to be replaced by a phase function $\alpha=\alpha(\omega,l)$ which incorporates all extra terms neglected when using these approximations. Therefore, it is in general a function of frequency and degree (cf Gough & Vorontsov 1995).

1.3.4 Variational principle

So far, we have described how given a numerical model of the Sun it is possible to obtain the frequencies of oscillation from solving numerically the four first order differential equations describing linear oscillations. However, if we want to estimate what contribution each region of the star gives to the global seismic properties we must obtain analytical descriptions on how a specific characteristic of the structure contributes to the frequencies.

Here, we present briefly the derivation of a such a theoretical relation, the objective being to determine how each frequency changes if we change slightly the structure. It is done by constructing a variational principle for adiabatic non-radial oscillations. First a brief description on how to obtain the expression for the variational principle from the perturbed hydrodynamic equations is given, including a discussion of the basic assumptions used. In order to write it in the appropriated form for later use we reduce the expression to the particular case of using the Cowling approximation (neglecting perturbations in the gravitational potential).

Lets start from the linearized equations of continuity and momentum, (B.2.13), in terms of the Eulerian perturbations as written in (1.3.2). Including also the adiabatic relation (1.3.1). As before quantities with subscript "0" correspond to the equilibrium configuration. Our equations are

$$\begin{aligned}
&\rho' + \nabla\cdot\left(\rho_0\,\vec{\xi}\right) = 0\\
&\omega^2\rho_0\,\vec{\xi} - \nabla P' + \rho_0\,\nabla\Phi' + \rho'\,\nabla\Phi_0 = 0\\
&\nabla^2\Phi' = -4\pi G\rho'\\
&P' - c_0^2\,\rho' = \left(c_0^2\,\nabla\rho_0 - \nabla P_0\right)\cdot\vec{\xi}\,.
\end{aligned} \tag{1.3.24}$$

Note that we maintain the dependence on time just to simplify the notation. However it has no effect in the following whether it is kept or not.

After using the first equation to eliminate ρ' in the others, we find from the last equation that

$$P' = -\rho_0 c_0^2\,\nabla\cdot\vec{\xi} - \vec{\xi}\cdot\nabla P_0\ . \tag{1.3.25}$$

This in turn can then be used to replace the perturbation of the pressure in the second equation (in vectorial form). After doing so, the system is reduced to a vectorial equation

in terms of the displacement vector and the perturbation of the gravitational potential only. This is

$$\omega^2\ \rho_0\ \vec{\xi} + \nabla\left(c_0^2\rho_0\ \nabla\cdot\vec{\xi} + \vec{\xi}\cdot\nabla P_0\right) + \rho_0\ \nabla\Phi' - \frac{\nabla\cdot\left(\rho_0\ \vec{\xi}\right)}{\rho_0}\ \nabla P_0 = 0\ . \tag{1.3.26}$$

Finally we eliminate Φ' by using the integral form of the Poisson equation, which is the third equation in (1.3.24). The integral form is

$$\Phi' = G\int_V \frac{\rho'(\vec{r}_\bullet)}{|\vec{r}_\bullet - \vec{r}|}\ \mathrm{d}^3\vec{r}_\bullet = -G\int_V \frac{\nabla_\bullet\cdot\left[\rho_0(\vec{r}_\bullet)\ \vec{\xi}(\vec{r}_\bullet)\right]}{|\vec{r}_\bullet - \vec{r}|}\ \mathrm{d}^3\vec{r}_\bullet\ . \tag{1.3.27}$$

Obtaining finally one vector equation in terms only of the displacement vector;

$$\begin{aligned}\omega^2\ \rho_0\ \vec{\xi} = &-\nabla\left(c_0^2\rho_0\ \nabla\cdot\vec{\xi} + \vec{\xi}\cdot\nabla P_0\right) + \frac{1}{\rho_0}\ \nabla\cdot\left(\rho_0\ \vec{\xi}\right)\ \nabla P_0 + \\ &+\rho_0\ \nabla\left\{G\int_V \frac{\nabla_\bullet\cdot\left[\rho_0(\vec{r}_\bullet)\ \vec{\xi}(\vec{r}_\bullet)\right]}{|\vec{r}_\bullet - \vec{r}|}\ \mathrm{d}^3\vec{r}_\bullet\right\}\ .\end{aligned} \tag{1.3.28}$$

Now, defining the linear operator $\mathcal{L}$ according to

$$\begin{aligned}\mathcal{L}(\vec{\xi}) = &-\frac{1}{\rho_0}\ \nabla\left(c_0^2\rho_0\ \nabla\cdot\vec{\xi} + \vec{\xi}\cdot\nabla P_0\right) + \frac{1}{\rho_0^2}\ \nabla\cdot\left(\rho_0\ \vec{\xi}\right)\ \nabla P_0 + \\ &+\nabla\left\{G\int_V \frac{\nabla_\bullet\cdot\left[\rho_0(\vec{r}_\bullet)\ \vec{\xi}(\vec{r}_\bullet)\right]}{|\vec{r}_\bullet - \vec{r}|}\ \mathrm{d}^3\vec{r}_\bullet\right\}\ ,\end{aligned} \tag{1.3.29}$$

we simplify the notation, with Eq. (1.3.26) becoming

$$\omega^2\vec{\xi} = \mathcal{L}(\vec{\xi})\ . \tag{1.3.30}$$

It can be shown that for the boundary condition using zero pressure at the surface the operator is also Hermitian (eg. Chandrasekhar 1963, 1964).

The next step is to consider the scalar product of Eq. (1.3.30) with $\vec{\xi}^*$ (the star denotes the complex conjugate of $\vec{\xi}$) multiplied by the density. We then integrate both sides over the total volume of the star;

$$\omega^2\int_V 4\pi\rho_o\ \vec{\xi}^*\cdot\vec{\xi}\ \mathrm{d}\vec{r} = \int_V 4\pi\rho_o\ \vec{\xi}^*\cdot\mathcal{L}(\vec{\xi})\ \mathrm{d}\vec{r}\,, \tag{1.3.31}$$

where the volume element, in spherical coordinates, is $\mathrm{d}\vec{r}{=}r^2\sin\theta\ \mathrm{d}r\mathrm{d}\theta\mathrm{d}\phi$.

Using the hermiticity of the linear operator $\mathcal{L}$ (as mention above it is true for the zero pressure boundary condition at the surface) it can be shown that first order perturbations in the eigenfunctions only have a second order effect on the eigenvalues (Chandrasekhar 1964). Therefore expression (1.3.31) is in fact a variational principle for the eigenfrequencies

ω. I.e., first order changes in the frequencies due to small changes in the equilibrium structure can be evaluated neglecting the changes in the eigenfunctions.

Since we are mainly interested in using solar p-modes in here we shall further consider the Cowling approximation by neglecting the term associated with the perturbation of the gravitational potential. In such a case the variational principle is reduced to a simpler expression by removing the term with the integral in the operator $\mathcal{L}$. We write instead that

$$\omega^2 \approx \frac{\int_V \vec{\xi}^* \cdot \left[\frac{\nabla P_0}{\rho_0} \nabla \cdot \left(\rho_0 \vec{\xi}\right) - \nabla\left(c_0^2 \rho_0 \nabla \cdot \vec{\xi} + \vec{\xi} \cdot \nabla P_0\right)\right] 4\pi \mathrm{d}\vec{r}}{\int_V 4\pi \rho_o \left(\vec{\xi}^* \cdot \vec{\xi}\right) \mathrm{d}\vec{r}} \,. \tag{1.3.32}$$

Replacing the last term by using

$$\begin{aligned} \int_V \vec{\xi}^* \cdot \nabla\left(c_0^2 \rho_0 \nabla \cdot \vec{\xi} + \vec{\xi} \cdot \nabla P_0\right) \mathrm{d}\vec{r} = & \int_V \nabla \cdot \left[\left(c_0^2 \rho_0 \nabla \cdot \vec{\xi} + \vec{\xi} \cdot \nabla P_0\right) \vec{\xi}^*\right] \mathrm{d}\vec{r} \\ & - \int_V \left(c_0^2 \rho_0 \nabla \cdot \vec{\xi} + \vec{\xi} \cdot \nabla P_0\right) \nabla \cdot \vec{\xi}^* \, \mathrm{d}\vec{r} \,, \end{aligned} \tag{1.3.33}$$

and further considering that

$$\int_V \nabla \cdot \left[\left(c_0^2 \rho_0 \nabla \cdot \vec{\xi} + \vec{\xi} \cdot \nabla P_0\right) \vec{\xi}^*\right] \mathrm{d}\vec{r} = \int_S \left(c_0^2 \rho_0 \nabla \cdot \vec{\xi} + \vec{\xi} \cdot \nabla P_0\right) \vec{n} \cdot \vec{\xi} \, \mathrm{d}s \,, \tag{1.3.34}$$

where $\vec{n}$ is the unit vector normal to the surface S of the star and the surface element is given by $\mathrm{d}s = r^2 \sin\theta \, \mathrm{d}\theta \mathrm{d}\phi$, the above expression can be simplified. Using the zero pressure boundary condition;

$$P_o \equiv 0 \qquad \text{and} \qquad \rho_o \equiv 0 \qquad \text{at the surface} \,,$$

equivalent to requiring $P' \equiv 0$ there, it follows that the right side of Eq. (1.3.34) is zero. Therefore, the variational principle can be written instead as

$$\omega^2 \approx \frac{\int_V \left[\frac{\vec{\xi}^* \cdot \nabla P_0}{\rho_o} \nabla \cdot \left(\rho_0 \vec{\xi}\right) + \left(c_0^2 \rho_0 \nabla \cdot \vec{\xi} + \vec{\xi} \cdot \nabla P_0\right) \nabla \cdot \vec{\xi}^*\right] 4\pi \mathrm{d}\vec{r}}{\int_V 4\pi \rho_o \left(\vec{\xi}^* \cdot \vec{\xi}\right) \mathrm{d}\vec{r}} \,. \tag{1.3.35}$$

Replacing the displacement vector by the expression given in the last equation of (1.3.2) and using the properties of the spherical harmonics giving

$$\nabla \cdot \vec{\xi} = \left[\frac{1}{r^2} \frac{\mathrm{d}}{\mathrm{d}r}\left(r^2 \xi_r\right) - \frac{L^2 \, \xi_h}{r}\right] \, Y_l^m \, \mathrm{e}^{\mathrm{i}\omega t} \,, \tag{1.3.36}$$

we can write that

$$\begin{aligned} \omega^2 \int_R 4\pi r^2 \rho_o \left(\xi_r^2 + L^2 \xi_h^2\right) \mathrm{d}r \approx \int_R \Bigg\{ & 2 \frac{\mathrm{d}P_0}{\mathrm{d}r} \xi_r \left[\frac{1}{r^2} \frac{\partial}{\partial r}\left(r^2 \xi_r\right) - \frac{L^2 \, \xi_h}{r}\right] \\ & + c_0^2 \rho_0 \left[\frac{1}{r^2} \frac{\partial}{\partial r}\left(r^2 \xi_r\right) - \frac{L^2 \, \xi_h}{r}\right]^2 \Bigg\} 4\pi r^2 \mathrm{d}r \end{aligned} \tag{1.3.37} \,.$$

Or in terms of mass,

$$\omega^2 \approx \frac{\displaystyle\int_M \left\{ -2g_0\ \xi_r \left[\frac{1}{r^2}\ \frac{\partial}{\partial r}\left(r^2\xi_r\right) - \frac{L^2\xi_h}{r}\right] + c_0^2\ \left[\frac{1}{r^2}\ \frac{\partial}{\partial r}\left(r^2\xi_r\right) - \frac{L^2\xi_h}{r}\right]^2 \right\} \mathrm{d}m}{\displaystyle\int_M \left(\xi_r^2 + L^2\xi_h^2\right) \mathrm{d}m} \ . \quad (1.3.38)$$

This can be written as

$$\omega^2 = I_2/I_1 \ , \quad (1.3.39)$$

where

$$I_1 = \int_R r^2\rho_0(\xi_r^2 + L^2\xi_h^2)\mathrm{d}r \ , \quad (1.3.40)$$

and

$$I_2 = \int_R \left\{ \frac{c_0^2}{r^4}\left[\frac{\mathrm{d}(r^2\xi_r)}{\mathrm{d}r}\right]^2 - \frac{g_0}{\rho_0}\ \frac{\mathrm{d}\rho_0}{\mathrm{d}r}\ \xi_r^2 + S_{l,0}^2 L^2\xi_h^2 - \right.$$

$$\left. - \frac{g_0}{r^4}\ \frac{\mathrm{d}(r^4\xi_r^2)}{\mathrm{d}r} - \frac{2S_{l,0}^2}{r}\ \xi_h\ \frac{\mathrm{d}(r^2\xi_r)}{\mathrm{d}r} + \frac{2g_0}{r}\ \xi_r L^2\xi_h \right\} r^2\rho_0\ \mathrm{d}r \ . \quad (1.3.41)$$

It follows that if we change the equilibrium configuration by small amounts $\delta\rho$ and δc^2 (within the Cowling approximation we are also neglecting variations of g), the eigenvalues will change from the initial value ω_0 to the new one, ω, according to

$$\delta\omega^2 = \omega^2 - \omega_0^2 = \frac{\delta I_2 - \omega_0^2\ \delta I_1}{I_1} = \frac{\delta I}{I_1} \ , \quad (1.3.42)$$

where

$$\delta I = \int_R \left\{ -\frac{2}{r}\ L^2\xi_h\ \frac{\mathrm{d}(r^2\xi_r)}{\mathrm{d}r} + \frac{1}{r^2}\ \left[\frac{\mathrm{d}(r^2\xi_r)}{\mathrm{d}r}\right]^2 + L^4\xi_r^2 \right\} \delta(\rho c^2)\ \mathrm{d}r -$$

$$- \int_R \left\{ -\frac{g_0}{r^2}\ \frac{\mathrm{d}(r^4\xi_r^2)}{\mathrm{d}r} + 2rg_0\ \xi_r L^2\xi_h - \omega_0^2 r^2(\xi_r^2 + L^2\xi_h^2) + r^2 g_0\xi_r^2\ \frac{\mathrm{d}}{\mathrm{d}r} \right\} \delta\rho\ \mathrm{d}r \ . \quad (1.3.43)$$

In writing this we used the fundamental fact that changes in the eigenfunctions could be neglected. This is the application of the variational principle for linear adiabatic nonradial oscillations in the Cowling approximation.

1.3.5 Structural kernels and frequency differences

Note that we can write formally the previous expression, obtained for the variational principle, as (see for example Gough & Thompson 1991 for a formal derivation of a relation of this type)

$$\frac{\delta\omega}{\omega} \approx \int_R \left[K_{\rho,c}^{\omega}(r)\ \frac{\delta\rho}{\rho_0} + K_{c,\rho}^{\omega}(r)\ \frac{\delta c}{c_0} \right] \mathrm{d}r \ , \quad (1.3.44)$$

after using hydrostatic equilibrium to eliminate one variable. The functions of the reference model, $K^{\omega}_{\rho,c}(r)$ and $K^{\omega}_{c,\rho}(r)$, are known since these depend in general on the structure of the reference model and its eigenfunctions. Therefore, this relation gives for a known reference model, the relative change in the frequencies that are associated with some specified small change relative to this reference structure, as described by $\delta\rho$ and δc. Since we are using the equation of hydrostatic equilibrium, these pair of variables can be replaced by any other pair of related thermodynamic quantities. Some possibilities are for example (c, Γ_1) or (c, υ) (Gough 1985, Gough & Thompson 1991, Christensen-Dalsgaard & Thompson 1996). Such expressions can provide the means to determine the expected frequency changes resulting from changes in the structure. Conversely, given a set of frequency differences we may try to invert the relation in order to infer what model differences were necessary to produce such frequency changes (cf Gough & Thompson 1991 and references therein).

2. Modelling Convective Overshoot

Sharp transitions in the internal stratification of a star give rise to a characteristic signature in normal p-mode frequencies. Various theoretical models of overshoot at the base of the convection zone predict the existence of a rather abrupt transition to sub-adiabatic stratification at the base of the overshoot region. Some of these models predicting such a behaviour are briefly reviewed.

Using a variational principle for non-radial adiabatic oscillations with the Cowling approximation we derive an expression for the signal in the frequencies. A comparison with other works is also included. The possible use of moderate degree data is considered by including an extra term in the expansion of the argument of the signal. The effects from uncertainties in the surface layers of the star are also discussed.

2.1 Introduction

From our ignorance of the physics of convection comes one of the present problems in stellar structure: the existence and extent of convective overshoot under stellar conditions and its effects on the equilibrium configuration and evolution of a star. An overshoot layer in the Sun is generally expected at the boundary between the convective stable radiative interior and the envelope where the fluid undergoes convective motions. Indeed, hydrodynamic simulations, and the observation of other transition layers in nature (see Zahn 1991 and references therein), suggest that convective motions within the gas do tend to penetrate beyond the convective unstable region into the region in radiative equilibrium, therefore affecting the structure beyond the region that is convective unstable as given by the Schwarzschild stability condition. Solar granulation is further evidence that overshoot indeed occurs at the top of the convection zone indicating again that we may expect a similar behaviour at the bottom of the envelope.

When modelling stars, overshoot from a convective envelope should be included (e.g. Alongi et al. 1991, Lattanzio et al. 1991). Even more significant is the similar process of overshoot from a convective core; this would add fuel to the nuclear-burning region of the

star and hence would strongly affect the evolution of the star (e.g. Maeder 1976, Lattanzio et al. 1991, Stothers & Chin 1992). But since we have no reliable theory to predict the penetration depth as a function of the local stratification, the effect is in general modelled through the introduction of a parameter (similar to the ratio α between mixing length and pressure scale height employed in mixing-length theory - eg. Stothers & Chin 1992). Such a parametric description must be constrained observationally if any predictive capability is to be retained from modelling stellar interiors. We also need even to establish the basic characteristics of such an overshoot layer, in particular, the temperature stratification and the effects on mixing, that the presence of overshoot imposes.

The work presented in this Chapter is an attempt to determine the effect on the frequencies of oscillation of an overshoot layer. By considering an overshoot region that is adiabatically stratified with a sharp transition to radiative stratification at its bottom, as expected in some models of this layer, we determine an asymptotic expression for the signature in the frequencies of oscillation. To do so, a variational principle for adiabatic nonradial oscillations with the Cowling approximation is used. A simple analogy is presented to elucidate the underlying physical reason for this signature and its periodicity. A comparison with other works is also presented.

If moderate-degree data are included the simple relation of the periodic signal with period given by the acoustic depth of the transition layer is destroyed. Hence we introduce a compensating higher-order term to allow the use of such moderate-degree data. A discussion of contributions, e.g. from the surface layers, is also presented in order to estimate the effect on the values inferred for the parameters of the signal.

2.2 Physical description of convective overshoot

How can we model convective overshoot? This is a question that can only be answered if we use a theory of convection, which is something we do not have. Therefore any attempt to model or estimate the behaviour of the gas at the border of a convective unstable layer is, a priori, very difficult if not impossible, considering our difficulties in describing the average properties for the motion of the gas within the proper convection zone. However some estimates have been proposed using simple analyses. We shall revise briefly some of these here in order to elucidate what type of configuration is expected for an overshoot region in stellar interiors.

The basic aspects which tend to be present in all descriptions discussed below can be reduced to the following basic points (see Fig. 2.1);

- The proper convection zone (above r_c) is superadiabatic in order to maintain the fluid in motion necessary for all flux to be transported - in the deep convection zone this

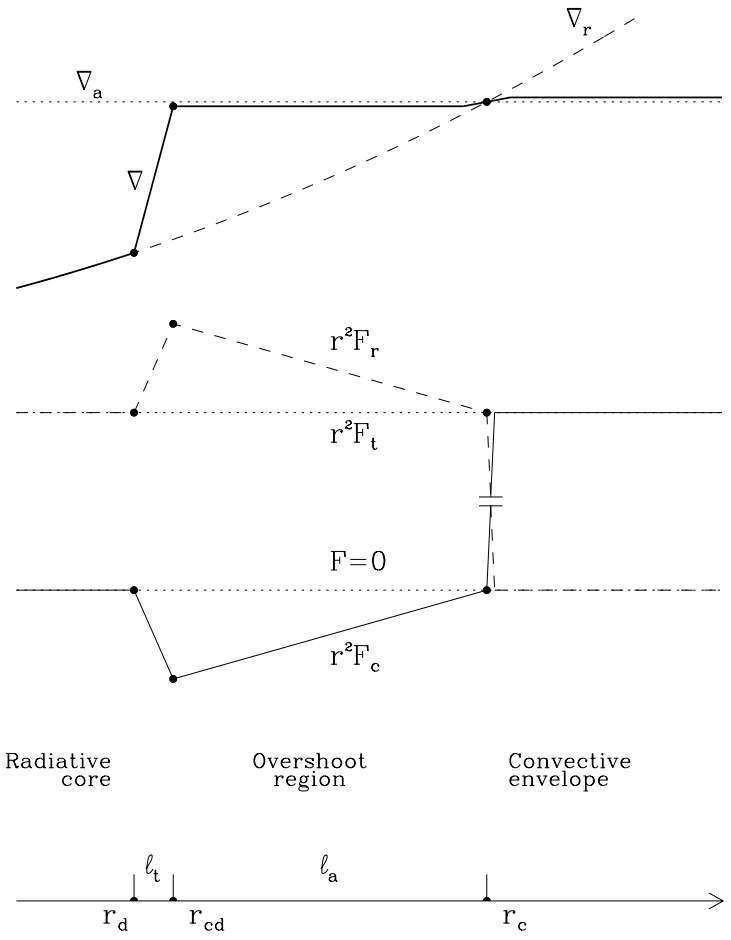

Fig. 2.1: Schematic configuration for the overshoot region. The top panel shows the behaviour of the temperature gradient ∇ together with the radiative ($\nabla_{\rm r}$) and adiabatic ($\nabla_{\rm a}$) gradients. While the other panel shows the fluxes; F_r carried by radiation, F_c carried by convection and the total flux F_t (there is no energy production in this region). The radial position $r_{\rm c}$ corresponds to Schwarzschild's instability condition, while $r_{\rm cd}$ is the bottom of the quasi adiabatically stratified zone. The actual base of the convection zone sis given by $r_{\rm d}$, if we define it as the region where there are convective motions of the fluid. So the total extent of the overshoot is $\ell_s \equiv r_{\rm c} - r_{\rm d} = \ell_t + \ell_a$. After Zahn (1991).

superadiabaticity is very small because the convective efficiency is extremely high and convective motions are very much subsonic.

- The proper convection zone ends where the fluid is no longer accelerated corresponding to the point $r_{\rm c}$ where the stratification becomes subadiabatic due to the effect of radiative transport of energy. However, this boundary is defined by a zero condition in the acceleration - not in velocity.
- Because of this non-zero velocity at the boundary the fluid penetrates beyond this boundary where due to the higher efficiency of radiation in transporting the flux the

stratification is subadiabatic and so the fluid motions are decelerated (region between $r_{\rm d}$ and $r_{\rm c}$).

- The extent ℓ_s and characteristics of this region are establish by the competing effects between the penetration of the fluid which tries to force a quasi adiabatic stratification and the radiation which tends to make it subadiabatic. The so-called region of overshoot ends ($r_{\rm d}$) where the radiation finally wins and the fluid comes to rest.

The important aspects of this scenario are the extent ℓ_s of the region and its characteristics. In particular, it is important to establish how strongly subadiabatic the overshoot region is and if part of it is quasi adiabatic what fraction (ℓ_t/ℓ_s) corresponds to the transition to a radiative stratification. These are the main answers we ask and they are addressed in the theoretical works reported briefly below. However, it should be noted that any of the theoretical estimates is a result of extremely simplified physics, with no account of extra contributions affecting convection and convective stability, like magnetic fields and rotation, and using a parametrization for the convective flux and velocity. So, as discussed latter, in a real star we do not known how representative such estimates are of what happens, since all these effects are certainly at work with a significant contribution to the stratification of the gas. This is one of the reasons why it is crucial to obtain observational constraints on the properties of an overshoot region, or even to establish whether it exists or not.

The first theoretical study of overshoot presented here is the one by van Ballegooijen (1982). Basically the same results have also been presented by Schmitt et al. (1984). In their works the plume equations are applied to solar conditions in the region of the subadiabatic gradient, just below the boundary of convective instability $r_{\rm c}$ (see Fig. 2.1), and the parameter space describing the convection characteristics is studied. We also consider the work by Zahn (1991) where mixing length type of arguments are again used to infer the properties of the overshoot region. The basic picture of an adiabatically stratified overshoot region extending over a few tenths of a pressure scale height is found by all authors, with a very thin transition region at the bottom. Other estimates have also been given by Shaviv & Salpeter (1973), Maeder (1975), Pidatella & Stix (1986), Skaley & Stix (1991) and Antia & Chitre (1993), with similar results. We do not discuss these here. As concluded by Renzini (1987) we do not really have a theory of overshooting and so only alternative sources of information, like numerical simulations of convection for example, may provide an alternative approach to this problem. However these present the problem that convective velocities depend crucially on the parameters and geometry of the simulation making it difficult to transpose the results to the Sun. We shall discuss some of these briefly.

2.2.1 Overshoot by van Ballegooijen and Schmitt et al.

In this Subsection, the works of van Ballegooijen (1982) and Schmitt, Rosner & Bohn (1984) are considered. The basic aspects of their methods to determine the characteristics of an overshoot layer at the bottom of the solar convective envelope can be reduced to the following equations describing how the trade-off between motions of the fluid and radiation stratifies the gas in an overshoot layer.

Let us start by neglecting fluctuations in density and assuming the motion to be adiabatic. Also, the fluctuations around the mean temperature T and entropy S are considered to be proportional to

$$T_1(z)\cos(kx)\,\mathrm{e}^{\gamma t} \qquad \text{and} \qquad S_1(z)\cos(kx)\,\mathrm{e}^{\gamma t}\,, \tag{2.2.1}$$

respectively. The constant k is the horizontal scale of the fluctuations and γ the inverse of the turnover time. The two functions T_1 and S_1 represent the dependence on the vertical depth z (from the Schwarzschild boundary r_c) of the amplitude of the fluctuations. A similar dependence is also written for the horizontal (u_x) and vertical (u_z) components of the velocity;

$$\vec{u}(x,z,t) \equiv \Big[u_x(z)\sin(kx)\,,\; u_z(z)\cos(kx)\Big]\,\mathrm{e}^{\gamma t} \tag{2.2.2}$$

The coordinate x is the horizontal direction, in planar geometry. Assuming the motion is adiabatic and using the continuity and momentum equations it is possible to write a system of four equations. By using the second law of thermodynamics, we replace the pressure in the equation of motion leaving the equations in terms of T_1, S_1, u_x and u_z. By using three of these to eliminate the first three variables, the following second order equation for the vertical component ρu_z of the mean flow (ρ is the density) can be found;

$$\begin{aligned}\frac{\mathrm{d}^2}{\mathrm{d}z^2}(\rho u_z) - \left(\frac{1}{H_\rho} + \frac{1}{C_P}\,\frac{\mathrm{d}S}{\mathrm{d}z}\right)\frac{\mathrm{d}}{\mathrm{d}z}(\rho u_z) \\ + \left[\frac{k^2}{\gamma^2}\,\left(C_P\,\frac{\mathrm{d}T}{\mathrm{d}z} - T\,\frac{\mathrm{d}S}{\mathrm{d}z}\right)\frac{1}{C_P}\,\frac{\mathrm{d}S}{\mathrm{d}z} - k^2\right](\rho u_z) = 0\,,\end{aligned} \tag{2.2.3}$$

where $H_\rho{=}(\partial \log\rho/\partial z)^{-1}$ is the density scale height and C_P is the specific heat at constant pressure. The second law of thermodynamics can then be used again to replace the temperature gradient by the entropy gradient. The equation is then complemented by two boundary conditions. One is that u_z goes to zero at infinity and the other is imposed from the conditions at the top of the overshoot region (bottom of the convection zone), i.e.,

$$\left[\frac{1}{\rho}\,\frac{\mathrm{d}}{\mathrm{d}z}(\rho u_z)\right]_{z=0} = -k v_c\,. \tag{2.2.4}$$

The quantity v_c is the typical velocity at the base of the proper convection zone imposed by the properties of convection in the unstable region (for z negative). To this van Ballegooijen adds a diffusion-like equation relating the entropy gradient and the convective

flux,

$$F_c = -\rho T D \frac{\mathrm{d}S}{\mathrm{d}z} , \tag{2.2.5}$$

where D is a diffusion coefficient given by

$$D = \frac{u_z^2}{\gamma} . \tag{2.2.6}$$

Eliminating the entropy between the two and using the conservation of total flux the second order differential equation for the vertical mass flow can be solved. For typical values of the parameters (γ, k, v_c) a stratification of the overshoot layer can therefore be determined.

Using an analytical treatment of such an equation van Ballegooijen finds an approximate expression for the depth of the overshoot region of a few tenths of the pressure scale height. For the transition region from this adiabatic overshoot to the radiative stratification van Ballegooijen determines an extent that is proportional to the relative kinetic energy at the base of the convection zone, giving a value which is much smaller than the extent of the adiabatically stratified fraction of the overshoot layer.

The results from the numerical integration of Eq. (2.2.3) support these findings when typical values of the parameters describing the basic properties of the region (efficiency of convection, relative cell lifetime and convective cells wavenumber), are used. The difference between the extents (ℓ_t) of the transition region and the adiabatic section (ℓ_a) of the overshoot layer imply a temperature gradient at the base of the envelope that "changes nearly discontinuously".

The final picture given there is very similar to the one represented in Fig. 2.1 where we have an overshoot region composed by an adiabatic section and a transition at the bottom which takes place over a distance much smaller than the previous. The actual values for both, however, depend crucially in parameters describing the convective properties of the fluid at the base of the convection zone, which are therefore unknown or extremely difficult to estimate with any certainty. However we must stress that this result is based on the assumption that convective motions within this overshoot region are strong enough to force a nearly adiabatic stratification. It is confirmed a *posteriori*, but as discussed by Renzini (1987) it is only confirmed if used a *priori*!

2.2.2 The approach of Zahn

Another estimation of convective overshoot in stellar interiors has been presented by Zahn (1991). The evaluation is done by assuming, again, that the properties of the fluid velocity field above in the proper convection zone are known. He further assumes that there is a quasi adiabatic section and a transition region (see Fig. 2.1). The basic arguments are as

follows. If the stratification is (quasi)adiabatic then the radiative flux can be written as

$$F_r = \chi \, \frac{T}{H_P} \, \nabla_{\rm a} \ , \tag{2.2.7}$$

where the radiative conductivity is given by

$$\chi = \frac{16\sigma T^3 C_P}{3k} \ . \tag{2.2.8}$$

The notation is as before, with k being the opacity and σ the Stefan-Boltzmann constant. So in this region, using the conservation of flux (and neglecting the contribution from the kinetic energy), we must have for the convective flux that

$$F_c = F_t - F_r \sim F_t - \left[F_r(r_{\rm c}) + \left(\frac{{\rm d}F_r}{{\rm d}r} \right)_{r_{\rm c}} (r - r_{\rm c}) \right] \ , \tag{2.2.9}$$

with F_t being the total flux and $F_r(r_{\rm c})=F_t$ by definition of $r_{\rm c}$. Assuming full ionization and neglecting the mass of the envelope we find

$$\left(\frac{{\rm d}F_r}{{\rm d}r} \right)_{r_{\rm c}} \sim F_t \left[\left(\frac{\partial \log \chi}{\partial r} \right)_{r_{\rm c}} - \frac{2}{r} \right] = -F_t \left(\frac{\chi_p}{H_P} + \frac{2}{r} \right)_{r_{\rm c}} \ ,$$

where $\chi_p \equiv \partial \log \chi / \partial \log P$. Further using the fact that $\chi_p \sim 3$ and $H_P \ll r_{\rm c}$ in this region, we arrive to

$$F_c \sim -F_t \, \frac{\chi_p}{H_P} \, (r_{\rm c} - r) \ . \tag{2.2.10}$$

At this point we need to relate this convective flux obtained by simple conservation of energy with the velocity field of the fluid. Zahn does it by assuming temperature and velocity perturbations given by $\delta T(z)h(x,y)$ and $W(z)h(x,y)$, respectively. Planar geometry, with z being the vertical coordinate and (x,y) the horizontal ones, is being used. The function $h(x,y)$ describes the horizontal structure of all fluctuations which have been therefore considered strongly correlated. It is defined such as to have the following properties;

$$\overline{h(x,y)} = 0 \ , \qquad \overline{h^2(x,y)} = f \qquad \text{and} \qquad \overline{h^2(x,y)\mu(x,y)} = 1 \ , \tag{2.2.11}$$

where the bar represents horizontal (over x and y) averages and $\mu(x,y)$ is just a mask which is zero everywhere except where h is positive taking the value one there.

Using horizontal averages the expression for the convective flux along z is simply

$$F_c \sim -f C_P \rho W \delta T \tag{2.2.12}$$

The next step is to use a simple kinematic (ballistic) argument; the fluid starts at $r=r_{\rm c}$ with vertical velocity W_0 and is decelerated by buoyancy due to its density fluctuation,

moving a distance ℓ_a before its velocity is too low ($\sim$0) to affect the stratification. In such a case the equation of motion is simply

$$\frac{1}{2}\,\frac{\mathrm{d}w^2}{\mathrm{d}z} = g\,\frac{\delta\rho}{\rho}\,h(x,y) = -gQ\,\frac{\delta T}{T}\,h(x,y)\,, \tag{2.2.13}$$

where Q is the coefficient of expansion of the gas. Multiplying by h and taking horizontal averages it gives that

$$\frac{\mathrm{d}W^2}{\mathrm{d}z} = -\frac{2gQ}{c_h}\,\frac{\delta T}{T} \sim -\frac{1gQF_t\chi_P}{c_h f\ C_P\rho H_P T}\,\frac{z}{W}\,, \tag{2.2.14}$$

where we have combined Eq. (2.2.10) and (2.2.12) to replace δT. The new parameter $c_h{=}\overline{h^2}/\overline{h^3}$ describes the degree of asymmetry of the flow. After integration (neglecting variations of all other quantities except W) we find

$$\frac{\ell_a}{H_P} = W_0^{3/2}\sqrt{c_h f}\,\left(\frac{3}{2}\,gQK\chi_p\nabla_{\rm a}\right)^{1/2}\,. \tag{2.2.15}$$

The radiative diffusivity is $K{=}\chi/(\rho C_P)$. Note that we can write this in another form,

$$\frac{\ell_a}{H_P} = \left[\frac{4}{3}\,(c_h f)\ \ \frac{\frac{1}{2}\,\rho W_o^2\cdot W_0}{F_t}\ \ \frac{H_{T,a}H_{\chi,a}}{H_P^2}\right]^{1/2}\,. \tag{2.2.16}$$

This just says, as we would expect, that the size of the adiabatically stratified overshoot layer is proportional to the geometrical mean of the typical lengths, namely for the temperature $H_{T,\rm a}{=}(\partial\log T/\partial r)^{-1}_{\rm a}$ and for the radiative conductivity $H_{\chi,\rm a}{=}(\partial\log\chi/\partial r)^{-1}_{\rm a}$, where the subscript "a" reminds that the stratification is assumed adiabatic. The proportionality is given by the ratio of the kinetic flux of the fluid at the Schwarzschild boundary and the total flux (the luminosity is assumed constant for this region). There is also the factor describing the degree of asymmetry of the flow $\sqrt{c_h f}$, which is unknown, but expected to be of order unity.

Using typical values for the Sun we have that $H_{T,\rm a}{\sim}5H_P/2$ and $H_{\chi,\rm a}{\sim}3H_P$, giving

$$\ell_a{\sim}1.6\times10^{-3}\sqrt{fc_h}\,\left(\frac{W_0}{100\mathrm{ms}^{-1}}\right)^{3/2}H_P\,. \tag{2.2.17}$$

Zahn goes further by substituting an expression for the convective flux inside the proper convection zone in order to replace W_0 in the above expression. He gives the following relation for the total flux close to $r_{\rm c}$, but above it,

$$F_t = \frac{2}{3}\,(c_h f)_\star\ \ \frac{\rho\chi_p W_0^3}{\nabla_{\rm a}}\,, \tag{2.2.18}$$

where the "$\star$" represents the values of c_h and f inside the convection zone. After substitution in Eq. (2.2.17) gives

$$\ell_a{\sim}\frac{1}{\chi_p}\,\left[\frac{c_h f}{(c_h f)_\star}\right]^{1/2}H_P\,. \tag{2.2.19}$$

Using again a typical value for χ_p of 3, we would say that ℓ_a is expected to be, according to this expression, about a few tenths of a pressure scale height. However, as Zahn points out, Eq. (2.2.18) predicts extremely high convective velocities, which is essential in order to arrive to the previous statement. This can also be understood considering (2.2.17) where only for a vertical component of the convective velocity much larger than $100\mathrm{ms}^{-1}$ will we obtain $\ell_a \sim 10\% H_P$.

In the calculation of this value it has been assumed that convective motions are sufficiently efficient to enforce an adiabatic stratification. However, in the picture where the fluid vertical velocity W is decelerated to zero, there comes a point where this assumption is no longer true. So, we have to consider what happens at this point, where the (negative) convective flux comes to a maximum and radiative diffusion dominates over convective motions. This is the transition region for which Zahn estimates an extent which is given by

$$\frac{\ell_t}{H_P} \sim \left[\frac{1}{c_h f} \, \frac{(\rho C_P \chi)^2}{Q \chi_p \nabla_{\mathrm{a}} g H_P} \, \frac{H_P}{\ell_a} \right]^{1/4} , \tag{2.2.20}$$

corresponding to the scale needed for the fluid to relax to the radiative stratification with a rapid decrease of the remaining vertical velocity. Using typical values for the proportionality function we find

$$\frac{\ell_t}{H_P} \sim \frac{2.5 \times 10^{-13}}{(c_h f)^{1/4}} \left(\frac{H_P}{\ell_a} \right)^{1/4} . \tag{2.2.21}$$

So, again the final picture is one of a quasi adiabatic overshoot layer penetrating a few tenths of the local pressure scale height with a transition region at the bottom to radiative stratification taking place over an extremely short distance.

2.2.3 Numerical simulations of convection

Numerical simulations of convection are presently one of the tools used to study stellar convection, granulation and overshoot. Overshoot in particular has been extensively studied; see for example Hurlburt, Toomre & Massaguer (1986), Roxburgh & Simmons (1993), Hurlburt et al. (1994) and Singh, Roxburgh & Chan (1995).

The fact that the gas overshoots from the convective unstable region into the stable regions is a feature common to all works. However, to infer the actual penetration distance for the particular case of having a stable region below the unstable layer from the simulations, for solar conditions, is not a simple task. The usual configuration of having initially a layer where the motions are still strong enough to force a quasi adiabatic stratification and the transition to radiative stratification at the bottom when the motions are too low to affect the local thermodynamics is present in most of the results. This can be seen

for example in the Fig. 8 of Roxburgh & Simmons (1993) where the numerical results are compared with the astrophysical solution without overshoot.

Hurlburt et al. (1994) also included a detailed study of how these two regions, which we refer as ℓ_a and ℓ_t in Fig. 2.1, depend on the relative stability between the stable and unstable regions. This parameter S is determined from the polytropic indices of the two layers which come from the configuration of the system trough the thermal conductivity. Their results indicate the existence of two distinct regimes. One corresponding to lower values for the relative stability with an extent ℓ_s dominated by the quasi adiabatic overshoot, i.e. with $\ell_s \sim \ell_a$, and having a very thin transition layer (small ℓ_t). The actual extent in this regime varies inversely with S. The second regime corresponds to high values of the stability parameter with the extent of the overshoot varying with $S^{-1/4}$ being dominated by the transition layer; $\ell_s \sim \ell_t$. The same behaviour is reported in Singh et al. (1995) where the actual extent of the overshoot region is plotted as a function of this stability parameter.

These results seem to indicate that the estimates reported before correspond to one of the regimes, namely the first having $\ell_s \sim \ell_a$. However an alternative configuration is possible where there is penetration of the fluid in the stable region but with a very weak effect on the local stratification. This would suggest that there may be effects on aspects like mixing, but not significantly on temperature stratification. This is one of the questions we need to answer using stellar seismic data. The possibility of discriminating between these two distinct behaviours is addressed later, in Chapters 3 and 5. However as a starting point let us consider what happens to the seismic properties of the Sun if the configuration of the overshoot layer corresponds to the one found for low values of the stability parameter and the theoretical estimations presented above.

2.3 Seismic effects of overshoot

The next point is, after considering the simplest possible configuration of an overshoot layer, to use it to estimate how the seismic properties of the star are affected. We shall do so by assuming that overshoot extends down in radius the adiabatically stratified envelope of the Sun. At the bottom of this added extra layer, a jump to radiative stratification takes place inducing a discontinuity in the sound speed derivative.

From this simple model we attempt to determine using a variational principle for the frequencies how these are changed relative to a model with a smoother transition. In this way we can estimate by how much the frequencies change, and more important, the functional dependence of the changes on mode frequency/order and degree, due to the presence of overshoot.

2.3.1 Variational analysis

In order to determine the effect on the seismic properties of the star from an overshoot layer we consider a variational principle for nonradial adiabatic oscillations, assuming zero pressure at the surface located at radius R as a boundary condition (Chandrasekhar 1964, Unno et al. 1979 - see Chapter 1 for some of the details). This gives an estimate on how each frequency changes due only to the overshoot layer by relating the frequency changes to the structural differences coming from the presence of such a layer.

For high order and high frequency acoustic modes one may neglect terms associated with the perturbation in the gravitational potential - Cowling approximation (Cowling 1941), to obtain an expression for the variational principle of the type (see Section 1.3.4)

$$\omega^2 = I_2/I_1 \ , \tag{2.3.1}$$

where

$$I_1 = \int_0^R r^2\rho(\xi_r^2 + L^2\xi_h^2)\mathrm{d}r \ , \tag{2.3.2}$$

and

$$I_2 = \int_0^R \left\{ \frac{c^2}{r^4}\left[\frac{\mathrm{d}(r^2\xi_r)}{\mathrm{d}r}\right]^2 - \frac{g}{\rho}\,\frac{\mathrm{d}\rho}{\mathrm{d}r}\,\xi_r^2 + S_l^2L^2\xi_h^2 - \right.$$
$$\left. - \frac{g}{r^4}\,\frac{\mathrm{d}(r^4\xi_r^2)}{\mathrm{d}r} - \frac{2S_l^2}{r}\,\xi_h\,\frac{\mathrm{d}(r^2\xi_r)}{\mathrm{d}r} + \frac{2g}{r}\,\xi_rL^2\xi_h \right\} r^2\rho \ \mathrm{d}r \ . \tag{2.3.3}$$

Here ω is the frequency of the mode, and r, ρ, c and g are distance from the centre, density, adiabatic sound speed and gravitational acceleration, respectively. The Lamb frequency is $S_l{=}Lc/r$ with $L^2{=}l(l{+}1)$, l being the degree of the mode, and the horizontal and vertical components of the displacement vector are, respectively, ξ_h and ξ_r.

Whether there is or not overshoot at the base of the convection zone, the region is characterized by a change from near adiabatic stratification to a radiative one. Regardless of how it changes from one to the other if such a transition occurs within a short distance compared with the wavelength of the oscillations then it is felt as a localized feature by the waves. In particular, we have the case of standard solar models where this transition is modeled with a discontinuity of the second derivative of the temperature. Or in a simple analysis of the overshoot region, the transition from adiabatic stratification, extended due to the penetration of the convective motions, to radiative energy transport can be regarded as discontinuous (see Section 2.2). This implies that instead of having a discontinuous second derivative of the sound speed due to the transition from convective unstable to stable regions we have a discontinuity in the first derivative resulting from the forced adiabatic stratification into the stable region. Our next step is to define a smooth model

in order to treat these features as localized perturbations to this smooth structure. The condition for smoothness has then to be that the scale height of the second derivative of the sound speed is much larger than the local wavelength of the modes.

The actual star differs from the smooth model by having small localized deviations $\delta\rho$ and δc^2 in its structure, resulting from smoothing the discontinuity at the base of the convective envelope. We now apply the variational principle to obtain the change in frequency, due to these small perturbations $\delta\rho$ and δc^2, from the value ω_0 for the smooth reference model. The expression is (see Eq. (1.3.42) and the discussion following it)

$$\delta\omega^2 = \omega^2 - \omega_0^2 = \frac{\delta I}{I_1} \, , \tag{2.3.4}$$

where

$$\delta I = \frac{\delta I_2 - \omega_0^2 \delta I_1}{I_1} = \int_0^R \left\{ -\frac{2}{r} \, L^2 \xi_h \, \frac{\mathrm{d}(r^2\xi_r)}{\mathrm{d}r} + \frac{1}{r^2} \, \left[\frac{\mathrm{d}(r^2\xi_r)}{\mathrm{d}r} \right]^2 + L^4 \xi_r^2 \right\} \delta(\rho c^2) \, \mathrm{d}r -$$

$$- \int_0^R \left\{ -\frac{g}{r^2} \, \frac{\mathrm{d}(r^4\xi_r^2)}{\mathrm{d}r} + 2rg \, \xi_r L^2 \xi_h - \omega_0^2 r^2 (\xi_r^2 + L^2 \xi_h^2) + r^2 g \xi_r^2 \, \frac{\mathrm{d}}{\mathrm{d}r} \right\} \delta\rho \, \mathrm{d}r \, . \tag{2.3.5}$$

All quantities correspond now to the equilibrium structure of the smooth star.

This is the expression that estimates the contribution to the eigenvalues ω coming from the base of the convection zone as described by $\delta(\rho c^2)$ and $\delta\rho$.

2.3.2 Expression for the changes in the frequency

The next step is to reduce the expression for the changes in the frequencies as given in Eq. (2.3.5) to a simpler form. We do so by integrating by parts, and neglecting the perturbation to the pressure, in order to reduce the equation to an integral of a sum of terms, each of which is an n^{th} derivative of the product of a smooth function and the perturbation in sound speed multiplied by an integral of the squared eigenfunction. If the $(n-1)^{th}$ derivative of δc^2 is discontinuous, the n^{th} derivative in the integral so obtained may be represented by a δ-function centred at the acoustic position of the discontinuity. Hence the integral is replaced by the value of the integrand at this position. If overshoot is present then n=2, while in its absence n=3. Substituting the asymptotic expression for the eigenfunction, it leads to an expression for the periodic component associated with δI that describes the changes in the frequencies due to the characteristics of the base of the convection zone.

First, the horizontal component of the displacement vector is eliminated by substituting (cf. Eq. (1.3.3) and Eqs. (1.3.4))

$$\xi_h = \frac{1}{\omega^2 - S_l^2} \, \left[\frac{g}{r} \, \xi_r - \frac{c^2}{r^3} \, \frac{\mathrm{d}}{\mathrm{d}r} (r^2 \xi_r) \right] \, , \tag{2.3.6}$$

in Eq. (2.3.5). Next, we replace integration over r by integration over acoustic depth τ defined by $\mathrm{d}\tau = -\mathrm{d}r/c$ and $\tau = 0$ at $r = R$; we also truncate the integration at the lower turning point r_t of the mode, since the eigenfunction is very small below this point.

The result is an expression of the form

$$\delta I = \int_0^{\tau_t} \left[f_1(r)\ E_{\mathrm{r}}^2 + f_2(r)\ \frac{\mathrm{d}E_{\mathrm{r}}^2}{\mathrm{d}\tau} + f_3(r)\ \left(\frac{\mathrm{d}E_{\mathrm{r}}}{\mathrm{d}\tau}\right)^2 \right] \mathrm{d}\tau\ ; \tag{2.3.7}$$

where the f_i's are functions of the background state and the perturbations $\delta\rho$ and $\delta(\rho c^2)$. Also, E_{r} is a scaled eigenfunction given by

$$E_{\mathrm{r}} = r\sqrt{\rho c}\ \ \xi_r\ . \tag{2.3.8}$$

The scaling factor is introduced in order to remove from ξ_r the dominant radial dependence of the amplitude within the propagating region (see Section 1.3.3). We now use

$$\left(\frac{\mathrm{d}E_{\mathrm{r}}}{\mathrm{d}\tau}\right)^2 = \frac{1}{2}\ \frac{\mathrm{d}^2E_{\mathrm{r}}^2}{\mathrm{d}\tau^2} - E_{\mathrm{r}}\ \frac{\mathrm{d}^2E_{\mathrm{r}}}{\mathrm{d}\tau^2}\ , \tag{2.3.9}$$

and substitute the asymptotic expression for the eigenfunction, valid in the interior of the resonance cavity, as given in Eq. (1.3.19),

$$\frac{\mathrm{d}^2E_{\mathrm{r}}}{\mathrm{d}\tau^2} \simeq -\omega^2(1-\Delta)\ E_{\mathrm{r}}\ , \tag{2.3.10}$$

with

$$\Delta \equiv \frac{S_l^2}{\omega^2} = \frac{l(l+1)c^2}{\omega^2 r^2}\ , \tag{2.3.11}$$

to obtain

$$\delta I = \int_0^{\tau_t} \left(\delta B_1\ E_{\mathrm{r}}^2 + \delta B_2\ \frac{\mathrm{d}E_{\mathrm{r}}^2}{\mathrm{d}\tau} + \delta B_3\ \frac{\mathrm{d}^2E_{\mathrm{r}}^2}{\mathrm{d}\tau^2}\right)\mathrm{d}\tau + \int_0^{\tau_t} \frac{\mathrm{d}\delta B_0}{\mathrm{d}\tau}\ E_{\mathrm{r}}^2\mathrm{d}\tau\ . \tag{2.3.12}$$

Here

$$\delta B_0 = \ \frac{g}{c}\ \frac{\delta c^2}{c^2} - \frac{g}{c}\ \frac{\delta(\Gamma_1 P)}{\Gamma_1 P} \tag{2.3.13}$$

$$\begin{aligned}
\delta B_1 = \ & \left\{ -\frac{\omega^2}{1-\Delta} + \frac{g}{c}\ \frac{\mathrm{d}}{\mathrm{d}\tau}\log\left(\frac{g}{\rho c}\right) - \frac{1-2\Delta}{(1-\Delta)^2}\ \frac{g}{c}\ \frac{\mathrm{d}}{\mathrm{d}\tau}\log\left(\frac{r^2}{\rho c}\right) - \right. \\
& \left. - \frac{1}{4}\ \frac{\Delta}{(1-\Delta)^2}\left[\frac{\mathrm{d}}{\mathrm{d}\tau}\log\left(\frac{r^2}{\rho c}\right)\right]^2 + \frac{\Delta(1-2\Delta)}{(1-\Delta)^2}\ \frac{g^2}{c^2}\right\}\ \frac{\delta c^2}{c^2} + \\
& + \left\{ \ \frac{g}{c}\ \frac{\mathrm{d}}{\mathrm{d}\tau}\log\left(\frac{g}{\rho c}\right) - \frac{1}{1-\Delta}\ \frac{g}{c}\ \frac{\mathrm{d}}{\mathrm{d}\tau}\log\left(\frac{r^2}{\rho c}\right) - \right. \\
& \left. - \frac{1}{4}\ \frac{1}{1-\Delta}\ \left[\frac{\mathrm{d}}{\mathrm{d}\tau}\log\left(\frac{r^2}{\rho c}\right)\right]^2 + \frac{\Delta}{1-\Delta}\ \frac{g^2}{c^2}\right\}\ \frac{\delta(\Gamma_1 P)}{\Gamma_1 P}
\end{aligned} \tag{2.3.14}$$

$$\delta B_2 = -\left\{\frac{1-2\Delta}{(1-\Delta)^2}\,\frac{g}{c}+\frac{1}{2}\,\frac{\Delta}{(1-\Delta)^2}\,\frac{\mathrm{d}}{\mathrm{d}\tau}\log\left(\frac{r^2}{\rho c}\right)\right\}\frac{\delta c^2}{c^2}-$$

$$-\left\{\frac{1}{1-\Delta}\,\frac{g}{c}-\frac{1}{2}\,\frac{1}{1-\Delta}\,\frac{\mathrm{d}}{\mathrm{d}\tau}\log\left(\frac{r^2}{\rho c}\right)\right\}\frac{\delta(\Gamma_1 P)}{\Gamma_1 P} \tag{2.3.15}$$

$$\delta B_3 = -\frac{1}{2}\,\frac{\Delta}{(1-\Delta)^2}\,\frac{\delta c^2}{c^2}+\frac{1}{2}\,\frac{1}{(1-\Delta)^2}\,\frac{\delta(\Gamma_1 P)}{\Gamma_1 P}\,. \tag{2.3.16}$$

We have used

$$\frac{\delta(\Gamma_1 P)}{\Gamma_1 P}=\frac{\delta(\rho c^2)}{\rho c^2}\qquad\text{and}\qquad\frac{\delta\rho}{\rho}=\frac{\delta(\Gamma_1 P)}{\Gamma_1 P}-\frac{\delta c^2}{c^2}\,. \tag{2.3.17}$$

Now an interval $[\tau_\mathrm{a},\tau_\mathrm{b}]$ is considered, with $0<\tau_\mathrm{a}<\tau_\mathrm{b}<\tau_\mathrm{t}$ and $\tau_\mathrm{b}-\tau_\mathrm{a}\ll\tau_\mathrm{t}$, such that $\delta c^2/c^2$, $\delta(\Gamma_1 P)/\Gamma_1 P$ and all their derivatives are equal to zero outside it. Integrating Eq. (2.3.12) by parts we obtain

$$\delta I=\int_{\tau_\mathrm{a}}^{\tau_\mathrm{b}}\left[\frac{\mathrm{d}^3\delta B_1}{\mathrm{d}\tau^3}\,\overline{\overline{\overline{E_\mathrm{r}^2}}}+\frac{\mathrm{d}^3}{\mathrm{d}\tau^3}(\delta B_2+\delta B_0)\,\overline{\overline{E_\mathrm{r}^2}}+\frac{\mathrm{d}^3\delta B_3}{\mathrm{d}\tau^3}\,\overline{E_\mathrm{r}^2}\right]\mathrm{d}\tau\,, \tag{2.3.18}$$

with

$$\overline{\overline{\overline{E_\mathrm{r}^2}}}(\tau)=\int^{\tau}\overline{\overline{E_\mathrm{r}^2}}(\tau_1)\,\mathrm{d}\tau_1=\int^{\tau}\int^{\tau_1}\overline{E_\mathrm{r}^2}(\tau_2)\,\mathrm{d}\tau_2\mathrm{d}\tau_1=\int^{\tau}\int^{\tau_1}\int^{\tau_2}E_\mathrm{r}^2(\tau_3)\,\mathrm{d}\tau_3\mathrm{d}\tau_2\mathrm{d}\tau_1\,. \tag{2.3.19}$$

We have asymptotically that in this region (see Eqs. (1.3.17) and (1.3.18))

$$E_\mathrm{r}(\tau)\sim E_0\,\cos\left[\omega\int_0^{\tau}(1-\Delta)^{1/2}\mathrm{d}\tau+\phi\right]=E_0\,\cos(\Lambda/2)\,, \tag{2.3.20}$$

where E_0 is the amplitude of the normalized eigenfunction, and we use $\Lambda(\tau)$ to represent twice the argument. It then follows, for example, that

$$\overline{\overline{\overline{E_\mathrm{r}^2}}}\sim\frac{1}{2}\,E_0^2\left[\frac{\tau^2+2e_1\tau+2e_2}{2}-\frac{\cos(\Lambda)}{4\omega^2(1-\Delta)}\right]\,, \tag{2.3.21}$$

where the e_i's are constants of integration. We are neglecting again, as in using the asymptotic result for example, derivatives of the equilibrium quantities in Δ.

We now have a relation between the local characteristics described by the derivatives of the δB_i functions and the local behaviour of the oscillation given approximately by the asymptotic eigenfunction E_r. Substituting the normalized eigenfunction and its integrals and keeping only the terms with a trigonometric function we find for the *periodic component* of $\delta\omega$,

$$\delta\omega_p\sim\frac{1}{4\omega^2\tau_\mathrm{t}}\int_{\tau_\mathrm{a}}^{\tau_\mathrm{b}}\Big[-\frac{\sin(\Lambda)}{4\omega^2(1-\Delta)^{3/2}}\,\frac{\mathrm{d}^3\delta B_1}{\mathrm{d}\tau^3}-\frac{\cos(\Lambda)}{2\omega(1-\Delta)}\,\frac{\mathrm{d}^3}{\mathrm{d}\tau^3}(\delta B_0+\delta B_2)$$

$$+\frac{\sin(\Lambda)}{(1-\Delta)^{1/2}}\,\frac{\mathrm{d}^3\delta B_3}{\mathrm{d}\tau^3}\Big]\quad\mathrm{d}\tau\,. \tag{2.3.22}$$

Note that we have used $I_1 \sim \tau_{\rm t} E_0^2/2$, obtained from Eqs. (2.3.2) and (2.3.20) after neglecting terms with Δ in the integral.

The next step is to substitute the functions δB_i. First we note that

$$\begin{aligned}
\frac{\delta B_1}{\omega^2} &\sim \left[-\frac{1}{1-\Delta} + \frac{g_0}{\omega^2 c_0}\,\frac{\mathrm{d}}{\mathrm{d}\tau}\log\left(\frac{g_0}{r_0^2}\right) + \mathcal{O}(\omega^{-4})\right]\ \frac{\delta c^2}{c_0^2} \\
\frac{\delta B_0 + \delta B_2}{\omega} &\sim \mathcal{O}(\omega^{-3})\quad \frac{\delta c^2}{c_0^2} \\
\delta B_3 &\sim -\frac{1}{2}\,\frac{\Delta}{(1-\Delta)^2}\quad \frac{\delta c^2}{c_0^2}\ ,
\end{aligned} \tag{2.3.23}$$

and recall that we are considering high frequency modes, i.e. p-modes. In this limit terms with higher powers of frequency dominate. Note also that it has been used the fact that $\Delta \sim \mathcal{O}(\omega^{-2})$.

In writing the above expressions we have neglected already the contribution from $\delta(\Gamma_1 P)$ since Γ_1 will be assumed constant and P is, as given by the hydrostatic equation, continuous one derivative further than the sound speed. However, we caution here that this simplification is not advisable if we go up to third derivatives of the sound speed. In such a case we have second derivatives of the pressure, which are also discontinuous in case of the presence of overshoot. We will discuss later the possible contributions of these extra terms in the analysis, but ignore them in the following.

The next step is to neglect terms of order $\mathcal{O}(\omega^{-3})$ or smaller in the integrand in Eq. (2.3.22), leaving

$$\begin{aligned}
\delta\omega_p \sim -\int_{\tau_{\rm a}}^{\tau_{\rm b}} &\left\{\frac{\mathrm{d}^3}{\mathrm{d}\tau^3}\left[\left(-\frac{1}{1-\Delta} + \Delta_c\right)\ \frac{\delta c^2}{c_0^2}\right] + 2(1-\Delta)\,\frac{\mathrm{d}^3}{\mathrm{d}\tau^3}\left[\frac{\Delta}{(1-\Delta)^2}\,\frac{\delta c^2}{c_0^2}\right]\right\} \\
&\times \quad \frac{\sin(\Lambda)}{16\omega^2\tau_{\rm t}(1-\Delta)^{3/2}}\ \mathrm{d}\tau\ .
\end{aligned} \tag{2.3.24}$$

Here

$$\Delta_c = \frac{g_0}{\omega^2 c_0}\,\frac{\mathrm{d}}{\mathrm{d}\tau}\log\left(\frac{g_0}{r_0^2}\right)\ . \tag{2.3.25}$$

Now, we neglect second derivatives of the equilibrium quantities (for the smooth model) which are negligible compared with lower derivatives (also done for the asymptotic analysis). Then, we take only the terms that are proportional to the second and third derivatives of the sound-speed difference, since at most the first derivative of the sound speed is discontinuous, the only terms that may contribute with a δ function are the second and third derivatives of the sound speed.

After using these considerations we are left with the following expression for the periodic signal

$$\delta\omega_p \sim \frac{1}{16\omega^2\tau_{\rm t}}\int_{\tau_{\rm a}}^{\tau_{\rm b}}\left\{\left[\frac{1-2\Delta}{1-\Delta} - \Delta_c\right]\frac{\mathrm{d}^3}{\mathrm{d}\tau^3}\left(\frac{\delta c^2}{c_0^2}\right)\right.$$

$$- \left[\frac{6\Delta(1+2\Delta)}{(1-\Delta)^2} \frac{\mathrm{d}}{\mathrm{d}\tau} \log\left(\frac{c_0}{r_0}\right) \right] \frac{\mathrm{d}^2}{\mathrm{d}\tau^2} \left(\frac{\delta c^2}{c_0^2}\right) \Bigg\} \frac{\sin(\Lambda)}{(1-\Delta)^{3/2}} \, \mathrm{d}\tau \,, \quad (2.3.26)$$

where, we recall, the interval of integration $[\tau_\mathrm{a},\tau_\mathrm{b}]$ is defined such that δc^2 and its derivatives are zero outside it. The effect of the small quantity Δ, which depends on the mode degree l, is very small for most of the modes considered here. However, we shall include the dominant terms in Δ, in our analysis, since its effect at low frequencies may be significant. The argument of the sine function is (see Eq. (2.3.20))

$$\Lambda(\tau) = 2\omega \int_0^\tau (1-\Delta)^{1/2} \mathrm{d}\tau' + 2\phi \,, \quad (2.3.27)$$

where ϕ is the phase.

2.4 Sound speed and the temperature gradient

Simple descriptions of overshoot (Section 2.2) and modelling of convection are typically expressed in terms of the behaviour of the temperature gradient $\nabla \equiv \mathrm{d}\log T/\mathrm{d}\log P$, where T is the temperature and P the pressure. However, the effects of sharp features on p-mode frequencies are most naturally expressed in terms of second and third derivatives of the squared sound speed

$$c^2 = \frac{\Gamma_1 P}{\rho} \,, \quad (2.4.1)$$

where ρ is density and $\Gamma_1 = (\partial \ln P/\partial \ln \rho)_S$ is the adiabatic exponent, the derivative being at constant entropy S. So, here we analyse these derivatives in terms of derivatives of ∇, using as independent variable the acoustic depth τ.

From the definition (2.4.1) of c^2 we obtain the first derivative of the squared sound speed, with respect to acoustic depth τ, as

$$\frac{\mathrm{d}\log c^2}{\mathrm{d}\tau} = \frac{\mathrm{d}\log \Gamma_1}{\mathrm{d}\tau} + \frac{\mathrm{d}\log P}{\mathrm{d}\tau} - \frac{\mathrm{d}\log \rho}{\mathrm{d}\tau} \,. \quad (2.4.2)$$

The derivative of the density can be eliminated by means of the thermodynamic relation (A.3.5) (e.g. Cox & Giuli 1968), assuming constant abundances:

$$\frac{\mathrm{d}\log \rho}{\mathrm{d}\tau} = \frac{1-\chi_T \nabla}{\chi_\rho} \frac{\mathrm{d}\log P}{\mathrm{d}\tau} \,, \quad (2.4.3)$$

where

$$\begin{aligned} \chi_T &= \left(\frac{\partial \log P}{\partial \log T}\right)_\rho = \frac{\gamma-1}{\gamma} \frac{1}{\nabla_\mathrm{a}} \\ \chi_\rho &= \left(\frac{\partial \log P}{\partial \log \rho}\right)_T = \frac{\Gamma_1}{\gamma} \\ \nabla &= \frac{\mathrm{d}\log T}{\mathrm{d}\log P} \,. \end{aligned} \quad (2.4.4)$$

Here γ is the ratio of the specific heats (eg. (A.3.10)). Note however that if we do not consider constant abundances, as in the case of diffusion for example, such a variation can be included by maintaining the term in $\nabla_\mu \equiv \partial \log \mu / \partial \log P$ in Eq. (2.4.3).

We now have for the density that

$$\frac{\mathrm{d}\log\rho}{\mathrm{d}\tau} = \frac{\gamma}{\Gamma_1}\left(1 - \frac{\gamma-1}{\gamma}\frac{\nabla}{\nabla_\mathrm{a}}\right)\frac{\mathrm{d}\log P}{\mathrm{d}\tau}\,, \tag{2.4.5}$$

and so,

$$\frac{\mathrm{d}\log c^2}{\mathrm{d}\tau} = \frac{\mathrm{d}\log\Gamma_1}{\mathrm{d}\tau} + \frac{\mathrm{d}\log P}{\mathrm{d}\tau}\left[1 - \frac{\gamma}{\Gamma_1}\left(1 - \frac{\gamma-1}{\gamma}\frac{\nabla}{\nabla_\mathrm{a}}\right)\right]\,. \tag{2.4.6}$$

In terms of acoustic depth the hydrostatic equation is

$$\frac{\mathrm{d}\log P}{\mathrm{d}\tau} = \frac{g\Gamma_1}{c}\,. \tag{2.4.7}$$

After substitution, we are left with

$$\frac{\mathrm{d}\log c^2}{\mathrm{d}\tau} = \frac{\mathrm{d}\log\Gamma_1}{\mathrm{d}\tau} + \frac{g}{c}\left[(\Gamma_1-\gamma) + (\gamma-1)\frac{\nabla}{\nabla_\mathrm{a}}\right]\,. \tag{2.4.8}$$

Given the assumption of constant abundances this equation is general. However, since we want to apply it to the region around the base of the convection zone, we shall further assume that

$$\frac{\mathrm{d}\Gamma_1}{\mathrm{d}\tau} = 0\,, \qquad \frac{\mathrm{d}\gamma}{\mathrm{d}\tau} = 0 \qquad \text{and} \qquad \frac{\mathrm{d}\nabla_\mathrm{a}}{\mathrm{d}\tau} = 0\,. \tag{2.4.9}$$

These are a very good approximation to the actual physics of the region since there the gas is almost fully ionized.

We may now obtain the final expressions for the sound speed and its derivatives. The first derivative becomes simply

$$\frac{\mathrm{d}c^2}{\mathrm{d}\tau} = gc\left[(\Gamma_1-1) + (\gamma-1)\frac{\nabla-\nabla_\mathrm{a}}{\nabla_\mathrm{a}}\right]\,, \tag{2.4.10}$$

While the second is now obtained by differentiating this relation, giving (G is the gravitational constant)

$$\begin{aligned}\frac{\mathrm{d}^2c^2}{\mathrm{d}\tau^2} = &-c^2\left(4\pi G\rho - \frac{2g}{r}\right)\left[(\Gamma_1-1) + (\gamma-1)\frac{\nabla-\nabla_\mathrm{a}}{\nabla_\mathrm{a}}\right] \\ &+ \frac{g^2}{2}\left[(\Gamma_1-1) + (\gamma-1)\frac{\nabla-\nabla_\mathrm{a}}{\nabla_\mathrm{a}}\right]^2 + \frac{gc(\gamma-1)}{\nabla_\mathrm{a}}\frac{\mathrm{d}}{\mathrm{d}\tau}(\nabla-\nabla_\mathrm{a})\,,\end{aligned} \tag{2.4.11}$$

where we used

$$\frac{\mathrm{d}g}{\mathrm{d}\tau} = -c\left(4\pi G\rho - \frac{2g}{r}\right)\,. \tag{2.4.12}$$

To calculate the third derivative we differentiate Eq. (2.4.11) once more, and use

$$\frac{\mathrm{d}\log\rho}{\mathrm{d}\tau} = \frac{g}{c}\left[1 - (\gamma-1)\frac{\nabla-\nabla_\mathrm{a}}{\nabla_\mathrm{a}}\right]\,, \tag{2.4.13}$$

to get

$$\begin{aligned}\frac{\mathrm{d}^3c^2}{\mathrm{d}\tau^3} = &- gc\left[4\pi G\rho\left(\Gamma_1+\frac{2c^2}{rg}\right)-\frac{6c^2}{r^2}\right]\left[(\Gamma_1-1)+(\gamma-1)\,\frac{\nabla-\nabla_\mathrm{a}}{\nabla_\mathrm{a}}\right]\\ &- 4gc\left(\pi G\rho-\frac{g}{r}\right)\left[(\Gamma_1-1)+(\gamma-1)\,\frac{\nabla-\nabla_\mathrm{a}}{\nabla_\mathrm{a}}\right]^2\\ &+\frac{2gc^2(\gamma-1)}{\nabla_\mathrm{a}}\left\{\frac{2}{r}-\frac{4\pi G\rho}{g}+\frac{3g}{4c^2}\left[(\Gamma_1-1)+(\gamma-1)\,\frac{\nabla-\nabla_\mathrm{a}}{\nabla_\mathrm{a}}\right]\right\}\frac{\mathrm{d}}{\mathrm{d}\tau}(\nabla-\nabla_\mathrm{a})\\ &+\frac{gc(\gamma-1)}{\nabla_\mathrm{a}}\,\frac{\mathrm{d}^2}{\mathrm{d}\tau^2}(\nabla-\nabla_\mathrm{a})\,. \end{aligned} \tag{2.4.14}$$

These can be expressed simply as

$$\frac{\mathrm{d}c^2}{\mathrm{d}\tau} = d_{10}+d_{11}\,\frac{\nabla-\nabla_\mathrm{a}}{\nabla_\mathrm{a}}\,, \tag{2.4.15}$$

$$\frac{\mathrm{d}^2c^2}{\mathrm{d}\tau^2} = d_{20}+d_{21}\,\left(\frac{\nabla-\nabla_\mathrm{a}}{\nabla_\mathrm{a}}\right)+d_{22}\,\left(\frac{\nabla-\nabla_\mathrm{a}}{\nabla_\mathrm{a}}\right)^2+d_{23}\,\frac{\mathrm{d}}{\mathrm{d}\tau}\left(\frac{\nabla-\nabla_\mathrm{a}}{\nabla_\mathrm{a}}\right)\,, \tag{2.4.16}$$

and

$$\begin{aligned}\frac{\mathrm{d}^3c^2}{\mathrm{d}\tau^3} = \;& d_{30}+d_{31}\,\left(\frac{\nabla-\nabla_\mathrm{a}}{\nabla_\mathrm{a}}\right)+d_{32}\,\left(\frac{\nabla-\nabla_\mathrm{a}}{\nabla_\mathrm{a}}\right)^2\\ &+d_{33}\,\frac{\mathrm{d}}{\mathrm{d}\tau}\left(\frac{\nabla-\nabla_\mathrm{a}}{\nabla_\mathrm{a}}\right)+d_{34}\,\frac{\mathrm{d}}{\mathrm{d}\tau}\left(\frac{\nabla-\nabla_\mathrm{a}}{\nabla_\mathrm{a}}\right)^2+d_{35}\,\frac{\mathrm{d}^2}{\mathrm{d}\tau^2}\left(\frac{\nabla-\nabla_\mathrm{a}}{\nabla_\mathrm{a}}\right)\,. \end{aligned} \tag{2.4.17}$$

The coefficients d_{ij} are continuous functions of the local stratification as given in (2.4.10), (2.4.11) and (2.4.14).

In determining the behaviour of the gradient ∇ with acoustic depth at the base of the convection zone, for the time being we shall assume that the transition from adiabatic stratification to radiative stratification occurs over a length scale much shorter than the wavelength of the modes. Furthermore, it is assumed that a possible overshoot layer is adiabatically stratified, with a jump to radiative stratification at its boundary. Effects of relaxing these assumptions are discussed in the next Chapter.

We start by writing

$$\nabla-\nabla_\mathrm{a} = (\nabla_\mathrm{r}-\nabla_\mathrm{a})\,f(\tau)\,, \tag{2.4.18}$$

where ∇_r is the radiative gradient. Also, we let τ_c be the acoustical depth of the transition from instability to stability according to the Schwarzschild condition (i.e., $\nabla=\nabla_\mathrm{a}=\nabla_\mathrm{r}$ at $\tau=\tau_\mathrm{c}$), whereas the depth at the edge of the overshoot region is denoted τ_d. If we restrict ourselves to the region around the base of the convection zone, the behaviour of the function f (see for example Fig. 2.1), is then given by

$$f(\tau)\simeq\begin{cases} 0^+ & ;\ \tau<\tau_\mathrm{c} \quad \text{Convection zone}\\ 0 & ;\ \tau=\tau_\mathrm{c} \quad \text{Schwarzschild point}\\ 0^+ & ;\ \tau_\mathrm{c}<\tau<\tau_\mathrm{d} \quad \text{Overshooting}\\ 1 & ;\ \tau\geq\tau_\mathrm{d} \quad \text{Radiative interior}\,. \end{cases} \tag{2.4.19}$$

The value of 0^+ in both the convection zone and the overshoot region reflects the fact that the value of ∇ near the base but inside the convection zone is slightly superadiabatic, while in the overshoot region ($\tau_c<\tau<\tau_d$) the stratification is slightly subadiabatic. If there is no overshoot layer, $\tau_d=\tau_c$.

Neglecting the small departures from adiabatic stratification on either side, to a very good approximation we may write

$$f(\tau) = H(\tau-\tau_d) \equiv \begin{cases} 0 & ;\ \tau<\tau_d \\ 1 & ;\ \tau\geq\tau_d \end{cases}, \tag{2.4.20}$$

where H is the Heaviside (or step) function. Substitution of this expression in Eq. (2.4.18) gives

$$\nabla-\nabla_a = (\nabla_r-\nabla_a)\ H(\tau-\tau_d)\ ; \tag{2.4.21}$$

and differentiating it we obtain

$$\frac{d}{d\tau}(\nabla-\nabla_a) = (\nabla_r-\nabla_a)\ \delta(\tau-\tau_d) + \frac{d\nabla_r}{d\tau}\ H(\tau-\tau_d)\ . \tag{2.4.22}$$

Further,

$$\frac{d^2}{d\tau^2}(\nabla-\nabla_a) = \ (\nabla_r-\nabla_a)\ \delta'(\tau-\tau_d) + 2\ \frac{d\nabla_r}{d\tau}\ \delta(\tau-\tau_d) + \frac{d^2\nabla_r}{d\tau^2}\ H(\tau-\tau_d)\ , \tag{2.4.23}$$

where δ' is the derivative of the δ function. Note that, in the case of no overshooting, $\nabla_r=\nabla_a$ at $\tau=\tau_c=\tau_d$; hence the terms in $\nabla_r-\nabla_a$ vanish.

We can now write the derivatives of the sound speed as combinations of two parts: one that contains the continuous terms and terms with step functions, denoted by the subscript '$_s$'; and a second which contains δ functions or derivatives thereof. As shown below, the contribution from the latter dominates the oscillatory signal. From expressions (2.4.15) and (2.4.21) we obtain

$$\frac{dc^2}{d\tau} = \left[\frac{dc^2}{d\tau}\right]_s\ ; \tag{2.4.24}$$

furthermore, from Eqs. (3.4.16), (2.4.21) and (2.4.22), and using the explicit expression for d_{23}, we have

$$\frac{d^2c^2}{d\tau^2} = \left[\frac{d^2c^2}{d\tau^2}\right]_s + gc(\gamma-1)\ \frac{\nabla_r-\nabla_a}{\nabla_a}\ \delta(\tau-\tau_d)\ . \tag{2.4.25}$$

In the case with no overshoot, the term in the δ function is zero. Here the oscillatory signal in the frequencies arises from the third derivative of sound speed. This is obtained from Eqs. (3.4.17) and (2.4.21) – (2.4.23) as

$$\begin{aligned}\frac{d^3c^2}{d\tau^3} = \left[\frac{d^3c^2}{d\tau^3}\right]_s &+ \frac{2gc(\gamma-1)}{\nabla_a}\ \delta(\tau-\tau_d)\ \left[\frac{d\nabla_r}{d\tau} - (\nabla_r-\nabla_a)\ \frac{d}{d\tau}\log\left(\frac{c^3}{g^2}\right)\right] \\ &+ \frac{gc(\gamma-1)}{\nabla_a}\ (\nabla_r-\nabla_a)\ \delta'(\tau-\tau_d)\ .\end{aligned} \tag{2.4.26}$$

If there is no overshoot we have only the contribution from $d\nabla_r/d\tau$.

2.5 Amplitude of the signal

We shall now determine an expression for the amplitude of the signal in the p-mode frequencies as a function of the thermodynamics in the reference model by substituting the sound speed derivatives in the expression for the periodic component of the signal obtained from the variational principle.

We recall that the sharp feature at the base of the convection zone is represented by the departure δc^2 in the squared sound speed from an assumed 'smooth' model, indicated by the subscript '$_0$'. This model has, by definition, no discontinuous derivatives (at least up to the third) of any thermodynamic quantity (in particular the sound speed), and hence has no δ function in any derivative of c_0^2 (in the equations below).

Starting from expression (2.3.26) for the periodic component of the frequency differences, the next step is to keep track explicitly only of those terms in the second and third derivatives of the sound-speed difference that involve a δ function or its derivative. Noting that from the third derivative of the sound-speed difference there are two such terms (from the second and third derivatives of c^2) and from the second derivative there is one, it can be shown that, using Eqs. (3.4.24)- (2.4.26),

$$\begin{aligned}
\frac{\mathrm{d}^2}{\mathrm{d}\tau^2}\left(\frac{\delta c^2}{c_0^2}\right) &= \left[\frac{\mathrm{d}^2}{\mathrm{d}\tau^2}\left(\frac{\delta c^2}{c_0^2}\right)\right]_{\mathrm{s}} + \frac{g_0(\gamma_0-1)}{c_0\ \nabla_{\mathrm{a}0}}\quad \delta(\tau-\tau_{\mathrm{d}})\ \ (\nabla_{\mathrm{r}0}-\nabla_{\mathrm{a}0})\,, \\
\frac{\mathrm{d}^3}{\mathrm{d}\tau^3}\left(\frac{\delta c^2}{c_0^2}\right) &= \left[\frac{\mathrm{d}^3}{\mathrm{d}\tau^3}\left(\frac{\delta c^2}{c_0^2}\right)\right]_{\mathrm{s}} + \frac{g_0(\gamma_0-1)}{c_0\ \nabla_{\mathrm{a}0}}\quad \delta'(\tau-\tau_{\mathrm{d}})\ \ (\nabla_{\mathrm{r}0}-\nabla_{\mathrm{a}0}) \\
&\quad + \frac{g_0(\gamma_0-1)}{c_0\ \nabla_{\mathrm{a}0}}\ \delta(\tau-\tau_{\mathrm{d}}) \times \left[2\frac{\mathrm{d}\nabla_{\mathrm{r}0}}{\mathrm{d}\tau} - (\nabla_{\mathrm{r}0}-\nabla_{\mathrm{a}0})\ \ \frac{\mathrm{d}}{\mathrm{d}\tau}\log\left(\frac{c_0^3}{g_0^2}\right)\right]\,.
\end{aligned} \tag{2.5.1}$$

Substituting in Eq. (2.3.26), the contributions from the δ functions and their derivatives to the integral give

$$\begin{aligned}
\delta\omega_p \sim\ & \frac{g_0(\gamma_0-1)}{16\omega^2\tau_{\mathrm{t}}c_0\nabla_{\mathrm{a}0}}\ \frac{\sin(\Lambda_{\mathrm{d}})}{(1-\Delta)^{3/2}}\left\{\frac{\mathrm{d}\nabla_{\mathrm{r}0}}{\mathrm{d}\tau}\left(\frac{1-2\Delta}{1-\Delta}-\Delta_c\right)\right. \\
& \left. -(\nabla_{\mathrm{r}0}-\nabla_{\mathrm{a}0})\left[\frac{1-2\Delta}{1-\Delta}\ \frac{\mathrm{d}}{\mathrm{d}\tau}\log\left(\frac{c_0^2}{g_0}\right) + \frac{\Delta(7-6\Delta)}{(1-\Delta)^2}\ \frac{\mathrm{d}}{\mathrm{d}\tau}\log\left(\frac{c_0}{r_0}\right)\right]\right\} \\
& - \frac{g_0(\gamma_0-1)}{8\omega\tau_{\mathrm{t}}c_0\nabla_{\mathrm{a}0}}\ \frac{\cos(\Lambda_{\mathrm{d}})}{1-\Delta}\ (\nabla_{\mathrm{r}0}-\nabla_{\mathrm{a}0})\left(\frac{1-2\Delta}{1-\Delta}-\Delta_c\right)\,,
\end{aligned} \tag{2.5.2}$$

where all quantities are now evaluated at τ_{d}. More succinctly, introducing coefficients a_1 and a_2, (and dropping the subscript "p" from $\delta\omega$)

$$\delta\omega \sim \frac{1-2\Delta}{(1-\Delta)^2}\ \left[\frac{a_1}{(1-\Delta)^{1/2}}\ \left(\frac{\tilde{\omega}}{\omega}\right)^2 \sin(\Lambda_{\mathrm{d}}) + a_2\ \left(\frac{\tilde{\omega}}{\omega}\right)\ \cos(\Lambda_{\mathrm{d}})\right]\,, \tag{2.5.3}$$

where $\tilde{\omega}$ is a reference frequency. The coefficients a_i are;

$$a_1 = \frac{g_0(\gamma_0-1)}{16\tilde{\omega}^2\tau_{\rm t}c_0\nabla_{\rm a0}}\left\{\frac{{\rm d}\nabla_{\rm r0}}{{\rm d}\tau}\left[1-\frac{\Delta_c(1-2\Delta)}{1-\Delta}\right]\right.$$
$$\left.+(\nabla_{\rm r0}-\nabla_{\rm a0})\left[(1-\Delta_c)\,\frac{2c_0}{r_0}\,h(\tau_{\rm d})-\frac{\Delta(7-6\Delta)}{(1-2\Delta)(1-\Delta)}\,\frac{\rm d}{{\rm d}\tau}\log\left(\frac{c_0}{r_0}\right)\right]\right\}, \qquad (2.5.4)$$
$$a_2 = -\frac{g_0(\gamma_0-1)}{8\tilde{\omega}\tau_{\rm t}c_0\nabla_{\rm a0}}\,(\nabla_{\rm r0}-\nabla_{\rm a0})\left[1-\frac{\Delta_c(1-2\Delta)}{1-\Delta}\right],$$

where the function $h(\tau)$ is

$$h(\tau) = \frac{1}{1-\Delta_c}\left[1-\frac{4\pi G r_0\rho_0}{2g_0}-\frac{r_0g_0}{2c_0^2}\,(\Gamma_{10}-1)-\frac{r_0g_0}{2c_0^2}\,(\gamma_0-1)\,\frac{\nabla_{\rm r0}-\nabla_{\rm a0}}{\nabla_{\rm a0}}\right]. \qquad (2.5.5)$$

To the order of the analysis we can consider the values of Δ_c and Δ to be evaluated at $\omega=\tilde{\omega}$. Then a_1 and a_2 are independent of frequency. Also, given that $\Delta\cdot\Delta_c$ and $\Delta\cdot{\rm d}\log(c_0/r_0)/{\rm d}\tau$ are of higher order in small quantities than is Δ_c, we may neglect the terms in a_1 and a_2 that depend on the degree. Therefore, both expressions are also independent of l. The signal is then simply, after redefining the phase ϕ in order to combine the trignometric functions in Eq. (2.5.3),

$$\delta\omega \sim A(\omega,\Delta)\,\cos(\Lambda_{\rm d}), \qquad (2.5.6)$$

with

$$A(\omega,\Delta) = \frac{1-2\Delta}{(1-\Delta)^2}\left[\frac{a_1^2(\tilde{\omega})}{1-\Delta}\,\left(\frac{\tilde{\omega}}{\omega}\right)^4+a_2^2(\tilde{\omega})\,\left(\frac{\tilde{\omega}}{\omega}\right)^2\right]^{1/2}. \qquad (2.5.7)$$

These are the expressions we shall consider when isolating the signal in the frequencies as discussed in the next Chapter. Before that, Eqs. (2.5.4) and (2.5.5) can be used to estimate the expected parameters of the signal for a solar model. This is discussed next.

2.5.1 Components of the amplitude

We have two terms contributing to the amplitude of the signal. One, a_1, is associated with the discontinuity of the third derivative of the sound speed and is always present whether there is overshoot or not. However, the other, a_2, is only different from zero if $\tau_{\rm d}\neq\tau_{\rm c}$, and therefore it only contributes when there is overshoot. Dropping the subscript '$_0$' from all quantities (remembering also that they are evaluated at $\tau=\tau_{\rm d}$) we have found that

$$a_1 = \frac{a_0}{\tilde{\omega}}\left[\frac{{\rm d}\nabla_{\rm r}}{{\rm d}\tau}+(\nabla_{\rm r}-\nabla_{\rm a})\,\frac{2c}{r}\,h(\tau_{\rm d})\right], \qquad (2.5.8)$$
$$a_2 = -2a_0\,\,(\nabla_{\rm r}-\nabla_{\rm a}),$$

where

$$a_0 = \frac{(\gamma-1)}{16\tilde{\omega}\tau_{\rm t}}\,\frac{g(1-\Delta_c)}{c\,\nabla_{\rm a}}. \qquad (2.5.9)$$

To facilitate the comparison between different models and expressions, we shall also consider the amplitude $A(\omega, \Delta)$ evaluated at a fiducial frequency and degree. We define

$$A_{2.5} \equiv A(\tilde{\omega}, \Delta{=}0) = \left(a_1^2 + a_2^2\right)^{1/2}$$
$$= \frac{(\gamma{-}1)}{16\tilde{\omega}\tau_{\rm t}} \; \frac{g(1{-}\Delta_c)}{c\,\nabla_{\rm a}} \left\{ 4\,(\nabla_{\rm r}{-}\nabla_{\rm a})^2 + \frac{1}{\tilde{\omega}^2}\left[\frac{{\rm d}\nabla_{\rm r}}{{\rm d}\tau} + (\nabla_{\rm r}{-}\nabla_{\rm a})\,\frac{2c}{r}\,h(\tau_{\rm d})\right]^2 \right\}^{1/2} . \quad (2.5.10)$$

Considering already the application to solar data, we take $\tilde{\omega}/2\pi{=}2500$ μHz. This expression gives the dependence of the amplitude $A_{2.5}$ on the acoustic position $\tau_{\rm d}$ of the transition, and so also the implicit dependence on the acoustic extent $\tau_{\rm d}{-}\tau_{\rm c}$ of the overshoot region.

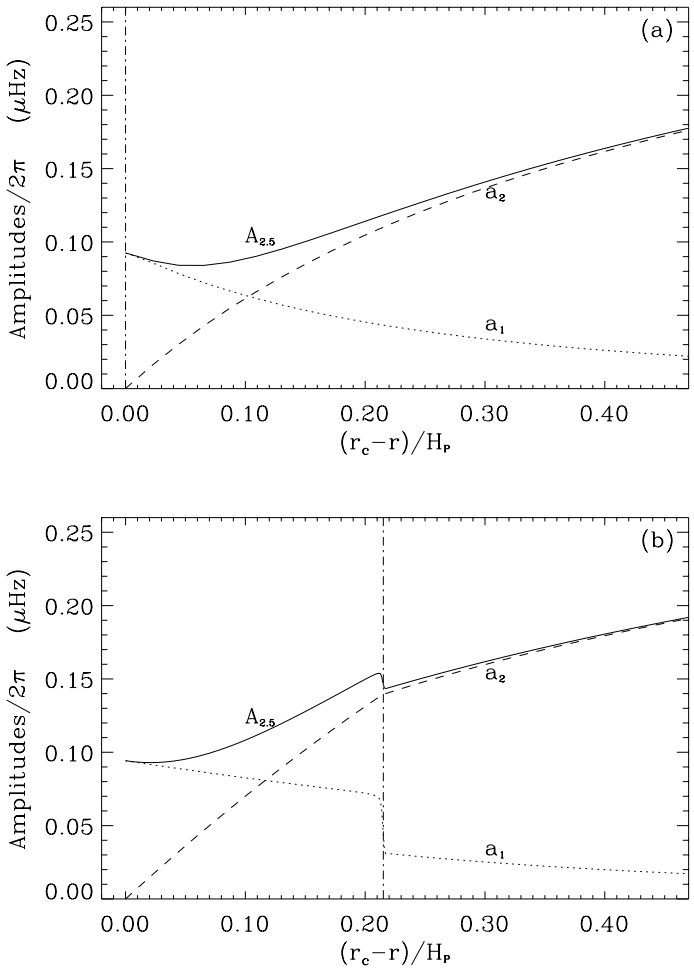

Fig. 2.2: (a) Plot of the amplitude $A_{2.5}$ (continuous line) and the components a_1 (dotted line) and a_2 (dashed line) for an evolved solar model which has no overshoot (model Z_0 - see next Chapter). (b) As (a) but for a model with overshoot (model Z_5 - see next Chapter). The extent of the overshoot layer in this model is $0.215H_P$ (H_P being the pressure scale height). The dash-dotted lines indicate the point corresponding to $r{=}r_{\rm d}$ for each model.

To study the actual variation of a_1, a_2 and $A_{2.5}$ with the extent of the overshoot region we need to know how the different functions of solar structure in Eqs. (2.5.8) - (2.5.10) vary when $\tau_{\rm d}$ and $\tau_{\rm c}$ are varied. Strictly speaking these expressions should be evaluated at the point $\tau_{\rm d}$ of the sharp feature in the model. However, to get some feel for how the amplitudes would vary with the actual extent of overshoot we have taken two models, one without and one with overshoot (see next Chapter for the details of these models), and have plotted the right-hand sides of Eqs. (2.5.8) and (2.5.10), evaluated at r, against $(r_{\rm c}-r)/H_P$, where $r_{\rm c}$ is the value of r at the edge of the unstable region and H_P is the pressure scale height. The results are shown in Fig. 2.2. As expected a_1 decreases from the value it has at the Schwarzschild boundary while a_2 increases from zero there. The cross-over between these two contributions gives rise to a shallow minimum in $A_{2.5}$ at a modest overshoot distance, as found by Roxburgh & Vorontsov (1994).

2.6 Argument of the signal

Clearly, for low-degree data the analysis of the signal is greatly simplified. In this limit we can ignore the contributions from terms on the degree of the mode leaving only the dependence on the frequency. Recalling the expression for the argument of the signal,

$$\Lambda_{\rm d} = 2\omega \int_0^{\tau_{\rm d}} (1-\Delta)^{1/2} {\rm d}\tau' + 2\phi \ , \tag{2.6.1}$$

if we neglect Δ, this becomes simply $\Lambda \sim 2\omega\tau_{\rm d} + 2\phi$. Hence we obtain a simple periodic signal with period equal to twice the acoustic depth $\tau_{\rm d}=\tau(r_{\rm d})$ of the discontinuity. This kind of periodic signature was identified in the frequencies of a solar model by Gough (1990) using *second differences* (see below), and was also investigated by Thompson (1988), Vorontsov (1988), and Gough & Sekii (1993). Such a periodic signal may in principle provide information for stars other than the Sun, where only low-degree modes are expected to be observed. It would indicate the presence of an abrupt transition in the star, and with sufficient observational precision the nature of the transition and its acoustic position may be constrained (eg Audard & Provost 1994; Audard, Provost & Christensen-Dalsgaard 1995). However for the Sun we have a large set of very accurate p-mode frequencies with degrees that can go up to the thousands. In order to use some of these we must extend our analysis further or the approximation discussed above will be inadequate to study the signal.

Another problem is that our simple asymptotic analysis breaks down near the surface where several aspects contribute to invalidate the expression we have used for the eigenfunction. This has an effect on the phase of the eigenfunction and therefore affects the phase of the signal. A simple analysis is presented in order to estimate how this can change the characteristics of the signal.

2.6.1 Low degree data

For low degree data (lets say $l<5$) the expected signal is a simple sinusoidal variation of the frequencies with frequency, given by

$$\delta\omega \sim \left[a_1^2 \left(\frac{\tilde{\omega}}{\omega}\right)^4 + a_2^2 \left(\frac{\tilde{\omega}}{\omega}\right)^2\right]^{1/2} \cos\left(2\omega\tau_{\rm d}+2\phi\right) \tag{2.6.2}$$

where we have replaced the integral in Eq. (2.6.1) by the dominant contribution (i.e., we neglect Δ). This is the expression we may hope to use to study other stars (eg. Audard & Provost 1994).

The expected amplitude for a standard model is of the order of 0.1μHz (see Fig. 2.2). Therefore any isolation of such a signal as given by the expression above will require observational errors below that value. This is a problem even for the Sun where low degree data is harder to obtain. The actual accuracy of the observations have been improving rapidly and solar data in this range of degree having observational errors below the 0.1μHz level are starting to appear. An example is the recent BISON data published in Elsworth et al. (1994). Kosovichev (1993) also proposes an alternative method to determine the base of the convection zone using low degree data. In his work the IPHIR data (Toutain & Fröhlich 1992) has been used to determine this position. Both sets of data could be used here, however they still have significantly higher observational errors than moderate degree data, and therefore would not add much to the determinations of the characteristics for the signal. See Section 4.3.2 in the next Chapter for a discussion on the selection of the mode set from currently available data for use in the analysis presented here.

2.6.2 Use of moderate degree data

Because current low-degree solar data still have a noise level significantly higher than moderate-degree data there is a great advantage in using the latter in order to be able to have a better measurement of the overshoot properties, although, evidently, restricted to modes with their lower turning point below the base of the solar convective envelope. With existing observations, modes in the range $5\leq l\leq 20$ are suitable. However, if such data are included, the analysis based on a simple periodic signal, as given in Eq. (2.6.2), proves to be inadequate.

The coherent behaviour of low-degree data is destroyed (see Fig. 2.3a) due to the effect of the l dependence. This has two possible sources. One arises because the amplitude $A(\omega,l)$ of the signal is a function of both degree and frequency. However, this effect is at most a second order term in S_l/ω; hence, for modes with small S_l/ω it is almost negligible. This l-dependence can be taken into account by including in the expression for

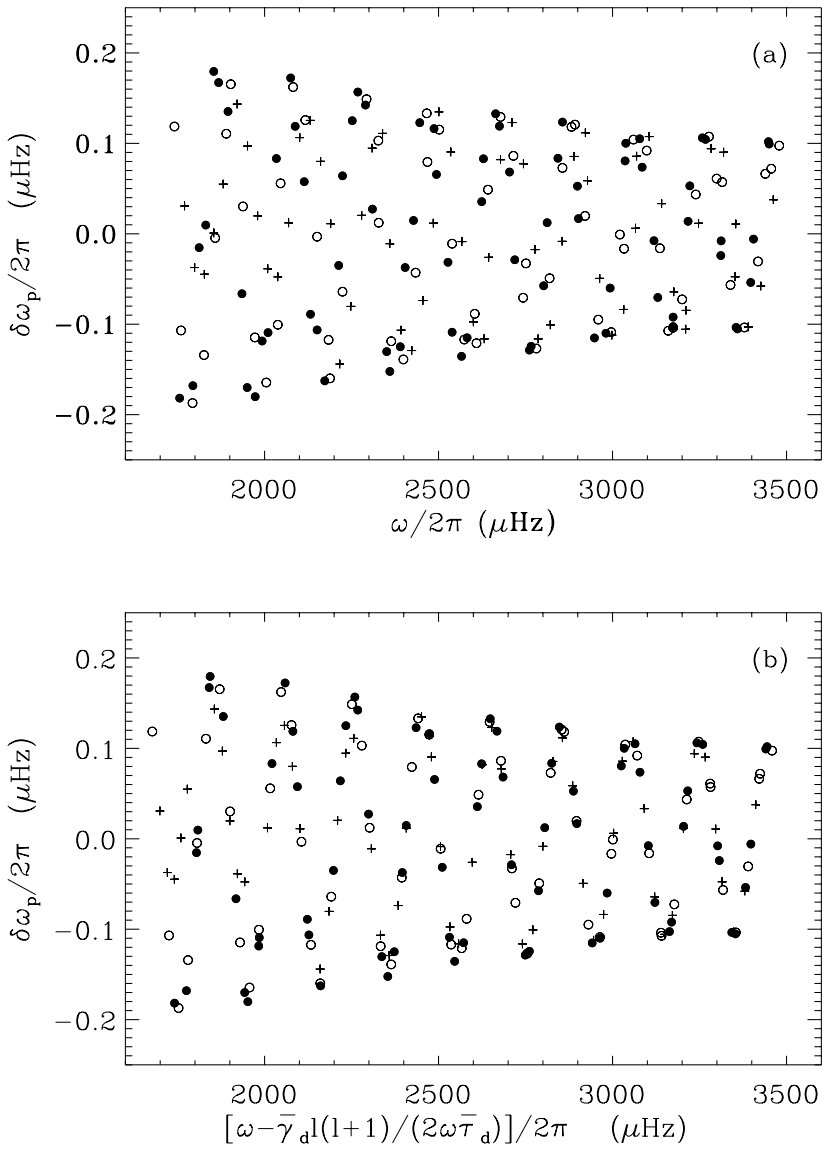

Fig. 2.3: (a) Artificial signal versus frequency for the following values of the parameters; τ_d=2311.3 s, $\gamma_d/2\pi$=13.12 μHz, $a_1/2\pi$=0.0265 μHz, $a_2/2\pi$=0.1410 μHz, Δ_d=0.304, ϕ_0=−4.17, a_ϕ=200.6 s, $a_\gamma/2\pi$=1.43 μHz [see Eq. (3.6.12)] and (b) the same signal but now plotted against $\omega-\overline{\gamma}_d L^2/2\omega\overline{\tau}_d$ to show the corrective effect of including $\overline{\gamma}_d$. The symbols are: (•) l=5−10, (○) l=11−15, and (+) l=16−20

the amplitude a parameter Δ_d depending on $[c(r_d)/r_d]^2$, according to

$$\Delta = \frac{l(l+1)}{\tilde{l}(\tilde{l}+1)} \left(\frac{\tilde{\omega}}{\omega}\right)^2 \Delta_d \,, \tag{2.6.3}$$

which represents the value of Δ at the frequency $\tilde{\omega}$ and degree $\tilde{l}$. In the results presented here I choose the reference value $\tilde{l}$=20. This expression for Δ is used in Eq. (2.5.7) for the dependence of $A(\omega, l)$ on l; the parameter introduced can then be determined as part of

the fit. However, because the effect of this term is very small for almost all the modes used in this analysis the fit is not expected to improve substantially.

The second contribution to the l-dependence is a phase shift; geometrically this arises because as l increases the ray paths through the convection zone depart more and more from the vertical, so that the path length from the surface to the discontinuity becomes longer. In order to use moderate-degree modes, without destroying the signal, we must account for this shift by including a first-order correction in Λ. As given in Eq. (2.6.1) the argument of the signal is in general given by

$$\Lambda_{\rm d}(\omega,l) = 2\omega \int_{r_{\rm d}}^{R} \left(1-\frac{S_l^2}{\omega^2}\right)^{1/2} \frac{{\rm d}r}{c} + 2\phi \,. \tag{2.6.4}$$

It is the term in S_l^2 that represents this shift of the phase for nonradial modes. The next step is to expand the square root in the integral in terms of the small quantity S_l^2/ω^2. This is

$$\left(1-\frac{S_l^2}{\omega^2}\right)^{1/2} \simeq 1 - \frac{S_l^2}{2\omega^2} - \frac{S_l^4}{8\omega^4} + \ldots \,, \tag{2.6.5}$$

following that to first approximation we have

$$\Lambda_{\rm d} \simeq 2\omega \int_{r_{\rm d}}^{R} \left(1-\frac{S_l^2}{2\omega^2}\right) \frac{{\rm d}r}{c} + 2\phi \,. \tag{2.6.6}$$

Therefore,

$$\Lambda_{\rm d} \simeq 2\omega\tau_{\rm d} - \gamma_{\rm d}\,\frac{L^2}{\omega} + 2\phi \,, \tag{2.6.7}$$

where

$$\gamma_{\rm d} \equiv \int_{r_{\rm d}}^{R} \frac{c}{r^2}\,{\rm d}r \,. \tag{2.6.8}$$

Fig. 2.3b shows the effect of introducing $\gamma_{\rm d}$. Evidently this accounts for essentially the full l-dependence of the signal, which demonstrates that the phase shift is the dominant cause of the disorderly appearance of Fig. 2.3a. This may also be argued as follows. The relative contribution to the amplitude (see Eq. (2.5.7)) from the degree is of order S_l^4/ω^4 if overshoot is present and $S_l^2/2\omega^2$ if it is not. Consider then the ratio of the latter to the change in $\delta\omega$ arising from the l-dependence of the phase (Eq. (2.6.5)). This ratio may be shown to be approximately $\frac{(c/r)^2}{(2\omega\gamma_{\rm d})}\,\cot\Lambda_{\rm d} \approx \frac{(\tilde{\omega}/\omega)}{20}\,\cot\Lambda_{\rm d}$. Except when ω is very small or $\cot\Lambda_{\rm d}$ happens to be large, the ratio is small and so the change in phase dominates. However, we shall maintain the contribution from l to the amplitude in order to confirm that it is indeed smaller than the correction from $\gamma_{\rm d}$ in the argument of the signal.

2.6.3 Contribution from the surface layers

Additional difficulties arise from the contribution of the surface layers to the characteristics of the mode; here the simple asymptotic analysis breaks down, and in addition, the uncertain effects of turbulent convection and energy transfer modify the properties of the oscillations. Consequently, ϕ becomes a function of frequency and degree (eg. Gough & Vorontsov 1995). Hence the determination of $\tau_{\rm d}$ and $\gamma_{\rm d}$ will be affected. However, modes with degree $l \leq 20$ propagate almost vertically near the surface, so the l-dependence should be weak. Thus, to estimate the first order effect, we write

$$\phi(\omega, l) = \phi_0 + a_\phi \omega + a_\gamma \frac{L^2}{2\omega} \, , \tag{2.6.9}$$

where ϕ_0, a_ϕ and a_γ are constants. Here the ω-dependence has been approximated as being linear, and we have retained only the l-dependent term that is functionally indistinguishable from the term in $\gamma_{\rm d}$, as defined in Eq. (2.6.7). Substituting this into that equation it follows that

$$\Lambda_{\rm d} \sim 2\omega\bar{\tau}_{\rm d} - \bar{\gamma}_{\rm d} \ \frac{l(l+1)}{\omega} + 2\phi_0 \, , \tag{2.6.10}$$

with

$$\bar{\tau}_{\rm d} = \tau_{\rm d} + a_\phi \, , \qquad \text{and} \qquad \bar{\gamma}_{\rm d} = \gamma_{\rm d} + a_\gamma \, . \tag{2.6.11}$$

The two constants (a_ϕ, a_γ) are therefore the dominant corrections to account for the surface effects.

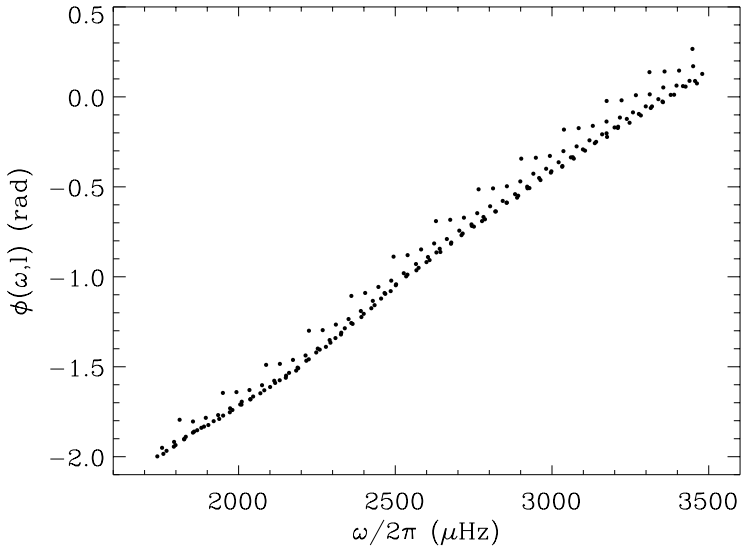

Fig. 2.4: Plot of the phase function $\phi(\omega, l)$ for a solar model, obtained from the acoustic phase α, determined by using the Duvall law - see (2.6.12) and (2.6.23). The same set of modes have been used as for Fig. 2.3.

For a model of known structure, and assuming adiabatic oscillations, ϕ can be determined. We do so by using the asymptotic result (eg. Eqs. (1.3.17) and (1.3.23)) that gives ϕ from the phase function $\alpha(\omega, l)$ through

$$\phi \sim \frac{\pi}{4} - \pi\ \alpha(\omega,l)\ , \tag{2.6.12}$$

(see for example (2.3.21) and (2.3.23)) where the phase function can be determined from a given model using the Duvall law

$$\int_{r_t}^{R} \left(1 - \frac{S_l^2}{\omega^2}\right)^{1/2} \frac{\mathrm{d}r}{c} \sim \pi\ \frac{n+\alpha(\omega,l)}{\omega} \tag{2.6.13}$$

(cf. Christensen-Dalsgaard & Pérez Hernández 1992 - see Section 1.3.3 for a brief discussion of this equation). The result is shown in Fig. 2.4, for one of the models discussed in Chapter 3. From these results we may estimate the value of a_ϕ to be of the order of 200s. Evidently, any determination of $\overline{\tau}_\mathrm{d}$ will only give τ_d if a_ϕ is known. However, asymptotically

$$a_\phi \sim -\pi\ \frac{\mathrm{d}\alpha}{\mathrm{d}\omega}\ , \tag{2.6.14}$$

and as is well known, $\frac{\mathrm{d}\alpha}{\mathrm{d}\omega}$ is undetermined observationally, and hence the period of the signal does not pin down the location of the discontinuity: unless model-dependent information is used, the determination of the location in acoustical depth is in error by an amount of order a_ϕ, i.e., about 200 s.

We also note here the difficulty of inferring radial distance from acoustic depth due to the uncertain treatment of the stellar surface layers. Because $|\mathrm{d}\tau/\mathrm{d}r| \equiv c^{-1}$ is relatively large there, any error in the physics of the outer few per cent of the star is substantially amplified in the radius determined from the acoustic depth. However, if an accurate measurement of γ_d is achieved this difficulty may be partially overcome. The reason is that γ_d, given by Eq. (2.6.8), is relatively insensitive to the surface layers of the star. Near $r{=}R$, the sound speed is much smaller than in the interior, which together with the factor $1/r^2$ reduces the effect of the uncertain outermost parts of the star's structure on the value of γ_d. The effect of a_γ must also be taken into account; but we may clearly hope to be able to use this method to constrain further the value of r_d for the Sun from solar frequency data.

The final expression for the signal in the frequencies of p-modes is now

$$\delta\omega = \frac{1{-}2\Delta}{(1{-}\Delta)^2} \left[\frac{a_1^2}{1{-}\Delta}\left(\frac{\tilde{\omega}}{\omega}\right)^4 + a_2^2\left(\frac{\tilde{\omega}}{\omega}\right)^2\right]^{1/2} \cos\left[2\omega\bar{\tau}_\mathrm{d} - \bar{\gamma}_\mathrm{d}\ \frac{l(l{+}1)}{\omega} + 2\phi_0\right]\ . \tag{2.6.15}$$

This is fitted to the data to determine the parameters $(a_1, a_2, \bar{\tau}_\mathrm{d}, \bar{\gamma}_\mathrm{d}, \phi_0, \Delta_\mathrm{d})$, as discussed in the next Chapter.

2.7 Other alternative analysis

Other authors have considered the possibility of isolating this signal. First proposed by Gough (1990), the second differences have been used in several works as the simplest and easiest way of identifying the signal in frequency data. Variations on this approach are for example the work by Monteiro, Christensen-Dalsgaard & Thompson (1993), Gough & Sekii (1993); Basu, Antia & Narasimha (1994); Basu & Antia (1994). A brief summary of some of these works is presented below.

Other authors, Vorontsov (1988), Roxburgh & Vorontsov (1994), have discussed the possibility of isolating the signal in the phase function of the oscillations. It is shown here that this method is equivalent to the one proposed by us. Since it uses the acoustic potential for the oscillation we start by considering a simpler example which makes the physics involved transparent. Their method is then presented and the expressions compared with the ones obtained above.

2.7.1 Second differences

The method proposed by Gough (1990) is simply to calculate the numerical second derivative of the frequencies as functions of mode order, for the same degree. This involves three modes, and the second difference for those modes of consecutive order is given by

$$S_d(\omega_{n,l}) = \omega_{n+1,l} - 2\omega_{n,l} + \omega_{n-1,l} \ . \tag{2.7.1}$$

An expression of this type removes a second order polynomial to the frequencies allowing the signal to become visible. Instead of using definition (2.7.1), Monteiro et al. (1993) used splines to fit the data, with the second differences coming naturally as the spline parameters. This prove to give a slightly clear signal than expression (2.7.1). In Fig. 2.5 the values of S_d for the frequencies of two models, one with and the other without overshoot are shown (see Chapter 3 for the details of these models). The difference in amplitude is clear and the periodic signature also. However in the figure only very low degree data has been used, otherwise the coherence of the points would be destroyed making it difficult to identify the signal. Note also that there are other components present, like the contribution from the helium ionization zone as a larger wavelength signal, which dominates at low frequencies.

If further derivatives are taken as in the work of Basu, Antia & Narasimha (1994), it is not a second order but a higher order polynomial that is taken out approaching the limit where only rapidly varying components of the frequencies as functions of mode order are left. However such a process can not be extended indefinitely because the degradation of the signal due to observational errors quickly surpasses the isolation of the signal provided

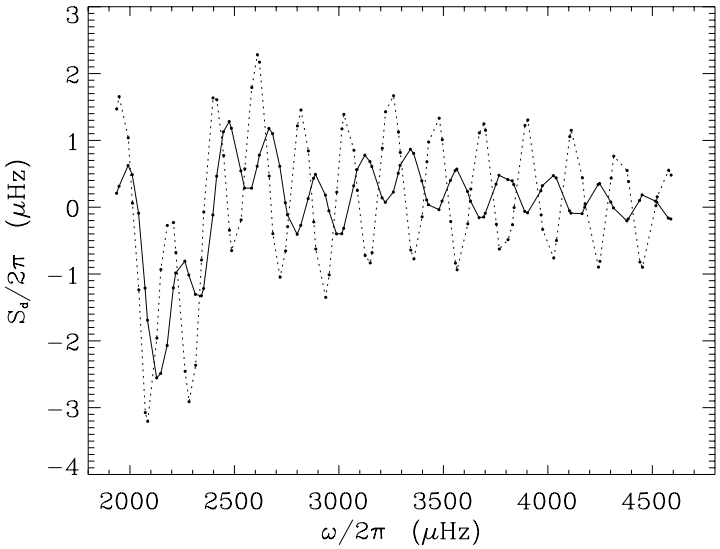

Fig. 2.5: Second differences S_d for frequencies of two models with (dotted line) and without (continuous line) overshoot - see next Chapter. Only low degree data ($0 \leq l \leq 4$) are shown.

by derivatives. The information associated with the frequency and/or degree dependence of the amplitude is also lost in a such a procedure.

2.7.2 Simple example

To illustrate the physical reason for the presence of the oscillatory signal we now consider a simple problem of a potential well. The advantage of this example, with an analytical solution, is that the analogy with stellar oscillations can be easily established.

For l=0 the eigenfunctions of the modes of oscillation for the Sun satisfy asymptotically an equation of the type

$$\frac{\mathrm{d}^2 Y}{\mathrm{d}\tau^2} + [\omega^2 - V^2(\tau)]\, Y = 0 \qquad (2.7.2)$$

(e.g. Vorontsov & Zharkov 1989, Gough & Vorontsov 1995), where $V(\tau)$ is an acoustic potential (independent of ω) and $Y(\tau)$ is the oscillation eigenfunction. Fig. 2.6 shows the potential for two solar models: one without and the other with overshoot at the base of the convection zone (as in Fig. 2.5). This potential includes terms in the first and the second derivative of the sound speed. Hence any discontinuity in the first derivative of the sound speed gives rise to a δ-function in V, while a discontinuity in the second derivative of the sound speed causes a step function in V. Clearly, since V depends on the structure of the star, the exact solution of Eq. (2.7.2) can be obtained only numerically for a realistic model.

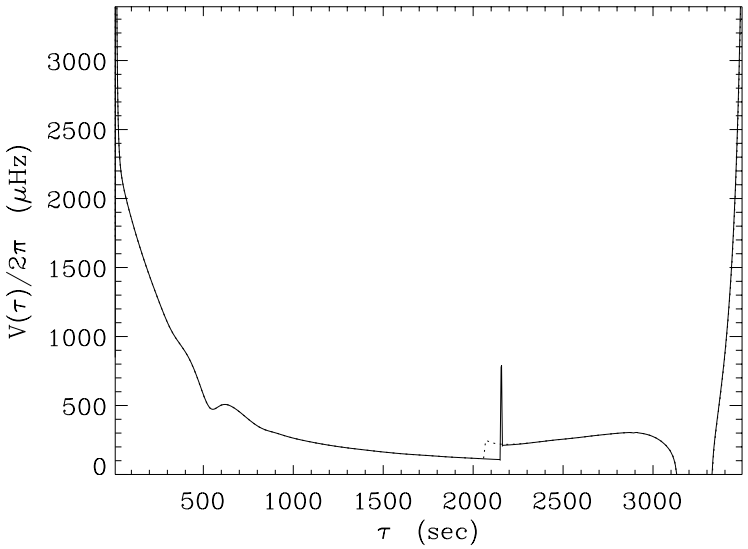

Fig. 2.6: Acoustic potential $V(\tau)$ with τ being the acoustic depth for two Models: a non-overshoot model (Y_1 - dotted line) and an overshoot model (Z_2 - continuous line). Both potentials are for $l = 0$. The expression used to determine the potential is given below in (2.7.17)

To simulate the effect on ω of a discontinuity in sound speed derivatives we consider instead simpler problems by defining potentials for which we can determine an exact solution. Starting from Eq. (2.7.2) we need to determine the eigenfunction $Y(\tau)$ which is the solution for the eigenvalue ω for a given potential $V(\tau)$. As boundary conditions we take rigid boundaries (Y=0) at τ=0 and τ=τ_t. Our reference solution is assumed to correspond to a constant potential everywhere, V=V_a, say. The solution for frequency ω_0, satisfying the boundary condition at τ=0, is

$$Y(\tau) = A_0 \ \sin\left[\int_0^{\tau} \left(\omega_0^2 - V_a^2\right)^{1/2} \ \mathrm{d}\tau\right] \ , \tag{2.7.3}$$

where A_0 is a constant. Imposing also the boundary condition at τ=τ_t, we obtain the following dispersion relation:

$$\omega_0^2 - V_a^2 = \left(\frac{n\pi}{\tau_t}\right)^2 \ , \tag{2.7.4}$$

n being an integer corresponding to the $(number\ of\ zeros - 1)$ of the eigenfunction.

To illustrate the effects of discontinuities or singularities, we consider two perturbations to the reference potential. The first is defined by

$$V_1(\tau) = \begin{cases} V_b & \text{for} \quad 0 \leq \tau < \alpha_1 \tau \\ \\ V_a & \text{for} \quad \alpha_1 \tau \leq \tau < \tau_t \ , \end{cases} \tag{2.7.5}$$

while the second is given by

$$V_2(\tau) = V_a + A_\delta \ \delta(\tau - \alpha_2 \tau_t) \tag{2.7.6}$$

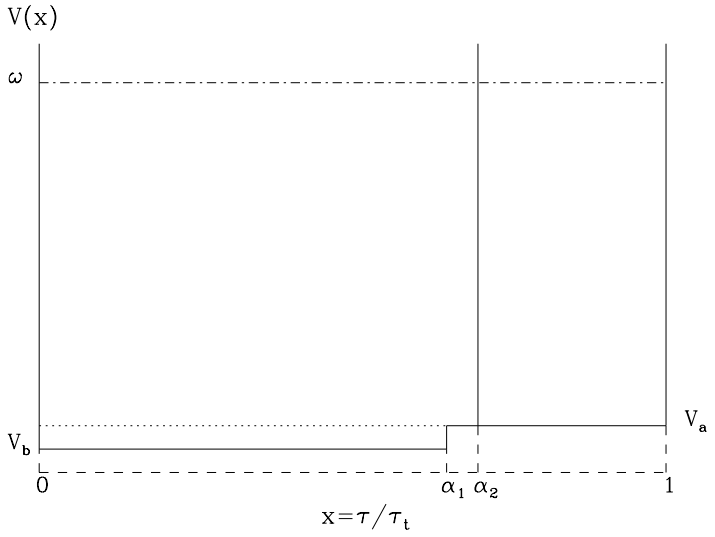

Fig. 2.7: Example of a potential which is constant everywhere in the interval $[0, \pi_t]$ and two types of perturbation: a step at $\alpha_1 \pi_t$ and a δ function at $\alpha_2 \pi_t$

(see also Fig. 2.7). Imposing the same boundary conditions, and requiring that $Y(\tau)$ be continuous everywhere, we find the solutions for the two cases as, respectively,

$$\begin{cases} Y_{11}(\tau) = A_1 \dfrac{\sin[\Lambda_b(\tau)]}{\sin[\Lambda_b(\alpha_1\pi_t)]} & \text{for } \; 0 \le \tau \le \alpha_1 \pi_t \\ Y_{12}(\tau) = A_1 \dfrac{\sin[\Lambda_a(\pi_t - \tau)]}{\sin[\Lambda_a(\pi_t - \alpha_1\pi_t)]} & \text{for } \; \alpha_1\pi_t \le \tau \le \pi_t \end{cases} \tag{2.7.7}$$

and,

$$\begin{cases} Y_{21}(\tau) = A_2 \dfrac{\sin[\Lambda_a(\tau)]}{\sin[\Lambda_a(\alpha_2\pi_t)]} & \text{for } \; 0 \le \tau \le \alpha_2 \pi_t \\ Y_{22}(\tau) = A_2 \dfrac{\sin[\Lambda_a(\pi_t - \tau)]}{\sin[\Lambda_a(\pi_t - \alpha_2\pi_t)]} & \text{for } \; \alpha_2\pi_t \le \tau \le \pi_t \; . \end{cases} \tag{2.7.8}$$

Here A_1 and A_2 are constants, and

$$\Lambda_j(\tau) = \int_0^\tau \left(\omega^2 - V_j^2\right)^{1/2} \mathrm{d}\tau = \left(\omega^2 - V_j^2\right)^{1/2} \tau \; ; \quad j = a, b \; . \tag{2.7.9}$$

We now need to impose a condition on $\mathrm{d}Y/\mathrm{d}\tau$. To do so, Eq. (2.7.2) is integrated around $\alpha_i \pi_t$ (i=1,2) giving,

$$\int_{\alpha_i\pi_t - \epsilon}^{\alpha_i\pi_t + \epsilon} \frac{\mathrm{d}^2 Y}{\mathrm{d}\tau^2} \, \mathrm{d}\tau = - \int_{\alpha_i\pi_t - \epsilon}^{\alpha_i\pi_t + \epsilon} \left(\omega^2 - V^2\right) \, Y \, \mathrm{d}\tau \; . \tag{2.7.10}$$

Substituting the potentials in Eqs. (2.7.5) and (2.7.6), and taking the limit $\epsilon \to 0$ of these

relations, we obtain the matching conditions

$$\left[\frac{\mathrm{d}Y_{12}}{\mathrm{d}\tau} - \frac{\mathrm{d}Y_{11}}{\mathrm{d}\tau}\right]_{\alpha_1\pi} = 0\,,$$

and (2.7.11)

$$\left[\frac{\mathrm{d}Y_{22}}{\mathrm{d}\tau} - \frac{\mathrm{d}Y_{21}}{\mathrm{d}\tau}\right]_{\alpha_2\pi} = A_\delta\ Y_{21}(\alpha_2\pi) = A_\delta\ Y_{22}(\alpha_2\pi)\,,$$

in each case, respectively. By using the solutions given in Eqs. (2.7.7) and (2.7.8), we finally derive the following two dispersion relations:

$$\tan[\Lambda_b(\alpha_1\pi)] = -\left(\frac{\omega^2-V_b^2}{\omega^2-V_a^2}\right)^{1/2}\tan[\Lambda_a(\pi-\alpha_1\pi)] \tag{2.7.12}$$

and

$$\tan[\Lambda_a(\alpha_2\pi)] = -\frac{\tan[\Lambda_a(\pi-\alpha_2\pi)]}{1-A_\delta(\omega^2-V_a^2)^{-1/2}\tan[\Lambda_a(\pi-\alpha_2\pi)]}\,. \tag{2.7.13}$$

These relations determine the values of ω satisfying the boundary conditions for the first case in terms of V_a, V_b and α_1, while in the second case in terms of V_a, A_δ and α_2.

We now expand the expressions to first order in the small quantities; $\delta\omega{=}\omega{-}\omega_0$, $\delta V^2{=}V_a^2{-}V_b^2$ and V_i^2/ω^2. For the step-function potential $V_1(\tau)$ we obtain the periodic component of $\delta\omega$, given by

$$\delta\omega_{p1} \sim \frac{\delta V^2}{4\pi\omega_0^2}\ \sin\left[2\Lambda_0(\alpha_1\pi)\right]\ , \tag{2.7.14}$$

while the delta-function potential $V_2(\tau)$ gives rise to a periodic component

$$\delta\omega_{p2} \sim \frac{A_\delta}{2\pi\omega_0}\ \cos\left[2\Lambda_0(\alpha_2\pi)\right]\ ; \tag{2.7.15}$$

here

$$\Lambda_0(\tau) = \int_0^\tau (\omega_0^2-V_a^2)^{1/2}\mathrm{d}\tau\,. \tag{2.7.16}$$

The nature of the signal in the frequencies for these simple cases is very similar to the result obtained for a star. Note the difference in the phase, and in the power of ω_0 in the amplitude of the signal, depending on whether the potential has a step or a δ-function. If many mode frequencies are available, we can in principle distinguish between the two types of potential on the basis of the phase and the frequency dependence of the amplitude, and determine δV^2 and $\alpha_1\pi$ in the first case, or A_δ and $\alpha_2\pi$ in the second case, hence obtaining the nature, position and magnitude of the perturbations.

The method used to obtain expressions (2.7.14) - (2.7.15) can also be used for a star - this is discussed below. In this approach, suitable matching conditions on the eigenfunction are imposed at the reflecting boundaries substituting the rigid boundaries we have considered here.

2.7.3 Roxburgh & Vorontsov method

Here, a combination of the method used by Roxburgh & Vorontsov (1994) - here after RV, and our own analysis is presented. As done for the cases of simple acoustic potentials in the previous section we shall consider here how discontinuities in the sound speed derivatives affect the acoustic potential. From there we just need to use the second order differential equation as written in (2.7.2) and determine the periodic component of the change in the eigenvalues due to the presence of the discontinuities. In their work RV considered not changes in the frequencies but changes in the phase function. They are related, to first order, by $\delta\omega{\sim}\pi\delta\alpha/\tau_{\rm t}$, where α is the phase function in the Duvall law - see Eqs. (2.6.12) and (2.6.13).

We start by considering the acoustic potential for the oscillations, which is (Vorontsov & Zharkov 1989, RV and references therein)

$$\begin{aligned} V^2(\tau) =& N^2 + \frac{c^2}{4}\,\left(\frac{2}{r}+\frac{N^2}{g}-\frac{g}{c^2}-\frac{1}{2c^2}\,\frac{{\rm d}c^2}{{\rm d}r}\right)^2 \\ & -\frac{c}{2}\,\frac{\rm d}{{\rm d}r}\left[c\left(\frac{2}{r}+\frac{N^2}{g}-\frac{g}{c^2}-\frac{1}{2c^2}\,\frac{{\rm d}c^2}{{\rm d}r}\right)\right] - 4\pi G\rho\,, \end{aligned} \tag{2.7.17}$$

N being the Brünt–Vässäla frequency defined in (1.3.5). A plot of this potential for two solar models is shown in Fig. 2.6 above.

Using again approximations (2.4.9), relations (2.4.10) - (2.4.11) and Eqs. (2.4.21) to (2.4.23) this can be written as

$$\begin{aligned} V^2(\tau) =& \left(\frac{g\Gamma_1}{2c}\right)^2 + \frac{2g}{r}\,(\Gamma_1{-}2) + \frac{2c^2}{r^2} - 2\pi G\rho\Gamma_1 \\ & + \left(\pi G\rho - \frac{g}{2r} - \frac{g^2\Gamma_1}{2c^2}\right)\left[\Gamma_1{-}1 + (\gamma{-}1)\,\frac{\nabla_{\rm r}{-}\nabla_{\rm a}}{\nabla_{\rm a}}\,H(\tau{-}\tau_{\rm d})\right] \\ & + \frac{g^2}{16c^2}\left\{(\Gamma_1{-}1)^2 + (\gamma{-}1)\,\frac{\nabla_{\rm r}{-}\nabla_{\rm a}}{\nabla_{\rm a}}\left[2(\Gamma_1{-}1) + (\gamma{-}1)\,\frac{\nabla_{\rm r}{-}\nabla_{\rm a}}{\nabla_{\rm a}}\right]H(\tau{-}\tau_{\rm d})\right\} \\ & - \frac{g}{4c}\left[(\gamma{-}1)\,\frac{\nabla_{\rm r}{-}\nabla_{\rm a}}{\nabla_{\rm a}}\,\delta(\tau{-}\tau_{\rm d}) + \frac{\gamma{-}1}{\nabla_{\rm a}}\,\frac{{\rm d}\nabla_{\rm r}}{{\rm d}\tau}\,H(\tau{-}\tau_{\rm d})\right]. \end{aligned} \tag{2.7.18}$$

Thus we obtain an expression of the form

$$V^2(\tau) = V_0^2(\tau) + A_H(\tau)\,H(\tau{-}\tau_{\rm d}) + A_\delta(\tau)\,\delta(\tau{-}\tau_{\rm d})\,, \tag{2.7.19}$$

where

$$\begin{aligned} V_0^2(\tau) &= \frac{g}{2r}\,(3\Gamma_1{-}7) + \frac{2c^2}{r^2} - \pi G\rho(\Gamma_1{+}1) - \frac{g^2}{16c^2}\,(\Gamma_1{+}1)(\Gamma_1{-}3)\,, \\ A_H(\tau) &= -\frac{g(\gamma{-}1)}{2r}\;\frac{\nabla_{\rm r}{-}\nabla_{\rm a}}{\nabla_{\rm a}}\;\bar{h}(\tau) - \frac{g(\gamma{-}1)}{4c\nabla_{\rm a}}\;\frac{{\rm d}\nabla_{\rm r}}{{\rm d}\tau}\,, \\ A_\delta(\tau) &= -\frac{g(\gamma{-}1)}{4c}\;\frac{\nabla_{\rm r}{-}\nabla_{\rm a}}{\nabla_{\rm a}}\,, \end{aligned} \tag{2.7.20}$$

and the function $\bar{h}(\tau)$ is

$$\bar{h}(\tau) = 1 - \frac{4\pi G r \rho}{2g} + \frac{rg(\Gamma_1+3)}{4c^2} - \frac{3rg}{8c^2}\,(\gamma-1)\,\frac{\nabla_{\rm r}-\nabla_{\rm a}}{\nabla_{\rm a}}\,. \tag{2.7.21}$$

It follows that the periodic signal in the frequencies is given by (see RV and Eqs. (2.7.14) - (2.7.15))

$$\begin{aligned}\delta\omega &\sim -\frac{A_H(\tau_{\rm d})}{4\omega^2\tau_{\rm t}}\,\sin(\Lambda) + \frac{A_\delta(\tau_{\rm d})}{2\omega\tau_{\rm t}}\,\cos(\Lambda) \\ &\sim \bar{a}_1\left(\frac{\tilde{\omega}}{\omega}\right)^2\sin(\Lambda) + \bar{a}_2\left(\frac{\tilde{\omega}}{\omega}\right)\cos(\Lambda)\,,\end{aligned} \tag{2.7.22}$$

with the components given by

$$\begin{aligned}\bar{a}_1 &= \frac{\bar{a}_0}{\tilde{\omega}}\,\left[\frac{{\rm d}\nabla_{\rm r}}{{\rm d}\tau} + (\nabla_{\rm r}-\nabla_{\rm a})\,\frac{2c}{r}\,\bar{h}(\tau_{\rm d})\right] \\ \bar{a}_2 &= -2\bar{a}_0\,(\nabla_{\rm r}-\nabla_{\rm a})\,.\end{aligned} \tag{2.7.23}$$

Where

$$\bar{a}_0 = \frac{1}{16\tilde{\omega}\tau_{\rm t}}\,\frac{g(\gamma-1)}{c\nabla_{\rm a}}\,, \tag{2.7.24}$$

and all quantities are evaluated at $\tau=\tau_{\rm d}$. These correspond to the expressions found using the variational principle, in particular (2.5.8) and (2.5.9).

The two sets of equations are approximately the same for $l=0$. Expressions (2.5.6) and (2.5.1) are quite similar to Eq. (2.7.22) if $l=0$, the same happening between Eqs. (2.5.8) - (2.5.9) and Eqs. (2.7.23) - (2.7.24). The main advantage of the variational principle is that it also gives the dependence on the degree l. The additional contribution from Δ_c in Eq. (2.5.9) also has some effect for $\tau_{\rm d}$ close to $\tau_{\rm c}$. The correction term in a_1 arising from $\nabla_{\rm r}-\nabla_{\rm a}$ also differs (the two functions h and $\bar{h}$ are different), but the difference is of little importance since the contribution of this term is small.

Roxburgh & Vorontsov present a simplified analysis which uses approximate dependences of the opacity on density and temperature at the base of the convection zone, to replace the equivalent to Eqs. (2.7.23) and (2.7.24), allowing then to write the explicit dependence of the amplitude on the penetration depth. The result is

$$A_{\rm RV}(\tilde{\omega}) = \frac{g}{12\tau_{\rm t}\tilde{\omega}\,c}\,\left[\left(\frac{g}{12\tilde{\omega}\,c}\right)^2\left(17-\frac{35}{\epsilon}+\frac{33}{\epsilon^2}\right)^2 + \left(1-\frac{1}{\epsilon}\right)^2\right]^{1/2}\,, \tag{2.7.25}$$

with

$$\epsilon = \left(1+\frac{2}{5}\,\frac{r_{\rm c}-r_{\rm d}}{H_P}\right)^{15/4}\,. \tag{2.7.26}$$

Here $r_{\rm c}$ and $r_{\rm d}$ are the radial positions corresponding to $\tau_{\rm c}$ and $\tau_{\rm d}$, respectively. As in expression (2.5.10), given a solar model, i.e. (g, c, H_P), this equation gives the expected amplitude for the signal. Note that, as referred above, Roxburgh & Vorontsov method does give almost the some values as our analysis, if we use our expressions for the effect

of overshoot in the temperature gradient. However, due to the simplifying assumptions used in deriving Eq. (2.7.25) a difference of about 10% is introduced. In the next Chapter several models are consider and the expected amplitude of the signal from both analysis is determined and compared with each other.

3. Measuring Solar Convective Overshoot

Using the analysis developed in the previous Chapter for the signal in the frequencies of oscillation we consider here the possibility of studying the solar overshoot layer using solar frequency data. First different solar models with and without overshoot are calculated in order to calibrate the expression obtained for the signal. Using this calibration we then proceed to study the solar signal and calculate the effect of observational errors in the determination. We further discuss some of our assumptions entering the analysis for the amplitude of the signal and try to quantify the possible sources of errors. The effect of relaxing the assumption of an abrupt transition from adiabatic to radiative stratification at the bottom of the overshoot layer is also considered.

We find no strong evidence for the existence of an overshoot region of the kind we consider here. Indeed if the overshoot consists of an essentially adiabatic extension of the convection zone followed by an abrupt transition to radiative stratification then we may put an upper limit of 0.1 local pressure scale heights on the extent of the adiabatically stratified overshoot layer.

3.1 Introduction

The work presented here is an attempt to determine, using solar seismic data, whether overshoot is present at the base of the solar convective envelope and to put an upper limit on its extent. The basic idea, developed in the previous Chapter, is that a localized or sharp feature in the Sun's internal structure will give rise to a characteristic periodic signal in the frequencies of global p-modes. Such a sharp feature occurs in standard solar models at the base of the outer convective envelope. An even sharper transition occurs in models incorporating an overshoot layer adiabatically stratified beneath the convection zone. Therefore, one expects to use the amplitude of the periodic signal in the seismic data to infer how this transition occurs. Pursuing this possibility we construct a method for isolating the signal in the frequencies and through the study of its characteristics provide a direct constraint on the penetration distance at the base of the convective envelope in the Sun.

Our method consists of an iterative process whereby a smoothing function is used to remove a 'smooth' approximation to the frequencies of oscillation, leaving in the residuals the periodic signal we are trying to study. We then fit to the residuals, considered as a function of mode frequency, an asymptotic expression obtained from a variational principle for adiabatic non-radial oscillations. Major complications in such an isolation procedure are the relatively small amplitude of the signal we are dealing with, and the contribution to the frequencies from other localized effects, such as the helium ionization zone.

The calibration from a sequence of solar models with increasing overshoot distance is used with the solar data to give an upper limit on the penetration distance ℓ_s for the Sun. We also investigate the effects from the observational errors and the uncertainties in some other aspects of the physics. We further consider the implications of relaxing the assumption of having a sharp transition from near adiabatic to radiative stratification at the bottom of the overshoot layer. This may be essential for interpreting the results from the data.

3.2 Solar Envelope Models

To test the method we use several solar models (see Table 3.1 below). Apart from the inclusion of overshoot, the models were calculated essentially as described by Christensen-Dalsgaard (1982), although with substantially higher numerical precisions and using opacities based on the Los Alamos Opacity Library. For simplicity, full evolution sequences were not computed; instead the hydrogen abundance was obtained by scaling from a suitable model of the present Sun, the scaling factor being determined, together with the mixing-length parameter, to obtain the correct solar luminosity and radius (cf. Christensen-Dalsgaard & Thompson 1991).

Some of the models also include a parametrized change in the opacities. These have been introduced according to the expressions presented for example in Christensen-Dalsgaard & Thompson (1991). We also consider models with thermal configurations that represent the possible effect of overshoot. Again it is done by using a parametric description of the temperature gradient at the base of the convection zone that reproduces the behaviour seen for simple descriptions of stellar overshoot. Both changes to what would be otherwise standard models are discussed in detail in the following subsections.

3.2.1 Models with overshoot

Static solar models with different extents of the overshoot layer at the base of the convection zone are considered. In order to study the applicability of the method proposed we have implemented overshoot in the simplest possible way, through a model which sim-

ulates the results of more detailed calculations, with a few adjustable parameters which may be used to specify the extent of overshoot and the thickness of the transition zone. The actual temperature gradient $\nabla = \mathrm{d}\ln T/\mathrm{d}\ln P$ is related to the adiabatic gradient ∇_a and the radiative gradient ∇_r, through the following parametric relations. Defining

$$x = 1 - \mathcal{C}\left(1 - \frac{\nabla_\mathrm{a} - \nabla_\mathrm{r}}{\mathcal{D}}\right) , \tag{3.2.1}$$

the gradient in the overshoot region is calculated from

$$\nabla = \begin{cases} \nabla_\mathrm{a} & ; x \le 0 \\ \nabla_\mathrm{r} + \mathcal{D}(1-x)^3 \left[\left(1-\frac{1}{\mathcal{C}}\right) + \left(3-\frac{2}{\mathcal{C}}\right)x + 3\left(2-\frac{1}{\mathcal{C}}\right)x^2\right] & ; x \ge 0 , \end{cases} \tag{3.2.2}$$

where $1-\mathcal{C} \le x \le 1$. While in the proper convection zone ∇ is computed from the usual mixing-length expression. Here $\mathcal{D}$ and $\mathcal{C}$ are adjustable parameters, determining, respectively, the extent of overshoot (in terms of $\nabla_\mathrm{a} - \nabla_\mathrm{r}$) and the fraction of it taken by the transition region from adiabatic stratification to radiative stratification. In our previous notation (see (2.4.19)), in terms of radius r or acoustic depth τ, to the Schwarzschild point (r_c and τ_c) corresponds $x = 1-\mathcal{C}$, while to the base of the overshoot region (r_d and τ_d) corresponds $x = 1$. We also have to introduce an intermediate point r_cd (and τ_cd) which separates the adiabatically stratified part of the overshoot layer and the transition region. This point corresponds to $x = 0$.

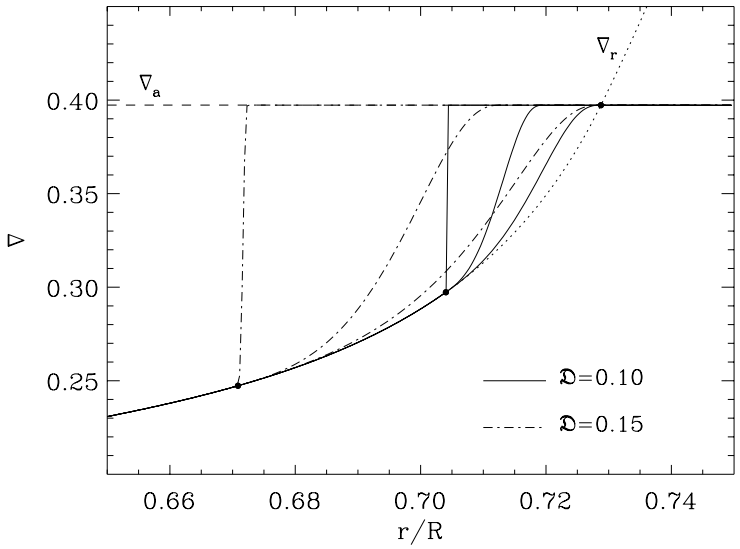

Fig. 3.1: Plot of the gradients as given by (3.2.2), for $\mathcal{D} = 0.1, 0.15$ as indicated. For each of these values there are three lines plotted for $\mathcal{C} = 1, 2, 10^5$ corresponding to increasing steepness of the transition.

Table 3.1: Characteristics of the models considered. The radial position r_c corresponds to the point where the radiative gradient equals the adiabatic gradient, while r_d is the position where the stratification changes to become finally radiative. Overshoot has been modelled according to Eqs. (3.2.1) - (3.2.2) using values for $\mathcal{D}$ from 0 up to 0.18 and with $\mathcal{C}=10^4$ giving a very thin ($r_{cd}\sim r_d$) transition zone with an adiabatic stratification over all the layer. The total solar radius is R.

Model	$\frac{r_c}{R}$	$\frac{r_d}{R}$	$\frac{r_c-r_d}{R}$	$\frac{r_c-r_d}{H_P}$
Z_0	0.72876	0.72876	0.00000	0.00000
Z_1	0.72871	0.72569	0.00302	0.03841
Z_2	0.72866	0.72246	0.00620	0.07886
Z_3	0.72857	0.71900	0.00957	0.12158
Z_4	0.72843	0.71529	0.01314	0.16693
Z_5	0.72823	0.71128	0.01695	0.21517
Z_6	0.72795	0.70692	0.02103	0.26683
Z_7	0.72759	0.70215	0.02544	0.32242
Z_8	0.72711	0.69690	0.03022	0.38256
Z_9	0.72650	0.69104	0.03546	0.44814

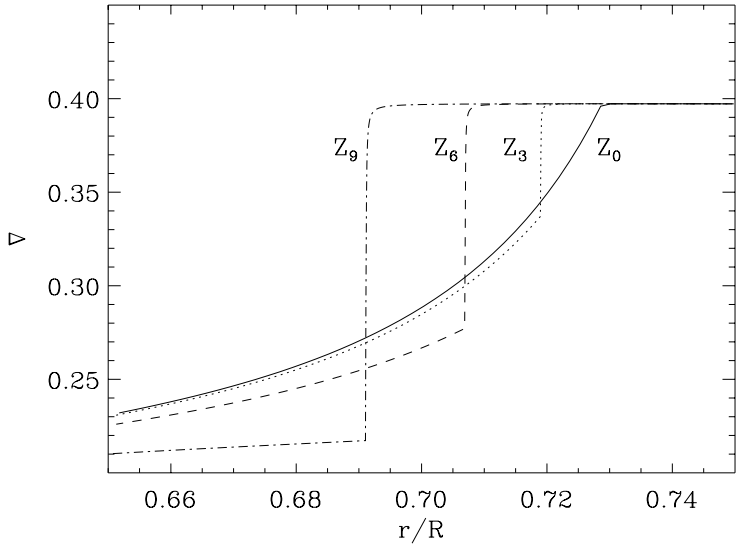

Fig. 3.2: Temperature gradient ∇ versus radius at the base of the convective envelope for some models constructed using Eq. (3.2.2). Different values of $\mathcal{D}$ (from 0 to 0.18) have been used with $\mathcal{C}=10^4$.

Expression (3.2.2) clearly has the desired form; in particular it has continuous first, second and third derivatives on both boundaries of the overshoot region (considering that the stratification is adiabatic in the proper convection zone above). Also it might be noted that the expression is purely local, and hence easily implemented. Since the thickness of the transition region is given by $\mathcal{D}/\mathcal{C}$, we have that $\mathcal{C}\geq 1$ and for $\mathcal{C}$ large ($\gtrsim 100$) there is a very abrupt transition. The values of $\mathcal{D}$ are chosen to obtain the desired depths of the

overshoot region. In Fig. 3.1 we illustrate some gradients as given by (3.2.2) for different values of the two parameters $\mathcal{D}$ and $\mathcal{C}$.

With the implementation of this expression in the code for calculating solar models we have obtained the ten models listed in Table 3.1 with different penetration depths of overshoot. Fig. 3.2 shows the temperature gradient at the base of the convection zone for some of them.

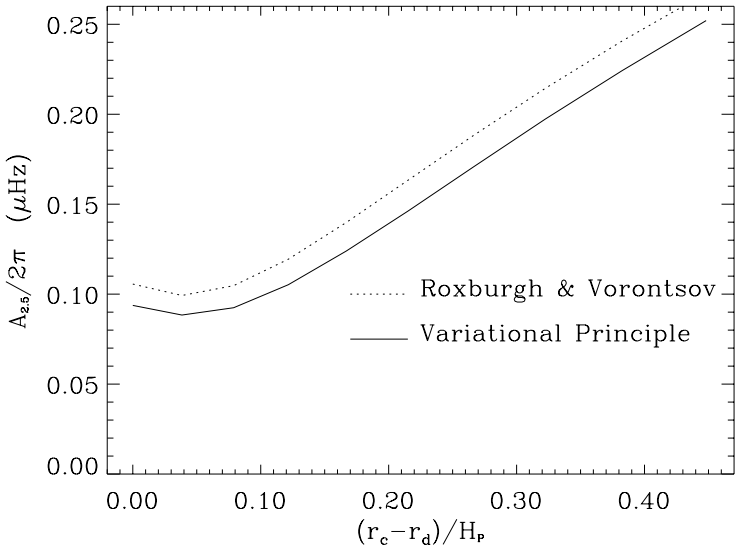

Fig. 3.3: Plot of the expected amplitude $A_{2.5}$ for models Z_{0-9} as given by expression (2.5.10) - continuous line, while the dotted line shows the amplitude A_{RV} as given by Eq. (2.7.25) - (2.7.26) and corresponding to the result of Roxburgh & Vorontsov (1994).

Given a model it is possible using the theoretical expressions for the amplitude of the signal to determine the expected value of the amplitude $A_{2.5}$ - Eq. (2.5.10). This has been calculated for all ten models listed in Table 3.1 and the results are plotted in Fig. 3.3, for both the expression from the variational principle, (2.5.10), and the Roxburgh & Vorontsov result, (2.7.25) - (2.7.26).

3.2.2 Effects of changes in other aspects of the physics

In order to test how uncertainties in other aspects of the physics affect our results we have also considered models without overshoot but with changes in the opacities. These variations were considered in order to model uncertainties in the surface layers and in the opacities for the radiative interior. The opacity changes have been incorporated as in Christensen-Dalsgaard & Berthomieu (1991) or Christensen-Dalsgaard & Thompson (1991),

where the actual opacity k_0 is replaced by k given according to

$$\log k = \log k_0 + A \exp\left[-\left(\frac{y}{\Delta}\right)^2\right] , \tag{3.2.3}$$

$$\text{with} \qquad y = \begin{cases} \log T - \log T_1 & ; \text{ for } \log T < \log T_1, \\ 0 & ; \text{ for } \log T_1 < \log T < \log T_2, \\ \log T - \log T_2 & ; \text{ for } \log T_2 < \log T \ . \end{cases}$$

Here, T_1 and T_2 are the values between which the logarithm of the opacity is changed by A, while Δ is a parameter, given in terms of $\log T$, which defines the steepness of the transition for the opacity from the borders T_1 and T_2, where it is k, to the real value k_0.

All models considered are listed in Table 3.2. One of the models (Y_3) is distinguished by having a localized opacity increase near the base of the convection zone, to see whether this can be distinguished from overshoot. Model Y_{2a} has a broader opacity change in order to increase the depth of the convective envelope relative to a standard model such that its base is at the location of the base of the overshoot region in an overshoot model (Y_2). To test the effect of near-surface uncertainties, models Y_{1a} and Y_{4a} differ from Y_1 and Y_4 in having different atmospheric opacities and hence different frequencies and phases ϕ. This causes the acoustic depth of the base of their adiabatic region to be slightly different from that in the corresponding model without opacity modification, though the atmospheric change hardly affects the depth in terms of radius.

Table 3.2: Base of the convection zone for seven models incorporating different changes in the physics, specifically; opacities and overshoot. Column 2 gives the radial location of the base of the convective envelope (including overshoot), while column 1 gives the radial location of the base of the convective unstable envelope according to the Schwarzschild criterion. **Notes: 1.** Model has reduced surface opacity, with $\delta \log \kappa = -0.3$ for $\log T \lesssim 4.2$. **2.** Models with overshoot (using $\mathcal{C}=10^5$). **3.** Model has a broad opacity increase, with $\delta \log \kappa = 0.093$ for $5 \lesssim \log T \lesssim 6.8$, in order to increase the depth of the convection zone. **4.** Model has higher opacity immediately beneath the convection zone, with $\delta \log \kappa = 0.093$ for $5 \lesssim \log T \lesssim 6.4$.

Model	$\frac{r_c}{R}$	$\frac{r_d}{R}$	$\frac{r_c - r_d}{R}$	$\frac{r_c - r_d}{H_P}$	Note
Y_1	0.72870	0.72870	0.00000	0.00000	–
Y_{1a}	0.72890	0.72890	0.00000	0.00000	1
Y_2	0.72830	0.71320	0.01510	0.19122	2
Y_{2a}	0.71320	0.71320	0.00000	0.00000	3
Y_3	0.71490	0.71490	0.00000	0.00000	4
Y_4	0.72730	0.69940	0.02790	0.35277	2
Y_{4a}	0.72750	0.69990	0.02760	0.34993	1

In order to compare with the overshoot models we also plot in Fig. 3.4 the temperature gradient for all Y models. Note that we have considered overshoot models with an even sharper transition by using a higher value of $\mathcal{C}$.

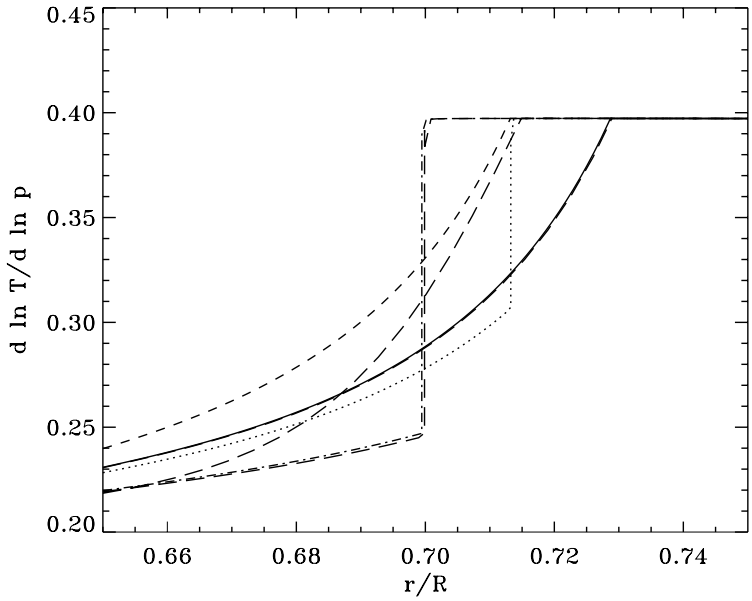

Fig. 3.4: Temperature gradient ∇ at the base of the convective envelope for models (see Table 3.2): Y_{1a} (continuous line), Y_{2a} (dashed line), Y_3 (long-dashed line), Y_2 (dotted line), Y_4 (dot-dashed line). Temperature gradients for models Y_1 and Y_{4a} are also depicted (as dashed lines), but these are virtually indistinguishable in the figure from those of models Y_{1a} and Y_4 respectively

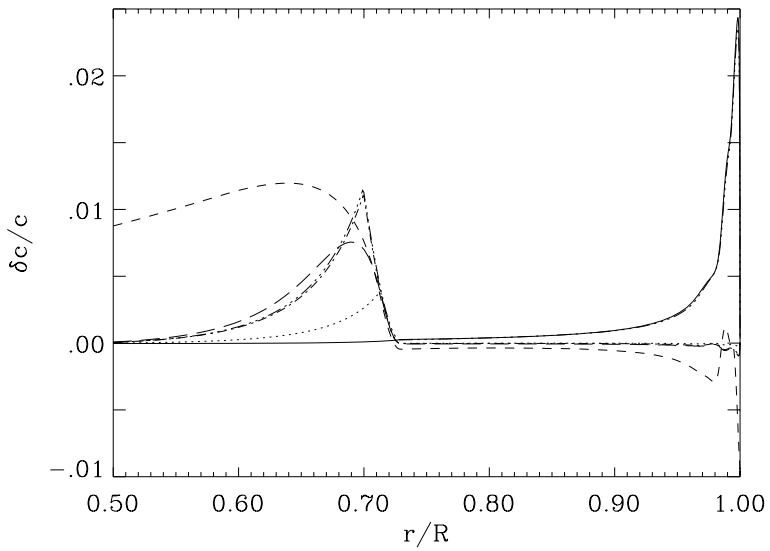

Fig. 3.5: Relative sound-speed differences $(c_i - c_1)/c_1$, at fixed r; here c_1 refers to Model Y_1, and c_i to the following Models: Y_{1a} (continuous line), Y_{2a} (dashed line), Y_3 (long-dashed line), Y_2 (dotted line), Y_4 (dot-dashed line), Y_{4a} (triple dot-dashed line)

The difference in adiabatic sound speed is important for understanding the differences in the model frequencies. Fig. 3.5 therefore shows relative sound-speed differences, at fixed

radius, between several models and model Y_1 (which is a standard solar model).

3.2.3 Effects of a gradual transition

We have so far assumed that there is an abrupt transition from the adiabatic to the radiative temperature gradient in the case of overshooting, leading to a discontinuity in ∇ at the point $r{=}r_{\rm d}$ where the transition to the radiative gradient occurs. To illustrate the effects of relaxing this assumption, we have also constructed models with the following structure for the overshoot region: from the boundary $r_{\rm c}$ of the unstable region to a point $r{=}r_{\rm cd}$ the stratification is assumed to be almost adiabatic, whereas between $r_{\rm cd}$ and the bottom $r_{\rm d}$ of the overshoot region there is a smooth sub-adiabatic transition to radiative stratification. This is considered just as a test for our method to analyse the signal and therefore has no physical grounds. However there are several aspects that can be represented by such a smooth transition. Even if the transition region is thin as expected by theoretical arguments, there may be time or position dependent variations of the location of this transition region in scales smaller than the period or length scales of the modes. The effect will be that modes will feel an average (over time or space) of this different positions simulating a smooth transition. Or, of course, our predictions may be wrong, so that the actual overshoot layer is predominantly sub-adiabatic. This corresponds to the other regime as discussed in Section 3.2 on the physical discussion of convective overshoot . We shall come back to this possibility in Chapter 5.

Table 3.3: Characteristics of the models. The parameter $\mathcal{D}$ gives the thickness of the transition while $\mathcal{C}$ characterises the fraction of it corresponding to the transition from adiabatic stratification to the radiative interior. The overshoot layer is modelled according to Eq. (3.2.2).

Model	$\mathcal{D}$	$\mathcal{C}$	$\frac{r_{\rm c}}{R}$	$\frac{r_{\rm cd}}{R}$	$\frac{r_{\rm d}}{R}$	$\frac{r_{\rm c}-r_{\rm cd}}{R}$	$\frac{r_{\rm c}-r_{\rm cd}}{H_P}$	$\frac{r_{\rm c}-r_{\rm d}}{R}$	$\frac{r_{\rm c}-r_{\rm d}}{H_P}$
W_1	0.05	1	0.72871	0.72871	0.71977	0.00000	0.00000	0.00894	0.11364
W_2	0.1	1	0.72862	0.72862	0.70522	0.00000	0.00000	0.02340	0.29737
W_3	0.1	2	0.72844	0.72061	0.70761	0.00783	0.09950	0.02084	0.26473
W_4	0.1	10^5	0.72822	0.71134	0.71134	0.01688	0.21431	0.01688	0.21434

The stratification for models of this nature, whose characteristics are given in Table 3.3, is illustrated in Fig. 3.6. There, the gradient in the overshoot region is shown. For comparison, we also show the gradient in models Z_0 (considered before) and W_4; the former is a standard model with no overshoot, the gradient changing from the adiabatic to the radiative value at the instability boundary, whereas the latter is an overshoot model with a very sharp transition. The new models are W_1, W_2 and W_3, which have a smoother

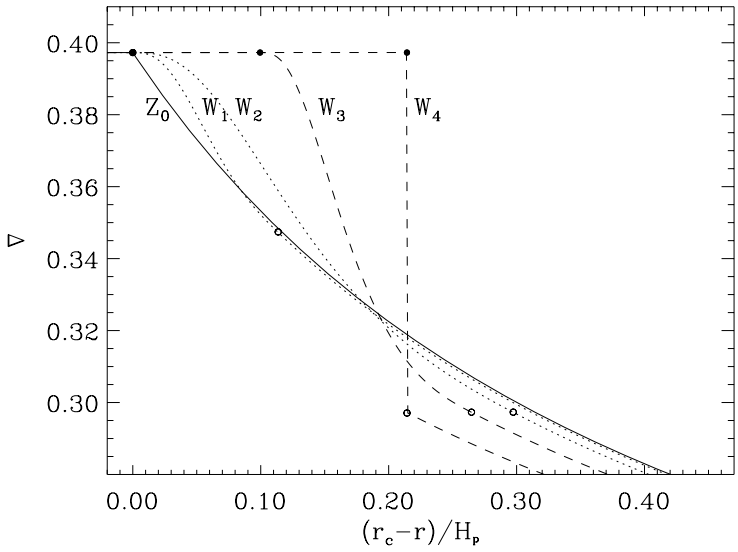

Fig. 3.6: Temperature gradient ∇ below the convection zone for five models (see the text and Table 3.3), plotted against the distance $r_c - r$ beneath the limit of the unstable region, in units of the pressure scale height H_P. Filled circles indicate the end of the adiabatically stratified layers while open circles show where the stratification becomes radiative.

transition from the adiabatic to the radiative value of the gradient in the overshoot region. For W_1 and W_2 there is no adiabatic stratification in the overshoot region, the models differing only in the extent of overshoot and hence of the smooth transition, while in W_3 half the overshoot region is adiabatically stratified, while the other half is the transition region.

3.3 Signal in the frequencies of oscillation

We now come to the point where we can compare the expected characteristics of the signal due to the base of the convection zone with the actual signal in the frequencies. First we take all the models calculated above and determine numerically their frequencies of oscillations. These were calculated as described in Appendix B, using a code for linear adiabatic nonradial oscillations. After having the frequencies we can then isolate the signal and by a least-squares method fit the expressions derived in the previous Chapter. These values can then be compared with the theoretically expected values according to our definitions of all six parameters.

In Table 3.4 the expected values of the parameters are given for all models we have described in the previous Section. Note that when comparing the expected values with the fitted ones, we must have in mind that the actual fit will give $\bar{\tau}_\mathrm{d}=\tau_\mathrm{d}+a_\phi$ and $\bar{\gamma}_\mathrm{d}=\gamma_\mathrm{d}+a_\gamma$

Table 3.4: Expected values for the parameters of the signal in all models considered. The amplitudes $a_1/2\pi$, $a_2/2\pi$ and $A_{2.5}/2\pi$ are all given in (μHz). While the acoustic depth $\tau_{\rm d}$ and a_ϕ are both given in (s) and $\gamma_{\rm d}/2\pi$ and $a_\gamma/2\pi$ in (μHz) also.

Model	$\frac{a_1}{2\pi}$	$\frac{a_2}{2\pi}$	$\frac{A_{2.5}}{2\pi}$	$\Delta_{\rm d}$	$\tau_{\rm d}$	a_ϕ	$\frac{\gamma_{\rm d}}{2\pi}$	$\frac{a_\gamma}{2\pi}$
Z_0	0.094	0.000	0.094	0.30	2069.3	200.6	12.12	1.43
Z_1	0.084	0.028	0.088	0.31	2076.6	200.7	12.33	1.42
Z_2	0.074	0.056	0.093	0.32	2087.0	200.9	12.64	1.42
Z_3	0.064	0.084	0.105	0.33	2098.0	200.7	12.97	1.43
Z_4	0.054	0.112	0.124	0.34	2109.7	200.6	13.34	1.42
Z_5	0.044	0.139	0.146	0.35	2122.3	200.6	13.74	1.43
Z_6	0.018	0.182	0.183	0.37	2154.9	201.0	14.84	1.42
Z_7	0.026	0.196	0.197	0.37	2150.5	200.7	14.68	1.40
Z_8	0.017	0.224	0.224	0.39	2166.5	200.7	15.25	1.42
Z_9	0.006	0.252	0.252	0.41	2184.2	200.6	15.90	1.43
Y_1	–	–	–	–	2068.5	201.0	12.10	1.43
Y_{1a}	–	–	–	–	2059.7	196.3	12.20	1.45
Y_2	–	–	–	–	2117.5	200.8	13.60	1.42
Y_{2a}	–	–	–	–	2120.7	198.9	13.59	1.43
Y_3	–	–	–	–	2116.4	201.0	13.54	1.40
Y_4	–	–	–	–	2160.0	200.9	15.02	1.44
Y_{4a}	–	–	–	–	2146.6	196.7	14.98	1.45
W_1	–	–	–	–	2095.5	200.7	12.90	1.43
W_2	–	–	–	–	2141.0	200.7	14.36	1.41
W_3	–	–	–	–	2133.6	200.7	14.11	1.43
W_4	–	–	–	–	2122.1	200.6	13.73	1.44

and not $\tau_{\rm d}$ and $\gamma_{\rm d}$ themselves.

The next step is then to use the p-mode frequencies of these models and submit them to a fitting procedure in order to find $(a_1, a_2, \bar{\tau}_{\rm d}, \bar{\gamma}_{\rm d}, \phi_0, \Delta_{\rm d})$. The actual function fitted is given in Eq. (2.6.15), with (2.6.3). The fitting procedure constructed to isolate the signal is described next in detail. It is not a trivial task to find a method which is insensitive to any of the other contributions to the frequencies coming from other sharp variations in the structure of the Sun.

The mode set also needs to be selected, in order to use the same modes for all models and for observational data. The main constraints determining the mode set to be used are of course the observationally available data and the physical restrictions on what modes can be used. One of these is, for example, the fact that only modes crossing the base of the convection zone can be affected directly by an overshoot layer. We also discuss what type of observational data is available and can be used.

Finally, we proceed to the determination of the signal characteristics. The results for all models and the Sun are presented in the last Sections. To determine the effect of observational errors on our results we constructed 100 realizations of randomly generated errors

and added these to the numerical frequencies of each model. The errors were independent and normally distributed with zero mean and standard deviations (which differed from one mode to another) given by the estimated uncertainties for the observational data of Libbrecht et al. (1990). In the light of the effect of the observational errors we can estimate the accuracy of the parameters found for the Sun (under the assumption that there are no systematic errors).

3.3.1 Method to isolate the signal in the frequencies

In this Section we outline the method developed to isolate the signal in the frequencies of oscillation given by Eq. (2.6.15) and hence determine the parameters $\overline{\tau}_{\rm d}$, $\overline{\gamma}_{\rm d}$, ϕ_0 and the function $A(\omega, l)$ as given in Eq. (2.5.7) with (2.6.3).

The basic idea is to fit all points ω_{nl}, for a given l, by a smooth function such as to leave in the residuals only the signal we are studying. The best values of the parameters for the signal are then obtained through a simultaneous least-squares fit to the residuals for different l. The smooth function must eliminate all variations of ω_{nl} on scales substantially longer than the contribution from the base of the convection zone which we wish to isolate, without affecting the characteristics of the latter. Oscillatory components in the frequencies arise from any region where the solar structure undergoes rapid variations (Gough 1990, Christensen-Dalsgaard & Pérez–Hernández 1992). Particularly significant is the region of second helium ionization near the surface, where the adiabatic exponent $\Gamma_1 = (\partial \ln P / \partial \ln \rho)_S$ (the derivative being at constant specific entropy S) changes rapidly on a short scale. This produces a corresponding signature in the sound speed, and hence induces an oscillatory signal in the frequencies, which is conceptually similar to the one we are considering although differing in the period and amplitude behaviour. We consider the possibility of using this signal to measure the helium abundance in Chapter 4. Such contributions are responsible for the difficulties surrounding the isolation of the signal from the base of the convection zone; care is required to avoid that they contaminate the inferred values of the parameters. This is achieved in our method through a gradual relaxation of the condition of smoothness in the fit; as a result, we are able to make a reliable determination of the parameters associated with the base of the convection zone.

Thus we have developed a process that will iterate on the six parameters to determine the minimum of

$$\mathcal{R} = \sum_l \left\{ \sum_n \left[(\omega_{nl} - \omega_{nl}^{(s)}) - f(\omega_{nl}) \right]^2 \right\} . \tag{3.3.1}$$

Here the function $f(\omega_{nl})$ is expressed as

$$f(\omega_{nl}) = \frac{1 - 2\Delta_{\rm d}\ \dfrac{l(l+1)}{\tilde{l}(\tilde{l}+1)}\ \left(\dfrac{\tilde{\omega}}{\omega_{nl}}\right)^2}{\left[1 - \Delta_{\rm d}\ \dfrac{l(l+1)}{\tilde{l}(\tilde{l}+1)}\ \left(\dfrac{\tilde{\omega}}{\omega_{nl}}\right)^2\right]^2} \quad \left[\frac{a_1^2\left(\dfrac{\tilde{\omega}}{\omega_{nl}}\right)^4}{1 - \Delta_{\rm d}\ \dfrac{l(l+1)}{\tilde{l}(\tilde{l}+1)}\ \left(\dfrac{\tilde{\omega}}{\omega_{nl}}\right)^2} + a_2^2\left(\frac{\tilde{\omega}}{\omega_{nl}}\right)^2\right]^{1/2}$$
$$\times\ \cos\left(2\omega_{nl}\overline{\tau}_{\rm d} - \overline{\gamma}_{\rm d}\ \frac{L^2}{\omega_{nl}} + 2\phi_0\right)\ , \tag{3.3.2}$$

with $\tilde{\omega}/2\pi$=2500μHz and $\tilde{l}$=20. The smooth frequency $\omega_{nl}^{(s)}$ is obtained separately for each degree l, by fitting a smoothing function of mode order n, to the reduced frequency

$$\omega_{nl}^{(r)} = \omega_{nl} - f(\omega_{nl})\ . \tag{3.3.3}$$

As smoothing functions are used the polynomials

$$\mathcal{P}_l(n) = \sum_{k=1}^{N_l} a_k^{(l)}\ n^{k-1}\ , \tag{3.3.4}$$

constructed for each l, given the N_l points $(n, \omega_{nl}^{(r)})$, by determining the values of the coefficients a_k (k=1, ..., N_l) that minimize

$$\sum_{i=1}^{N_l}\left\{\left[\mathcal{P}_l(n_i) - \omega_{n_i l}^{(r)}\right]^2 + \lambda\left(\frac{{\rm d}^3\mathcal{P}_l}{{\rm d}n^3}\right)_{n_i}^2\right\}\ . \tag{3.3.5}$$

The actual numerical procedure is not done in terms of ω and n but in normalized variables obtained from these with linear transformations to the interval $[-1, 1]$. It is done in order to normalized the effect/value of λ for all l values, with the added advantage that numerical errors are more strongly controlled. If λ=0, $\mathcal{P}_l$ will interpolate all points; however for non-zero λ the second term will try to reduce the third derivative of $\mathcal{P}_l$, making it smoother. The choice of a smoothing condition based on derivatives of frequency comes from the fact that components varying over a shorter scale in frequency dominate in higher derivatives. Therefore, we have selected the lowest derivative of $\omega(n)$ for which the signal from the base of the convection zone dominates over the signal from the helium ionization zone, and at the same time the smooth component of the frequencies is removed.

The actual numerical procedure consists in finding the parameters a_1, a_2, $\overline{\tau}_{\rm d}$, $\overline{\gamma}_{\rm d}$, ϕ_0 and $\Delta_{\rm d}$ minimizing $\mathcal{R}$ using two iterative cycles. The inner cycle iterates, given a value of λ, the values of the parameters in $f(\omega_{nl})$ in order to decrease $\mathcal{R}$; thus, using the same λ we repeat the cycle:

$$\text{find } \omega_{nl}^{(r)} \quad \rightarrow \quad \text{smooth } \omega_{nl}^{(r)} \quad \rightarrow \quad \text{fit } \left[\omega_{nl} - \omega_{nl}^{(s)}\right] \text{ by } f(\omega_{nl}).$$

This iteration is surrounded by an outer cycle, where λ is successively reduced by a factor two. In the initial step of these cycles we take $f(\omega_{nl})\equiv 0$ when determining $\omega_{nl}^{(r)}$, since in this step all parameters are unknown.

This group of steps will isolate from ω_{nl} a component of the form given by Eq. (3.3.2), returning the best values of the parameters, in a least-squares sense, characterizing the signal. The initial value λ_0 of λ determines the period of the signal to be isolated. If λ_0 is chosen to be larger, the smoothing step fails to remove the signal associated with the helium ionization zone, which would then dominate the least-squares fit (3.3.1). When studying overshoot, we have used the same λ_0 $(= 10^{-8})$, in the fits to all model and observed frequencies.

3.3.2 Selection of the mode set

The reason why we consider different solar envelope models is mainly because we will need ultimately to calibrate the amplitude in order to use solar frequency data. Therefore, our selection of the modes to be used in the analysis is dictated not only by physical reasons, like the fact that we can only choose modes that cross the base of the convection zone, but also by what data we have for the Sun.

There were different sets of data available at the time this analysis was done. As our starting point we have taken the data from the compilation by Libbrecht, Woodard & Kaufman (1990). Nowadays there is also the IRIS data (Toutain & Fröhlich 1992) and the more recent BISON data published in Elsworth et al. (1994). The latter have much better observational precision than the low degree data listed by Libbrecht et al.. However that data is still significantly noisier than moderate degree data and does not add much to the determination of the signal characteristics. So, such modes are not used in the analysis reported here. Nevertheless, we address the possibility of using low degree data in a latter Section, and present the signal for such data. In Fig. 3.7 we plot the region in the plan (l, ω) from which we select our set of modes. Also included are the more recent observations.

The first condition we have is that only modes that are reflected below $r\sim 0.7R$ can be used. This gives a condition for ω/L, plotted in Fig. 3.7 as a dotted line. We now introduce the observational limitations by demanding that the quoted observational error has to be smaller than 0.1μHz. This value has been chosen considering that the expected amplitude for a standard solar model is of the order of 0.1μHz (see Table 3.4). It is also necessary to eliminate any group of modes corresponding to an l value for which there is less than four consecutive (in mode order) frequencies, because we try to fit a polynomial using a smooth condition for the third derivative, so we need at least to have four points

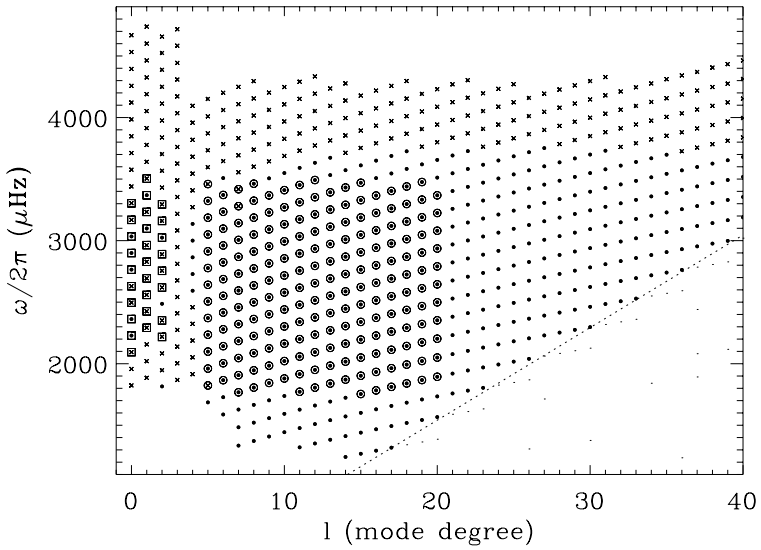

Fig. 3.7: Plot of solar seismic data from Libbrecht et al. (1990). The symbols are: filled circles are for quoted errors smaller than 0.1μHz while (x) is for frequencies with an error superior to that value. Also represented by small points are modes with their lower turning point above the base of the convection zone. The set of modes selected for our analysis is indicated by open circles around the symbol for that mode. Also indicated as squares are data from Elsworth et al. (1994) having quoted observational errors below our limit of 0.1μHz.

to be able to do so. We further ignore high degree modes since our expansion in terms of the Lamb frequency is only valid for small S_l^2/ω^2 (Eqs. (2.6.5) and (2.6.9)). Low frequency modes whose frequencies are dominated by the signal from the second helium ionization zone are also omitted. These two limits when imposed led us to remove all $l>20$ and $\omega/2\pi<1800\mu$Hz modes.

After applying all restrictions our selected set ended with 197 modes having degrees between 5 and 20 (inclusive) and for frequencies between 1800 and 3500μHz. In the main results presented here we have not used the data for low-l (l=0−4) modes. However we consider briefly their possible use in the light of the recent improvements on the observation of solar and stellar oscillations.

Note that the observational uncertainties σ_{nl} have not been included in the expressions (3.3.1) and (3.3.5) used in the method to isolate the signal. Because σ_{nl} increases with ω or n, as shown in Fig. 3.8, taking the uncertainties into account in the least-squares fits would give relatively more weight to low-frequency data, where the signal from the helium ionization zone has a larger amplitude. The result would be a systematic error in the inferred value of $\overline{\tau}_{\rm d}$ due to the contamination of the smooth function from such a signal, as well as of the fitting. One can of course take the uncertainties on individual mode frequencies into account while introducing an extra weighting to compensate for the

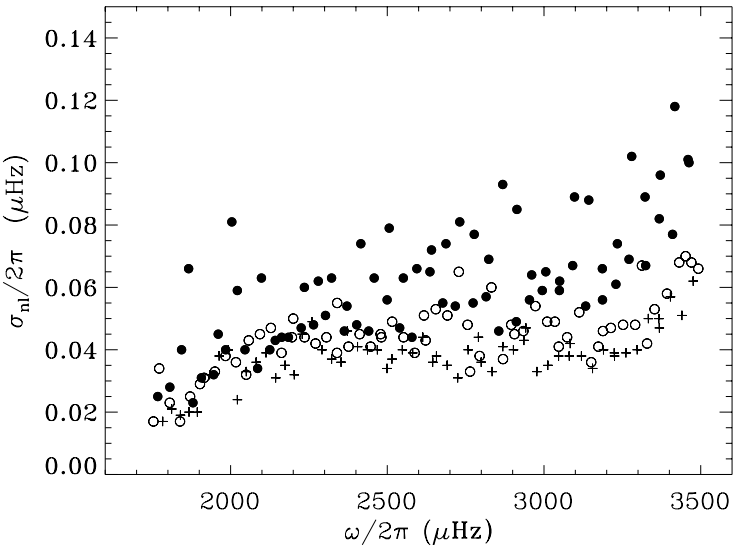

Fig. 3.8: Plot of the quoted observational errors for modes used in this work and taken from the data of Libbrecht et al. (1990). The symbols are: fill circles for $5 \leq l \leq 10$, open circles for $11 \leq l \leq 15$ and crosses for $16 \leq l \leq 20$.

general trend of the uncertainties with frequency, but we have chosen not to do so, given the arbitrariness of such a weighting.

3.3.3 Results for the models

We have submitted the frequency sets for all models to our method to isolate the signal. The same set of frequencies is always used for every model considered, and the process each set goes trough is also the same. In order to estimate the effect of the observational errors we calculate the effect of these through the fitting procedure by considering 100 sets of realizations of randomly generated errors, with the σ from the corresponding solar modes as quoted by the observers, added to the frequencies.

The results obtained for all models are given in Table 3.5 - both the mean values and the standard deviations. The results for error free data are not shown since they are in very good agreement with the results from averaging over the 100 realizations, indicating that random data errors do not introduce any significant systematic error into our procedure. As expected, the amplitude increases with the extent of the overshoot layer. We plot in Fig. 3.9 the comparison between the amplitude $A_{2.5}$ from the fit and the function obtained from the models by using expression (2.5.10). The results of the fit if we neglect the contribution from $\Delta_{\rm d}$ are also shown. The effect on $A_{2.5}$ of neglecting Δ is very small. There is a more significant effect on the value of $\bar{\gamma}_{\rm d}$: this is natural, given that

Table 3.5: List of the inferred values of $A_{2.5}/2\pi$ (μHz) ($A_{2.5}$ being the amplitude evaluated at $\omega/2\pi$=2500μHz and l=0), $\overline{\tau}_{\rm d}$ (s), $\overline{\gamma}_{\rm d}/2\pi$ (μHz), ϕ_0 (rad) and $\Delta_{\rm d}$, resulting from fitting expression (3.3.2) to the frequencies of the models. The mean values and the standard deviation for 100 error realizations of randomly generated errors, with the corresponding solar σ value added to the frequencies of the models, are both shown.

Model	Mean values					Standard deviation				
	$\overline{\tau}_{\rm d}$	$\frac{\overline{\gamma}_{\rm d}}{2\pi}$	ϕ_0	$\frac{A_{2.5}}{2\pi}$	$\Delta_{\rm d}$	$\sigma_{\overline{\tau}_{\rm d}}$	$\frac{\sigma_{\overline{\gamma}_{\rm d}}}{2\pi}$	σ_{ϕ_0}	$\frac{\sigma_{A_{2.5}}}{2\pi}$	$\sigma_{\Delta_{\rm d}}$
Z_0	2258.3	11.6	1.31	0.0756	0.32	22.2	2.9	0.34	0.0092	0.03
Z_1	2261.2	12.5	1.30	0.0826	0.33	21.6	3.2	0.34	0.0084	0.02
Z_2	2268.6	12.1	1.19	0.0867	0.33	19.4	2.7	0.29	0.0085	0.02
Z_3	2283.0	12.3	1.07	0.1072	0.32	16.3	1.9	0.25	0.0090	0.02
Z_4	2293.6	13.3	1.00	0.1201	0.32	16.9	1.7	0.27	0.0093	0.02
Z_5	2310.4	13.1	0.89	0.1438	0.31	14.6	1.4	0.23	0.0085	0.01
Z_6	2326.8	13.8	0.81	0.1656	0.30	11.0	1.4	0.18	0.0093	0.01
Z_7	2346.0	14.2	0.71	0.1925	0.30	10.1	1.1	0.16	0.0117	0.03
Z_8	2366.3	14.8	0.63	0.2178	0.30	08.4	1.2	0.13	0.0104	0.01
Z_9	2383.6	16.1	0.56	0.2430	0.30	08.0	1.1	0.13	0.0106	0.01
Y_1	2262.9	11.5	1.25	0.0778	0.32	24.4	2.7	0.39	0.0080	0.03
Y_{1a}	2247.5	12.0	1.45	0.0776	0.32	24.9	2.8	0.39	0.0087	0.04
Y_2	2309.3	12.7	0.81	0.1350	0.31	14.2	1.7	0.23	0.0082	0.02
Y_{2a}	2325.3	13.2	1.02	0.0874	0.20	21.9	2.4	0.34	0.0097	0.12
Y_3	2328.2	13.4	0.97	0.1106	0.27	18.9	1.9	0.28	0.0089	0.08
Y_4	2359.3	14.5	0.60	0.2110	0.30	08.6	1.1	0.14	0.0095	0.01
Y_{4a}	2346.2	14.3	0.81	0.2168	0.30	09.1	1.0	0.14	0.0097	0.01
W_1	2267.2	11.6	1.19	0.0836	0.32	22.2	2.8	0.32	0.0090	0.02
W_2	2280.1	12.2	1.09	0.0938	0.32	20.5	2.3	0.31	0.0095	0.02
W_3	2299.7	12.5	0.90	0.1227	0.31	15.2	1.8	0.24	0.0083	0.02
W_4	2317.6	13.0	0.78	0.1491	0.31	11.4	1.4	0.18	0.0090	0.02

$\bar{\gamma}_{\rm d}$ determines the dependence on degree of the argument of the signal (cf. Eq. (2.6.10)). Comparison of the values of the amplitude predicted by Eq. (2.5.10) with the ones found by the fitting shows good agreement for overshooting distances larger than $0.1H_P$. However, for small overshoot distances the fit seems to give systematically smaller values. Also, the expression for the variational principle displays a local minimum in the amplitude at small overshoot distance, first noted by RV using their simplified expression for the amplitude. It was seen already for the predictions shown in Fig. 3.3. It is interesting that the fit does not show such a minimum, although there is a noticeable departure from linearity at small $r_{\rm c}-r_{\rm d}$. We return to this point later.

Other important information in the signal is of course the frequency dependence of the amplitude. To see how this may be used we illustrate in Fig. 3.10, $(\omega/\tilde{\omega})^2 A(\omega)$ for some of the models. As predicted by Eq. (2.5.7) the frequency dependence of the amplitude differs by a factor of ω between models with and without overshoot. This is particularly evident from a comparison of Models Z_3 and Y_3 where the overall level of the amplitude is

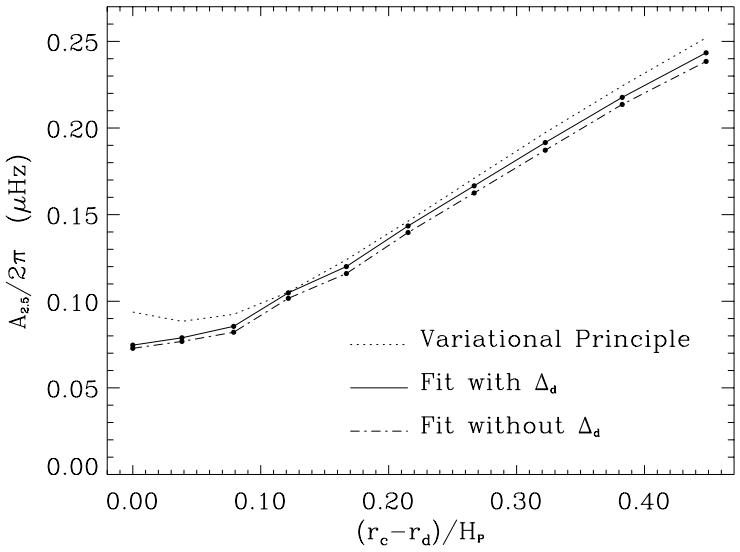

Fig. 3.9: Plot of the amplitude $A_{2.5}$ for models Z_{0-9} (filled circles). The continuous line corresponds to the values given by the fit if the dependence of the amplitude on the mode degree is considered. The dot-dashed line corresponds to neglect the degree dependence of the amplitude by fitting with Δ_d=0. The theoretical values, as predicted by expression (2.5.10), are also plotted (dotted line) for all models.

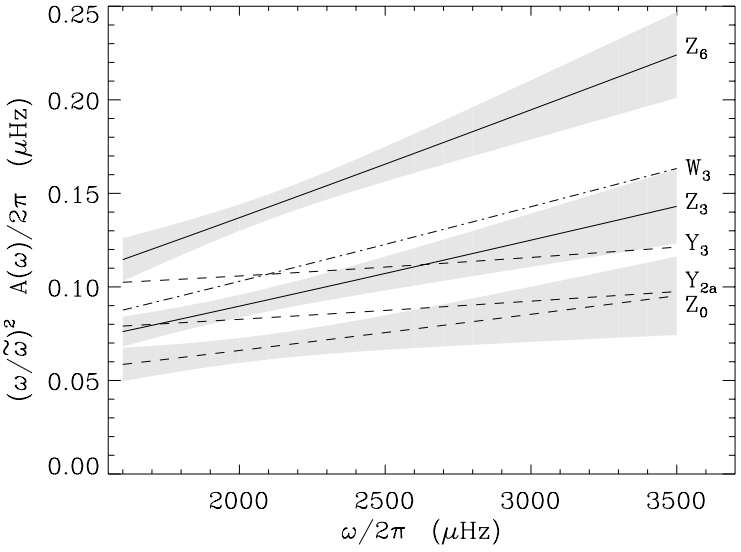

Fig. 3.10: Inferred amplitudes multiplied by $(\omega/\tilde{\omega})^2$ (cf Eq. (2.5.7) with l=0) for some models as indicated; the shadowy areas show 1σ deviations obtained from 100 error realizations for those models (all other models have a similar behaviour). Dashed lines are used for models without overshoot while continuous lines are for models with overshoot (Z type models - see Table 3.1). Also shown is a model with a smoother transition at the base of the overshoot layer (dash-dotted line).

similar (having very similar amplitudes at $\omega/2\pi$=2500μHz); these results suggest that the frequency dependence of the amplitudes might be used to distinguish between overshoot and a localized change in the opacity. However, we caution that the distinction in $A(\omega)$ between overshoot and non-overshoot models can be blurred by the presence of data errors. For significant amounts of overshoot the variation with $(\omega/\tilde{\omega})$ of the amplitude is quite clear, and so in this limit we can safely hope to use this dependence if the Sun presents such a behaviour.

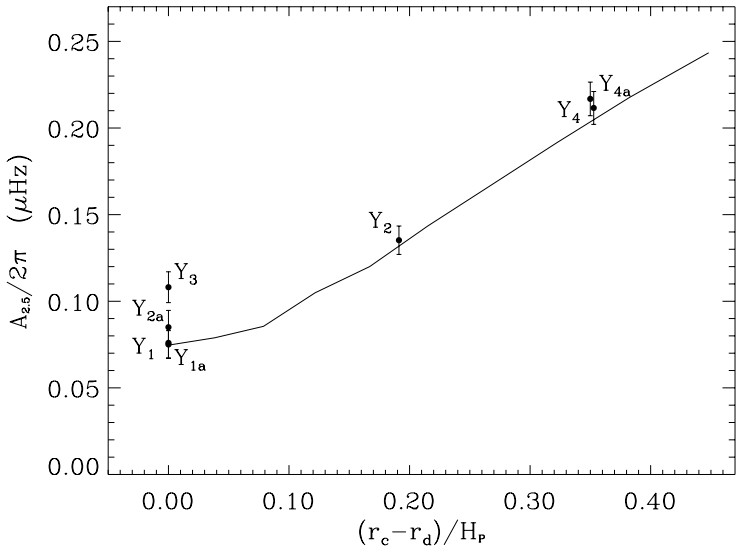

Fig. 3.11: Amplitude $A_{2.5}$ of the signal, in terms of cyclic frequency, at $\omega/2\pi$=2500μHz, versus penetration depth r_c-r_d for all Y models (see text). The continuous line is the result for the ten overshoot (Z) models shown before.

The effect of changes in other aspects of the physics on the value of $A_{2.5}$ are plotted in Fig. 3.11. The model with a localized increase in opacity (Y_3) has a fairly large amplitude which, though smaller than the corresponding overshoot model Y_2, comes close to the amplitude for Model Z_3. However we note that the behaviour of the amplitude with frequency differs significantly between the two. Models with neither overshoot nor a very localized opacity increase have substantially smaller amplitudes. The two pairs of models; (Y_1,Y_{1a}) and (Y_4,Y_{4a}) which differ only in their surface layers do not show a significant difference in the amplitude for the signal. However the value of $\bar{\tau}_d$ found varies by up to 15s, as we would expect due to the changes in sound speed near the surface coming from the difference in surface opacities (see Fig. 3.5). As discussed in Chapter 2, the inferred "depth" $\bar{\tau}_d$ is a poor estimate of the actual acoustic depth τ_d of the base of the adiabatic layer but is rather an estimate of τ_d+a_ϕ (cf. Eqs. (2.6.11) and (2.6.14)). For the models considered the values of a_ϕ are very similar, all being of the order of 200s (Table 3.4).

Therefore the inferred value of $\bar{\tau}_{\rm d}$ can adequately be corrected, within the accuracy of approximating ϕ by expression (2.6.9), to give an estimate of the actual acoustic depth. The overall standard deviations are reasonably modest. In particular, the uncertainty in the amplitude (less than ~ 0.01) is small ($\lesssim 10\%$ of $A_{2.5}$). The uncertainty in the inferred $\bar{\tau}_{\rm d}$ is up to 25s for models without overshoot and less than 15s for models with significant convective penetration. The systematic change with penetration distance is as one would expect, given that the signal amplitude for the larger distances is greater, so that the signal characteristics should be easier to determine.

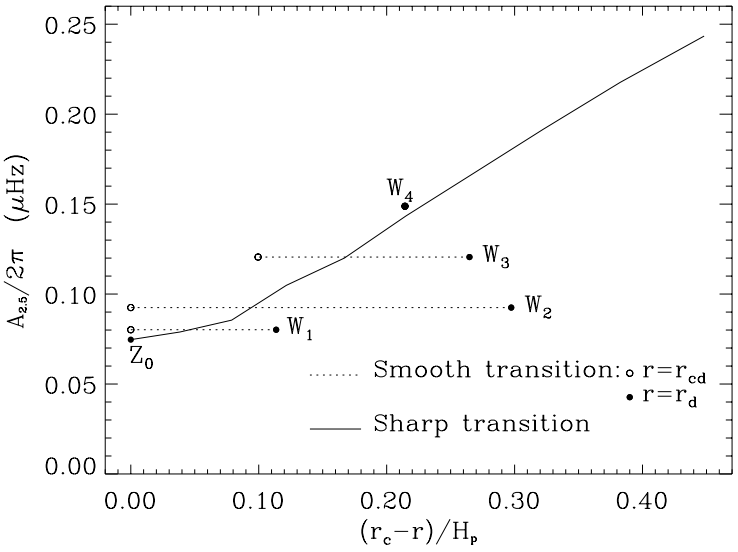

Fig. 3.12: Plot of amplitude versus penetration distance for the overshoot models $Z_0 - Z_9$ (continuous line) and the new models $W_1 - W_4$. For these models we represent as a dashed line the region between the point $r_{\rm cd}$ (open circle) where the region starts deviating from the adiabatic gradient and the point $r_{\rm d}$ (filled circle) where the gradient is finally radiative.

In order to understand how the assumption of a sharp transition to radiative stratification at the base of the overshoot layer affects the results, we have considered above models W (see Table 3.3). In Fig. 3.12 each of these is indicated by a horizontal line at the amplitude obtained from the fit: the left-hand end corresponds to the radius $r_{\rm cd}$ where the adiabatic stratification imposed by the overshoot ends, and the right-hand end corresponds to the point $r_{\rm d}$ where the stratification finally becomes radiative. Interestingly, even though the gradients in models $W_1 - W_3$ are smooth, the transition gives rise to a larger maximum value of $|{\rm d}\nabla/{\rm d}\tau|$ than for the non-overshoot model; thus, on the scale of the modes the behaviour mimics that of an overshoot model, causing a modest increase in the amplitudes. This is similar to what happen for the model with a localized change in the opacities; Y_3. The fitted amplitudes for the smooth models can be converted to a

distance scale by calibrating against the fitted amplitudes of models with sharp overshoot regions. The inferred effective extent of overshoot for the smooth models is greater than the extent of the exactly adiabatic region (open circles) but less than the distance from the base of the convective unstable region to the point where the stratification becomes radiative (filled circles). Roughly speaking, one may say that the fitted amplitude is an indicator of the extent of the region which is adiabatic to within ∼80% of ∇_a.

3.3.4 Results for observational data

The solar data of Libbrecht, Woodard & Kaufman (1990) were used in this study. The modes were selected according to the criteria discussed in Subsection 3.3.2, leaving a set of 197 modes with $5 \leq l \leq 20$ and $1800\mu\text{Hz} \leq \omega/2\pi \leq 3500\mu\text{Hz}$, having a mean for the quoted errors of $\sim 0.05\mu$Hz (cf. Fig. 3.8). This set of modes was used also for the tests on models, described before, and the same procedures were used on both observational and artificial data.

Table 3.6: List of the inferred values of; $\overline{\tau}_d$ (s), $\overline{\gamma}_d/2\pi$ (μHz), ϕ_0 (rad), $A_{2.5}/2\pi$ (μHz), and Δ_d, resulting from fitting expression (3.3.2) to solar frequencies given by Libbrecht et al. (1990).

	$\overline{\tau}_d$	$\frac{\overline{\gamma}_d}{2\pi}$	ϕ_0	$\frac{A_{2.5}}{2\pi}$	Δ_d
Sun	2336.5	12.98	0.64	0.0853	0.29

The results of fitting the solar data are given in Table 3.6. In Fig. 3.13 the solar signal isolated, with the error bars from the quoted observational errors, is plotted. It is clear that the signal is well defined and above the observational uncertainties for this set of modes. Note that as expected, the amplitude of the solar signal is marginally above our upper limit on the quoted observational errors used when selecting the frequencies. This means, as discussed in Subsection 3.3.2, that the low degree data given by Libbrecht et al. (1990) can not be used.

However, the same is not true for the more recent observations of low-l modes (Toutain & Fröhlich 1992 and Elsworth et al. 1995) which have on average an observational error below this limit. There is still the problem for l=4, since no frequency for these modes have been observed with sufficiently high accuracy. The signal obtained when using Elsworth et al. data is shown in Fig. 3.14 where it is possible to see that the error bars are still to high, removing any possible advantage in using this low degree frequencies to isolate the signal. But in the case of having only very low l modes we note that a detection of

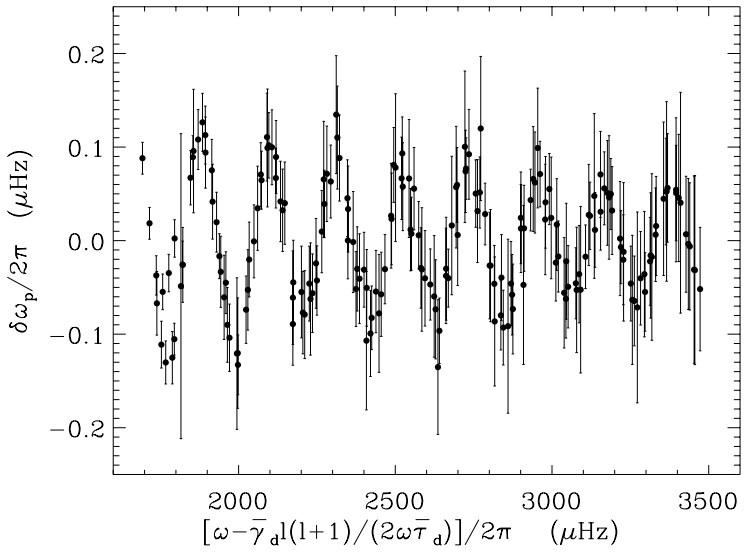

Fig. 3.13: Solar signal versus reduced frequency. The error bars correspond to the observational errors for the solar data as quoted by Libbrecht et al. (1990).

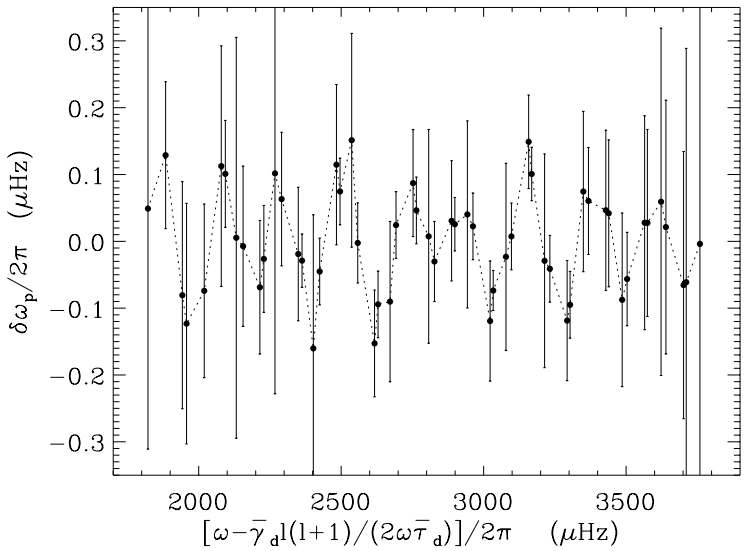

Fig. 3.14: Solar signal versus reduced frequency for modes with $l \leq 3$ from data of Elsworth et al. (1994). Note that the errors are still to high when compared with error bars in the previous figure. The dotted line connects consecutive points to guide the eye.

the signal is already marginally possible for observational errors as in the low l solar data considered.

When looking to the values that have been obtained for the Sun, given in Table 3.6,

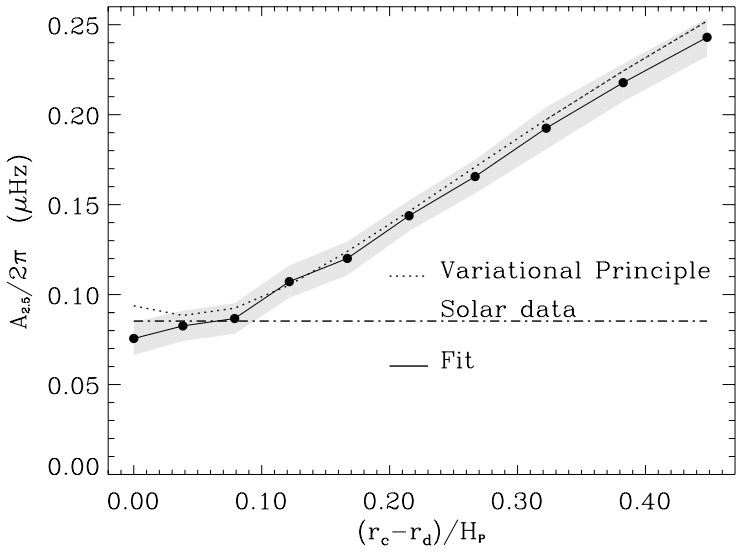

Fig. 3.15: Plot of the amplitude $A_{2.5}$ for the fit (continuous line) and the expression from the variational analysis (dotted line) for all models Z_{0-9}. The result for the solar data (see Table 3.6) is also plotted. The shaded area indicates the error as determined from 100 error realizations for the models.

the basic information from the signal we hope to use is the amplitude. We can now take the values found for the models to compare with solar result. This comparison is presented in Fig. 3.15 where the amplitude for the models is plotted, with the corresponding errors from the error realizations, together with the solar value. The solar data have a lower amplitude than most of the overshoot models. On the other hand, the solar amplitude is over 1 s.d. greater than those of Model Z_0 (a standard model), and is closest to the overshoot Model Z_2. Although the statistical analysis is somewhat uncertain, a simple reading of Fig. 3.15 gives an estimate that overshoot of the nature considered here does not exceed $0.1H_P$ in the Sun, or using Fig. 1.4, $0.008R$. In terms of acoustic depth the Sun is between Models Z_6 and Z_7, indicating a deeper convection zone than for standard Model Z_0.

Having in mind the difficulties of using it, Fig. 3.16 also suggests that the solar data favour the frequency dependence of the amplitude shown by models with modest overshoot (i.e., $A(\omega) \propto 1/\omega^2$) instead of models with large overshoot layers (with $A(\omega) \propto 1/\omega$). Indeed, for the entire frequency interval considered the solar amplitude is within 1σ of the amplitude found for model Z_2 or W_1 as shown in the figure. Note that the latter is a model without overshoot but having a smooth transition such as the gradient does not become radiative at the Schwarzschild boundary, simulating a weak thermodynamic impact of convection below this transition.

The values of ϕ_0 (see Table 3.5) also show a systematic variation with extent of the

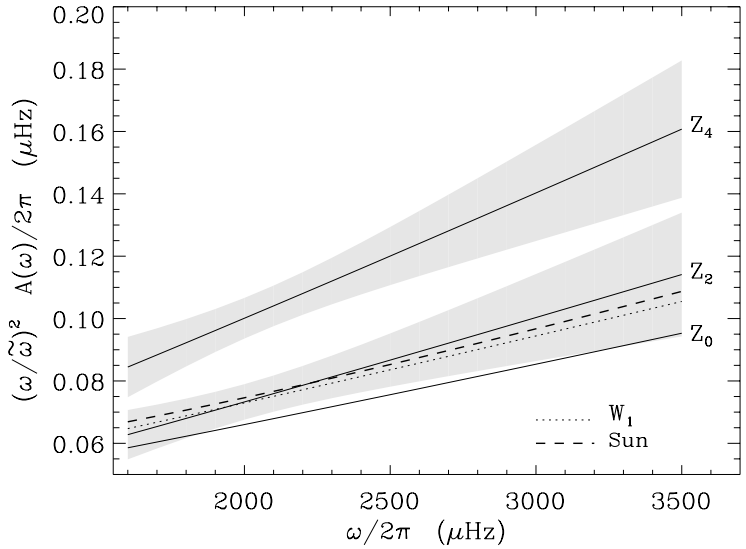

Fig. 3.16: Inferred amplitudes multiplied by $(\omega/\tilde{\omega})^2$ for some models, as indicated, and the Sun. The shadowy areas show 1σ deviations obtained from 100 error realizations for models Z_2 and Z_4. The behaviour obtained for solar data is shown as a thick dashed line, while continuous lines are for overshoot models and the dotted line for a model with a smooth transition to radiative stratification.

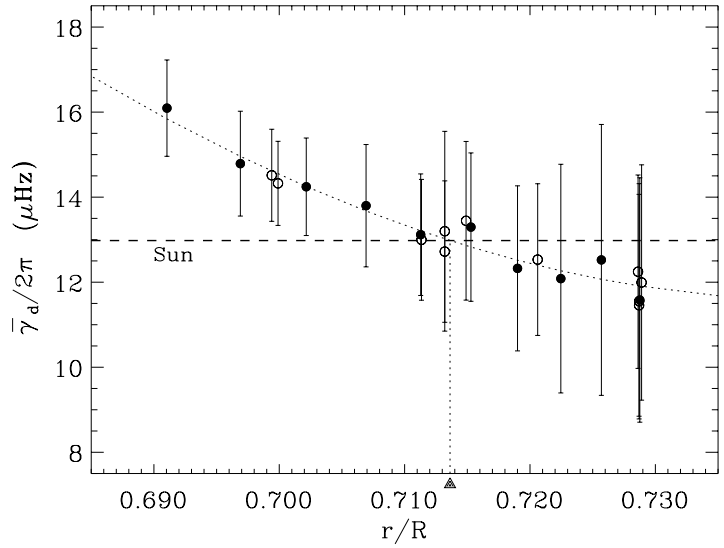

Fig. 3.17: Plot of $\overline{\gamma}_{\rm d}$ versus the radial position of the base of the convective envelope for all models. The error bars correspond to the standard deviation for 100 error realizations while the thick dashed line is the value inferred for the solar data. The dotted line is a least square fit of a polynomial to all points. Open circles represent both Y and W models while filled circles are for the Z models.

overshoot layer, in accordance with expectations. However, the still high uncertainties

due to the observational errors, make ϕ_0 of little use yet for analyzing the solar data. As mentioned in Section 2.6.3, $\overline{\gamma}_{\rm d}$ should in principle be less sensitive to the surface layers of the Sun, and therefore give a better estimate of the position of the base of the adiabatically stratified region, than $\overline{\tau}_{\rm d}$. Fig. 3.17 shows $\overline{\gamma}_{\rm d}$ versus $r_{\rm d}$ for all models, with error bars given by the 1σ deviations found from the 100 error realizations. The value obtained for the solar data is shown as a dashed line. The observational errors clearly limit the accuracy with which we may currently determine the solar value of $\overline{\gamma}_{\rm d}$; however, it seems to confirm that $r_{\rm d}$ is between $0.71R$ and $0.72R$, in accordance with the value found by Christensen-Dalsgaard, Gough & Thompson (1991). Obviously, this statement assumes that the contribution from a_γ can be considered as a shift in Fig. 3.17, not strongly affecting the relative positions on the plot. From Table 3.4, we see that $a_\gamma/2\pi$ varies from model to model by at most 0.05μHz. Provided the differences in the surfaces layers of the models reflect the possible differences between models and the Sun, we conclude that this corresponds to an uncertainty in $r_{\rm d}$ from $\overline{\gamma}_{\rm d}/2\pi$ of about $5\times10^{-4}R$. This is much smaller than the uncertainty introduced in the determination of $r_{\rm d}$ from $\tau_{\rm d}$ due to the uncertainties in the sound speed behaviour near the surface as determined from helioseismic inversions. We cannot exclude, however, that neglected effects in the near-surface layers of the Sun might make additional significant contributions to $\overline{\gamma}_{\rm d}$, beyond those that have been considered here. Nonetheless, $\overline{\gamma}_{\rm d}$, may well prove very useful as an extra position indicator, especially if more accurate data become available (the reduction to half of the present uncertainties would allow a meaningful determination of $r_{\rm d}$) for the determination of $\overline{\gamma}_{\rm d}$.

3.3.5 Comparison with other methods

By calibrating the amplitude for ten models with different overshoot distances we may put an upper limit to the extent of the overshoot layer at the base of the solar convective envelope of $0.008R$ (corresponding to $0.1H_P$, where H_P is the local pressure scale height). Also using the assumption that the transition is sharp, other authors: Basu et al. 1994; Gough & Sekii 1994; Roxburgh & Vorontsov 1994, have also inferred that the extent of any overshoot region if present is much less than one pressure scale height. For example, the findings of Basu et al. (1993) are very similar to ours. They have extended the idea of using second differences of frequencies to higher-order differences. Provided this is not taken too far, it enhances the signal from the base of the convection zone without the effect of data errors becoming dominant. Basu et al. conclude that a two-sigma upper limit of $0.1H_P$ can be placed on the extent of overshoot.

Some alternative works which deal with the use of this signal have also been briefly

discussed. However, the only other theoretical expression for the amplitude for such a signal has been given by Roxburgh & Vorontsov (1994). Their result is reproduced using our analysis. They also use a power law for the opacity to write the terms that appear as the radiative gradient or its derivative in our expression. Their method does give almost the same expression when used together with our analysis. The main advantage of using the variational principle is that correction terms of about 10 per cent in magnitude can be included, together with the dependence of the amplitude on the degree of the modes. These two effects can account for up to 20 per cent of the amplitude associated with the term in the third derivative of the sound speed.

4. Second helium Ionization Zone

One of the present problems in solar physics is the determination of the envelope helium abundance. We propose to extent the fitting method developed in the previous Chapter in order to determine this abundance. Because the second helium ionization zone is confined to a very thin region the effects on the structure can be treated as the result of a localized perturbation to an otherwise smooth behaviour. Therefore, we may hope to be able to measure the amplitude of the periodic signal in the frequencies due to such a layer. This amplitude is dependent on the surface helium abundance.

By using solar models with different helium abundances we attempt to calibrate the amplitude for application to solar data. Two important factors determine how meaningful an answer from such a calibration is. These are the equation of state used to construct the models for the calibration and the observational uncertainties. Both are discussed and some suggestions are made on how to improve the results found.

4.1 Introduction

When modelling the structure of the Sun we usually use the helium abundance by mass as a fitting parameter in order to adjust the luminosity to its observed value (see Appendix A). If the value we find from the calculations could be compared with the actual solar helium abundance an extra restriction on the physics of the models would be available. However, because all important helium lines fall into the ultraviolet or infrared parts of the spectrum, being produced in the chromosphere and corona under conditions which largely deviate from local thermodynamic equilibrium, the error in the observational determination of the helium abundance is far too large. Any other method, as measuring the abundance in the solar wind, provides even worse measurements of what the actual helium abundance in the solar envelope is.

With the observation of solar oscillations of very high precision some attempts have been done using these data to measure seismologically the abundance; Däppen & Gough (1986); Däppen, Gough & Thompson (1988); Dziembowski, Pamyatnykh & Sienkiewicz (1991); Vorontsov, Baturin & Pamyatnykh (1991, 1992); Guzik & Cox (1992); Kosovichev (1993);

Pérez Hernández & Christensen-Dalsgaard (1994) and Basu & Antia (1995). However the dependence of the results on the errors and also on the equation of state used in the reference models poses a serious problem (e.g. Kosovichev et al. 1992, Antia & Basu 1994). Here we propose an alternative by using the method described in the previous Chapters, and developed to study convective overshoot. Sharp/localized variations in the structure of the Sun (as the one occurring at the base of the convective envelope) create a periodic signal in the frequencies of oscillation. The characteristics of such a signal are related to the location and thermodynamic properties of the star at the point where the sharp variation occurs. The study of such a signal coming from the zone of the second ionization of helium can provide information regarding the solar envelope helium abundance. Such a signal has also been used by Vorontsov, Baturin & Pamyatnykh (1991, 1992), Pérez Hernández & Christensen-Dalsgaard (1994) or Gough & Vorontsov (1995), but in the phase function and not directly in the frequencies. Pérez Hernández & Christensen-Dalsgaard (1994), for example, have given a value of Y=0.242 $\pm$ 0.003 based on variations of the amplitude of the signal with abundance.

By using a variational principle we first determine how the second helium ionization zone through the derivative of the squared sound speed can indeed be considered a localized perturbation to an otherwise "smooth" model. In the next section we present the analysis and the predicted characteristics of the signal. We then consider the frequencies of several models which have different envelope helium abundances and have been calculated with different equations of state to compare the measured amplitudes by fitting the signal and the predicted values. In this way we also calibrate the method which is then applied to the observed solar data of Libbrecht et al. (1990). The Chapter ends with some considerations on how to improve and extend the results obtained here.

4.2 Frequency changes

In order to establish by how much the frequencies are affected due to the region of second ionization of the helium we shall take again a variational principle for nonradial linear adiabatic oscillations. As discussed in Section 1.3.4, in writing it we have assumed zero pressure at the surface located at radius R as a boundary condition and since we are considering high-order acoustic modes, we also neglect the perturbation in the gravitational potential. The expression used here is as given in Eq. (1.3.42) with (1.3.43) where now the model differences are associated with the region of the second ionization zone of the helium. The smooth model relatively to which we calculate the differences is of course a model without the second ionization of helium.

One of the thermodynamic quantities entering in the oscillations equations which is

more strongly affected by the ionization is the adiabatic exponent Γ_1. In order to obtain the dominant contributions to the frequencies from such a region we must write the variational principle in terms of model changes that better represent the presence of ionization. With this objective we have considered a variable θ associated with the derivative of the squared sound speed, and so, to the derivative of Γ_1, normalized by gravity. This is similar to the method used for overshoot, with the difference being that now it is not discontinuities that we model but a "bump" in θ confined to a narrow region in acoustic depth. By integrating for such a behaviour of the model differences we can write an expression for the signal in the frequencies.

4.2.1 Variational analysis

The variational principle has been written in a form (see Chapter 2) that gives the frequency changes in terms of products of three functions δB_i and the eigenfunctions. These δB_i's describe the variations between the actual star and the reference star (without the second ionization of helium). The change in the eigenvalues ω due to these differences are given from these functions according to;

$$\delta\omega^2 = \frac{\delta I}{I_1} \, . \tag{4.2.1}$$

Where,

$$I_1 \sim \frac{1}{2} \, \tau_t E_o^2 \, , \tag{4.2.2}$$

and

$$\delta I \sim \int_0^{\tau_t} \left[\left(\delta B_1 + \frac{\mathrm{d}\delta B_0}{\mathrm{d}\tau} \right) E_r^2 + \delta B_2 \, \frac{\partial E_r^2}{\partial \tau} + \delta B_3 \, \frac{\partial^2 E_r^2}{\partial \tau^2} \right] \mathrm{d}\tau \, . \tag{4.2.3}$$

Here, τ_t is the total acoustic depth of the Sun and E_r the normalized radial eigenfunction (see (1.3.18)) of constant amplitude E_o^2. The δB_i's are as given in (2.3.13) to (2.3.16) but now in terms of $\delta\rho$ and δc^2;

$$\delta B_0 = - \frac{g}{c} \, \frac{\delta\rho}{\rho} \tag{4.2.4}$$

$$\begin{aligned} \delta B_1 = \; & \left\{ - \frac{\omega^2}{1-\Delta} + \frac{2g}{c} \, \frac{\mathrm{d}}{\mathrm{d}\tau} \log\left(\frac{g}{\rho c}\right) - \frac{1-3\Delta/2}{1-\Delta} \, \frac{2g}{c} \, \frac{\mathrm{d}}{\mathrm{d}\tau} \log\left(\frac{r^2}{\rho c}\right) - \right. \\ & \left. - \frac{1}{4} \, \frac{1}{(1-\Delta)^2} \left[\frac{\mathrm{d}}{\mathrm{d}\tau} \log\left(\frac{r^2}{\rho c}\right) \right]^2 + \frac{\Delta(1-3\Delta/2)}{(1-\Delta)^2} \, \frac{2g^2}{c^2} \right\} \frac{\delta c^2}{c^2} + \\ & + \left\{ \frac{g}{c} \, \frac{\mathrm{d}}{\mathrm{d}\tau} \log\left(\frac{g}{\rho c}\right) - \frac{1}{1-\Delta} \, \frac{g}{c} \, \frac{\mathrm{d}}{\mathrm{d}\tau} \log\left(\frac{r^2}{\rho c}\right) - \right. \end{aligned}$$

$$- \frac{1}{4} \frac{1}{1-\Delta} \left[\frac{\mathrm{d}}{\mathrm{d}\tau} \log\left(\frac{r^2}{\rho c}\right)\right]^2 + \frac{\Delta}{1-\Delta} \frac{g^2}{c^2} \Bigg\} \frac{\delta\rho}{\rho} \tag{4.2.5}$$

$$\delta B_2 = - \left\{ \frac{1-3\Delta/2}{(1-\Delta)^2} \frac{2g}{c} - \frac{1}{2} \frac{1-2\Delta}{(1-\Delta)^2} \frac{\mathrm{d}}{\mathrm{d}\tau} \log\left(\frac{r^2}{\rho c}\right) \right\} \frac{\delta c^2}{c^2} -$$

$$- \left\{ \frac{1}{1-\Delta} \frac{g}{c} - \frac{1}{2} \frac{1}{1-\Delta} \frac{\mathrm{d}}{\mathrm{d}\tau} \log\left(\frac{r^2}{\rho c}\right) \right\} \frac{\delta\rho}{\rho} \tag{4.2.6}$$

$$\delta B_3 = \frac{1}{2} \frac{1}{1-\Delta} \frac{\delta c^2}{c^2} + \frac{1}{2} \frac{1}{(1-\Delta)^2} \frac{\delta\rho}{\rho} \, . \tag{4.2.7}$$

We consider again an interval $[\tau_\mathrm{a}, \tau_\mathrm{b}]$, with $0<\tau_\mathrm{a}<\tau_\mathrm{b}<\tau_t$ and $\tau_\mathrm{b}-\tau_\mathrm{a} \ll \tau_t$, such that $\delta c^2/c^2$, $\delta\rho/\rho$ and all their derivatives are equal to zero outside it. Integrating by parts δI we obtain

$$\delta I = \int_{\tau_\mathrm{a}}^{\tau_\mathrm{b}} \left[\frac{\partial \delta B_1}{\partial \tau} \overline{E}_r^2 + \frac{\partial}{\partial \tau} (\delta B_2 + \delta B_0) E_r^2 + \frac{\partial \delta B_3}{\partial \tau} \frac{\partial E_r^2}{\partial \tau} \right] \mathrm{d}\tau \, . \tag{4.2.8}$$

Recalling that (as found in Section 2.3.2)

$$\begin{aligned} \overline{E}_r^2 &\sim \frac{E_o^2}{2} \frac{\sin(\Lambda)}{2\omega(1-\Delta)^{1/2}} \\ E_r^2 &\sim \frac{E_o^2}{2} \cos(\Lambda) \\ \frac{\partial E_r^2}{\partial \tau} &\sim -\frac{E_0^2}{2} 2\omega(1-\Delta)^{1/2} \sin(\Lambda) \, , \end{aligned} \tag{4.2.9}$$

where the argument of the trigonometric functions is

$$\Lambda(\tau) = 2\omega \int_0^\tau (1-\Delta)^{1/2} d\tau + 2\phi \, , \tag{4.2.10}$$

we have that

$$\begin{aligned} \delta B_1 \cdot \frac{1}{\omega} &\sim \left[\mathcal{O}(\omega^1) + 3 \text{ terms in } \mathcal{O}(\omega^{-1}) + \mathcal{O}(\omega^{-3})\right] \frac{\delta c^2}{c^2} + \ldots \frac{\delta\rho}{\rho} \\ \delta B_0 + \delta B_2 &\sim \left[2 \text{ terms in } \mathcal{O}(\omega^0)\right] \frac{\delta c^2}{c^2} + \ldots \frac{\delta\rho}{\rho} \\ \delta B_3 \cdot \omega &\sim \left[\mathcal{O}(\omega^1)\right] \frac{\delta c^2}{c^2} + \ldots \frac{\delta\rho}{\rho} \, . \end{aligned} \tag{4.2.11}$$

The dominant contributions are now taken, corresponding to terms in $\mathcal{O}(\omega^1)$ and $\mathcal{O}(\omega^0)$, with all terms in $\delta\rho$ being neglected. This is done assuming that the major change in sound speed comes predominantly from the change in Γ_1 associated with ionization (Christensen-Dalsgaard & Däppen 1992, Pérez Hernández & Christensen-Dalsgaard 1994). So, the actual relative changes of pressure and density are assumed to contribute much less to derivatives

of the relative model differences than the sound speed (through Γ_1). The expression we are left with is

$$\delta I \approx -\frac{E_o^2}{2} \int_{\tau_a}^{\tau_b} \left\{ \frac{\omega}{2} \frac{3-2\Delta}{\sqrt{1-\Delta}} \frac{\mathrm{d}}{\mathrm{d}\tau} \left(\frac{1}{1-\Delta} \frac{\delta c^2}{c^2} \right) \sin\Lambda + \right.$$
$$\left. + \frac{\mathrm{d}}{\mathrm{d}\tau} \left[\frac{2-3\Delta}{(1-\Delta)^2} \frac{g}{c} \frac{\delta c^2}{c^2} \right] \cos\Lambda \right\} \mathrm{d}\tau \,. \tag{4.2.12}$$

Neglecting again terms with a derivative of equilibrium quantities and substituting in

$$\delta\omega_p \sim \frac{\delta I}{\omega \tau_t E_0^2} \,, \tag{4.2.13}$$

we find for the periodic signal in the frequencies,

$$\delta\omega_p \sim -\frac{1}{2\tau_t} \int_{\tau_a}^{\tau_b} \left[\frac{3-2\Delta}{2(1-\Delta)^{3/2}} \sin\Lambda + \frac{g}{\omega c} \frac{2-3\Delta}{(1-\Delta)^2} \cos\Lambda \right] \frac{\mathrm{d}}{\mathrm{d}\tau} \left(\frac{\delta c^2}{c^2} \right) \mathrm{d}\tau \,. \tag{4.2.14}$$

The next step is to substitute the derivative of the sound speed difference at the ionization zone by the relative difference of a new variable (associated with Γ_1) that better describes the ionization zone.

4.2.2 Description of the ionization zone

In order to study the effect on the frequencies due to ionization as given by the variational principle we need to choose the best way in which represent the model differences associated with this region. There is not a unique choice. The criterion we use is that whatever combination of thermodynamic variables we take, it must represent the dominant changes in the models and can be substituted by a simple integrable and localized function.

Considering that the dominant effect of ionization on the frequencies comes from the changes in the adiabatic exponent we introduce the function θ, given by

$$\theta = \frac{1}{g} \frac{dc^2}{dr} \,. \tag{4.2.15}$$

This is the same function as used in Däppen et al. (1988), but with different notation. One of the reasons why this is a convenient function is because it can be determined from seismic data. In Fig. 4.1 we plot θ for a standard solar model in the region of the second helium ionization zone. The contribution from this region corresponds to the bump of the function around an acoustic depth of 600s. From (4.2.15) we get that

$$\frac{d}{d\tau} \left(\frac{\delta c^2}{c^2} \right) \sim -\frac{\theta g}{c} \left(\frac{\delta\theta}{\theta} - \frac{\delta c^2}{c^2} \right) \,. \tag{4.2.16}$$

In writing this equation the change of the gravitational acceleration has been neglected. After substituting in the expression for the frequency changes and taking only terms in $\delta\theta$ we find that

$$\delta\omega_p = \frac{1}{2\tau_t} \int_{\tau_a}^{\tau_b} \frac{\theta g}{c} \left[\frac{3-2\Delta}{2(1-\Delta)^{3/2}} \sin\Lambda + \frac{g}{\omega c} \frac{2-3\Delta}{(1-\Delta)^2} \cos\Lambda \right] \frac{\delta\theta}{\theta} \mathrm{d}\tau \,. \tag{4.2.17}$$

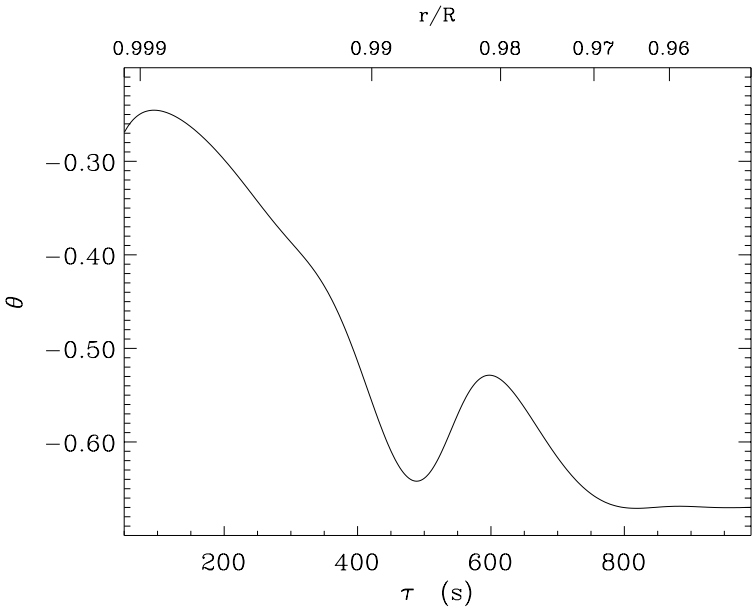

Fig. 4.1: Plot of θ, as defined in Eq. (4.2.15), versus acoustic depth τ for a standard solar model. The bump between $\tau\sim$500s and $\tau\sim$800s is due to the second ionization of the helium. It is the effect of this variation in θ on the frequencies of oscillation that we want to model.

Note that to obtain this expression we have assumed that relative variations of the sound speed derivative dominate over relative differences of the sound speed itself. So, any contribution from $\delta c^2/c^2$ is considered to be negligible compared to $\delta\theta/\theta$. Now, within the order of the analysis, we further consider that the quantities for the smooth model do not vary over the interval $[\tau_{\rm a},\tau_{\rm b}]$ (i.e. derivatives of these quantities are negligible). In the region around $\tau\sim$600s we are already well below the superadiabatic layer, where the structure changed rapidly, therefore it is within the order of the analysis (as when we neglect $\delta c^2/c^2$ for example) to assume that g, c or θ for the smooth model do not vary in the zone of the second ionization of helium. Such an assumption gives the following expression for the dominant contribution to the signal in the frequencies,

$$\delta\omega_p = \left(\frac{\theta g}{2\pi_{\rm t} c}\right)_{\tau_{\rm d}} \left[\frac{3-2\Delta}{2(1-\Delta)^{3/2}} \int_{\tau_{\rm a}}^{\tau_{\rm b}} \sin\Lambda \ \frac{\delta\theta}{\theta}\,{\rm d}\tau + \left(\frac{g}{\tilde{\omega}c}\right)_{\tau_{\rm d}} \frac{2-3\Delta}{(1-\Delta)^2} \left(\frac{\tilde{\omega}}{\omega}\right) \int_{\tau_{\rm a}}^{\tau_{\rm b}} \cos\Lambda \ \frac{\delta\theta}{\theta}\ {\rm d}\tau \right] . \qquad (4.2.18)$$

All quantities outside the integrals are now evaluated at $\tau=\tau_{\rm d}$. Again, we have introduced a constant $\tilde{\omega}$ corresponding to a reference frequency. The value of $\tilde{\omega}/2\pi$=2000μHz is used everywhere in this Chapter.

The next step is to substitute $\delta\theta$ by a simpler function in order to solve the integrals present in Eq. (4.2.18). The simplest possible choice is to replace $\delta\theta/\theta$ by a triangle (see

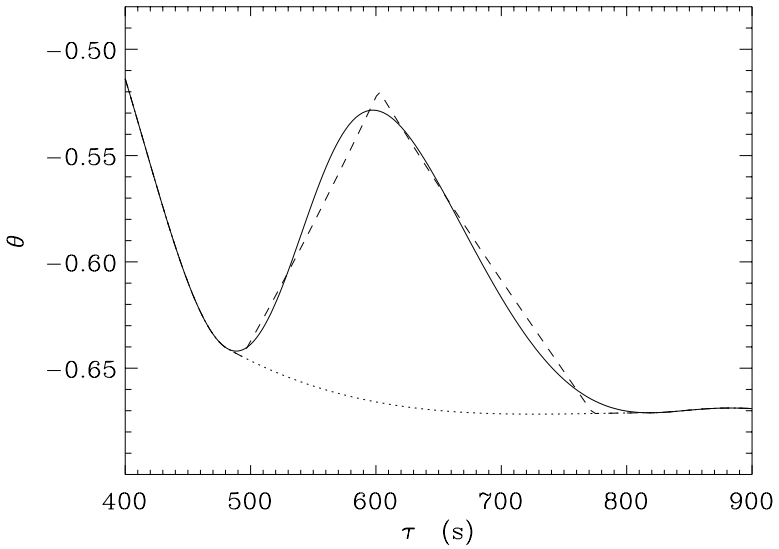

Fig. 4.2: Plot of θ (continuous line) and an estimation of what is our smooth model (dotted line) corresponding to an envelope without the second ionization of helium. Also shown as a dashed line is our simple fit by a triangle of this "bump" in θ with half of the base being taken as 140s. Note that the triangle is actually fitted to $\delta\theta/\theta$ and not $\delta\theta$ itself.

Fig. 4.2). We then write that

$$\frac{\delta\theta}{\theta} \equiv \begin{cases} \left(\dfrac{\delta\theta}{\theta}\right)_d \dfrac{\tau-\tau_{\rm a}}{\tau_{\rm d}-\tau_{\rm a}} & ;\ \tau_{\rm a} \leq \tau \leq \tau_{\rm d} \\ \left(\dfrac{\delta\theta}{\theta}\right)_d \dfrac{\tau_{\rm b}-\tau}{\tau_{\rm b}-\tau_{\rm d}} & ;\ \tau_{\rm d} \leq \tau \leq \tau_{\rm b} \\ 0 & ;\ \text{elsewhere}\ . \end{cases} \tag{4.2.19}$$

We also define more two quantities; I_θ and β which describe the global effect of the ionization zone. These are given by

$$I_\theta = \theta_{\rm d} \int_{\tau_{\rm a}}^{\tau_{\rm b}} \frac{\delta\theta}{\theta}\ {\rm d}\tau \qquad \text{and} \qquad \beta = \frac{\tau_{\rm b}-\tau_{\rm a}}{2}\ . \tag{4.2.20}$$

The quantity I_θ is just the area of the bump while β measures the width and I_θ/β the height of the maximum. Note that with this definition the acoustic depth $\tau_{\rm d}$, or the corresponding radial position $r_{\rm d}$, is associated with the maximum of $\delta\theta/\theta$.

We are now in conditions to calculate the integrals in Eq. (4.2.18). After substituting

definition (4.2.19) the integrals are simply

$$\int_{\tau_a}^{\tau_b} \sin\Lambda \ \frac{\delta\theta}{\theta}\,\mathrm{d}\tau \sim \left(\frac{\delta\theta}{\theta}\right)_{\tau_d} \beta \ \sin\Lambda_d \ \frac{\sin^2\left(\omega\beta\sqrt{1-\Delta}\right)}{\left(\omega\beta\sqrt{1-\Delta}\right)^2}$$
$$\int_{\tau_a}^{\tau_b} \cos\Lambda \ \frac{\delta\theta}{\theta}\,\mathrm{d}\tau \sim \left(\frac{\delta\theta}{\theta}\right)_{\tau_d} \beta \ \cos\Lambda_d \ \frac{\sin^2\left(\omega\beta\sqrt{1-\Delta}\right)}{\left(\omega\beta\sqrt{1-\Delta}\right)^2} \ . \tag{4.2.21}$$

The argument Λ_d being

$$\Lambda_d = 2\omega\int_0^{\tau_d}(1-\Delta)^{1/2}\mathrm{d}\tau + 2\phi \ . \tag{4.2.22}$$

(the notation is equivalent to what we have used in Chapter 2 for the study of overshoot). These expressions are now used in Eq. (4.2.18) to obtain the explicit dependence of the signal on the local equilibrium conditions.

4.2.3 Expression for the signal

We have now an estimate on how much the frequencies are affected because there is the second ionization of helium. This is given by Eq. (4.2.18) when we use Eqs. (4.2.21). The periodic signal (the subscript "p" shall be dropped from $\delta\omega_p$) is then found to be given by,

$$\delta\omega \sim \frac{3I_\theta g}{4\pi_t c} \ \frac{\sin^2\left(\omega\beta\sqrt{1-\Delta}\right)}{\left(\omega\beta\sqrt{1-\Delta}\right)^2} \ \left[\ \frac{1-2\Delta/3}{(1-\Delta)^{3/2}} \ \sin\Lambda_d + \frac{4g}{3\tilde{\omega}c} \ \frac{1-3\Delta/2}{(1-\Delta)^2} \ \left(\frac{\tilde{\omega}}{\omega}\right) \ \cos\Lambda_d\right]. \tag{4.2.23}$$

All equilibrium quantities are evaluate at $\tau{=}\tau_d$. To simplify the notation this expression is written as

$$\delta\omega \sim \frac{\sin^2\left(\omega\beta\sqrt{1-\Delta}\right)}{\left(\omega\beta\sqrt{1-\Delta}\right)^2} \left[a_1^2 \ \frac{(1-2\Delta/3)^2}{(1-\Delta)^3} + a_2^2 \ \frac{(1-3\Delta/2)^2}{(1-\Delta)^4} \ \left(\frac{\tilde{\omega}}{\omega}\right)^2\right]^{1/2} \cos\Lambda_d \ , \tag{4.2.24}$$

where we have introduced the amplitude components

$$a_1 = a_0 \qquad \text{and} \qquad a_2 = a_0 \ \frac{4g}{3\tilde{\omega}c} \ , \qquad \text{with} \qquad a_0 = \frac{3I_\theta g}{4\pi_t c} \ . \tag{4.2.25}$$

Note that any information associated with the helium abundance and the equation of state is contained in the two parameters describing the ionization zone, namely I_θ and β. The quantity Δ, which depends on the degree l of the modes, is written as

$$\Delta = \Delta_d \ \frac{l(l+1)}{\tilde{l}(\tilde{l}+1)} \ \left(\frac{\tilde{\omega}}{\omega}\right)^2 \ , \tag{4.2.26}$$

with the reference value $\tilde{l}$ taken as being 140. As far, we have four parameters associated with the amplitude of the signal which are; a_1, a_2, β and Δ_d.

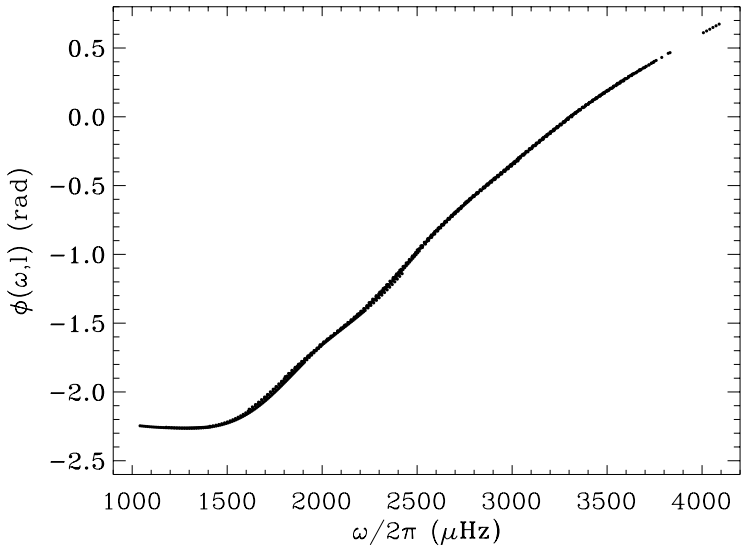

Fig. 4.3: Plot of the phase function $\phi(\omega, l)$, calculated using the Duvall law (Eqs. (2.6.13) and (2.6.12)), versus frequency. A standard solar model (H_2 in Table 4.1) is used and we show modes with $30 \lesssim l \lesssim 140$. Note the weak dependence of ϕ on the degree when compared with lower degree data shown in Fig. 2.4.

We still have to replace the argument of the signal by an approximate expression which can be fitted to the frequencies. However, the analysis presented for the overshoot has to be adapted to this particular case. The reason is that now we need to use high degree modes with l going from a few tens up to the hundreds. In spite of this, and using the fact that for these modes $(c/r)^2$ is now much smaller cancelling to some degree the higher values of l we still need to consider the expansion of the square root of the integrand in the argument as done in Eq. (2.6.5). In this way we still have $\gamma_{\rm d}$, as defined in Eq. (2.6.8), present in the argument of the signal.

However, when considering the possible dependence of the phase function ϕ on the frequency and degree of the modes we do not have the same behaviour as seen in Fig. 2.4. For the type of modes we shall be using here the phase function is shown in Fig. 4.3. Note that now the dependence on degree is very weak, while the linear dependence on frequency, used in Eq. (2.6.9) is far from being valid now, in particular for the limits of low and very high frequencies. As a first order approximation, and to avoid to introduce any extra parameter in the argument, we consider nevertheless ϕ as independent of degree and a linear function of frequency (valid really only for frequencies between 1500 and 3500 μHz). The implications are that $\tau_{\rm d}$ is affected by the phase variation, and so again we shall be fitting $\bar{\tau}_{\rm d}$ and not $\tau_{\rm d}$, but the same does not happen to $\gamma_{\rm d}$, contrary to what we have seen for overshoot. The fact that we are replacing the dependence of ϕ on frequency

(Fig. 4.3) by a linear relation also introduces some degree of indeterminacy in the values or both $\bar{\tau}_{\rm d}$ and ϕ_0. However, we do not expect any significant contribution to $\gamma_{\rm d}$.

Having these considerations in mind, we write the signal as being

$$\delta\omega \sim A(\omega,l)\ \ \cos\left[2\omega\bar{\tau}_{\rm d} - \gamma_{\rm d}\ \frac{l(l+1)}{\omega} + 2\phi_0\right]\ , \tag{4.2.27}$$

with the amplitude given by

$$A(\omega,l) \equiv \frac{\sin^2\left[\left(\frac{\omega}{\tilde{\omega}}\right)\tilde{\omega}\beta\sqrt{1-\Delta}\ \right]}{\left[\left(\frac{\omega}{\tilde{\omega}}\right)\tilde{\omega}\beta\sqrt{1-\Delta}\ \right]^2}\ \ \left\{a_1^2\ \frac{\left(1-\frac{2\Delta}{3}\right)^2}{(1-\Delta)^3} + a_2^2\ \frac{\left(1-\frac{3\Delta}{2}\right)^2}{(1-\Delta)^4}\ \left(\frac{\tilde{\omega}}{\omega}\right)^2\right\}^{1/2}\ . \tag{4.2.28}$$

In order to compare the amplitude for different models an amplitude $A_{2.0}$ is defined for l=0 and $\tilde{\omega}/2\pi$=2000μHz. It is given by

$$\begin{aligned} A_{2.0} \equiv A(\omega{=}\tilde{\omega},l{=}0) &= \frac{\sin^2(\tilde{\omega}\beta)}{(\tilde{\omega}\beta)^2}\ \sqrt{a_1^2+a_2^2} \\ &= \frac{3I_\theta g}{4\pi_{\rm t} c}\ \frac{\sin^2(\tilde{\omega}\beta)}{(\tilde{\omega}\beta)^2}\ \left[1+\left(\frac{4g}{3\tilde{\omega}c}\right)^2\right]^{1/2}\ . \end{aligned} \tag{4.2.29}$$

If the structure of a model is known then using this equation it is possible to estimate the expected amplitude (and form) of the signal for such a model.

4.3 Solar models

In order to estimate how well the analysis presented above represents the effect of the helium ionization zone on the structure and frequencies of oscillation we consider several solar envelope models. Their characteristics have been described in Chapter 1 (and Appendix A). Because we need to establish what is the effect of using different equations of state (EOS) on the calculation of the models we shall also consider here models constructed with different EOS. In particular we have considered the CEFF equation of state (eg. Christensen-Dalsgaard & Däppen 1992) with Cox & Tabor (1976) opacities, and also a simpler EOS, as described in Appendix A, using just the Saha equations for hydrogen and helium ionization and including an *ad hoc* total ionization at high pressures.

The characteristics of all envelope models are given in Table 4.1. These have been constructed having the same total mass, luminosity, radius, heavy elements abundance (Z=0.02) and with the base of the convection zone at the same position ($r_{\rm d}$=0.713R). Convection has been modelled using the mixing length theory. In order to illustrate the effect of using different equations of state we show, in Fig. 4.4, θ for all models listed in Table 4.1. Note the fact that the major difference is a shift in acoustic depth of the maximum (corresponding to our definition of $\tau_{\rm d}$) of the bump due to ionization of the

Table 4.1: Solar envelope models with different hydrogen (X) and helium (Y) mass abundances. The position $r_{\rm d}$, of the maximum of $\delta\theta/\theta$, resulting from the second helium ionization is given in the second column. The equation of state used in their calculation is also indicated.

Model	$r_{\rm d}/R$	X	Y	EOS
H_1	0.98186	0.7330	0.2470	CEFF
H_2	0.98209	0.7170	0.2630	"
H_3	0.98234	0.7010	0.2790	"
H_4	0.97951	0.7330	0.2470	SEOS
H_5	0.97979	0.7170	0.2630	"
H_6	0.98006	0.7010	0.2790	"

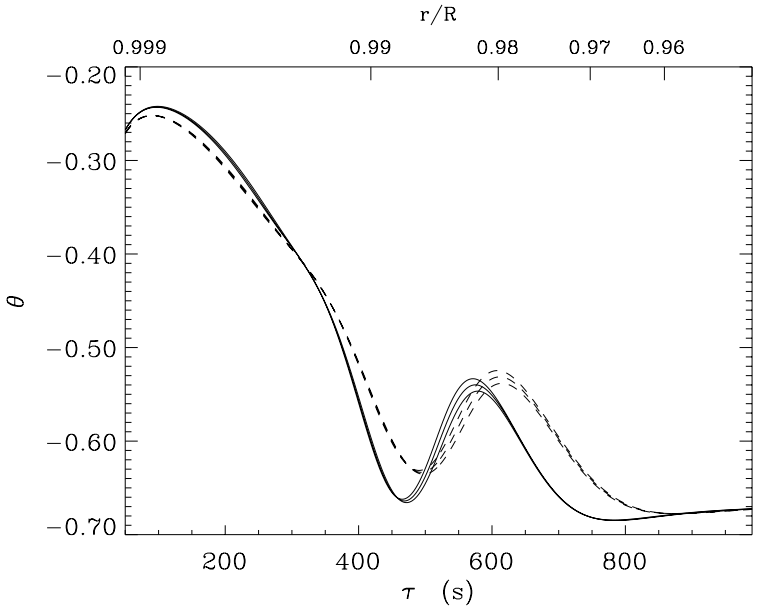

Fig. 4.4: Plot of θ - see Eq. (4.2.15), versus acoustic depth τ for several solar models. The continuous line is for models H_{1-3} constructed using the CEFF equation of state and the dotted line for models H_{4-6} using our simple equation of state SEOS.

helium, with the simplest equation of state giving the deepest acoustic location for this maximum. There is also a barely noticeable different in the width of the bump for different equations of state. This is the characteristic associated with β.

The next step is, using the fact that $\delta\theta_d$ (and therefore also I_θ) depends on the helium abundance (Y) in the envelope, to calibrate the amplitude $A_{2.0}$ of the signal given by Eq. (4.2.29) as a function of Y.

4.4 Signal in the frequencies

From the solar envelope models with different helium abundances and calculated using different equations of state we can now determine how the signal in the frequencies is affected by each of these aspects. The main problem in doing so comes from the difficulty of defining our smooth model, which is necessary in order to determine the amplitude of the signal, contrary to what happen for the study of overshoot where the smoothness condition where imposed on the derivatives.

We also note that we have not considered here an extensive representation of different values of abundances or the physics for that matter. In particular we note that all our models have the base of the convection zone at the same position. However, the change in that aspect leads to changes in the position of the second helium ionization zone, and therefore affects the function θ (Däppen et al. 1988). The objective is just to present the possibilities of the method and how it can complement other determinations of the solar envelope helium abundance.

Table 4.2: Expected values of the parameters for all models. The amplitude $A_{2.0}/2\pi$ and $\gamma/2\pi$ are given in (μHz). While the quantity I_θ and the acoustic depth $\tau_{\rm d}$ are both given in (s). In order to find $A_{2.0}$ we have used β=140s (see the text).

Model	I_θ	$\frac{A_{2.0}}{2\pi}$	$\Delta_{\rm d}$	$\tau_{\rm d}$	$\frac{\gamma}{2\pi}$
H_1	17.70	1.552	0.476	581.70	0.1119
H_2	18.52	1.643	0.466	577.19	0.1090
H_3	19.56	1.749	0.458	574.53	0.1072
H_4	17.38	1.408	0.544	619.68	0.1368
H_5	18.34	1.498	0.535	617.02	0.1344
H_6	19.44	1.602	0.525	613.73	0.1316

From a model and using expressions (4.2.20), (4.2.25), (4.2.26) and the definitions of the parameters in the argument as given in (4.2.27), we can estimate the values expected for each of the parameters. Such values are given in Table 4.2 for all models considered. The values for the amplitude $A_{2.0}$ versus helium abundance are also shown in Fig. 4.5. There is a significant shift due to the equation of state we are using to construct the models. However, we note that our SEOS models are an extreme case.

Included in Table 4.2, and used to calculate $A_{2.0}$, is an estimation of I_θ for each of the models. We must, however, note that there is not a unique way of calculating it, since the result depends on what we take as being the smooth model. Here we have chosen to adjust a polynomial with continuous first derivatives on both sides of the bump (at about $\tau\sim$450s and $\tau\sim$800s). The value of I_θ is calculated according to Eq. (4.2.20) using this

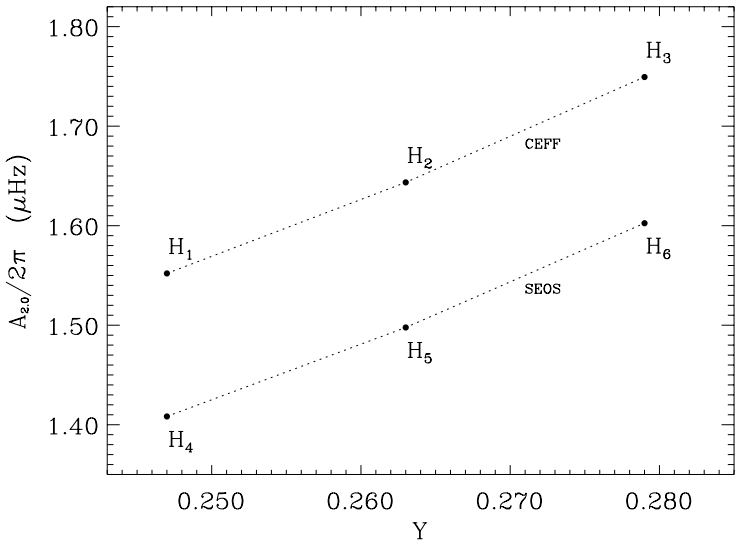

Fig. 4.5: Plot of the expected amplitudes $A_{2.0}$ versus the helium abundance by mass. The dotted line connects points corresponding to models constructed using the same EOS as indicated. See the text and Table 4.1 for more details on the models.

smooth θ. By definition the parameter β is half of the base of a triangle whose top vertex have an height of $(\delta\theta)_{\tau_d}$ and with an area equal to I_θ. There are other possibilities of determining these two parameters, but most of them would give the same values to within 5%. From such an exercise we have found that β is similar (within less than 20s) for all models, being around 140s. Deviations from a unique value, as used here, can be either physical, being associated with the equation of state and the helium abundance, or just numerical resulting from the particular method used to define the smooth θ.

Here, we have chosen not to consider β as a fitting parameter. We do so because there is already a parameter associated with the effect of the helium ionization (I_θ) and we have other six parameters, with two of then describing the amplitude. Also, we note that the effect of β in the frequency dependence of the amplitude is mixed with the effects coming from the other two amplitude parameters. Such a mixing leads to a ill define dependence which makes it difficult to find the actual behaviour by least squares fitting. So, we leave any possible variation in each model from β =140s to be accommodated by the two parameters associated with the amplitude dependence on frequency, namely a_1 and a_2. We shall be back to this point later, when analysing the results, considering how this assumption for β can affect the value of $A_{2.0}$.

4.4.1 Fitting the signal

The method we have used here to isolate the signal in the frequencies is the same as

presented for the case of overshoot, in Section 3.3.1. The only difference is that now we have used $\lambda_0=10^{-6}$, since the signal we want to isolate has a longer wavelength. The numerical procedure is exactly the same, and the seismic data for all the models reported here go through the same analysis.

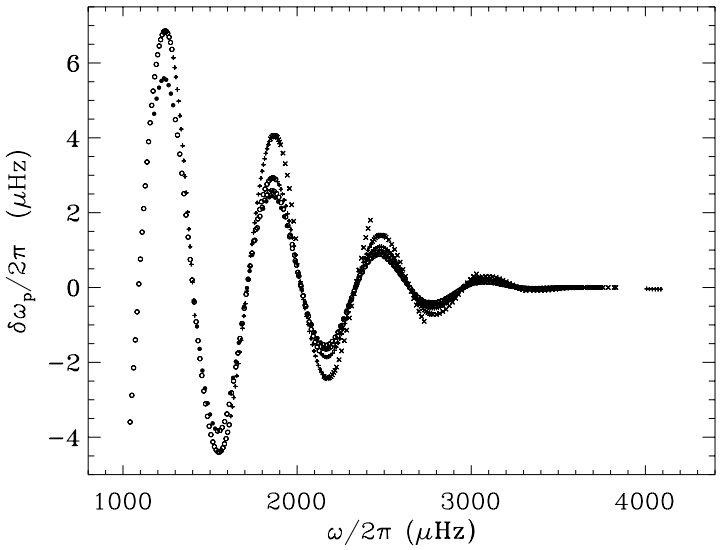

Fig. 4.6: Plot of the expected signal using Eq. (4.4.2) for model H_2 and the values of the parameters as given in Table 4.2. The symbols are as follows: (closed circles) $l\leq 40$, (open circles) $41\leq l\leq 69$, (crosses) $70\leq l\leq 99$ and (x) $100\leq l$.

The parameters coming from the fitting are;

$$\bar{\tau}_{\rm d},\ \gamma_{\rm d},\ \phi_0,\ a_1,\ a_2,\ \text{ and }\ \Delta_{\rm d}\ ; \tag{4.4.1}$$

and the expression fitted being given by (see Eqs. (4.2.27) and (4.2.28))

$$\begin{aligned} f(\omega_{nl}) =& \frac{\sin^2\left[\left(\frac{\omega_{nl}}{\tilde{\omega}}\right)\tilde{\omega}\beta\left(1-\Delta_{\rm d}\,x\right)^{1/2}\right]}{\left[\left(\frac{\omega_{nl}}{\tilde{\omega}}\right)\tilde{\omega}\beta\left(1-\Delta_{\rm d}\,x\right)^{1/2}\right]^2} \quad \cos\left[2\omega_{nl}\bar{\tau}_{\rm d}-\gamma_{\rm d}\,\frac{l(l+1)}{\omega}+2\phi_0\right] \\ & \times\left[a_1^2\ \frac{\left(1-\frac{2}{3}\,\Delta_{\rm d}\,x\right)^2}{\left(1-\Delta_{\rm d}\,x\right)^3}+a_2^2\ \frac{\left(1-\frac{3}{2}\,\Delta_{\rm d}\,x\right)^2}{\left(1-\Delta_{\rm d}\,x\right)^4}\ \left(\frac{\tilde{\omega}}{\omega_{nl}}\right)^2\right]^{1/2}, \end{aligned} \tag{4.4.2}$$

where $\quad x=\dfrac{l(l+1)}{\tilde{l}(\tilde{l}+1)}\ \left(\dfrac{\omega_{nl}}{\tilde{\omega}}\right)^2$.

The two reference values used are $\tilde{l}=140$ and $\tilde{\omega}/2\pi=2000\mu$Hz. Also, as discussed above, we set $\beta=140$s.

4.4.2 Selection of the mode set

The basic rule for choosing the modes whose frequencies will be used to study the signal from the second helium ionization zone is the observational error. To this we also add the fact that we take out all modes that also cross the base of the convection zone, avoiding in this way any possible contamination from the signal associated with this region. Finally only modes whose lower turning point is below the zone under study can be used.

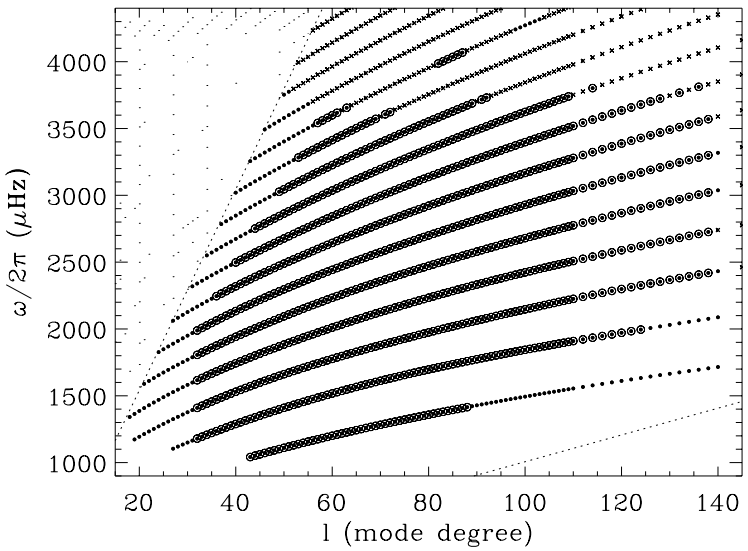

Fig. 4.7: Plot of solar seismic data from Libbrecht et al. (1990). The symbols are: fill circles are for modes with quoted errors smaller than 0.15μHz while (x) is for frequencies with an error superior to that value. Represented by small points are modes with their lower turning point below the base of the convection zone. The set of modes selected for our analysis is indicated by open circles around the symbol for that mode.

These last two conditions are shown as dotted lines in Fig. 4.7. Also indicated are modes with errors below (filled circles) or above (crosses) the value of 0.15μHz from the data compiled by Libbrecht et al. (1990). The actual modes used here are indicated by the circles around the symbol corresponding to the mode. The set of selected frequencies has 816 values with an average error of about 0.04μHz, for l between 32 and 138 and frequencies from 1000 to 4000μHz. The same set of frequencies is considered for all the envelope models.

Note that according to Fig. 4.3 we should most probably remove modes with frequencies below 1500μHz. However, it would reduce the range in frequency in which the expression of the signal is fitted (and has a higher amplitude) worsening the indeterminacy for the parameters associated with the frequency dependence of the amplitude. We have chosen to maintain those modes since the amplitude is the most important parameter

we are trying to measure. Even if it means decreasing the significance of the parameters associated with the argument.

The frequencies were calculated using the code for linear adiabatic non-radial oscillations as described in Appendix B. To estimate the effect of observational uncertainties randomly generated errors with zero mean and standard deviation for each mode as given by the corresponding quoted observational error, were added to the numerical frequencies. In this way 100 sets of frequencies were generated for one of the models (H_2) and the parameters for the signal determined for each of those. The estimated errors presented here correspond to the standard deviation of these 100 results.

4.5 Results

The method to isolate the signal (described Section 3.3.1) was used on all sets of frequencies for the models under consideration in order to find the parameters of signal. The expression fitted is given in (4.4.2) and the frequencies included in the data sets described above. All frequency data were submitted to the same procedure.

Table 4.3: Parameters obtained by fitting the frequency data with the expression of the signal as given in Eq. (4.4.2). The acoustic depth is given in 'sec' while $\gamma_{\rm d}$ and the amplitudes are given is 'μHz'. The parameters obtained for the solar data given in Libbrecht, Woodard & Kaufman (1990) are listed in the last row.

Model	$\bar{\tau}_{\rm d}$	$\frac{\gamma_{\rm d}}{2\pi}$	$\frac{A_{2,0}}{2\pi}$	Δ_d
H_1	673.41	0.162	2.637	0.551
H_2	665.36	0.143	2.714	0.536
H_3	653.44	0.131	2.820	0.524
H_4	725.81	0.242	1.975	0.542
H_5	723.83	0.243	1.993	0.531
H_6	708.34	0.217	2.098	0.519
Sun	649.00	0.140	2.766	0.454

The results for the parameters found for each of the models are listed in Table 4.3. The effect of the errors is very small being below 1% for most of the parameters. These very low errors due to the observational uncertainties are not surprising when comparing with the results for overshoot. Not only is the amplitude much larger, but the number of frequencies used is larger with the frequencies having on average lower observational errors. These three factors together are responsible for such a low effect on the determination of the parameters from the observational errors.

We plot in Fig. 4.8 the results for all models considered here. If included, the error bars in the plot would be smaller than the size of the symbols. Note that there is a systematic

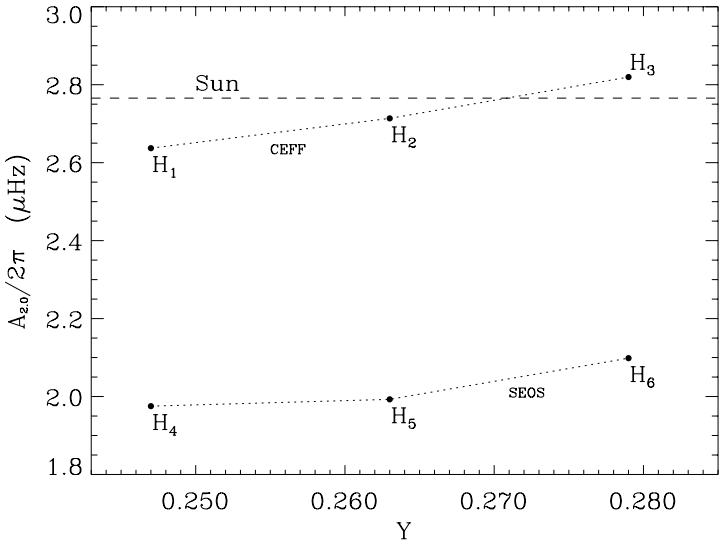

Fig. 4.8: Plot of the fitted amplitude $A_{2,0}/2\pi$ for the signal versus the helium abundance Y for all models considered, H_{1-6} (see Table 4.2) as indicated. The dotted lines connect points corresponding to models using the same equation of state as given in Table 4.1. The value obtained for the solar data is also shown as the horizontal dashed line. The error bars ($\lesssim 0.003\mu$Hz) are smaller than the size of the filled circles.

increase of the amplitude with increasing surface helium abundance if the same equation of state is used. Such a variation is well above the observational uncertainties. However, there is a strong dependence of the amplitude on the equation of state used to calculate the model. This effect is by far the dominant one. There is also a clear difference between the predicted value for the amplitude and the ones found from the fitting. This is most probably associated with the fact that the determination of I_θ is not correct. Therefore a calibration is essential to measure the solar helium abundance using this method, unless the theoretical value can be correctly determined for a given model. The discrepancy between theoretical and fitted values is also associated with the fact that here we are using the same β for all models, therefore once again introducing an extra contribution to the value found for the amplitude if the actual value for the models is not the one used in the fitting. In spite of this the clear dependence of the amplitude on the helium abundance is according to the expected behaviour.

The effect of the parameter β in the description of the signal is mixed with the other two parameters associated with the amplitude. In the light of Eqs. (4.2.20), it is clear that the parameter β is also associated with what I_θ is, and so we cannot avoid affecting the latter with what we do with the former. Therefore before any save conclusions are drawn from our results it is necessary to separate these dependences clearly, with each parameter being associated with a specific characteristic of the ionization zone. In particular with

a parameter for the dependence on the helium abundance (most probably a_1 and a_2) while leaving the dependence on the equation of state to some other parameter (the one replacing for example β).

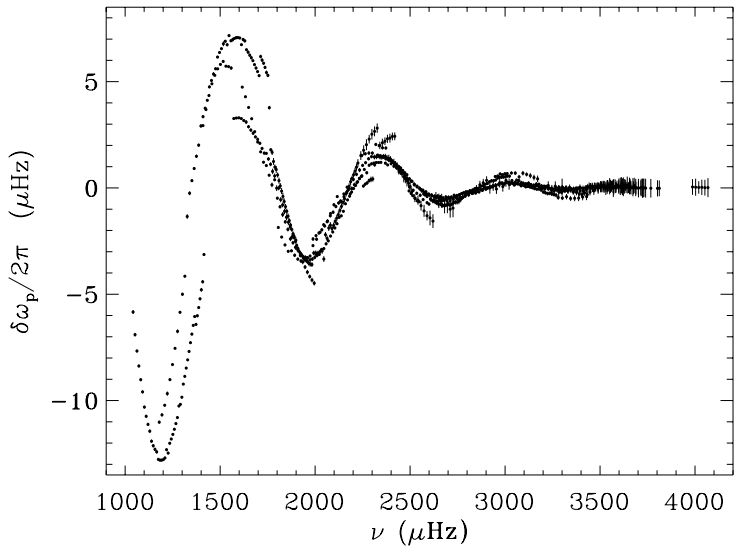

Fig. 4.9: Plot of the solar signal in the data of Libbrecht et al. (1990). The error bars correspond to 3σ of the quoted observational errors.

We have also submitted the solar data to the same fitting procedure. The results for the parameters are given in the last row of Table 4.3 and the amplitude plotted as a dashed line in Fig. 4.8. To these values corresponds the signal shown in Fig. 4.9. Note the fact that the error bars are also plotted there, with a factor of 3 otherwise would be barely visible. This is the reason, as discussed above, of why the values of the fitted parameters are so insensitive to the observational errors.

4.6 Comments

In this Chapter we have not presented definite results but only suggested a possible application of the same technique as used for studying overshoot. The fact that this method can be used to isolate the signal is in my point of view demonstrated. In particular the very high precision, given an equation of state, with which we may attempt to determine the abundance. Considering the error in the determination of the amplitude, as given from 100 error realisations obtained by adding random errors normally distributed with the sigma for each frequency being the corresponding quoted observational error, we have obtained an uncertainty in the fitting of $A_{2.0}$ of less than 0.003μHz. To such a value corresponds an uncertainty in the determination of the helium abundance below 5%.

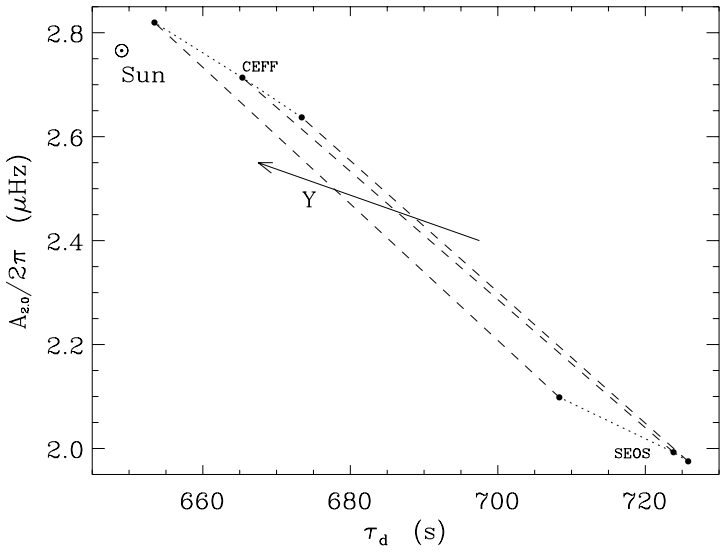

Fig. 4.10: Plot of the fitted amplitude $A_{2,0}/2\pi$ for the signal versus the acoustic depth $\bar{\tau}_d$ of the ionization zone of all models (Table 4.3). The dotted lines connect points corresponding to models using the same equation of state (as indicated), while dashed lines connect models having the same envelope helium abundance with the value increasing as indicated by the arrow. The value obtained for the solar data of Libbrecht et al. (1990) is also shown ($\odot$).

The results are shown in Fig. 4.10 in a plot of amplitude versus acoustic depth of the ionization zone. These are still unable to provide a direct measurement of the surface helium abundance but they are clear evidence that we may expect to do so when a more complete analysis of the effect on the frequencies from the ionization zone is done. We have discussed that it is mainly the envelope of the amplitude as function of frequency, provided by the measure of the thickness in acoustic depth of the ionization zone, that is dominating the incompleteness of the description presented here. However it can be extended further if this thickness is included as a free parameter. We have not done so because the separation between the amplitude parameters (a_1,a_2) and β is still not clear, introducing a indeterminacy when all three quantities are used as fitting parameters. The problem can be solved if a more detailed model of the ionization zone in the function θ is used. Here we have modelled it simply as a triangle in $\delta\theta/\theta$ where the differences are relative to a model without the second ionization of the helium. However, a better representation would remove the indeterminacy of the three quantities associated with the amplitude, leaving the dependence on the helium abundance solely to the quantity we introduced here as I_θ.

Also important, but not addressed here is how the signal is affected when we move the position of the ionization zone by changing the convection zone, for example. This aspect

has been considered by Däppen et al. (1988) when studying the function θ. In their work, it is possible to see that not only the position but also the width of the bump in θ changes when the mixing length parameter α changes (or equivalently, the base of the convection zone). The work presented here seems to indicate that the area of the bump would still be the same but only an extensive investigation on the dependence of the signal on these two aspects, eos and convection theory, may clarify how the latter affects the applicability of the method.

5. Constraints on Theories of Convection

Some alternatives to the traditional mixing-length theory (*MLT*) have been proposed for modelling convective heat transport inside stars. Presently we only have descriptions which still involve at least one free parameter. Having adjusted such a parameter to obtain the observed solar radius, we cannot discriminate non-seismically between different convective theories, regardless of how low-efficiency convection is treated. Here we consider how the additional information provided by global p-mode frequencies can be used to understand this regime of convection present at the top of the solar convective envelope.

We do so by considering a parametrization which in addition to the mixing length has two further parameters: one which regulates the relative degree of overadiabaticity (or inefficiency) of convection, and a second that affects the transition between the regimes of efficient and inefficient convection. Our parametrization includes traditional *MLT* and the theory of Canuto & Mazzitelli as particular cases. The effect of varying these parameters are study by constructing a series of envelope models with the same depth of the convection zone and computing their oscillation frequencies.

Using solar seismic data we further consider how the present tests may contribute to the understanding of the solar frequency discrepancies relatively to model frequencies. In particular we discuss how numerical simulations of solar convection may help in the understanding of this and other effects associated with the superadiabatic layer which may contribute to the discrepancy found for solar frequencies.

5.1 Introduction

Traditionally, convective energy transport in stars has been modelled using the *mixing-length theory* (*MLT*), proposed by Böhm-Vitense (1958). Recently, some alternative formulations have been proposed (Canuto & Mazzitelli 1991, 1992 – henceforth *CM*; Lydon, Fox & Sofia 1992; Balmforth 1992ab; Canuto 1995). It has long been recognized (e.g. Gough & Weiss 1976) that a solar model can always be constructed to match the observed radius, provided our description of convection has a free parameter to be adjusted. This is true regardless of how the low-efficiency regime is modelled: due to the almost adiabatic character of the deep convection zone, a small change is enough to accommodate any change at the top of the solar convective envelope where, due to the low density, convection is highly

inefficient at transporting heat. However, we now have at our disposal a large amount of extra data with very small observational errors, in the form of oscillation frequencies, which can be used to probe this region of the Sun.

In spite of the goal of finding a description without free parameters, in helioseismic studies it is very important to match the solar radius accurately and so at present a free parameter must be retained. We wish to address the question of whether, having adjusted this parameter to match the solar radius, one can still discriminate between the descriptions, to choose on the basis of observed seismic data which is the closer representation of solar convection. We address this question by investigating the effect that changing the description of convection has on the frequencies of solar envelope models. The envelopes have convection zones of the same depth $d_{\rm b}$ to isolate the effect of just one aspect of the model, namely the structure of the super-adiabatic layer at the top of the convection zone, where convection is inefficient. This condition substitutes the usual boundary condition requiring complete models to have the same radius.

With current solar models the dominant sources of discrepancy between the observed and the computed frequencies are confined to the superficial layers of the Sun, including the superadiabatic region of the convection zone (e.g. Christensen-Dalsgaard, Däppen & Lebreton 1988): with suitable scaling, the solar frequencies are lower than those of the models by typically 10-15 μHz at frequencies around 4000 μHz. Thus it is essential to determine the likely magnitude of the frequency errors introduced by the uncertainties in the treatment of convection. Furthermore, there is some hope that the observations can be used to test theories of convection, provided other sources of uncertainty with similar effects on the frequencies, such as non-adiabaticity and effects of atmospheric structure, can be constrained.

We propose a rather general parametrization which simulates some of the present uncertainties in the formulations of convective heat transport in stars. It has as particular cases the usual mixing-length theory and the *CM* theory. Thus we seek to unify and generalize some earlier investigations by e.g. Paternò et al. (1993), Basu & Antia (1994) and Baturin & Mironova (1995). The bulk of our investigation considers only local mixing-length theories, neglects the effects of turbulent pressure on the equilibrium structure and the oscillations, and assumes the oscillations to be adiabatic. However, we discuss briefly the expected effect on the frequencies of some of these aspects. In particular we address the advantages of using numerical simulations of solar convection to discriminate between the various proposed simpler parametrizations and estimate the possible contributions from other effects associated with convection which are not accounted for in our modelling.

The Chapter starts by describing the proposed parametrization. We then analyse the effects on the modelling of the superadiabatic region of envelope solar models, by

calculating envelopes with the same depth of the convection zone but different superadiabatic layers. We use the framework of the Grossman, Narayan & Arnett (1993) steady-state theory of convection to consider further the physical meaning of our parameter β_c and furthermore to argue for the plausibility of its taking a higher value than in the *MLT*. The seismic properties of the models are then determined, and the behaviour analysed in terms of kernels relating changes in frequencies to changes in the structure of the superadiabatic layer. We conclude from our investigation that errors of up to 10μHz should be expected due to the present uncertainties in modelling low-efficiency convection based only on the steepness of the temperature variation at the top of the convective envelope. A brief discussion of the possible effects of turbulent pressure, which has not been considered, and the non-adiabaticity of the oscillations is also included. We end by presenting some tentative conclusions for the Sun considering solar seismic data and its differences from frequencies for solar models. At the moment it is still difficult to establish how much of the frequency differences are due to the modelling of convection, however, based on simulations of convection and our study, a qualitative discussion of the main problems to be considered when modelling stellar convection can be done.

5.2 Parametrization of Convection

Our objective in this work is to understand how the frequencies of oscillation are affected by the particular formulation we use to model the solar convective envelope. Because we will be evaluating different formulations, like the standard Mixing Length Theory or the formulation by Canuto & Mazzitelli (1991), which differ basically on the behaviour for the limits of highly efficient and inefficient convection, we have developed a parametrization which reproduces the variation of these limiting behaviours with a parameter. In this way we can include both formulations in a global one which have them as particular cases for specific values of that parameter. So, we consider a expression for the gradient which in addition to the usual mixing-length parameter has two further parameters. One, β_c, is associated with the *strength* of the superadiabatic gradient in the regime of efficient convection compared to that in the regime of inefficient convection. The other, m, only affects the *transition* between the two regimes.

Since we are only considering local theories, the temperature gradient is given as the solution of an equation whose coefficients depend on local conditions. This may be written in terms of a variable Σ, which is related to the convective efficiency. The solution will then give the gradient $\nabla \equiv \mathrm{d}\log T/\mathrm{d}\log P$ at each point (where P and T are the pressure and temperature). The variable is defined as

$$\Sigma \equiv 4A^2\,(\nabla - \nabla_{\mathrm{a}})\,. \tag{5.2.1}$$

Here $\nabla_{\rm a}$ is the adiabatic temperature gradient; as usual, it corresponds to the gradient at constant entropy. The quantity A is a function of the local conditions given by

$$A^2 = \frac{C_P^2 Q\, \rho^3 g^2}{162 K^2 P}\, \ell^4 \,, \tag{5.2.2}$$

where C_P, Q, ρ, g and K are, respectively, the specific heat at constant pressure, the expansion coefficient, density, gravitational acceleration and radiative conductivity; and ℓ is a typical length scale over which the turbulent eddies travel before mixing with the surrounding fluid. The radiative conductivity is given by $K{=}4acT^3/3k\rho$, where a is the radiation constant, c the speed of light and k the opacity.

We obtain Σ from the equation

$$[1{+}\Phi(\Sigma)]\Sigma = 4A^2(\nabla_{\rm r}{-}\nabla_{\rm a}) \,, \tag{5.2.3}$$

where the function Φ characterizes the specific formulation of the theory. The radiative gradient, $\nabla_{\rm r}$, is defined as the value the gradient would have for all energy to be carried by radiation. Note that the left-hand side of this equation is only a function of Σ (see also Eq. (5.2.8) below) while the right-hand side is known at every point. Therefore, at each point of the model this equation allows the determination of Σ as function of the local structure, giving the local temperature gradient ∇ by inverting definition (5.2.1). In this formulation we have that $\nabla_{\rm a}{\le}\nabla{\le}\nabla_{\rm r}$ with Φ being just a measure of the degree of superadiabaticity. Noting that

$$\Phi = \frac{\nabla_{\rm r}{-}\nabla}{\nabla{-}\nabla_{\rm a}} \,, \tag{5.2.4}$$

it follows that near the top of the convection zone, where due to the low efficiency of convection ∇ must be closer to $\nabla_{\rm r}$ than $\nabla_{\rm a}$, we have that Φ is very small. On the other hand, in the deep convection zone, where convection forces an almost adiabatic stratification with $\nabla{\simeq}\nabla_{\rm a}$, Φ becomes very large.

For the typical length ℓ we use the expression

$$\ell = \alpha_c\, H_P \,, \tag{5.2.5}$$

where the mixing-length parameter α_c is introduced as a fitting parameter and H_P is the pressure scale height. Some authors argue that other expressions are preferable (see *CM*), such as ℓ being proportional to depth. For the time being we shall only use definition (5.2.5), however in a later Section we introduce a mixing length proportional to depth as suggested by Canuto & Mazzitelli (1992). This alternative removes the locality of the formulation but does not change the formalism presented here. The only difference being that in such a case ℓ depends on the position of the top of the convection zone.

The convective flux is given by

$$F_c = K\, \Delta\nabla T\, \Phi \,, \tag{5.2.6}$$

where the superadiabatic temperature gradient is

$$\triangle\nabla T = \frac{T}{H_P}\,(\nabla - \nabla_{\rm a})\,. \tag{5.2.7}$$

The next step is to define an expression for Φ, which varies with the formulation we may consider. It should in principle be given by the physics of convection/turbulence, but only its asymptotic behaviour is known (Gough & Weiss 1976). Here, an expression for Φ that allows direct comparison with both *MLT* and the *CM* formulation is used. Following *CM*, we write

$$\Phi(\Sigma) \equiv a_1 \Sigma^m\ \left[(1+a_2\Sigma)^n - 1\right]^p\ . \tag{5.2.8}$$

To this, we add conditions relating n and p to m by using the asymptotic limits for the optically thin and thick regimes (Gough & Weiss 1976):

$$\begin{aligned} \Phi &\propto \Sigma^2 \qquad \text{for } \Sigma \ll 1 \\ \Phi &\propto \Sigma^{1/2} \qquad \text{for } \Sigma \gg 1\,, \end{aligned} \tag{5.2.9}$$

giving that

$$n = \frac{1}{2}\,\frac{1-2m}{2-m} \qquad \text{and} \qquad p = 2-m\,. \tag{5.2.10}$$

Three parameters (m, a_1, a_2) therefore define a specific formulation.

5.2.1 Convection theories

This formulation is still general in the sense that other than choosing the formal dependence of Φ on Σ we still have not defined the values of the three parameters (m, a_1, a_2). When doing so we end with a particular formulation. Mixing Length Theory and the *MLT* are such type of particular cases.

For the *MLT* we just have m=-1, a_1=9/8 and a_2=1 (e.g. Böhm-Vitense 1958; Cox & Giuli 1968; Gough & Weiss 1976), giving Φ as

$$\Phi_{MLT}(\Sigma) \equiv {}^9\!/_8\ \Sigma^{-1}\ \left[(1+\Sigma)^{1/2} - 1\right]^3\ . \tag{5.2.11}$$

This is the standard convection "theory" used in most stellar structure and evolution codes.

In their formulation, Canuto & Mazzitelli (1991, 1992) - referred to as *CM*, used analytic closures of the Navier-Stokes equations to determine the values of these parameters. They obtain m=0.14971, a_1=24.868 and a_2=0.097666, giving instead Φ as

$$\Phi_{CM}(\Sigma) \equiv \left({}^9\!/_8\right)\ 22.105\ \Sigma^{0.14972}\ \left[\left(1 + \frac{\Sigma}{10.239}\right)^{0.18931} - 1\right]^{1.8503}\ . \tag{5.2.12}$$

In the case of solar models the really important values are the ones for a_1 and a_2 since they define the proportionality constants for the limits in (5.2.9). While the value of m only affects the transition from small values of Σ to large values, which for the Sun occurs over a very thin region in radius, and so has no significant effects on the actual temperature stratification of the model.

5.2.2 Parametrization of the convective efficiency

The objective now is to introduce an extra parameter which may allow us to have these two formulations as particular cases. We do so by considering the parameter β_c defined such that, when β_c is greater than unity (the *MLT* value), convection becomes less efficient for low values of Σ (we decrease the convective flux by decreasing Φ in this limit) and more efficient (the convective flux is increased by increasing Φ) in the limit of high values of Σ, relative to the *MLT* values. Specifically, we impose the following conditions:

$$\begin{aligned} \lim_{\Sigma\to 0} \frac{\Phi}{\Phi_{MLT}} &= \frac{1}{\beta_c} \\ \lim_{\Sigma\to \infty} \frac{\Phi}{\Phi_{MLT}} &= \beta_c \, . \end{aligned} \tag{5.2.13}$$

To related this parameter to the values of a_1 and a_2 we consider a function Ω, for arbitrary m, a_1 and a_2, as

$$\Omega(\Sigma) \equiv \frac{\Phi}{\Phi_{MLT}} = \frac{a_1}{\overline{a}_1}\, \Sigma^{m+1}\, \frac{\left[(1+a_2\Sigma)^n - 1\right]^p}{\left[(1+\Sigma)^{1/2} - 1\right]^3} \, , \tag{5.2.14}$$

with $\overline{a}_1$=9/8. The values of p and n are as given in Eqs. (5.2.10). In the limits of very large and very small Σ we therefore have that

$$\begin{aligned} \Omega_S = \lim_{\Sigma\to 0} \Omega &= \frac{a_1}{\overline{a}_1}\, 2^3 \lim_{\Sigma\to 0} \left[(a_2 n)^p \Sigma^{m+p-2}\right] \\ &= \frac{a_1}{\overline{a}_1}\, 2^{m+1} \left(\frac{a_2}{2}\right)^{2-m} \left(\frac{1-2m}{2-m}\right)^{2-m} \, , \end{aligned} \tag{5.2.15}$$

and

$$\begin{aligned} \Omega_L = \lim_{\Sigma\to \infty} \Omega &= \frac{a_1}{\overline{a}_1} \lim_{\Sigma\to \infty} \left[a_2^{np} \Sigma^{m+np-1/2}\right] \\ &= \frac{a_1}{\overline{a}_1}\, a_2^{(1-2m)/2} \, . \end{aligned} \tag{5.2.16}$$

Note that, by definition, Ω is constant and equal to unity for $(m, a_1, a_2) = (-1, \overline{a}_1, 1)$. For the *CM* formulation (see previous Subsection and Canuto & Mazzitelli 1991), these are

$$\Omega_S = \frac{1}{9.1684} \qquad \text{and} \qquad \Omega_L = 9.7146 \, . \tag{5.2.17}$$

We now consider the new parameter β_c, as in conditions (5.2.13), giving that, after using Eqs. (5.2.14) to (5.2.16),

$$\begin{aligned} \frac{a_1}{\overline{a}_1}\ 2^{m+1}\, a_2^{2-m}\ \left(\frac{1-2m}{2-m}\right)^{2-m} &= \frac{1}{\beta_c}\ , \\ \frac{a_1}{\overline{a}_1}\ a_2^{(1-2m)/2} &= \beta_c\ . \end{aligned} \tag{5.2.18}$$

After solving these for a_1 and a_2, we find

$$\begin{aligned} a_1 &= \overline{a}_1\ \left[\frac{\beta_c^{5-4m}}{2^{2m^2+m-1}}\ \left(\frac{1-2m}{2-m}\right)^{2m^2-5m+2}\right]^{1/3}\ , \\ a_2 &= \left[\frac{1}{\beta_c^2\ 2^{m+1}}\ \left(\frac{2-m}{1-2m}\right)^{2-m}\right]^{2/3}\ . \end{aligned} \tag{5.2.19}$$

It is now sufficient to give the values of (m, β_c) to define a specific theory of convection. It follows from relations (5.2.17) that the *CM* formulation, which has $m \simeq 0.15$, corresponds approximately to $\beta_c \simeq 10$.

5.3 Grossman et al. Theory of Convection

The parameter β_c can be given a physical interpretation in the context of the steady-state local convection theory of Grossman et al. (1993). We do not do so in order to validate/justify the use of β_c, which have been introduced just to parametrize the uncertainties, but instead as a way to justify that within the mixing length type of theories this parameter does reflect real uncertainties in those descriptions. Any Mixing Length type of theory needs to introduce several length scales describing the geometry of the turbulent eddies and the dissipation processes. In particular the mixing length ℓ, used to describe the distance that the eddies move on average before losing their identity. A given local theory of convection corresponds to defining the particular dependence of each length scale on the local conditions.

We have considered the derivation of Grossman et al. because it allows us to maintain some of these lengths unspecified, replacing them by the ratio relative to each other. When doing this, we make the strong assumption that the ratio of the lengths to one another is independent of position. This is not necessary so, and most probably it is not, however unless we specify some functional dependence for these as we do for ℓ we can not construct a formulation. Note that the usual *MLT* (and for that matter the *CM* formulation also) in a similar way assumes implicitly that the ratios are constant for all the star (see for example the derivation of the expression for the convective flux by Gough 1977).

After presenting the basics of their derivation we use the expression for steady state local convection to relate the scaling of the typical lengths of convection with the parameter β_c.

5.3.1 Typical length scales

In their work, Grossman, Narayan & Arnett (1993) develop a Boltzmann transport theory for turbulent fluid elements. The turbulent viscosity is modelled through a turbulent viscosity coefficient

$$\nu_{\rm turb} = \sigma\, \ell_\omega \ , \tag{5.3.1}$$

where σ is the local velocity dispersion of the turbulent eddies and ℓ_ω is a typical length for the momentum exchange between blobs. Similarly, they model the turbulent diffusion of heat through a diffusion coefficient

$$\chi_{\rm turb} = \sigma\, \ell_\theta \ , \tag{5.3.2}$$

where ℓ_θ is also a typical thermal length associated with the diffusion of heat. The other two lengths considered are the vertical (ℓ_v) and horizontal (ℓ_h) dimensions of the turbulent eddies. As is typical of mixing-length theories, they also introduce the mixing length ℓ which is defined as the distance that the turbulent eddies travel on average before losing identity.

The standard process of constructing the expressions for the *MLT* (Böhm-Vitense 1958; Cox & Giuli 1968) has some implicit assumptions which relate these different lengths, and which are normally included in what are described as geometric coefficients. Since we want to explore some features of the hidden assumptions in constructing the expressions, all lengths shall be kept.

5.3.2 Convective flux

Because we are interested in the mixing-length theory, we restrict ourselves to the case described by Grossman et al. as *steady-state local convection*. This corresponds to the case where any time dependence is ignored, there are no mean bulk motions and all third moments are set equal to zero (defining the closure conditions). Turbulent pressure and microscopic viscosity are considered to be negligible compared with the thermal pressure and turbulent viscosity, respectively.

The expression for the convective flux is

$$F_c = \frac{\rho C_P T}{Qg} B \sigma^3 \ ; \tag{5.3.3}$$

here the velocity dispersion σ is determined as

$$\sigma = \frac{D}{2E}\left[\left(1 + 4Qg\,\frac{\Delta\nabla T}{T}\,\frac{E}{BD^2}\right)^{1/2} - 1\right] \ , \tag{5.3.4}$$

where the superadiabatic temperature gradient $\Delta\nabla T$ is given by Eq. (5.2.7). The expressions for B, D and E given by Grossman et al. are

$$\begin{aligned} B &= \frac{2\ell_\omega}{\ell_h^2} \,, \\ D &= \frac{K}{\rho c_p}\left(\frac{1}{\ell_v^2}+\frac{2}{\ell_h^2}\right) \,, \\ E &= \frac{2\ell_\theta}{\ell_h^2} \,, \end{aligned} \tag{5.3.5}$$

with K being the radiative conductivity, as in Eq. (5.2.2).

Using our notation (see previous Section), we write these expressions as

$$F_c = K\Delta\nabla T\ \Phi \,, \tag{5.3.6}$$

with

$$\Phi = \frac{a_1}{\Sigma}\left[(1+a_2\Sigma)^{1/2}-1\right]^3 \,. \tag{5.3.7}$$

Also

$$\Sigma = \frac{2Qg}{3^4}\,\frac{\Delta\nabla T}{T}\,\left(\frac{\rho c_p}{K}\right)^2 \ell^4 \,, \tag{5.3.8}$$

and

$$\begin{aligned} a_1 &= \frac{9}{8}\,\frac{\ell_\omega \ell^4}{54\,\ell_h^2\ell_\theta^3}\left(\frac{2+\ell_h^2/\,\ell_v^2}{3}\right)^3 \\ a_2 &= \frac{18\,\ell_h^4\ell_\theta}{\ell^4\ell_\omega}\left(\frac{3}{2+\ell_h^2/\,\ell_v^2}\right)^2 \,. \end{aligned} \tag{5.3.9}$$

Relation (5.3.8) is of course equivalent to definition (5.2.1) used before.

At this point we have some freedom in choosing each length; a group of relations defines a particular theory of convection. The "traditional" mixing-length theory (Böhm-Vitense 1958), for example, is recovered with the following relations

$$\ell_h = \ell_v = \ell_\omega = \sqrt{3}\,\ell_\theta = \left(6\sqrt{3}\right)^{-1/4}\ell \,. \tag{5.3.10}$$

The last relation follows from the condition for the onset of convection (see Grossman et al.) corresponding to a critical Rayleigh number of $60\sqrt{3}$. To be definite, we constrain the prescriptions considered to have this critical Rayleigh number, leading to the following relation between the mixing length ℓ and the other relevant lengths:

$$\ell^4 = 6\sqrt{3}\,\ell_h^4\left(\frac{5}{3+2\,\ell_h^2/\,\ell_v^2}\right)\left(\frac{3}{2+\ell_h^2/\,\ell_v^2}\right) \,. \tag{5.3.11}$$

We note that relations (5.3.10) - (5.3.11) are not the only way to recover the *MLT* expressions: these only require a_1=9/8 and a_2=1. However, they are the closest to the

physical arguments employed by different authors when deriving such expressions in a phenomenological approach, particularly in imposing $\ell_h{=}\ell_v$ and $\ell_v{\sim}\ell_\omega{\sim}\ell_\theta{\sim}\ell$.

To complete expressions (5.3.8) - (5.3.9) and (5.3.11), it is also necessary to relate ℓ to the local stratification. One of the options more frequently used is to expressed the mixing length as being proportional to the pressure scale height; $\ell{=}\alpha_c H_P$. The constant of proportionality α_c is a parameter traditionally called "the mixing-length parameter".

5.3.3 Convective efficiency and the length scales

We now introduce the parameters α_h, α_ω and α_θ, replacing some of the lengths, by the following relations:

$$\ell_h = \alpha_h\, \ell_v \ , \quad \ell_\omega = \alpha_\omega\, \ell_h \ , \quad \ell_\theta = \alpha_\theta\, \ell_h \ . \tag{5.3.12}$$

Note that α_h simply measures the asymmetry of the eddies, i.e, horizontal typical size versus vertical size. After substitution of Eqs. (5.3.11) and (5.3.12) into Eqs. (5.3.9), we obtain

$$\frac{8}{9}\, a_1 = \frac{\alpha_\omega}{3\sqrt{3}\ \alpha_\theta^3} \left(\frac{5}{3{+}2\alpha_h^2}\right) \left(\frac{2{+}\alpha_h^2}{3}\right)^2 \ ,$$

$$a_2 = \frac{\sqrt{3}\ \alpha_\theta}{\alpha_\omega} \left(\frac{3{+}2\alpha_h^2}{5}\right) \left(\frac{3}{2{+}\alpha_h^2}\right) \ . \tag{5.3.13}$$

To relate this to our parameter β_c, we use conditions (5.2.18). As we have found that the results depend little on the value of m we shall assume $m{=}{-}1$, the *MLT* value. Thus conditions (5.2.18) yield

$$\frac{8}{9}\, a_1\, a_2^3 = \frac{1}{\beta_c} \ ,$$

$$\left(\frac{8}{9}\, a_1\right)^2 a_2^3 = \beta_c^2 \ . \tag{5.3.14}$$

We can now use these conditions with expressions (5.3.13) to obtain two conditions involving α_ω, α_θ, α_h and β_c. These are

$$\frac{1}{\alpha_\omega^2} \left(\frac{3{+}2\alpha_h^2}{5}\right)^2 \left(\frac{3}{2{+}\alpha_h^2}\right) = \frac{1}{\beta_c} \ ,$$

$$\frac{1}{3\sqrt{3}\ \alpha_\omega \alpha_\theta^3} \left(\frac{3{+}2\alpha_h^2}{5}\right) \left(\frac{2{+}\alpha_h^2}{3}\right) = \beta_c^2 \ . \tag{5.3.15}$$

Eliminating α_ω between the two equations leaves

$$\alpha_\theta = \frac{1}{\sqrt{3}\ \beta_c^{5/6}} \left(\frac{2{+}\alpha_h^2}{3}\right)^{1/2} \ , \tag{5.3.16}$$

while the first equation simply gives

$$\alpha_\omega = \beta_c^{1/2} \left(\frac{3+2\alpha_h^2}{5}\right)\left(\frac{3}{2+\alpha_h^2}\right)^{1/2} . \tag{5.3.17}$$

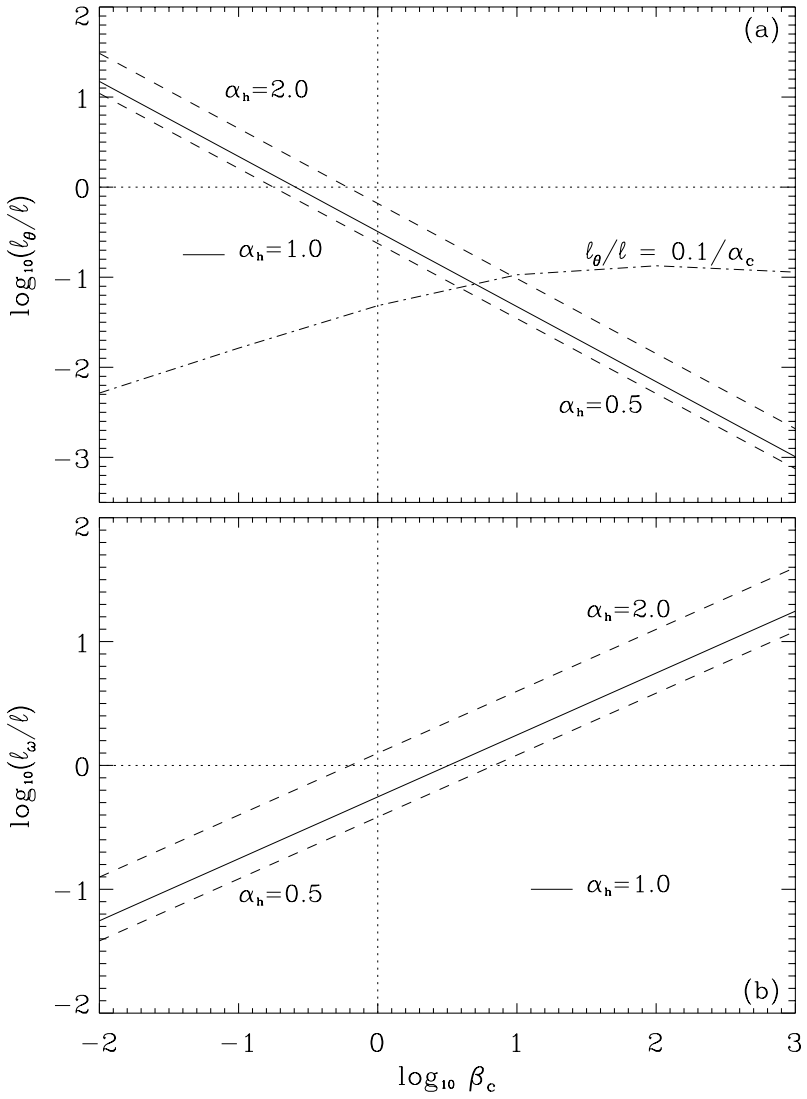

Fig. 5.1: (a) Plot of the ratio between the length associated with the turbulent diffusion of heat (ℓ_θ) and the mixing length ℓ, versus the parameter β_c. As indicated, the solid and dashed lines correspond to different values of α_h, which measures the asymmetry of the eddies. Also plotted is the condition ℓ_θ/ℓ=0.1/α_c corresponding to the upper limit given by the study of the overshoot region at the bottom of the solar convection zone (cf. Chapter 3 and Section 5.7). (b) As (a), but for the ratio between the length associated with the turbulent diffusion of momentum (ℓ_ω) and the mixing length ℓ.

If we further ignore the asymmetry of the eddies in the geometrical factors (by using α_h=1) it is clear that the effect of β_c being different from unity is to rescale the typical

length scales for the diffusion processes. Note that the factors associated with the asymmetry of the eddies are expected to be of order unity. From Eqs. (5.3.16) - (5.3.17) and using Eq. (5.3.11) it follows that

$$\frac{\ell_\theta}{\ell} = \frac{1}{\left(54\sqrt{3}\right)^{1/4}\beta_c^{5/6}}\left(\frac{3+2\alpha_h^2}{5}\right)^{1/4}\left(\frac{2+\alpha_h^2}{3}\right)^{3/4} ,$$

$$\frac{\ell_\omega}{\ell} = \frac{\beta_c^{1/2}}{\left(6\sqrt{3}\right)^{1/4}}\left(\frac{3+2\alpha_h^2}{5}\right)^{5/4}\left(\frac{3}{2+\alpha_h^2}\right)^{1/4} . \tag{5.3.18}$$

For α_h=1 and β_c=1, the *MLT* values, we have that ℓ_θ=32% ℓ and ℓ_ω=56% ℓ. Ignoring the factors of order unity due to α_h, the dependence of ℓ_θ and ℓ_ω on β_c is given simply as,

$$\frac{\ell_\theta}{\ell} \sim \frac{1}{\beta_c^{5/6}} \qquad \text{and} \qquad \frac{\ell_\omega}{\ell} \sim \beta_c^{1/2} . \tag{5.3.19}$$

One effect of changing the value of β_c is therefore to rescale the typical length scales for the diffusion of heat and momentum. Thus for high values of β_c, $\ell_\theta \ll \ell$ (see Fig. 5.1a) indicating that in this limit thermal relaxation is much faster, whereas the opposite is true of ℓ_ω (see Fig. 5.1b): in other words, thermal fluctuations are more rapidly damped, and velocity fluctuations less rapidly damped. As a consequence, for high β_c the thermal stratification is more nearly adiabatic in the bulk of the convection zone, whereas the convective transport is *less* efficient near the surface; and in any overshoot region beneath the convection zone, the near-adiabatic stratification would extend less deeply if β_c were increased, even though the velocity fluctuations would penetrate more deeply into the radiative interior.

5.4 Envelope Models

In order to test the response of the frequencies of oscillation to the parameters β_c and m, we construct several Parametrized Temperature Gradient (*PTG*) envelope models using the formalism described in Section 5.2, with different combinations of values for the two parameters. All envelopes were constructed using the CEFF equation of state (Christensen-Dalsgaard & Däppen 1992), which includes in the EFF equation of state (Eggleton, Faulkner & Flannery 1973) a Debye–Hückel approximation for the Coulomb term. The opacities of Cox & Tabor (1976) were used. We note that, in this study, only model and frequency differences are considered; hence the precise choice of physics, including opacity, is not important as long as the same choice is used consistently for all models. The envelopes all have the same surface mass M, radius R and luminosity L, and the same chemical composition (with abundances by mass of helium and heavy elements of, respectively,

0.247 and 0.020). The chemical profile used is a scaling of a chemical profile for an evolved solar model at the present solar age. The value of α_c was determined in each case by requiring the base of the convection zone to be at the helioseismically measured depth $d_{\rm b}$=0.287 R (Christensen-Dalsgaard, Gough & Thompson 1991). For more details on the calculation of the models see Appendix A. Characteristics for all envelopes calculated are listed in Table 5.1.

Table 5.1: Parameters and characteristics of the envelope models determined using our parametrization of convection. Given the values of m and β_c, the condition requiring the depth of the convection zone to be $d_{\rm b}$=0.287R gives the value of the mixing-length parameter α_c. The fifth column lists the maximum value of the temperature gradient in the envelope, which occurs very near the top of the convection zone.

Model	m	$\log_{10}(\beta_c)$	α_c	max(∇)	Theory
$PTG_{\rm a1}$	-2	-2	19.2984	0.6806	
$PTG_{\rm a2}$	"	-1	6.1135	0.6821	
$PTG_{\rm a3}$	"	0	2.0506	0.8501	
$PTG_{\rm a4}$	"	1	0.9256	1.8135	
$PTG_{\rm a5}$	"	2	0.7400	2.6760	
$PTG_{\rm a6}$	"	3	0.8766	2.9270	
$PTG_{\rm b1}$	-1	-2	19.2995	0.6807	
$PTG_{\rm b2}$	"	-1	6.1220	0.6843	
$PTG_{\rm b3}$	"	0	2.0678	0.8573	*MLT*
$PTG_{\rm b4}$	"	1	0.9398	1.7944	
$PTG_{\rm b5}$	"	2	0.7466	2.6583	
$PTG_{\rm b6}$	"	3	0.8784	2.9223	
$PTG_{\rm c1}$	-0.4	-2	19.3056	0.6811	
$PTG_{\rm c2}$	"	-1	6.1444	0.6899	
$PTG_{\rm c3}$	"	0	2.1006	0.8672	
$PTG_{\rm c4}$	"	1	0.9642	1.7631	
$PTG_{\rm c5}$	"	2	0.7575	2.6299	
$PTG_{\rm c6}$	"	3	0.8815	2.9146	
$PTG_{\rm d1}$	0.15	-2	19.4646	0.6888	
$PTG_{\rm d2}$	"	-1	6.3334	0.7179	
$PTG_{\rm d3}$	"	0	2.2613	0.8893	
$PTG_{\rm d4}$	"	1	1.0604	1.6506	*CM*
$PTG_{\rm d5}$	"	2	0.7976	2.5308	
$PTG_{\rm d6}$	"	3	0.8929	2.8867	

To illustrate the structural characteristics of the envelopes, Fig. 5.2a shows the adiabatic, radiative and actual temperature gradients for the *MLT* model while Fig. 5.2b is the same plot but for $PTG_{\rm d4}$, which corresponds approximately to the *CM* formulation. It is evident that the superadiabatic gradient takes higher values in the latter case. Outside the superadiabatic layer, the envelopes are very similar. Table 5.1 illustrates, for several values of m, the effect of varying β_c: for increasing values of β_c we get increasingly high values of the maximum of the superadiabatic gradient in the model, as expected. To keep

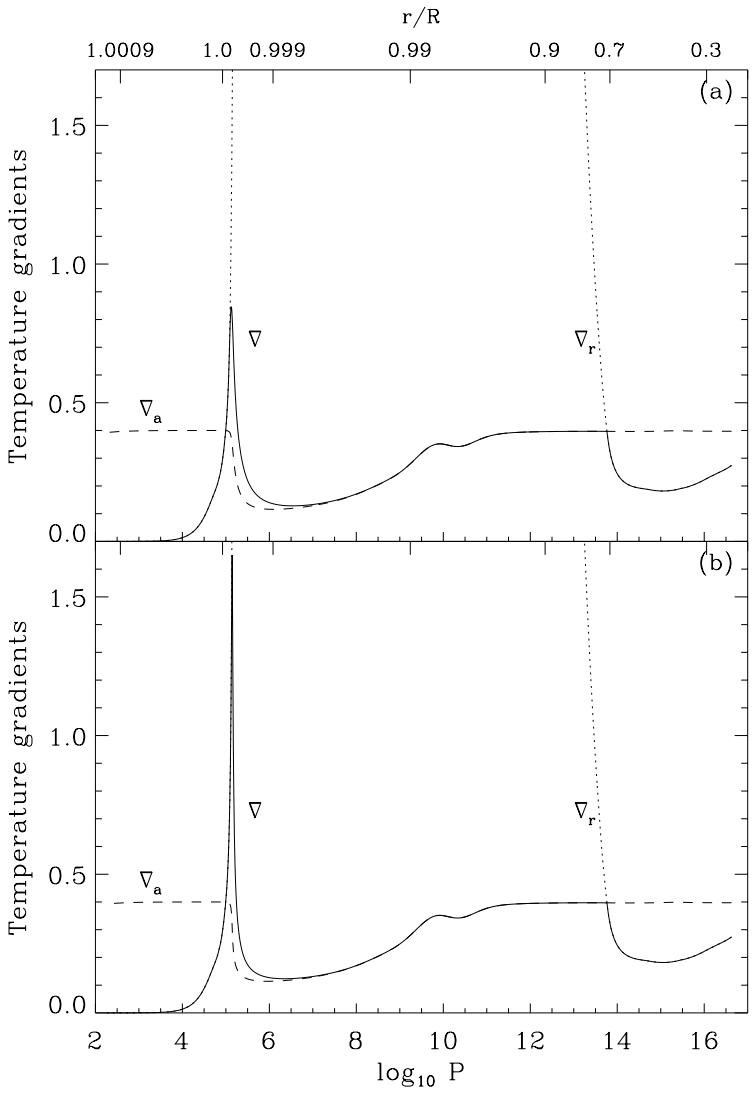

Fig. 5.2: Adiabatic $\nabla_{\rm a}$ (dashed line), radiative $\nabla_{\rm r}$ (dotted line) and actual ∇ (continuous line) temperature gradients for (a) the standard mixing-length theory envelope ($PTG_{\rm b3}$) and (b) model $PTG_{\rm d4}$ corresponding approximately to the *CM* formulation. Note that the models only differ in a very thin region at the top of the convection zone, being essentially the same everywhere else.

the base of the convection zone at the same position, the nearly adiabatically stratified region has to extend further up to compensate for the steeper variation of the temperature in the superadiabatic layer. Thus the mixing-length parameter α_c must decrease. It is interesting to note that the value of α_c becomes almost independent of β_c for very high values. This limit corresponds to the value of α_c for a model with a discontinuous jump of the temperature at the top, and an adiabatically stratified convection zone everywhere.

In Fig. 5.3a the temperature gradient is plotted for models with different values of β_c but with the same m, and also for different values of m but with same β_c. The value of m

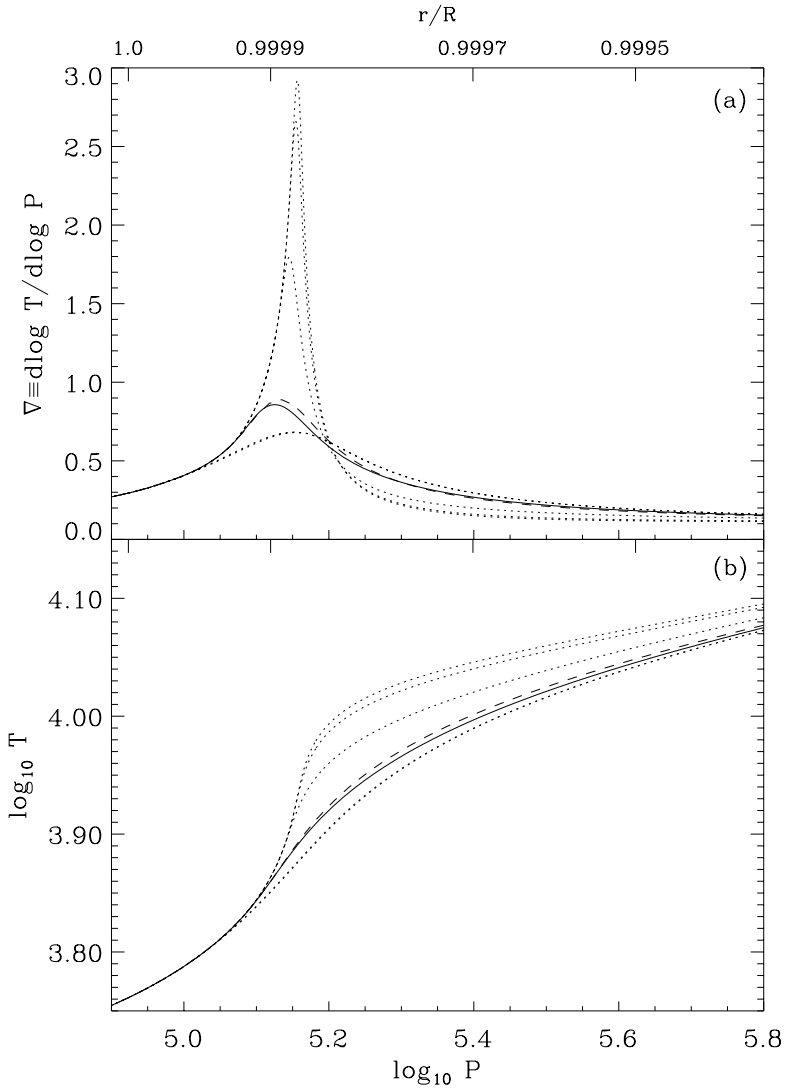

Fig. 5.3: (a) Temperature gradient for the *MLT* model $PTG_{\rm b3}$ (continuous line) and all the other $PTG_{\rm b}$ models (dotted lines) which have m=−1 and increasing values of β_c (corresponding to increasing maximum of ∇). Model $PTG_{\rm d3}$ (dashed line) is also shown, for comparison with $PTG_{\rm b3}$: both have β_c=1 but they have different values of m. (b) Plot of the temperature at the top of the convection zone for the same models as in (a).

does not affect the model significantly, since it is only important in a very thin layer between the two regimes of inefficient and highly efficient convection. To show the integrated effect on the temperature of such gradients, in Fig. 5.3b we plot temperature against pressure, indicating the different behaviour in the models at the top of the convection zone; they are the same everywhere else.

5.5 Oscillations

How the seismic properties of the models are affected by changes in the convection theory are now determined. Keeping in mind that any difference between the models is confined to a very thin region at the top of the convective envelope, it is important to understand what exactly differs between the models constructed with different values of β_c or/and m. A discussion about these differences and its analysis in terms of *kernels* is given. Quantitative and qualitative comparisons are done and the changes in the frequencies induced by such variations on the modelling of convection are analysed.

5.5.1 Model differences

The structural differences between the envelope models give rise to differences in their p-mode frequencies. Assuming that differences are sufficiently small for linear perturbation theory to be used, the frequency differences can be related to structural differences by kernels (e.g. Gough 1985, see also Chapter 1).

Since the models are in hydrostatic equilibrium, the structural differences pertinent to calculating adiabatic frequencies can be described by just two independent functions. There is great freedom of choice in which pair of functions to use. Here we shall work in terms of the adiabatic sound speed c and $v \equiv \Gamma_1/c$ (cf. Eq. (1.2.4)). This slightly unusual choice is motivated by the use of similar variables by Christensen-Dalsgaard & Pérez Hernández (1992) in their study of the influence of the upper layers of a star on p-mode frequencies. A further freedom is how to take the model differences. The conventional choice is to evaluate the differences at constant fractional radius; however, for near-surface model changes the structural differences are more nearly confined to the surface, and the frequency differences thus easier to interpret, if differences at constant fractional mass (Lagrangian differences) are used (Christensen-Dalsgaard & Thompson 1996).

Lagrangian relative differences $\Delta c/c$ and $\Delta v/v$ in sound speed and v between some envelopes and the *MLT* envelope are shown in Fig. 5.4. The effects of varying m or β_c are both illustrated. The main effect of changing the convective efficiency (or superadiabaticity) in the models is to move the hydrogen ionization zone. This gives rise to the structural differences shown in Fig. 5.4. In particular, if the convective efficiency is decreased in the superadiabatic layer (simulated in our models by increasing the value of β_c) then the region of partial hydrogen ionization is moved closer to the surface. This leads to a negative Lagrangian perturbation in Γ_1. Furthermore, we note that $v = \sqrt{\Gamma_1/u}$, where $u = P/\rho$ and ρ is density; the increased superadiabatic gradient leads to a more rapid increase in temperature, and hence in u, with depth, also contributing to the negative Δv shown in Fig. 5.4.

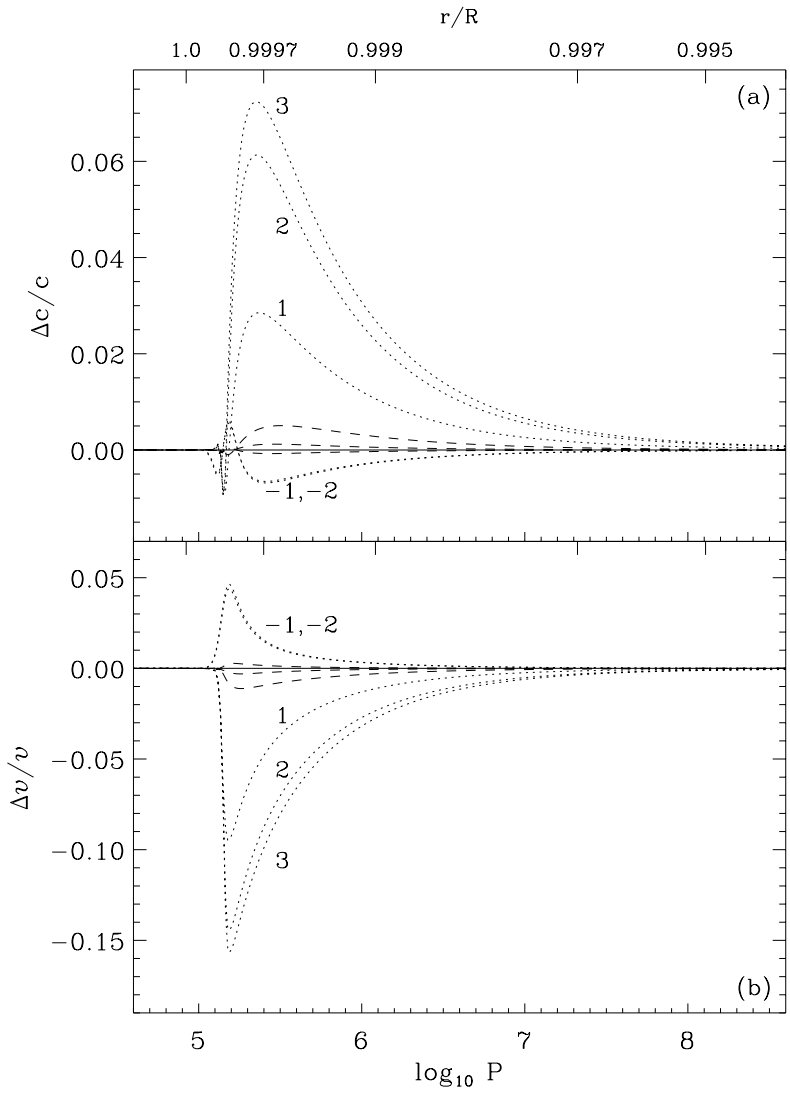

Fig. 5.4: (a) Fractional sound-speed differences, evaluated at constant mass fraction, of all $PTG_{\rm b}$ models relative to model $PTG_{\rm b3}$ showing the effect of changing β_c (dotted lines); the curves are labelled by the values of $\log_{10}\beta_c$. Also shown are the differences of models $PTG_{\rm a3,c3,d3}$ minus $PTG_{\rm b3}$ to illustrate the effect of changing m (dashed lines). (b) As (a), but for fractional differences of $\upsilon{=}\Gamma_1/c$.

5.5.2 Frequency differences

The difference in frequency ω of a mode of degree l and order n between different models is related to the structural differences by (see Section 1.3.5)

$$\frac{\delta\omega_{nl}}{\omega_{nl}} \;=\; \int_0^R \left[K_{nl}^{(\upsilon,c)}(r)\;\frac{\Delta\upsilon}{\upsilon} \;+\; K_{nl}^{(c,\upsilon)}(r)\;\frac{\Delta c}{c}\right] \mathrm{d}r\;. \tag{5.5.1}$$

The kernels $K_{nl}^{(\upsilon,c)}$ and $K_{nl}^{(c,\upsilon)}$ are known functions, and the integration is from the centre of the model to a point above the photosphere, e.g. the temperature minimum. In the

present case the region where Δv or Δc are non-zero is essentially restricted to the superadiabatic region; thus the integration only needs to extend over the envelope. The fact that we do not have a full model makes therefore no difference. The frequency differences contain two contributions, i.e., the two integrated terms on the right of Eq. (5.5.1). These contributions, together with the actual frequency difference, are shown in Fig. 5.5 for l=50 modes and the model pair $PTG_{\rm b6}$ and $PTG_{\rm b3}$. Note that the contribution from $\Delta c/c$ is very small, with this choice of variable pair: the frequency differences are almost completely described by the change in v. This is indeed true more generally for near-surface model changes (Christensen-Dalsgaard & Thompson 1996). This makes v a very convenient variable for describing the effect of such model changes on p-mode frequencies.

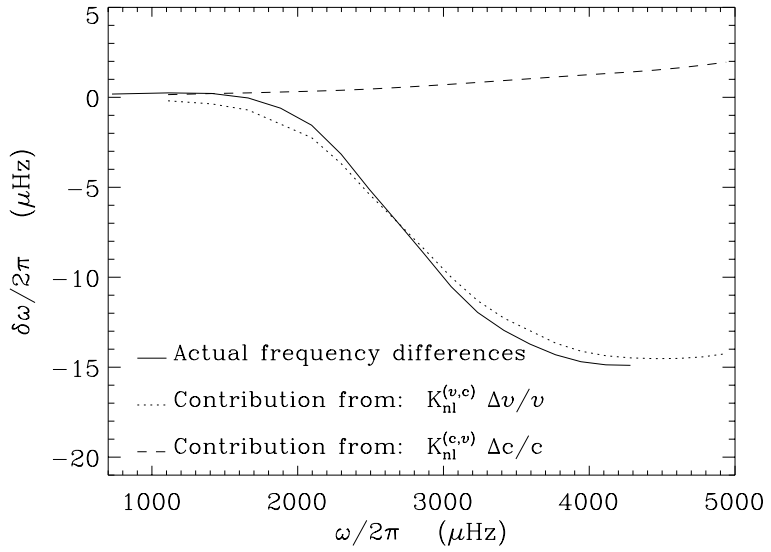

Fig. 5.5: Frequency differences in the sense $PTG_{\rm b6}$ minus $PTG_{\rm b3}$ for l=50 modes (connected by the continuous line). Also shown are the integrated contributions from sound-speed differences $[K_{nl}^{(c,v)}]$ and v differences $[K_{nl}^{(v,c)}]$ according to Eq. (5.5.1), for the same modes, using the differences shown in Fig. 5.4.

The variation of the p-mode frequency differences as a function of frequency can be understood by inspecting the kernels $K_{nl}^{(v,c)}$ (Fig. 5.6). Note that kernels for low-frequency (low-order) modes are close to zero in the region where $\Delta v/v$ is significantly non-zero. This behaviour is associated with the fact that the upper turning points of low-frequency modes lie below the superadiabatic region, so that the modes are evanescent in the superadiabatic layer. Such behaviour clearly indicates that low-frequency modes should not be affected by how low-efficiency convection is modelled. This is confirmed by Fig. 5.5, where frequency differences for modes with $\omega/2\pi \lesssim 2000\mu$Hz are close to zero. However, for higher frequencies the differences go up to 15μHz.

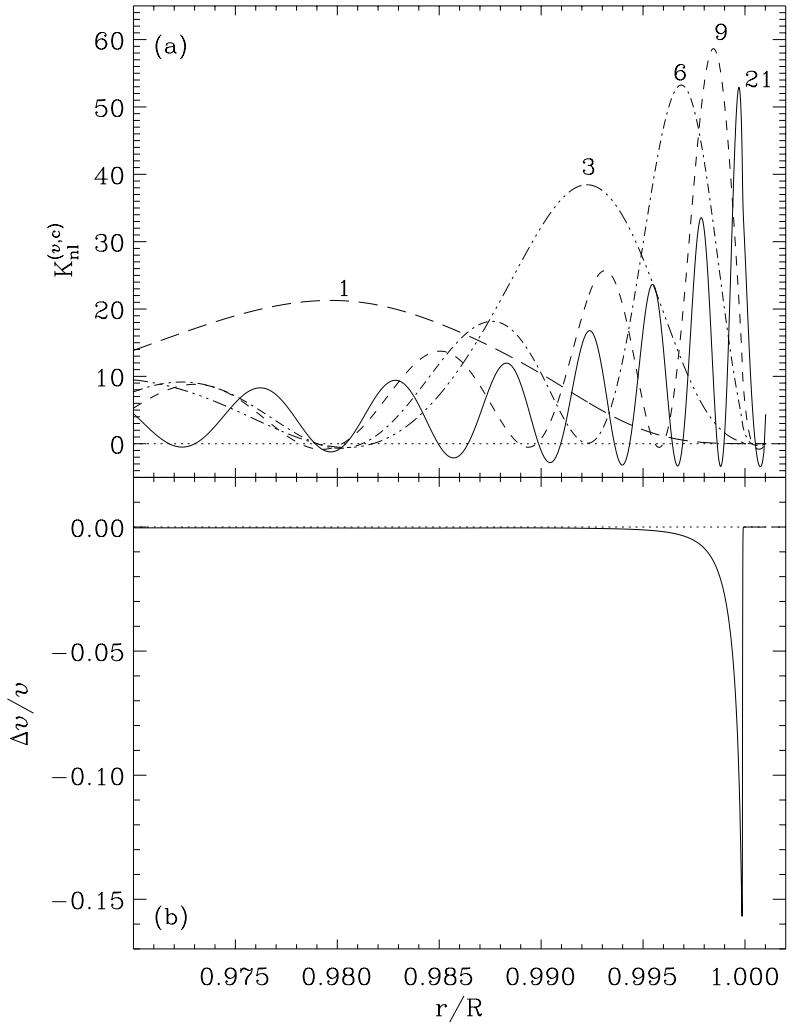

Fig. 5.6: (a) Kernels $K_{nl}^{(v,c)}$ for modes with l=50. The mode order is indicated by the number. (b) Lagrangian differences of v between models $PTG_{\rm b6}$ and $PTG_{\rm b3}$.

We have calculated differences between frequencies of various models, relative to the *MLT* model $PTG_{\rm b3}$, for p-modes with degrees l=20,30,40,50,100,200,300. The frequency differences for a given model pair essentially lie on a single curve provided the differences are first scaled by

$$Q_{nl} = E_{nl} / \overline{E}_{l=20}(\omega_{nl}) \; , \tag{5.5.2}$$

where the normalized mode energy E_{nl} is defined to be

$$E_{nl} = \frac{4\pi}{M} \frac{\displaystyle\int_0^R \left[\xi_{r,nl}^2(r) + l(l{+}1)\,\xi_{h,nl}^2(r)\right] r^2 \rho \, {\rm d}r}{\xi_{r,nl}^2(R) + l(l{+}1)\,\xi_{h,nl}^2(R)} \; . \tag{5.5.3}$$

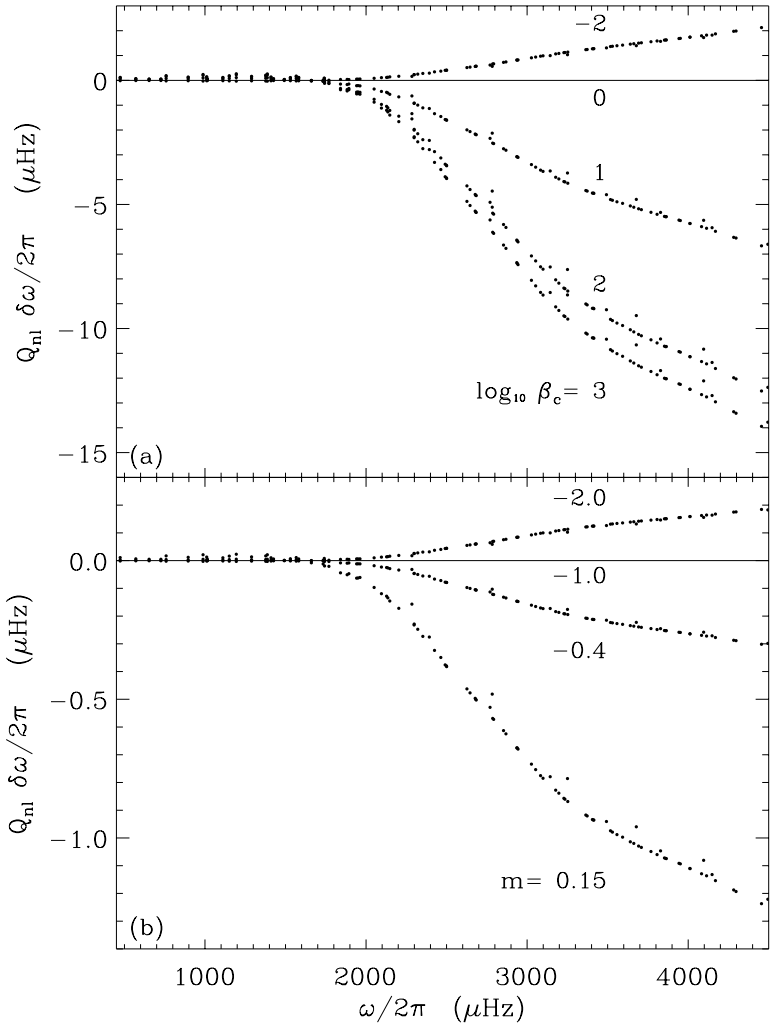

Fig. 5.7: (a) Scaled differences between frequencies of models $PTG_{\rm b1}$, $PTG_{\rm b4} - PTG_{\rm b6}$ and the reference *MLT* model $PTG_{\rm b3}$. Note that all models have the same value of m=−1, and increasing values of β_c as shown. (b) Scaled frequency differences between models $PTG_{\rm a3}$, $PTG_{\rm c3}$, $PTG_{\rm d3}$ and model $PTG_{\rm b3}$. All models have β_c=1 but different m as indicated. Outlier points correspond to the highest values of l.

Here $\xi_{r,nl}(r)$ and $\xi_{h,nl}(r)$ are respectively the radial and horizontal components of the eigenfunction of the mode (n,l) with frequency ω_{nl}, at the radius r. By $\overline{E}_{l=20}(\omega_{nl})$ we mean the value obtained by interpolating the mode energy of l=20 modes to the frequency ω_{nl}. In Fig. 5.7a scaled frequency differences are shown for models with same value of m but varying values of β_c, while Fig. 5.7b shows the effect of varying m, keeping β_c constant. The reference model used in both plots is the *MLT* model $PTG_{\rm b3}$. Low-frequency modes are indeed not affected by our change of the envelope model relative to the *MLT* as shown in these figures. By comparing the vertical scales of the two figures it is obvious that the

effect produced by changing m is an order of magnitude smaller than the effect of changing β_c.

5.6 Turbulent pressure and other effects

As far we have done a simple comparison of frequencies between models which differ only in their superadiabatic layer. This is only possible if all other aspects of the physics are the same for both models being compared. However if we extend, as we want to, this analysis to solar data in order to established if some description is favoured, and is therefore a better representation of solar convection, care must be taken with the possibility of many other effects being contributing to the frequency differences.

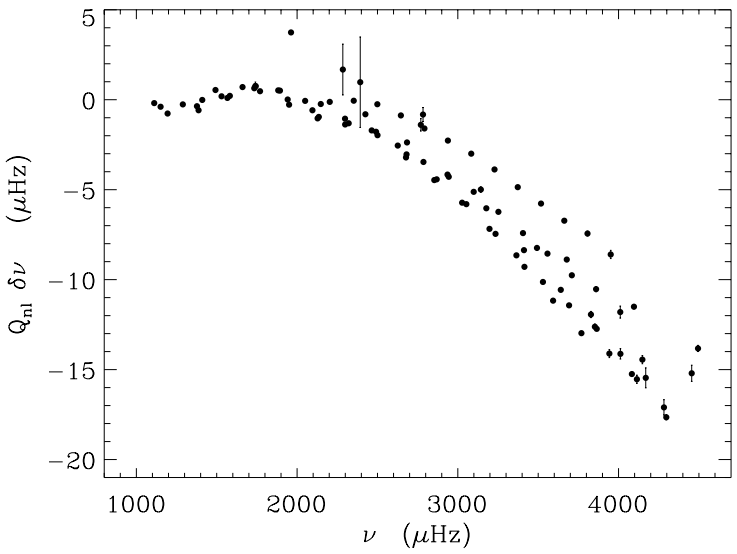

Fig. 5.8: Scaled differences between frequencies of the Sun from Libbrecht et al. (1990) and a standard solar model (in the sense *Sun-Model*) for the same set of modes as in Fig. 5.7. The model has been calculated using *MLT* and the best available physics. The error bars represent the quoted observational errors.

In Fig. 5.8 we show as an example frequency differences between the Sun (data from Libbrecht et al. 1990) and a standard solar model calculated using Mixing Length Theory to model convection. We are of course tempted to say that indeed the behaviour seen when increasing the superadiabatic gradient is similar to the one seen in this figure. This is the basic reason why several authors have found that the theory of Canuto & Mazzitelli (1991,1992) does indeed improve the matching of observed and theoretical frequencies. But such an improvement can be just coincidental due to the fact that increasing the superadiabatic gradient simulates the effect of some other aspect of the physics, while the

actual gradient is far from the predicted one. In this Section we try to present an overview of some possibilities and on how we may hope to constrain further the modelling of the convective flux in stellar interiors.

One possibility of going further in our understanding of convection is of course numerical simulations of stellar convective envelopes. The extra insight is given by the possibility of having a closer representation of the fluid motions in the star, having some control over the other physics that also contribute to the overall state. We address in particular the contribution to the mean stratification of the turbulent pressure. Due to the significant fluid velocities compared with the local sound speed in the superadiabatic layer it is expected that the total pressure is significantly different from the gas pressure and therefore having turbulent pressure an important contribution to the support against gravity (eg. Balmforth 1992b).

We also review briefly the fact that the usual assumption of adiabatic oscillations, being a very good approximation for most of the star, is quite unsatisfactory in the superadiabatic layer where the oscillations are expected to be non-adiabatic. This is yet another effect contributing to the frequency differences and coming from the same layers of the star.

There is also another aspect of convection, the intrinsic non-locality of the fluid motions, which is usually ignore when using expressions for the flux that depend only on the local conditions. We do know of course that convection cannot be local, and overshoot is one of the confirmations of this. Presently, there are some non-local theories of convection that try do reproduce to some degree how the average properties of the fluid at a given point depend on the rest of the star, and in particular, on all of the convection zone.

5.6.1 Turbulent pressure and non-locality of convection

In a first order approach to the effect of turbulent pressure we can say that the dominant effect of this extra pressure is to change the hydrostatic equation by adding an extra contribution for the support of the gas. The response is a decrease of the gas pressure (and temperature) which is translated as a decrease in convective efficiency and therefore has a similar effect when calculating a model to decrease a priori the convective efficiency. This is one of the effects that turbulent pressure has on the average structure in the superadiabatic region, however the interaction with the oscillations is also possible. This has been modelled to some degree by using time dependent convection theories (e.g. Gough 1977). The indication is that the actual frequencies can be changed up to 2μHz as calculated by Balmforth (1992b). However, he concludes that the largest contribution is not this but comes from differences in the mean structure resulting from the non-locality of convection

as modelled there. This characteristic of the convection theory developed is shown to be responsible for changes in frequencies of oscillation that can go up to 10 μHz. A value of this order of magnitude is found above, in our parametrization, for steeper gradients when compared with *MLT*. Such type of gradients have also been found for a mixing length proportional to depth, as given by

$$\ell = \left(1-\frac{\alpha_c}{10^4}\right) r_u - r \ , \tag{5.6.1}$$

where r_u is the radial position of the upper boundary of the convection zone. This type of mixing length introduces to a small degree some non-locality of convection (Canuto & Mazzitelli 1991, 1992). A model calculated with this expression is compared below with one where the mixing length is proportional to the pressure scale height. The main difference is in the superadiabatic gradient, which now has higher values resulting from the fact that the mixing length is smaller near the surface where $r_u - r < H_P$ - see Fig. 1.4. This has a very similar effect to increasing the parameter β_c considered before, on the structure of the upper layers of the convection zone. Some other nonlocal convection models have been proposed (eg. Xiong & Chen 1992 and references therein) but it is still difficult to estimate the seismic effects of such theories.

So, as a final summary we would say that the main contribution to the seismic properties of the star associated with the superadiabatic layer, coming from turbulent pressure, is its effect on the mean structure of the region. With the actual interaction with the oscillations giving only a small correction. We come back to this when discussing numerical simulations of convection. Other important factor that we must have in mind is the possible effect of the non-locality of convection. Its true effect is presently difficult to estimate, but tentative modelling indicates that it must be significant.

5.6.2 Adiabaticity of the oscillations

Also significant is the effect that our assumption of considering the oscillations adiabatic may have on the calculated frequencies. When comparing observations with numerical values we must have in mind that this is an effect that is contributing to the discrepancy between the two since the oscillations in the Sun are known (e.g. Unno et al. 1989, Balmforth 1992a, Guenther 1994) to deviate significantly from begin adiabatic at the top of the convection zone. The calculations by Balmforth (1992b) indicate that the effect on the calculated frequencies due to neglecting non-adiabatic effects are small compared with for example the effect on the mean structure from turbulent pressure. More recent calculations by Houdek, Balmforth & Christensen-Dalsgaard (1996) using the same nonlocal mixing length theory of Gough (1977) as in Balmforth's work, have been used by Rosenthal et al. (1996) to estimate the effect of using the adiabatic approximation. They found that

the non-locality of the theory gives lower frequencies, however the non-adiabaticity of the oscillations increases the frequencies relatively to the adiabatic values. The results are not yet conclusive but they seem to indicate that the two effects are opposite canceling each other to some degree. Therefore, we may say that at least the effect of the non-adiabaticity of the oscillations is to reinforce the fact that the mean structure in the superadiabatic layer has to be different from what mixing length theory predicts.

5.6.3 Results from numerical simulations of convection

Simulations of convection can provide a close representation of solar and stellar convection. For interior convection there are many such simulations whose main objective is to study the basic properties and average structure of highly efficient convection in order to compare with theories (eg. Chen et al. 1991, and references therein). However, when modelling the superadiabatic layer more care is needed because of the added difficulty of having to take into account radiative transfer. The diffusive approximation is no longer valid and so the radiative losses have to be included in the energy exchange of the fluid. This type of studies has been done by Nordlund & Dravins (1990) for different stellar masses. They have modelled the surface layers of the solar-type stars, including the photosphere and the superadiabatic layer.

The simplest analysis of this data is to calculate a horizontally and temporally averaged structure from such a simulation and use it to construct a solar model. If we then compare this model with a model that uses the same physics and has the same interior, the differences can be confined to the superadiabatic layer. Therefore any difference of the seismic properties between these models can be unambiguously attributed to the superadiabatic layer.

To illustrate the point we consider the average structure of the top 2% of a solar envelope from calculations by Nordlund (see Stein & Nordlund 1989; and Nordlund & Dravins 1990 for the details about these simulations). To this structure we add an interior model by integrating the structure equations from the base of such an average structure, using similar physics and considering the gradient to be adiabatic. The last assumption is reasonable since the simulations go deep enough for convection to be in the high efficiency regime at the bottom of the domain of the simulations. In order to compare with this envelope we have also computed three other models using the same physics and basic values (like abundances, mass and radius) but different formulations of convection. To restrict the differences to the superadiabatic layer these models have been calculated having the same depth for the convection zone as the model constructed from the simulations (with $r_{\rm d}$=0.70056R). This assures that all models are very similar except at the top of the

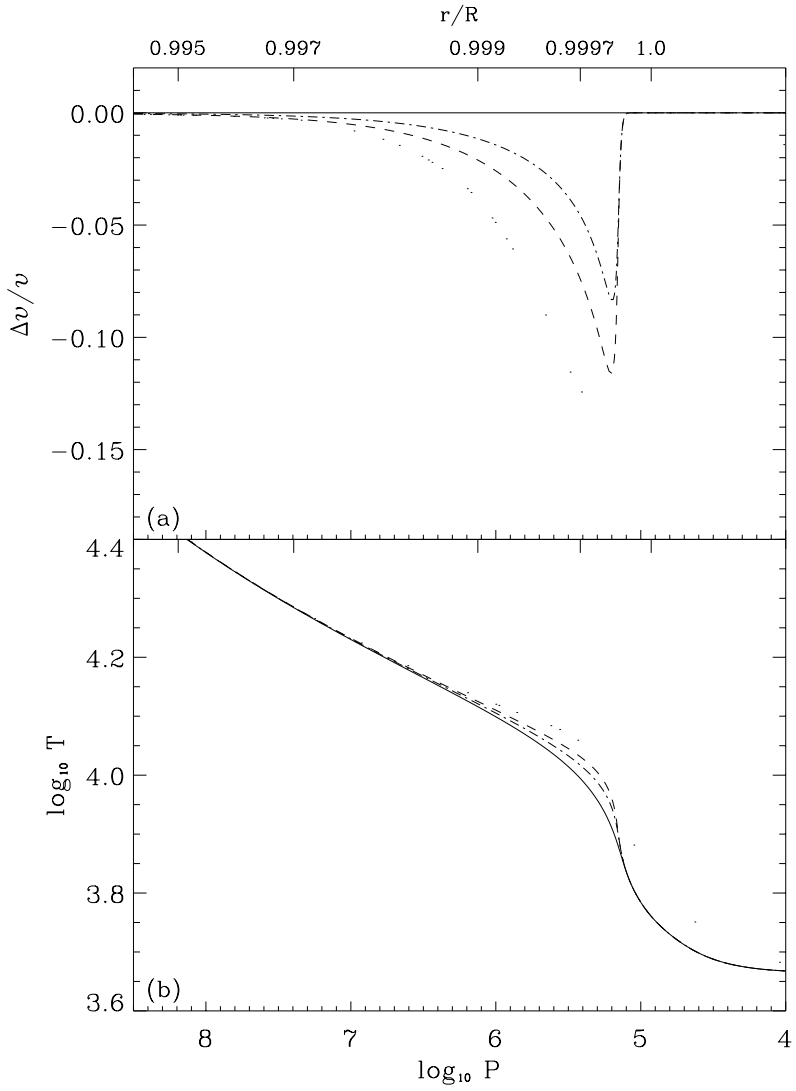

Fig. 5.9: (a) Fractional differences of $\upsilon=\Gamma_1/c$, evaluated at constant mass fraction. Differences for two *CM* models relative to a *MLT* envelope are shown. One, $CM_{\rm h}$, uses $\ell=\alpha_c H_P$ (dash-dotted line) while the other, $CM_{\rm z}$, has ℓ proportional to depth (dashed line) - see Eq. (5.6.1). The third model (dots) is the envelope constructed from the average structure of numerical simulations of the superadiabatic layer. (b) Logarithmic temperature for the same models as in (a). As in the previous panel, the continuous line is for the *MLT* model.

convection zone. One of the theoretical models is a *MLT* model while the other two are *CM* models but using difference expressions for the mixing length ℓ as given in Eqs. (5.2.5) and (5.6.1).

In Fig. 5.9 we show relative differences of $\upsilon=\Gamma_1/c$ between three of the models (simulations and *CM*) and the *MLT* model. Note that the difference between the two types of *CM* models is in the steepness of the temperature gradient. However, for the simulations the differences cannot be only modelled by a variation of the temperature gradient. In

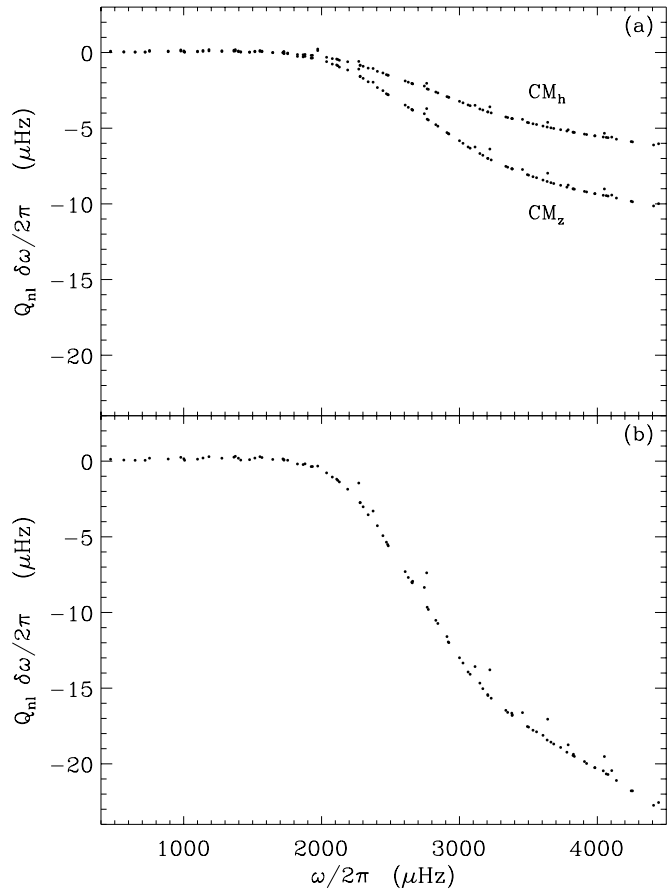

Fig. 5.10: (a) Scaled differences between frequencies of models $CM_{\rm h}$ and $CM_{\rm z}$ and the correspondent reference model *MLT*. (b) The same as (a) but now between the model constructed from the numerical simulations of convection and the same *MLT* reference model. After Rosenthal et al. (1996a).

order to understand the differences of v we also need to include the variations of Γ_1 due to turbulent pressure (Rosenthal et al. 1996a). This is also confirmed by the use of a nonlocal theory of convection as discussed above. The changes in the frequencies coming from changes in the averaged structure are mainly due to variations in Γ_1 resulting from turbulent pressure and not only from changes in the superadiabatic gradient. We also show in Fig. 5.10 frequency differences for our three models in order to illustrate this. The change of mixing length expressions between $CM_{\rm h}$ and $CM_{\rm z}$ is mainly translated in an increase of the temperature gradient since the latter has smaller values for the mixing length near the top (Fig. 1.4). This could be represented by an artificial model with a higher value of β_c. However, increasing β_c is not sufficient to reproduce the frequency differences found for the model constructed from the simulations. An actual comparison of the gradients indicates that the model $CM_{\rm h}$ shown here has already a temperature

gradient larger than the simulations in the superadiabatic zone (compare Fig. 5.2 with Fig. 1 of Rosenthal et al. 1996, for example).

5.7 Comments on seismic evidence

We note that, to improve the agreement between the observed and the computed frequencies, β_c must be fairly large, corresponding to a sharper superadiabatic gradient than obtained with mixing-length theory. Indeed, previous investigations have found that using the formulation proposed by Canuto & Mazzitelli (1991), based on a more complete description of turbulence, instead of the *MLT* formulation in solar models leads to apparently better agreement with the observed p-mode frequencies (e.g. Paternó et al. 1993; Basu & Antia 1994, 1995; Baturin & Mironova 1995). This corresponds in our formulation to using $\beta_c \simeq 10$.

Independent information about the properties of convection may be obtained by considering conditions at the base of the convection zone. Discontinuities associated with the adiabatic stratification of a possible overshoot region give rise to a signal in the frequencies which may be isolated from the observations (see Chapters 2 and 3). From such analyses we get an upper limit for the extent of this region of less than 10 per cent of the local pressure scale height. Given that this layer only exists as long as the turbulent diffusion of thermal heat is unable to adjust, the limit indicates, within the description of Grossman et al. (1993), that

$$\ell_\theta \lesssim 0.1\, H_P \quad \text{i.e.,} \quad \frac{\ell_\theta}{\ell} \lesssim \frac{0.1}{\alpha_c}\,. \tag{5.7.1}$$

The line corresponding to this limit is plotted in Fig. 5.1a, indicating that it is consistent with $\beta_c \simeq 10$, i.e., with the *CM* formulation.

Thus there appears to be some consistency between on the one hand the results based on the direct comparison of observed and computed frequencies and reflecting the properties of the superadiabatic region, and on the other the seismic limits on near-adiabaticity below the lower convective boundary. This is hardly compelling, since we have assumed that the ratio of the various length scales is independent of position, as is also done implicitly in the *MLT* and *CM* formulations. Nonetheless, both pieces of evidence suggest that stratifications similar to those in models using higher values of the parameter β_c are not inconsistent with our present helioseismic information about the physics of the Sun.

Frequency differences of 10μHz or more are considerably larger than the observational uncertainties with which many p-mode frequencies are measured. Hence one can in principle use the frequencies to investigate the effects of convection, for example differentiating between various simpler formulations of convection and results of numerical simulations. However, comparison with the observations is not a simple task, since other errors in the

calculation of solar models and frequencies (in the treatment of, for example, atmospheric opacity or non-adiabaticity) can have an effect on the frequencies of similar magnitude (e.g. Cox, Guzik & Kidman 1989; Christensen-Dalsgaard 1990; Balmforth 1992b). Likewise, it is clear from the magnitude of the frequency shifts obtained that uncertainties in the modelling of convection potentially affect attempts to use frequency differences between observation and theory to iterate on the construction of a solar model in order to improve some other aspect of the physics (e.g. Guzik & Cox 1993; Guenther 1994).

6. Conclusions

A summary of the topics discussed in this thesis is presented with a brief review of the main results and conclusions. The implications of some of the results on our understanding of solar/stellar physics are also presented.

A discussion on further studies following the work presented here is included. I also consider some of the necessary extensions of the analyses that have been discussed here which are expected to improve some of the results reported.

6.1 Summary

The core of this work has been divided in four Chapters, addressing three subjects associated with the solar convective envelope. The first subject taking two Chapters has been the problem of detecting and measuring, using solar seismic data, a possible layer of convective overshooting at the base of the convection zone. The theoretical analysis of the effect in the frequencies of an overshoot layer, as indicated by simple models, was first presented. The subject is completed with a second part including the applications to solar models and observational data. It has been done by developing a method to isolate the signal in the frequencies due to the base of the convective envelope.

I then attempt to use the same method, as for overshoot, to study the region of the second ionization of the helium. An analysis of the periodic signal in the frequencies generate by the presence of this thin layer near the surface is developed to estimate the helium abundance and constrain the equation of state. The potential of this method is shown and some tentative conclusions/results have been put forward. This part of the work has not been presented as a conclusive study but more as a demonstration that some precise and valuable information is indeed accessible using our method.

Finally, the third subject addressed is the possibility of using frequencies of oscillation to constraint formulations to model convective energy transport in stellar structure. I have used a parametrization of convection first to estimate quantitatively how important the

modelling of low efficiency convection is in terms of the frequencies. This is an artificial parametrization, however I also include an interpretation in terms of the relative intensity of thermal and momentum diffusion scales for the fluid, for the extra parameter that is used. In that way it is shown that within the present state of convection theories it represents our uncertainty and so, our results provide a quantitative study of how uncertainties in local theories can affect the seismic properties of solar models. The study is extended further in order to try to establish if it is possible to identify the properties that are associated with the observed differences between the Sun and our standard models. However, the evidence from different sources is still unclear. I have included some general views on these, in order to present a tentative analysis of what aspect associated with convection may be affecting the frequencies of oscillation. Some suggestions on the subject are reviewed here.

6.2 Convective Overshoot

Our approach to the study of convective overshoot has been separated in two Chapters. The first deals mainly with the study of the theoretically expected effect on the frequencies of oscillation if a sharp transition is present at the base of the convection zone. To do so, we either consider a standard transition from the adiabatic stratification to a radiative one occurring at the Schwarzschild boundary or a scenario where overshooting extends the adiabatic zone beyond this instability boundary, with a jump to radiative stratification at the bottom of the overshoot layer. In the other Chapter we have presented a numerical method to isolate the signal in the frequencies and consider several solar models to calibrate such a signal. Some of the information we try to obtain for the base of the convection zone in the Sun is to establish the existence of an overshoot layer, its extent, configuration and position. Some of the results found are reviewed below.

Our analysis is based upon the assumption that the transition from the convective region and overshoot layer to the radiative interior beneath takes place over a distance much shorter than the wavelength of the modes. This is indeed consistent with theoretical predictions that the extent of the transition region is very small (less than a few km). It is the abruptness of the transition that allows us to model its effect in terms of discontinuities of the derivatives of the sound speed. Such a sharp transition in the solar structure gives rise to a quasi-periodic signal in the p-mode frequencies. We have derived a theoretical expression for the amplitude of this signal, by considering a variational principle for nonradial linear adiabatic oscillations using the Cowling approximation. The presence of overshoot, according with our assumption of a sharp transition, is seen by the waves as a discontinuity of the sound speed derivative, while a standard model without overshoot

has a discontinuity in the second derivative. We have shown that the signal associated with the near-discontinuity of the second derivative is proportional to the derivative of the radiative gradient (and so to the derivative of the opacity at the base of the convection zone), while the signal associated with the near-discontinuity of the second derivative, which is present only if there is convective overshoot, is proportional to the difference between the radiative and adiabatic gradients at the point where the transition occurs. We have further shown that there is a different frequency dependence of the amplitude between the cases of larger overshooting distances and no overshoot.

6.2.1 Comments on the method

If overshoot does force a quasi-adiabatic stratification with a sharp transition to radiative equilibrium our method provides the extent of such a layer. This has been shown by the fact that for models of this type the amplitude found is equal to the expected values, for overshooting layers extending more than about 10% of a pressure scale height (H_P). From such a safe basis we can state that if overshoot in the Sun has this configuration then its extension is no more than $0.1H_P$. However, as indicated first by Roxburgh & Vorontsov (1994) and also seen in the analysis presented here, there is a theoretically expected non-monotonic behaviour for very small penetration distances. I propose that this is the result from the incompleteness of the analysis, while our method to isolate the actual signal in the frequencies still provides the correct values for the amplitude. Such a position comes from the fact that the method can not perform worse for smaller overshoot depths since the amplitude is similar. Considering the assumptions used in the derivation of the expression for the signal, and the previous argument, the discrepancy must be due to an incompleteness of the analysis with the fitted amplitude being correct. Assuming this is so, there is a small evidence that some sort of overshooting, or at least a different behaviour from the standard model, is present.

In order to estimate how the conclusions are affected by our assumption of a sharp transition other models with a smoother transition and changed opacities have been considered. In such conditions the method provides an amplitude which is higher than the value for the standard model since any such alteration in that region tends to increase the derivative of the radiative gradient, on which the amplitude depends. The Sun can clearly be such a case. However, in order to improve the quality of the conclusions we must complement the information coming from the amplitude $A_{2.5}$, with other characteristics of the signal. The behaviour with frequency of the amplitude is such an example. This can allow us to understand what type of transition is taking place at the base of the convection zone. However, our method to isolate the signal still has difficulties in finding

such a dependence for the current observational errors. Finally, it was also shown that the method can provide a reasonable estimation of a parameter associated with the argument of the signal which provides a measurement of the position where the transition occurs. The precision with which it is found is still very low, however, due to the observational errors.

6.2.2 Amplitude of the signal

I stress again that the fundamental point upon which our result for the upper limit on ℓ_s is based, is the assumption that the overshoot region is nearly adiabatically stratified with the transition to the radiative interior occurring over a very short length. If this is not the case, then the above conclusions concerning the extent of the overshoot layer must be modified. We have also considered models in which the transition from nearly adiabatic stratification to the substantially subadiabatic stratification of the radiative interior takes place over an extended region, though the transition still takes place within a fraction of one wavelength. In this case we found that the fitted amplitude, when calibrated against the amplitudes from models with a sharp transition, is a reasonable indicator of the radius at which the stratification begins to deviate by more than $\sim$20% of being adiabatic, but not of the point where the overshoot region finally peters out and the temperature gradient becomes radiative. The extended transition region in our models could represent a sub-adiabatic overshoot region in the Sun, extending beneath the adiabatic fraction of the overshoot layer, where the convective velocity field is non-zero but has only a weak effect on the thermodynamics of the layer. Hence a more precise interpretation of our present result, and similar published results, is that any adiabatically stratified overshoot region beneath the Sun's convective envelope cannot be more than a small fraction of a pressure scale height deep. We do not rule out a substantially deeper sub-adiabatic overshoot region in which weak mixing takes place. It is worth to note the similarities we have found between the solar signal and the signal for model W_1 which has no adiabatically stratified overshooting but has a significant subadiabatic layer below the Schwarzschild boundary due to overshoot (however the observational errors are still too high, as discussed above, to allow a definite conclusion). It must also be noted, that our analysis assumed a spherically symmetric solar model. In reality, the overshoot probably has the form of plumes with a distribution of penetration depths in space and time; hence, although each plume quite likely exhibits the structure obtained in simple models, with a nearly adiabatic region followed by an abrupt transition to radiative transport, the average structure felt by the modes of oscillation is likely to be more fuzzy (see for example Rieutord & Zahn 1995 for a discussion on plumes and their effects on the mean structure). Additional apparent

fuzziness might result from a possible oblateness of the base of the convection zone or interaction with magnetic fields (Petrovay 1991). Therefore, if on physical grounds we prefer to assume that overshoot must be present, the results obtained here should be interpreted as constraining the simplest possible model, with overshoot extending the adiabatically stratified region below the Schwarzschild boundary, with a sharp spherically symmetric transition to the stratification corresponding to radiative energy transport. With improved data, as is expected from observational programs like GONG, we hope to place tighter constraints on the transition from adiabatic to radiative stratification, and in this way test average properties of more realistic hydrodynamical models for convective overshoot.

6.2.3 Argument of the signal

The other important information potentially provided by the analysis of the solar data is the radial position r_d of the transition. But, as shown, in the oscillatory signal the acoustic position occurs in combination with a term resulting from the effect of the surface layers; here the turning point depends on the frequency of the mode, causing a phase shift that is frequency dependent and observationally undetermined. Furthermore, to determine radial position from acoustic depth, accurate knowledge of the sound speed near the surface is required.

I point out that a different parameter of the fitting carries information about the location of the transition, while being less sensitive to uncertainties near the surface. However, since it is of higher order than $\tau_{\rm d}$ in the expansion of the signal, it is more strongly affected by current observational errors, limiting the precision of the r_d determination to $0.01R$ (see Fig. 3.17). To this accuracy, the results are in agreement with the value determined by Christensen-Dalsgaard et al. (1991). We also note that the absolute value of $\gamma_{\rm d}$ is affected by the l-dependence of the surface phase; however, our model calculations indicate that this is unlikely to produce a significant relative difference between the models and the Sun when going from $\gamma_{\rm d}$ to $\overline{\gamma}_{\rm d}$. Therefore, in determining r_d from relative values of $\overline{\gamma}_{\rm d}$ the expected error from this source is less than $5 \times 10^{-4} R$. The analysis of the propagation of the errors from the frequencies to the value of $r_{\rm d}$ give us hope that a reduction by half on the present uncertainties may allow a significative determination of $r_{\rm d}$.

The last information from the argument of the signal is the phase constant ϕ_0. It is also an indicator of the type of transition, and the models do show a dependence of it on the penetration distance. However the present observational and theoretical uncertainties still make it very difficult to use this information. Improvements on the understanding

of the oscillations phase α as a function of frequency and degree may provide a better understanding on how the argument is affected, providing a better estimation of ϕ_0 and the other parameters in the argument of the signal.

6.2.4 Conclusions for the Sun

If we put together all information, having in mind all possible sources of errors as discussed above, it can be said that the Sun consistently favours the behaviour seen in models with almost no adiabatically stratified overshoot. There is also some indication that some sort of overshoot with only a small effect on the temperature stratification may be present which have implications on the currently available formulations describing convective overshoot. In particular it seems to indicate that the dissipation of momentum, and so the braking of the fluid motions within the convective stable region, is much less efficient than the thermal relaxation, which reaches thermal equilibrium for the penetrating gas in a much shorter time scale. As discussed in Section 2.2.3 this is also seen in numerical simulations of convective overshoot. The basic implication is that on average the dominant effect of overshoot in stellar structure and evolution is through mixing, for example. Some authors have also argued that such a configuration would also help in storing magnetic flux at the top of the radiative interior (van Ballegooijen 1982, Petrovay 1991, Moreno Insertis, Schüssler & Feniz Mas 1992). Petrovay & Marik (1995) suggest that the sharp transition can be removed if we relax the assumption that velocity and temperature fluctuations are correlated (as was done in Sections 2.2.1 and 2.2.2).

Concerning the position of the base of the convective envelope we can say that again the consistency points to values deeper than standard models (Z_0 in Table 3.1 is an example of these) usually indicate for the Schwarzschild boundary, putting it close to the measurement of Christensen-Dalsgaard et al. (1991). The use of new, more accurate data, as is expected for example from GONG, will certainty allow much more definite conclusions to be made on this. Just as an example, I plot in Fig. 6.1 the behaviour of the uncertainty in the determinations of the parameters as functions of the average ($\hat{\sigma}$), over all data used, of the errors in the frequencies. The data used above, from which our main conclusions have been draw, correspond to $\hat{\sigma} \equiv \overline{\sigma}_{nl} \sim 0.05 \mu$Hz. We note that halving the errors would improve significantly the quality of the conclusions, by providing a clear identification of the amplitude behaviour, for example, which we need to complement the information provided by a single value, as the $A_{2.5}$ used here.

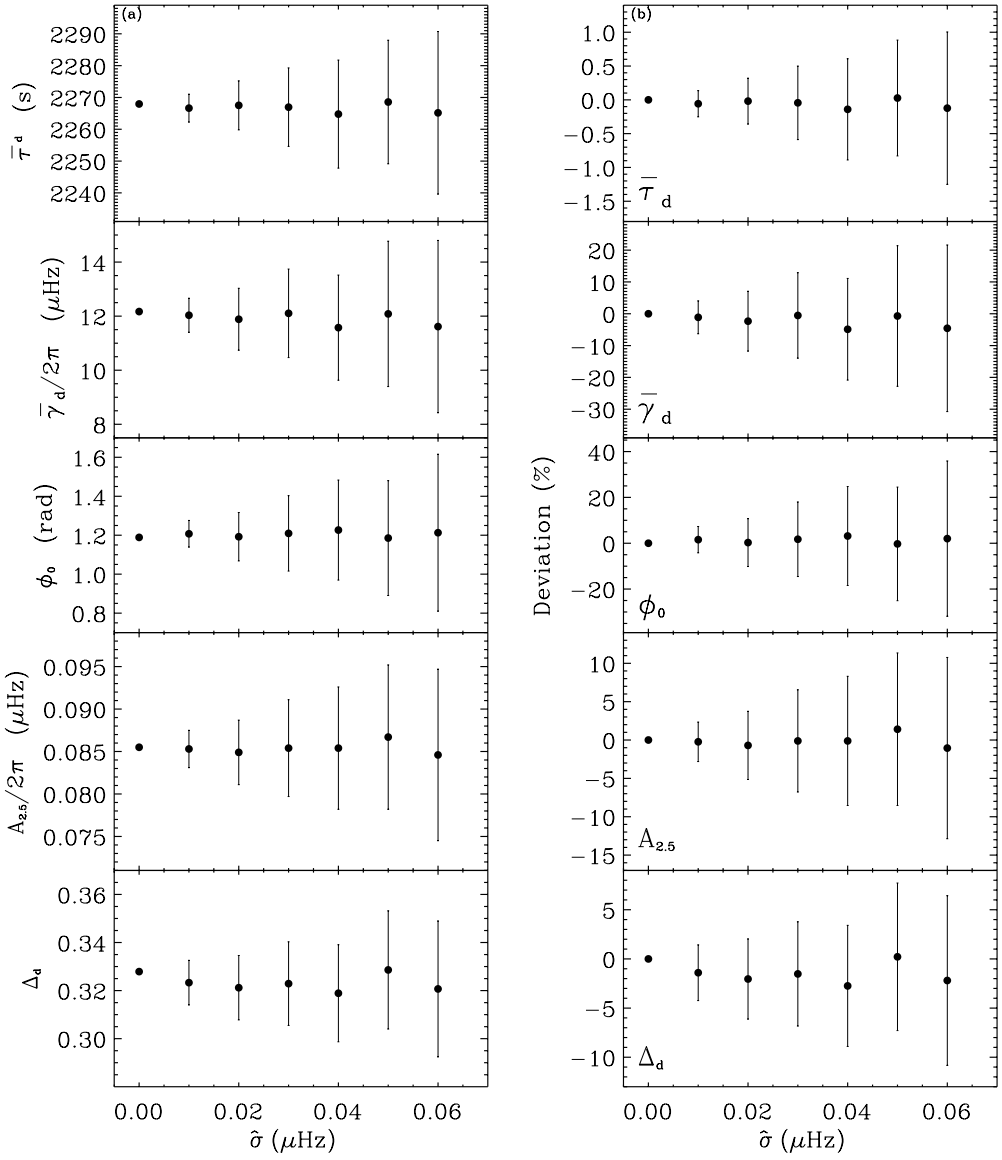

Fig. 6.1: (a) Plot of the uncertainties in the determination of the parameters as functions of the average error $\hat{\sigma}$ for the set of modes used in the fit. The relative differences between different mode errors have been maintained by normalizing the actual quoted values with the averaged error $\overline{\sigma}_{nl}$. The model whose frequencies we use here is Z_2 (Table 4.1) because of the very similar values for the amplitude that this model has when compared with the Sun. (b) Deviation (in percentage) for all parameters relatively to the error free value. Note that the statistics are beginning to fail for the higher values of $\hat{\sigma}$.

6.3 Helium abundance

By taking further the method developed for detecting convective overshoot I have discussed the possibility of studying the second helium ionization zone. It has been demonstrated that this method of isolating the signal in the frequencies can provide a very precise tool to

investigate this region. It has also been seen that the results depend not only on the helium abundance, which was our initial objective, but also on the equation of state. Therefore, the preliminary results obtained for the simplest possible description of the effect on the structure from the ionization seem to indicate, not surprisingly, that we can also apply this method to study the equation of state used to calculate our models. This has been done already by other authors when considering the same type of effect, but using different methods to extract the information from the frequencies. Due to the different effects that abundance or EOS have on the properties of the signal I have also suggest that both can be separated to some degree. However, the theoretical analysis of the effect of the ionization zone has to be redone in order to separate the dependence on these two different effects in different parameters of the signal. Unless we do so, the expression we are fitting is incomplete and do not represent the actual signal in frequency data. Therefore, I was still unable to provide here a direct measurement of the surface helium abundance.

This zone, in terms of the function θ, has been modelled as a triangle in $\delta\theta/\theta$ where the differences are relatively to a model without the second ionization of the helium. This defines the envelope dependence on frequency of the signal, and therefore affects the resulting amplitudes. If a better representation is used, the dependence on the helium abundance of the fitted expression of the signal, through the quantity we introduced here as I_θ, would be closer to the actual signal dependence on it. At the same time it would leave the dependence on the EOS to the amplitude behaviour with frequency, associated with what here I represented by β.

Also not considered here are the possible effects that other physics may have by moving the position of the ionization zone. For example, changes in the superadiabatic gradient do change significantly both helium and hydrogen ionization zones. Only a more extensive study of this and other effects may clarify how important for the characteristics of the signal are other aspects entering the models. Only after these are understood can we safely use the calibration from solar models to compare with the measured solar signal.

6.4 Theories of convection

By considering a parameter β_c that regulates the relative strength of the superadiabatic gradient in inefficient and highly efficient regions of convection, we have investigated the effect on p-mode frequencies of currently proposed local formulations of convective heat transport. Our parametrized formulation for modelling convective energy transport is of course artificial. However, it reproduces some of the currently proposed formulations, corresponding to a wide variety of behaviours of the superadiabatic region. In particular, as pointed out in Section 5.4, at high β_c our models come close to the limit corresponding to a discontinuous jump in temperature at the top of the convection zone. This suggests that the envelope models we have presented span the likely range of uncertainty regarding the thermal stratification of the super-adiabatic layer. From this aspect alone, Fig. 5.7 indicates that uncertainties in the scaled frequencies of about 10μHz are possible. The uncertainties in the actual unscaled frequencies can be much larger for shallowly penetrating high-degree modes, because the scaling factor is small for such modes.

This type of differences are also found when comparing solar seismic data with standard solar models. However, we propose that preliminary results using numerical simulations of convection question the validity of modelling the frequency differences by simple decreasing of the convective efficiency in the superadiabatic layer. There is also the added difficulty of separating additional contributions from other aspects of convection like turbulent pressure. We have addressed briefly some possible contributions of these and other effects, like non-adiabaticity of the oscillations, to the presently observed discrepancy of the solar frequencies of oscillation relatively to solar standard models.

6.4.1 Implications for theories of convection

One point that I would like to stress is the clear fact that the recipe we may use to model convection in our solar models can introduce frequency differences that go up to 15μHz. This alone is a clear evidence that surface effects, other than convection, should not be studied by simple comparisons of frequencies between models and the Sun, in order to iterate for that particular effect.

Also, it is clear evidence that we can no longer hide behind the mixing length parameter (or similar) when doing stellar structure and evolution. Of course, as I hope it has been shown here, we still can not use the observations to say what theory to model convection is adequate. This is the result of the final configuration being the unknown combination of many effects intrinsically connected to convection. Turbulent pressure, non-locality or non-adiabaticity are some of the ones we have touched upon here. Each of them is contributing in some way which is difficult to quantify. Therefore the solar

frequencies have to be used in a careful way to constrain convection theories.

An example is the fact that if we use the simulated effect of changing the efficiency of convection by reducing it where it is low, and increasing where it is high, the frequencies can be closer to the observed values. This happens for example with Canuto & Mazzitelli (1991) formulation. I have also note that, in spite of the weakness of the argument, this change in the convection theory is consistent with the results obtained from the study of the overshoot layer. This together with the fact that the construction of the *CM* formulation is a better physical description by including the modelling of this highly turbulent regime, contrary to what *MLT* does, leads to a tentative statement that it is a better representation of convection. As argued by Canuto (1996), such a formulation is indeed more defendable than the traditional Mixing Length Theory - whether we use theoretical arguments of laboratory evidence.

Important effects on the solar models and frequencies, which have been neglected in the present calculations, arise from turbulent pressure caused by the near-sonic velocities in the superadiabatic layer. This can reduce the gas pressure, leading to a decrease in the density, with a corresponding decrease in the convective efficiency. Other important effects may also arise from the dynamic effect of turbulent pressure on the oscillations; in particular, if one neglects the Lagrangian perturbation to the turbulent pressure which is associated with the oscillations, the effect on the frequencies is quite similar to the modifications induced by the *CM* formulation (Rosenthal et al. 1996). In terms of modelling stellar structure this implies the use of an extra differential equation, at least, which makes the task of solving the structure equations much more difficult. But, as indicated by simulations of convection or more detailed calculations, in seismic studies such inclusion is necessary, and being possible, should be done.

6.4.2 Evidence from numerical simulations of convection

An extra source of information regarding convection is provided by the numerical simulations of convection. These should be used together with seismic studies in order to isolate possible different contributions to the frequency differences, allowing the constraining on the formulations of convection. The sharp superadiabatic gradient, for example, corresponding to a large value of β_c, can be compared with results of hydrodynamical simulations of near-surface convection. Unfortunately, the current evidence from such simulations is somewhat contradictory. Lydon et al. (1992), who parametrised the equations for convective energy transport on the basis of numerical simulations, found no evidence for such a sharp gradient. On the contrary, the superadiabatic gradient was lower than for conventional mixing-length models, corresponding to using a value of β_c less than unity.

Thus they produced models with frequencies shifted in the opposite sense to those computed using higher values of β_c or, e.g. , the *CM* formulation. However, their simulations did not represent adequately the details of the physical conditions at the top of the solar convection zone, including radiative transfer, ionization, etc. More recent calculations by the same group (Kim et al. 1995), using more detailed physics in the near-surface region, predicted a much sharper temperature gradient which now corresponds to a higher value of β_c than for *MLT*. However, these calculations imposed a vanishing vertical velocity at the top of the convective unstable region, thus reducing the efficiency of convection in the uppermost parts of the convection zone and very likely contributing to the steep temperature gradient in this region.

In contrast, the simulations of Stein & Nordlund (1989), which allowed penetration into the atmosphere and included a careful treatment of the radiative transfer, led to an average temperature profile quite similar to that obtained from mixing-length theory. These simulations seem also to indicate that decreasing convective efficiency is not enough to reproduce the results from the simulations. In order to illustrate this I have taken the average structure from simulations by Nordlund and construct a model from such a surface structure. The simulations cover all the superadiabatic layer, and so, the differences between this and the other models reflect only what we want to isolate. The point that the steepness of the temperature is not enough is clear from such an exercise. Some small degree of non-locality has been also compared with the model from the simulations by incorporating a mixing length proportional to depth. The resulting model again shows that more effects are at play, with the indication that increasing the superadiabatic gradient only changes the frequencies in the right direction, but do not reproduce the thermodynamics of the region. Also clear from the simulations, is the fact that other effects, like turbulent pressure, have to be considered when modelling the convection zone, contrary to what is usually done.

6.5 Future

Clearly our study of overshoot can be pushed further. We have now come to a point where, with new solar data becoming available, more detailed studies of the base of the convection are possible. Natural extensions of the work presented here can be done for effects associated with an overshoot layer in the Sun. One example is the spherical symmetry, implicitly used here, which should be checked in order to understand how much in the signal is intrinsically attributable to the characteristics of overshoot. Also, with models associating the magnetic activity in the Sun to an overshoot region at the base of the envelope, it is expected that properties of such a region would vary with the solar cycle. Frequencies are indeed known to change along the solar cycle (Bachman & Brown 1993, Rüdiger & Branderburg 1995). With the improved seismic data from GONG, variations of the signal characteristics can be detected, and so we now have the possibility to establish in an absolute way if the solar cycle is indeed rooted deep in the interior of the Sun as expected by most dynamo theories. Also we could understand how important is overshoot in generating magnetic fields if we can determine how its configuration changes with activity levels. Not considered here, but possible to estimate by extending our analysis, is the effect of diffusion of the properties of the signal (cf. Basu & Antia 1994).

Of course our study of the second helium ionization zone has not been completed. It is still necessary to take it further by improving the theoretical description of the ionization zone and its effect on the frequencies by better represent the changes in the structure introduced by the second ionization of the helium. The possibilities of the method have been establish in my opinion. We must now improve it in order to extract from the observations useful information about the Sun and its physics.

Finally, with our study of convection we have found that there are a few things we still do not fully understand. We have started to dissect some of the parts, and further progress is, I believe, possible. It is fundamental that we quantify some of these problems in order to be able to advance in some way on the modelling of convection in stellar interiors. The discussion of possible effects that must be considered have been presented here. These studies are being pursued; the preliminary results presented in Rosenthal et al. (1996) are an example of this effort. Some observations for other stars, of solar type, also seems to indicate that the same discrepancy between the observed and expected frequencies is present (Christensen-Dalsgaard, Bedding & Kjeldsen 1995, and Christensen-Dalsgaard et al. 1996). Because the significance of the superadiabatic region in stars with masses different from the solar, like the case of η-Bootis, is different, the discrepancies between theory and observations for them may help us in a unique way to establish which properties of convection are more determinant in such a region and how we must go about

improving our theories of convection. As more and better observations for other stars became available, I hope we will come to a point where we can say why and what in a particular formulation is not correct. On the other hand, the use of numerical simulations of convection, and the implementation of more complete theories of convection can still provided us with valuable information. Such studies must be pursued together with the use of seismic data.

A. Calculation of a Static Solar Model

Here we describe how static solar models are constructed in order to be used in the work reported in the main text. Since we are only calculating static models (no time evolution) the chemical profile has to be given, corresponding to a particular age of the sun. Having this, we can then integrate numerically the equations of stellar structure.

We start by giving a summary of the main equations and relations necessary to determine a model. Then, a description of the assumptions related to the physics is presented. In particular, the equation of state, emissivity, opacities and the description of convective heat transport. After presenting the reduced variables used in the code we give a brief description of the numerical method applied to solve the problem.

A.1 General considerations

The problem addressed in this Appendix is how to calculate the structure of a star given its mass, luminosity and radius/effective temperature. Here we shall not consider the problem of how to model the change of the structure with time. We avoid this by using the results of other evolution codes which provide the run of the chemical profile with radius/mass of a present age Sun. This is not consistent, since the result of the evolution is affected by the physics that are used however for the applications considered in this Thesis, where we are mainly interested in model/frequency differences, it is not really important as long as we use the same chemical profile for all models.

In the construction of a model there are different aspects contributing for the result. First there is the set of assumptions considered in order to simplify the problem. Among them, spherical symmetry/no rotation and time independence are the most important. Second there are the ones going in establishing the physics that rule the behaviour of the gas within the star. Among them we need to establish how energy is produced and transported, how the fluid properties are related between them and how radiation interacts with the fluid. These are some of the important ones. For other detailed discussions on

the calculation of solar models see Christensen-Dalsgaard (1982, 1996), Turck-Chièze et al. (1993), or Turck-Chièze & Lopes (1993).

Here we shall start by listing the basic equations quoting the extra physics needed. Some of the physical aspects present in the basic equations, like convection, equation of state or opacities are then separately discussed. The transport of energy by convection is more extensively presented considering that it is one of the subjects of the Thesis. We also discuss in some detail a simple equation of state which shall be used to test the dependence of the results for the Helium abundance on the equation of state used to construct the model.

A.2 Basic equations of stellar structure

The basic equations of stellar structure are composed by four first order non linear differential equations obtained by assuming equilibrium, no rotation and spherical symmetry. The dependent variables are the functions to be found given the relations describing the physics and the boundary conditions. If the independent variable used is

$$r \; - \text{ radial distance from the centre of the star ,}$$

then the dependent variables to be determined are

$$\begin{aligned} m_r &- \text{mass within a sphere of radius } r \\ P &- \text{pressure} \\ L_r &- \text{luminosity crossing the sphere with radius } r \\ T &- \text{temperature .} \end{aligned} \tag{A.2.1}$$

It is also common to use m_r as the independent variable, however we have chosen not to do so here since we shall be mainly discussing the calculation of solar envelope models. For these type of models mass is not the most convenient variable since it changes very little for most of the envelope where the density is low. This option for the independent variable will only be used when determining the central regions of a full solar model.

To calculate a solar/stellar model, i.e. the run of the four dependent variables with radius, we need to define the boundary conditions. These are imposed at r=0 and r=R, where R is the total radius of the star. Using these we then find the solution by integrating the set of four differential equations given as

$$\frac{\mathrm{d}m_r}{\mathrm{d}r} = 4\pi r^2 \rho(r) \tag{A.2.2a}$$

$$\frac{\mathrm{d}P}{\mathrm{d}r} = -\frac{G m_r(r)}{r^2}\,\rho(r) \tag{A.2.2b}$$

$$\frac{\mathrm{d}L_r}{\mathrm{d}r} = \frac{\mathrm{d}m_r}{\mathrm{d}r}\ \varepsilon(r) \tag{A.2.2c}$$

$$\frac{\mathrm{d}T}{\mathrm{d}r} = \frac{T(r)}{P(r)}\ \frac{\mathrm{d}P}{\mathrm{d}r}\ \nabla(r)\ . \tag{A.2.2d}$$

These have to be solved together with relations giving the density ρ, energy production rate ε and the temperature gradient ∇ at each point, depending on r and the other four variables. Those functions also depend on the chemical profile (and since we are not calculating time evolution, this has to be given) through the hydrogen X, helium Y and heavy elements Z abundances by mass. Knowing two of them, for example $Y{=}Y(r)$ and $Z{=}Z(r)$, the third can be determined from

$$X(r) = 1 - Y(r) - Z(r)\ . \tag{A.2.3}$$

The functions needed are first, the equation of state (EOS), which gives the density and other thermodynamic functions. Formally, it provides the following dependences

$$\begin{aligned}
&\rho = \rho(r;P,T,X,Y)\\
&\nabla_{\mathrm{a}} \equiv \left(\frac{\mathrm{d}\log T}{\mathrm{d}\log P}\right)_S = \nabla_{\mathrm{a}}(r;P,T,X,Y)\\
&Q = Q(r;P,T,X,Y)\\
&C_P = C_P(r;P,T,X,Y)\\
&\Gamma_1 \equiv \left(\frac{\mathrm{d}\log P}{\mathrm{d}\log \rho}\right)_s = \Gamma_1(r;P,T,X,Y)\ ,
\end{aligned} \tag{A.2.4}$$

where ∇_{a}, Q, C_P and Γ_1 are respectively the adiabatic gradient, expansion coefficient, specific heat at constant pressure and adiabatic exponent (the derivative is taken at constant entropy S). The second function is the nuclear reactions rate

$$\varepsilon = \varepsilon(r;\rho,T,X,Y)\ , \tag{A.2.5}$$

giving the energy produced by unit mass. The third is the opacity law (necessary to find ∇)

$$k = k(r;\rho,T,X,Y)\ , \tag{A.2.6}$$

which describes the interaction between the gas particles and the radiation. The last relation also needed is an equation giving the temperature gradient

$$\nabla(r) \equiv \frac{\mathrm{d}\log T}{\mathrm{d}\log P} = \nabla(r;\rho,T,X,Y)\ , \tag{A.2.7}$$

which describes the energy transport in the star. Depending on the dominant process used by the star this function has different expressions. The basic options (but not only

these) are convection, conduction and radiation. For the cases considered here the actual temperature gradient will depend on two gradients; $\nabla_{\rm a}$ and a radiative gradient defined as

$$\nabla_r \equiv \left(\frac{{\rm d}\log T}{{\rm d}\log P}\right)_r = \frac{3}{2^6\pi\sigma G}\,\frac{L_r k P}{m_r T^4}\,. \qquad \text{(A.2.8)}$$

The latter corresponds to the temperature gradient needed for all flux to be transported by radiation. Therefore in regions where radiation is highly inefficient in transporting energy this gradient becomes very large.

Particular expressions for some of these functions are given in the Sections below. Some of those are not discuss in great detail, we just give a brief introduction to what has been used in calculating some of the models reported in the main text of the thesis.

Table A.1: Physical constants with their values in CGS units. The usual name and symbol by which they are known, and referred in the text, are also included.

Name	Symbol	Definition	Value	Units
Gravitational constant	G	–	6.67232×10^{-8}	dyn cm^2 g^{-2}
Speed of light in the vacuum	c	–	2.99792458×10^{10}	cm s^{-1}
Electron rest mass	m_e	–	9.1093897×10^{-28}	g
Electron elementary charge	e	–	4.803250×10^{-10}	esu
Plank's constant	h	–	6.6260755×10^{-27}	erg s
Atomic mass unit	u	–	1.660531×10^{-24}	g
Boltzmann's constant	k	–	1.380658×10^{-16}	erg k^{-1}
Radiation constant	a	$\frac{8\pi^5k^4}{15h^3c^3}$	7.5659×10^{-15}	erg cm^{-3}k^{-4}
Gas constant	$\mathcal{R}_{\rm g}$	$\frac{k}{u}$	8.314557×10^{7}	erg k^{-1}mole^{-1}
Stefan-Boltzmann constant	σ	$\frac{a\,c}{4}$	5.67051×10^{-5}	erg cm^{-2} s^{-1} K^{-4}
Hydrogen atomic mass	$A_{\rm H}$	–	$1.007825\ u$	g
Helium atomic mass	$A_{\rm He}$	–	$4.002603\ u$	g
H ionization energy	$\chi_{\rm HI}$	$\frac{2\pi^2e^4m_e}{h^2}$	13.595	eV
First He ionization energy	$\chi_{\rm HeI}$	–	24.587	eV
Second He ionization energy	$\chi_{\rm HeII}$	–	54.403	eV

A.2.1 Constants and observational data

For the sake of completeness all constants used here for the calculation of solar models (or frequencies of oscillation for that matter) are given here with the values that have been adopted throughout the different subjects addressed in the thesis. Two tables are included.

The first, Table A.1, lists all physical constants that at some point enter the calculations not only of solar models but also other calculations reported in the Thesis. These values have been taken mainly from Lang (1980).

Table A.2: Solar characteristics with their values in CGS units. The usual symbol and name by which they are known, and referred in the text, are also included.

Name	Symbol	Value	Units
Mass	$M_\odot$	1.989×10^{33}	g
Radius	$R_\odot$	6.9599×10^{10}	cm
Luminosity	$L_\odot$	3.846×10^{33}	erg s^{-1}
Effective temperature	$T_{\rm eff_\odot}$	5778	k

The other, Table A.2, lists the values for the basic characteristics of the Sun. These values are used when doing any of the solar calculations (structure models or oscillations, for example).

A.2.2 Boundary conditions

To complete our system of differential equations in order to solve them numerically we need four boundary conditions. These are imposed at the surface and at the centre (or somewhere in the envelope if we are not calculating a full model). We recall that we are not modelling evolution and so what defines our model is that for a given chemical profile our star has a total mass M, a total luminosity L and a radius R (or effective temperature $T_{\rm eff}$). Therefore our boundary conditions come from imposing such a configuration and requiring that there is no point mass or luminosity source at the centre. These give for the surface (r=R) the following conditions

$$\begin{aligned} m_r(r{=}R) &= M \\ L_r(r{=}R) &= L \ , \end{aligned} \tag{A.2.9}$$

while at the centre (r=0) we have

$$\begin{aligned} m_r(r{=}0) &= 0 \\ L_r(r{=}0) &= 0 \ . \end{aligned} \tag{A.2.10}$$

There are four first order differential equations, so these boundary conditions are sufficient to define a solution. Note however that the other four values have not been specified yet. These follow from finding a solution satisfying the boundary conditions. So, the solution found will define the following four values, at the surface

$$\begin{aligned} P(r{=}R) &= P_s \\ T(r{=}R) &= T_s \ ; \end{aligned} \tag{A.2.11}$$

and at the centre

$$\begin{aligned} P(r{=}0) &= P_c \\ T(r{=}0) &= T_{\rm c} \ . \end{aligned} \tag{A.2.12}$$

However, if we now take the temperature at the surface as being the effective temperature we need to introduce a parameter in order to be able to select the solution that has the chosen surface temperature ($T_s{=}T_{\rm eff}$). If we further integrate the equations for the stellar atmosphere the answer we obtain is the run of the pressure, and so its value at the surface, P_s. But again another free parameter has to be considered to choose the solution that has this surface pressure. In a full solar model these two extra parameters are associated to the chemical abundances and to the convective energy transport. As shall be discussed latter these are the envelope helium abundance Y and the mixing length parameter α_c.

If only an envelope is calculated there is no need for parameters since the two boundary conditions corresponding to (A.1.10) are not used. However in the models discussed here we have added a new condition, which is equivalent to a boundary condition, by requiring that the base of the convection zone is at a given position. In doing so, the parameter present in the modelling of the temperature gradient is maintained in order to choose the solution that satisfies this requirement.

A.2.3 Reduced variables

All the calculations are done not using the actual physical quantities but instead reduced variables which are dimensionless. This has the advantage of reducing all variables to values of the same order of magnitude improving the accuracy of the calculations. It also simplifies to some degree the equations and the structure of the code. This normalization can be done in many different ways. Here we use the process used for example by Schwarzschild (1958). It consists in removing the physical dimensions by using the total mass, radius and luminosity of the star together with the gravitational and gas constants.

According to this, for the independent variable we use the relative radius $x{\equiv}r/R$.

While for dependent variables of integration we define

$$\begin{aligned} z_1 &= \frac{m}{M} \\ z_2 &= P\,\frac{R^4}{GM^2} \\ z_3 &= \frac{L_r}{L} \\ z_4 &= T\,\frac{\mathcal{R}_{\rm g} R}{GM}\ , \end{aligned} \tag{A.2.13}$$

where, as before, M and L are the total mass and the total luminosity, respectively. For the same reason it is also convenient to define

$$c_p = \frac{C_P}{\mathcal{R}_{\rm g}} \qquad , \qquad \tilde{\varepsilon} = \frac{M}{L}\,\varepsilon \qquad \text{and} \qquad \tilde{\rho} = \rho\,\frac{R^3}{M}\ . \tag{A.2.14}$$

After substituting these definitions in the differential Eqs. (A.2.2) the new set of equations in terms of the new variables are

$$\begin{aligned} \frac{{\rm d}z_1}{{\rm d}x} &= 4\pi x^2 \tilde{\rho} \\ \\ \frac{{\rm d}z_2}{{\rm d}x} &= -\frac{z_1 \tilde{\rho}}{x^2} \\ \\ \frac{{\rm d}z_3}{{\rm d}x} &= \frac{{\rm d}z_1}{{\rm d}x}\ \tilde{\varepsilon} \\ \\ \frac{{\rm d}z_4}{{\rm d}x} &= \frac{z_4}{z_2}\,\frac{{\rm d}z_2}{{\rm d}x}\ \nabla\ . \end{aligned} \tag{A.2.15}$$

The boundary conditions (A.2.9) and (A.2.10) become, at the surface (x=1),

$$z_1(x{=}1) = z_3(x{=}1) = 1\ ; \tag{A.2.16}$$

while at the centre (x=0) ,

$$z_1(x{=}0) = z_3(x{=}0) = 0\ . \tag{A.2.17}$$

To complete the set of expressions to be used in the code we still need to add the "physics", i.e., the emissivity, the EOS and the opacity. Also, because our equation for the derivative of the temperature is not valid in the atmosphere, we still need to describe the set of equations to be used there. These are addressed in the next Section. After doing so we are in conditions to calculate the structure of the Sun.

A.2.4 Modelling the atmosphere

The integration of the atmosphere not only provides the structure of a region of the star that affects some of the modes of oscillation, but also provides one of the upper boundary conditions by establishing the value of the surface pressure.

The method used in our code is to take a known relation between temperature and optical depth τ_k and integrate the mass and pressure equation in this thin region using τ_k as the independent variable. The optical depth is related to distance by the opacity according to

$$\mathrm{d}\tau_k \equiv -\, k\rho \, \mathrm{d}r \ . \tag{A.2.18}$$

By using this equation we can write the hydrostatic equation for the pressure and the mass equation in terms of τ_k. In doing so we end with three differential equations (and the relation for temperature) that can be solved if the opacities and the equation of state are known. These are,

$$\begin{aligned} \frac{\mathrm{d}r}{\mathrm{d}\tau_k} &= -\frac{1}{k\rho} \\ \frac{\mathrm{d}m}{\mathrm{d}\tau_k} &= -\frac{4\pi r^2}{k} \\ \frac{\mathrm{d}P}{\mathrm{d}\tau_k} &= \frac{Gm}{r^2 k} \ . \end{aligned} \tag{A.2.19}$$

The relation giving the temperature as function of τ_k we have chosen to use here is the expression given by Krishna Swamy (1966) determined from a fitting to the results obtained from observed line profiles for the Sun. It is given as

$$T^4 = \frac{3}{4}\, T_{\mathrm{eff}}^4 \Big[\tau_k + 1.39 - 0.815 \, \exp\left(-2.54 \ \tau_k\right) - 0.025 \, \exp\left(-30 \ \tau_k\right) \Big] \ . \tag{A.2.20}$$

The surface corresponds to τ_k=0.312156$\equiv\tau_{ks}$. There are other model atmospheres determined using more complete physics (see for example Gingerich et al. 1971, for the Harvard-Smithsonian reference atmosphere). However we have decided in favour of this expression because of its simplicity and easy application.

Once again we redefine the variables in order to improve the accuracy of the calculations. For the atmosphere it is important to do so, specially due to the very low densities. The new variables are

$$f_1 = \frac{r}{R} - 1 \quad , \qquad f_2 = 1 - \frac{m}{M} \quad , \qquad f_3 = z_3 \qquad \text{and} \qquad \tilde{k} = \frac{M}{R^2}\, k \ . \tag{A.2.21}$$

The differential equations became,

$$\begin{aligned} \frac{\mathrm{d}f_1}{\mathrm{d}\tau_k} &= -\frac{1}{\tilde{k}\tilde{\rho}} \\ \frac{\mathrm{d}f_2}{\mathrm{d}\tau_k} &= 4\pi \, \frac{(f_1{+}1)^2}{\tilde{k}} \\ \frac{\mathrm{d}f_3}{\mathrm{d}\tau_k} &= \frac{1{-}f_2}{\tilde{k}(f_1{+}1)^2} \ , \end{aligned} \tag{A.2.22}$$

which have to be integrated between the top of atmosphere where the density goes to zero and the photosphere. To complement the equations we also have the following boundary conditions,

$$r(\tau_k{=}\tau_{ks}) = R \quad , \qquad m(\tau_k{=}0) = M \qquad \text{and} \qquad P(\tau_k{=}0) = 0 \; . \tag{A.2.23}$$

The top of the atmosphere corresponds to $\tau_k{=}0$ while the photosphere is at $\tau_k{=}\tau_{ks}$. These conditions in terms of the variables (A.2.21) are

$$f_2(\tau_k{=}0) = 0 \quad , \qquad f_3(\tau_k{=}0) = 0 \qquad \text{and} \qquad f_1(\tau_k{=}\tau_{ks}) = 0 \; . \tag{A.2.24}$$

The system of three differential equations with these three boundary conditions can now be integrated. The solution gives the structure of the atmosphere, and so also the value of the pressure P_s at the surface ($r{=}R$). Note that for these boundary conditions we need to correct the interior boundary condition for the reduced mass z_1, by writing instead that $z_1(x{=}1) = 1{-}f_2(\tau_k{=}\tau_{ks})$.

The singularity at $\tau_k{=}0$ can be easily removed by integrating analytically the first step. The numerical integration is then initiated at some deeper point and not the actual top of the atmosphere. We have taken this point as being $\tau_k{=}10^{-5}$.

Finally we have to force a smooth transition from the atmosphere to the solution for the interior. The problem is associated to the fact that we are changing from a solution for a $T{-}\tau_k$ relation to a solution determined from solving a differential equation for the temperature in the diffusive approximation. To get around this problem we have used the method proposed by Henyey, Vardya & Bodenheimer (1965) where near the bottom of the atmosphere the transition to the diffusivity approximation is done by writing the actual radiative gradient, not as defined in (A.2.8), but instead as

$$\begin{aligned} &\nabla_{\rm r} \rightarrow \nabla_{\rm r} \left(1 + \frac{{\rm d}q_\tau}{{\rm d}\tau_k} \right) \; , \\ &\qquad \text{with} \qquad q_\tau(\tau_k) = \frac{4}{3} \left(\frac{T}{T_{\rm eff}} \right)^4 - \tau_k \\ &\qquad\qquad\qquad = 1.39 - 0.815 \, \exp\left(-2.54 \; \tau_k\right) - 0.025 \, \exp\left(-30 \; \tau_k\right) \; . \end{aligned} \tag{A.2.25}$$

The temperature T has been replaced from (A.2.20) above. This introduces a correction that rapidly goes to zero below the photosphere reducing the temperature equation to its diffusive approximation. It is due to the rapid increase of the optical depth resulting from the variation of the density and opacity as given by

$$\frac{{\rm d}\tau_k}{{\rm d}x} = -\tilde{k}\tilde{\rho} \; . \tag{A.2.26}$$

This extra equation has to be kept in the calculation of the interior as long as the correction to $\nabla_{\rm r}$ is significant, what happens only for a very thin layer above the convection zone.

So, given the abundances, the opacity, the equation of state and of course the $T{-}\tau_k$ relation we have the structure of the atmosphere.

A.3 Equation of state

The main role of the equation of state (EOS) is to describe the thermodynamic behaviour of the fluid. In particular it provides the gas density and the adiabatic gradient, among others, needed for the structure equations.

Here we will just present the basic equations for a simple equation of state. This is the one for a perfect gas with radiation pressure and including only the ionization of hydrogen and helium, as described by the correspondent Saha equations. For high pressures we substitute this by the equation for a fully ionized gas with a continuous transition being imposed at some interval of intermediate values for the pressure where the results from the two cases are similar.

Also used in our code, but not discussed here, is an equation of state known as the CEFF equation of state (cf. Christensen-Dalsgaard & Däppen 1992). It includes a Debye-Hückel approximation for the Coulomb term to the EFF equation of state, proposed by Eggleton, Faulkner & Flannery (1973). This and the simple EOS are the only options we have used in constructing models with our code.

The implementation of the more complex CEFF equation of state has been done by using the subroutines developed by Christensen-Dalsgaard.

A.3.1 Basic thermodynamic relations

Formally, the equation of state can be written as a relation giving the density as function of pressure and temperature, for example, and of course of the abundances. I.e.,

$$\rho \equiv \rho(P, T, X, Z) \ . \tag{A.3.1}$$

Using such a relation we can define some functions which describe specific aspects of how the gas responds. Here we shall consider some of these functions, defining them and listing some basic relations among them, which are used along the main text.

From Eq. (A.3.1) we can formally write that

$$\mathrm{d}\rho = \left(\frac{\partial\rho}{\partial P}\right)_{T,X} \mathrm{d}P + \left(\frac{\partial\rho}{\partial T}\right)_{P,X} \mathrm{d}T + \left(\frac{\partial\rho}{\partial X}\right)_{P,T} \mathrm{d}X \ . \tag{A.3.2}$$

In writing this we have assumed that the abundance by mass of the heavy elements is constant. Or, in term of log's,

$$\frac{\mathrm{d}\log\rho}{\mathrm{d}\log P} = \left(\frac{\partial\log\rho}{\partial\log P}\right)_{T,X} + \left(\frac{\partial\log\rho}{\partial\log T}\right)_{P,X} \frac{\mathrm{d}\log T}{\mathrm{d}\log P} + \left(\frac{\partial\log\rho}{\partial\log X}\right)_{P,T} \frac{\mathrm{d}\log X}{\mathrm{d}\log P} \ . \tag{A.3.3}$$

Introducing the following definitions

$$\begin{aligned} \nabla &\equiv \frac{\mathrm{d}\log T}{\mathrm{d}\log P} \qquad \text{and} \qquad \nabla_X \equiv \frac{\mathrm{d}\log X}{\mathrm{d}\log P} \\ \chi_\rho &\equiv \left(\frac{\partial \log P}{\partial \log \rho}\right)_{T,X} = \frac{\chi_T}{Q} \\ \chi_T &\equiv \left(\frac{\partial \log P}{\partial \log T}\right)_{\rho,X} \\ \chi_X &\equiv \left(\frac{\partial \log P}{\partial \log X}\right)_{\rho,T} , \end{aligned} \tag{A.3.4}$$

the relation can be reduced to

$$\chi_\rho \frac{\mathrm{d}\log \rho}{\mathrm{d}\log P} = 1 + \chi_T \nabla + \chi_X \nabla_X . \tag{A.3.5}$$

In the case that the mean molecular height μ, defined as the average mass per particle, is independent of the temperature and pressure, as happens if the gas is fully ionized, we can replace X by μ in these equations since both functions became equivalent.

Also important are the specific heats, defined as

$$\begin{aligned} &\text{at constant pressure} \qquad C_P \equiv \left(\frac{\mathrm{d}Q_e}{\mathrm{d}T}\right)_P \\ &\text{at constant volume} \qquad C_V \equiv \left(\frac{\mathrm{d}Q_e}{\mathrm{d}T}\right)_\rho , \end{aligned} \tag{A.3.6}$$

where Q_e is the heat exchanged by the system. Using the definitions introduced above, we can write that

$$C_P - C_V = \frac{P}{\rho T}\,\frac{\chi_T^2}{\chi_\rho} . \tag{A.3.7}$$

Finally, introducing the *Gammas*, as the derivatives taken at constant entropy (i.e., zero $\mathrm{d}Q_e$)

$$\begin{aligned} \Gamma_1 &\equiv \left(\frac{\mathrm{d}\log P}{\mathrm{d}\log \rho}\right)_S \\ \Gamma_2 &\equiv \frac{1}{1-\nabla_\mathrm{a}} \\ \Gamma_3 &\equiv 1 + \left(\frac{\mathrm{d}\log T}{\mathrm{d}\log \rho}\right)_S , \end{aligned} \tag{A.3.8}$$

where

$$\nabla_\mathrm{a} \equiv \left(\frac{\mathrm{d}\log T}{\mathrm{d}\log P}\right)_S , \tag{A.3.9}$$

we find the following relations (Cox & Giuli 1968)

$$\gamma \equiv \frac{C_P}{C_V} = 1 + \frac{\chi_T}{\chi_\rho}\,(\Gamma_3 - 1) = \frac{\Gamma_1}{\chi_\rho} = \frac{\Gamma_3 - 1}{\chi_\rho}\,\frac{\Gamma_2}{\Gamma_2 - 1} . \tag{A.3.10}$$

Using these in Eq. (A.3.5) gives

$$\frac{\mathrm{d}\log \rho}{\mathrm{d}\log P} = \frac{1}{\Gamma_1}\,\left[1 - (\gamma - 1)\,\frac{\nabla - \nabla_\mathrm{a}}{\nabla_\mathrm{a}} - \gamma \chi_X \nabla_X\right] . \tag{A.3.11}$$

Note that only three between $(\Gamma_1, \Gamma_2, \Gamma_3, \gamma)$ are independent, so we can choose any combination. Here we have kept Γ_1, γ and Γ_2 trough $\nabla_{\rm a}$, which are also the thermodynamic exponents used in the main text.

A.3.2 A simple equation of state

One of the reasons to consider a simple equation of the state (SEOS) was to be able to test other parts of the code without much effort going into the calculation of the density and other thermodynamic quantities. However, in the Chapter 4, where we discussed the importance of the EOS on the results, some of the models considered have been calculated using this equation.

The basic characteristics describing our fluid are of an ideal gas subject to the radiation pressure and with inclusion of the hydrogen and helium ionization modelled by the corresponding Saha equations. Total ionization at high pressures is imposed by considering a smooth transition (not consistently), from the general equations to the special case of full ionization, as function of pressure. This transition takes place over an interval of pressure for which both cases give almost the same results.

The relation between pressure, temperature and density for such a fluid is

$$P = \frac{\mathcal{R}_{\rm g}}{\mu(T,P)}\,\rho T + \frac{aT^4}{3}\,. \tag{A.3.12}$$

The mean molecular height $\mu(T,P)$ describes the ionization of the particles in the gas. It is related to the abundances of the chemical elements and can be written as a function of the number E of free electrons per atom, according to

$$\mu = \frac{\mu_0}{E{+}1} \qquad \text{where} \qquad \mu_0 = \left(\frac{X}{A_{\rm H}} + \frac{Y}{A_{He}} + \frac{Z}{< A_i >}\right)^{-1} \sim \frac{4}{2X{-}Y{+}2}\,. \tag{A.3.13}$$

If we consider only the ionization of hydrogen and helium, the number of free electrons per atom is given by

$$\frac{E}{\mu_0} = \frac{X}{A_{\rm H}}\,x_{\rm HI} + \frac{Y}{A_{\rm He}}\,(x_{\rm HeI} + 2x_{\rm HeII})\,, \tag{A.3.14}$$

where the A's are the atomic mass of the elements and the x the ionization fraction, i.e., the number of particles in that ionization level divided by the total number of particles of that species. The ionization fractions are here given by the Saha equations for each ionization level as

$$\begin{aligned}
\frac{x_{\rm HI}}{x_{\rm H}}\,\frac{E}{E{+}1} &= \left(\frac{2\pi m_e}{h^2}\right)^{3/2}\frac{(kT)^{5/2}}{\beta P}\,\exp\left(-\frac{\chi_{\rm HI}}{kT}\right)\\
\frac{x_{\rm HeI}}{x_{\rm He}}\,\frac{E}{E{+}1} &= 4\left(\frac{2\pi m_e}{h^2}\right)^{3/2}\frac{(kT)^{5/2}}{\beta P}\,\exp\left(-\frac{\chi_{\rm HeI}}{kT}\right)\\
\frac{x_{\rm HeII}}{x_{\rm HeI}}\,\frac{E}{E{+}1} &= \left(\frac{2\pi m_e}{h^2}\right)^{3/2}\frac{(kT)^{5/2}}{\beta P}\,\exp\left(-\frac{\chi_{\rm HeII}}{kT}\right)\,,
\end{aligned} \tag{A.3.15}$$

with $x_{\rm H}+x_{\rm HI}=1$ and $x_{\rm He}+x_{\rm HeI}+x_{\rm HeII}=1$. See Table A.1 for the definition of the notation used for the constants present in these expressions, and the values they have.

To complete our set of equations we also need the energy per unit mass which is given as

$$u = \frac{3}{2}\frac{\mathcal{R}_{\rm g}}{\mu}T + \frac{aT^4}{\rho} + \frac{X}{A_{\rm H}}\chi_{\rm HI}x_{\rm HI} + \frac{Y}{A_{\rm He}}\left[\chi_{\rm HeI}x_{\rm HeI} + (\chi_{\rm HeI}+\chi_{\rm HeII})\,x_{\rm HeII}\right]. \qquad \text{(A.3.16)}$$

With these equations we can determine all the thermodynamic quantities, like density, adiabatic gradient, expansion coefficient, specific heats, etc, that we need to calculate the model.

One of the problems with the Saha equations is the fact that for high pressures, like the ones occurring in the deep interior of the Sun, it predicts recombination of the electrons. This is known not to be true, so a correction needs to be added to force full ionization at high pressures. Such a correction can be introduced consistently in the equations considered above (Christensen-Dalsgaard 1978). However it also introduces some complexity to the process of solving the above equations. In order to keep the EOS as simple as possible we have chosen not to do so. Opting instead by forcing the equation of state to take the values for the simpler expressions, resulting from assuming a priori full ionization of all species, in the limit of high pressures. The transition occurs for $14\leq\log_{10}P\leq15$, with the actual values in the interval being given by linear interpolation according to

$$w(P) = w_f(P)\,\left(\log_{10}P-14\right) + w_i(P)\,\left(15-\log_{10}P\right). \qquad \text{(A.3.17)}$$

We have used w to represent any of the thermodynamic quantities to be determined, with w_f being its value for that pressure if full ionization is assumed while w_i is the value it has if the Saha equations are used to model the ionization. Note that in this way all quantities change continuously.

A.4 Temperature gradient

Another important aspect of the physics that goes into modelling solar and stellar structure and evolution is the energy transport. The star produces energy in its interior in order to sustain its self-gravity. Therefore as a consequence of this there is a flux of energy from the central regions to the surface where the star finally looses the energy by radiating it away. The actual structure of the star is for that reason a consequence of how the stars manage to transport this energy up to the surface. There are different processes available to the star for transporting the flux, however depending on the local conditions there will be a dominant one. Some of the options are of course, radiation, conduction, neutrinos and convection. In principle we can say that the star will choose the easiest, which means

the one corresponding to the minimum energy state. In terms of structure this translates as the one that will need the lowest temperature gradient for transporting all the flux. However in some conditions more than one may be used simultaneously if neither of them is capable of taking care of all the energy flux.

Our objective here is therefore to describe a formulation that provides, given the local thermodynamic conditions, how the stratification in temperature will be, depending on the particular processes of transport that may intervene at that local. Using the diffusive approximation, valid for the interior of the Sun to a very high accuracy, we can calculate how much flux the radiation/photons transport from what we define previously as the radiative gradient $\nabla_{\rm r}$. It is also possible to include in this expression any small contribution that may exist from conduction of heat by the particles. But, in some regions due to the high opacity of the material which translates the degree of obscurity of the fluid to radiation, the photons are unable to take care of the job. The initial response is to increase the temperature gradient to compensate for this obscurity. But it soon comes to a point that the fluid becomes unstable to small perturbations entering a state of convective instability. We are then in what is call convection. For the star one of the effects is that now a new type of energy transport can take place due to the motions of the fluid.

In terms of modelling this is the most problematic type of transport. The reason is simply because to describe the average properties of a highly turbulent fluid as expected in the interior of the Sun is something we do not know how to do. What we do have are estimates on how such a fluid contributes to the transport of energy and so, estimates on how the average properties of the star are if such a regime is present.

In this section we present the expressions used to describe the average temperature gradient in such conditions. We have chosen to present a general formulation which has as special cases some formulations discussed in the main text. We have implemented these expressions for an easy application to all cases studied.

A.4.1 Criterion for instability

Only in regions that are unstable to fluctuations due to a non-real Buoyancy frequency ((1.3.5)) we need to consider a theory of the convective transport of energy. Therefore a criterion determining where such regions are for the model, depending on the local conditions, must be used. In our code such a criterion is the Schwarzschild Criterion which is simply (Schwarzschild 1958),

$$\begin{cases} \nabla_{\rm r} \geq \nabla_{\rm a} & \rightarrow \qquad \text{Convection theory giving } \nabla{=}\nabla(\nabla_{\rm a}, \nabla_{\rm r}) \\ \nabla_{\rm r} < \nabla_{\rm a} & \rightarrow \qquad \nabla = \nabla_{\rm r} \ . \end{cases} \tag{A.4.1}$$

Because it is fundamental to have a mesh point exactly where the boundaries of the

convection zone are, we have implemented an iterative method that finds for each boundary the radial position at which the transition occurs forcing a mesh point to be placed there.

When constructing a model we simply use $\nabla_{\rm r}$ in regions that are radiative while we must use a theory of convection, providing us with ∇, in order to integrate the differential equation for the temperature. The implementation of this is discussed below.

A.4.2 Basic Equations for modelling convection

The most common way to include in the structure code the equations for the temperature gradient within a convective unstable region is to have an equation for the convective efficiency. All the coefficients of such an equation are known functions at each given point and therefore provide the value of the convective efficiency at that point through this equation. Note that this is possible only because we are only considering local theories of convection, where the temperature gradient is assumed as being dependent only on the conditions at a specific radius. The gradient of the temperature is then calculated from the root of that equation. Here we describe a general formulation which has some parameters associated. The reason why we do so is associated to the fact that we need to construct models using different formulations which are particular cases of the more general equations presented here.

The basic equation relating the convective efficiency to the local structure is

$$\frac{9}{4}\,\Omega(\Gamma)\,\Gamma^3+\Gamma(\Gamma+1)=A^2(\nabla_{\rm r}-\nabla_{\rm a})\;, \tag{A.4.2}$$

where $\nabla_{\rm r}$ and $\nabla_{\rm a}$ are respectively the logarithmic ($\nabla=\mathrm{d}\log T/\mathrm{d}\log P$) radiative and adiabatic temperature gradients. The function which associates the root of this equation with the local structure is

$$A^2=\left(\frac{G}{12\sqrt{2}\,ac}\right)^2\frac{QC_P^2k^2\rho^5m_r^2}{r^4T^6P}\,\ell^4\;, \tag{A.4.3}$$

with the constants being as given in Table A.1 while the structural functions Q, C_P and k correspond, respectively, to the expansion coefficient, specific heat at constant pressure and opacity. The others are as before. The mixing length, formally defined as the typical length over which on average a portion of fluid travels before mixing with the surroundings, is ℓ. Finally we have the function defining a particular formulation. The general expression we consider here, for the time being, is

$$\Omega(\Gamma)=\frac{8a_1}{9}\,\Sigma^{m+1}\,\frac{[(1+a_2\Sigma)^n-1]^p}{\left[(1+\Sigma)^{1/2}-1\right]^3}\;, \tag{A.4.4}$$

with

$$\Sigma=4\Gamma(\Gamma+1)\;. \tag{A.4.5}$$

Two of the exponents are related to the third, as imposed by the limiting behaviour of highly efficient and highly inefficient convection. In particular we have (see Chapter 5 for more details on why this is so)

$$n = \frac{1}{2}\,\frac{1-2m}{2-m} \qquad \text{and} \qquad p = 2-m \ . \tag{A.4.6}$$

For given values of (m,a_1,a_2), and since at each point of the star we have $A^2(\nabla_{\rm r}-\nabla_{\rm a})$ (assuming we know ℓ also), these expressions can be solved for Γ (or Σ). In doing so we may then obtain ∇ through

$$\nabla = \nabla_{\rm a} + \frac{\Gamma(\Gamma+1)}{A^2} \ . \tag{A.4.7}$$

A particular case is the standard Mixing Length Theory, referred in the text as *MLT*, which corresponds to

$$\textit{MLT}: \qquad (a_1, a_2, m) = (9/8, 1, -1) \ . \tag{A.4.8}$$

Other options are also considered, for example the case of the formulation proposed by Canuto & Mazzitelli (1991, 1992), for example, and a general parametrization in terms of an extra parameter β_c which defines the value of a_1 and a_2. These alternatives are extensively discussed in the main text so we do not go further on this here. The actual implementation in the code is the same regardless of the values used for a_1, a_2 or m.

One other point still unspecified is the mixing length ℓ. In general this is only a function of the position in local theories. For such a case the implementation is trivial. An example is the usual option of writing

$$\ell = \alpha_c H_P \ , \tag{A.4.9}$$

where α_c is a parameter to be determined from the boundary conditions and H_P is the pressure scale height. We have also consider other options, which are not local but still of simple implementation. One of them is to write

$$\ell = \left(1 + \frac{\alpha_c}{10^4}\right) r_u - r \ , \tag{A.4.10}$$

where r_u is the upper boundary of the convective envelope. The number 10^4 has only been consider to make the value of α_c of the order of unity. So, the mixing length is approximately proportional to the depth from the top of the convection zone. This has been argued as being a better choice, than the previous one, by Canuto & Mazzitelli (1992). However in their proposal no parameters were used. But considering that we are constructing solar models for seismic studies a parameter is still necessary due to the fact that we need to make sure that our model has the observed radius.

A.4.3 Implementation of the convection theory

The actual calculations involved when using a formulation described above in a region of convection is reasonably simple. Here we describe briefly how it is done.

Again, all calculations are done in terms of reduced variables as defined before. According to this philosophy we also replace the mixing length ℓ by

$$\lambda = \frac{\ell}{H_P} \ , \tag{A.4.11}$$

with H_P being the pressure scale height. If we use for the mixing length the option $\ell \propto H_P$, then λ is constant and equal to α_c. However in general we have $\lambda = \lambda(r)$.

We further write

$$A^2 = \overline{A}^2 \ \lambda^4 \qquad \text{with} \qquad \overline{A}^2 = \frac{{\mathcal{R}_{\rm g}}^8}{2(12ac)^2(GR)^5 M} \ b(x) \ , \tag{A.4.12}$$

being

$$b = \frac{Q c_p^2 k^2 z_1^4 z_2^3 \tilde{\rho}}{x^2 z_4^6} \ . \tag{A.4.13}$$

Now, noting that

$$\frac{9}{4} \ \Omega \ \Gamma^3 = \frac{1}{4} \ a_1 \Sigma^{m+1} \left[(1+a_2\Sigma)^n - 1 \right]^p \ , \tag{A.4.14}$$

and introducing a new variable "s" as

$$s = \frac{\Sigma}{4\overline{A}^2} \ , \tag{A.4.15}$$

we construct a function $g = g(s)$ from Eq. (A.4.2) as

$$g(s) = 1 - s \ \ \frac{1 + b_1 s^m \left[(1+b_2 s)^n - 1 \right]^p}{\lambda^4(s) \ (\nabla_{\rm r} - \nabla_{\rm a})} \ , \tag{A.4.16}$$

with

$$b_1 = a_1 \left(4\overline{A}^2 \right)^m \qquad \text{and} \qquad b_2 = a_2 \left(4\overline{A}^2 \right) \ . \tag{A.4.17}$$

Then, the root s_0 (which is such as $0 \leq s_0 \lesssim \nabla_{\rm r} - \nabla_{\rm a}$) of $g(s)$ is used to determine the actual temperature gradient;

$$\nabla = \nabla_{\rm a} + \frac{s_0}{\lambda^4} \ . \tag{A.4.18}$$

This is the value we need at each point to be used in the structure equation for the temperature within the convection zone.

A.5 Other physics

Still needed to complete all our equations for calculating the structure of the Sun (or for that matter of a star) are the opacities k and the emissivity ε. These are the ingredients that together with the equation of state form the set of physics going into our modelling of the solar structure.

A.5.1 Opacities

What we actually need is a function that describes the interaction of radiation with the gas. So, given a temperature and the gas density (for specified abundances) the opacity is the function that provides this relation.

In the code described here, and used to determine most of the solar models reported in Thesis, we have used the subroutines provided by Christensen-Dalsgaard which interpolate opacity tables. The tables from Cox & Tabor (1976) have been used in all cases.

We also present and discuss results obtained for models that have not been calculated with our code (Chapter 3). But are instead from Christensen-Dalsgaard stellar structure code (cf Christensen-Dalsgaard 1982, also described in Christensen-Dalsgaard, Proffitt & Thompson 1993). It uses the more recent opacities from the Los Alamos Opacity Tables (Rogers & Iglesias 1992; Iglesias, Rogers & Wilson 1992).

A.5.2 Emissivity

In order to have a star in equilibrium there must be energy generation in the interior. When modelling the internal structure we must therefore provide a relation that gives the energy produced for a given temperature and density (for known abundances). Because we are mainly interested in solar and solar like models, the only contributions we have considered are the ones coming from the PP chain (in its three branches) and the small contribution due to the CNO chain.

The actual expressions implemented are given below (see Section 18 of Kippenhahn & Weigert 1990, references therein, and also Lang 1980). For the PP chain we have used

$$\varepsilon_{\rm PP} = \frac{\varepsilon_0}{0.980}\,\phi(\alpha)\,\Big(0.980\,F_1 + 0.960\,F_2 + 0.721\,F_3\Big) \qquad \text{erg g}^{-1}\ \text{s}^{-1} \tag{A.5.1}$$

$$\varepsilon_0 = 2.38{\times}10^6\,X^2\rho T_6^{-2/3}\Big(1 + 0.0123\,T_6^{1/3} + 0.0109\,T_6^{2/3} + 0.00095\,T_6\Big) \times \exp\Big(-33.81\,T_6^{-1/3} + 0.27\,\rho^{1/2}T_6^{-3/2}\Big)$$

$$T_6 = 10^{-6}\,T$$

$$\phi(\alpha) = 1 - \alpha + \alpha\sqrt{1{+}2/\alpha}$$

$$\alpha = 1.2\times10^{17}\left(\frac{1-X-Z}{4X}\right)^2 \mathrm{e}^{-100\ T_6^{-1/3}}$$
$$F_1 = \frac{\sqrt{1+2/\alpha}-1}{\sqrt{1+2/\alpha}+3}$$
$$F_2 = \frac{1-F_1}{1+8.94\times10^{15}\ \frac{X}{4-3X}\ T_6^{-1/6}\mathrm{e}^{-102.65\ T_6^{-1/3}}}$$
$$F_3 = 1-F_1-F_2\ .$$

While for the CNO chain we have considered

$$\begin{aligned}\varepsilon_{\rm CNO} =& 8.67\times10^{27}\, Z_{\rm CNO} X\ \rho T_6^{-2/3}\Big(1+0.0027\ T_6^{1/3}+0.00778\ T_6^{2/3}+0.000149\ T_6\Big)\\ &\times\exp\Big(-152.28\ T_6^{-1/3}\Big) \qquad\qquad \mathrm{erg\ g^{-1}\ s^{-1}}\ .\end{aligned} \tag{A.5.2}$$

Here, $Z_{\rm CNO}$ is the abundances by mass of the elements C, N and O. For the models using simplest physics we consider this to be the actual heavy elements abundance Z, while for the others we have taken Grevesse's heavy elements abundances for the individual species as listed in Iglesias et al. (1992).

The actual emissivity is the sum of the two,

$$\varepsilon(\rho,T) = \varepsilon_{\rm PP} + \varepsilon_{\rm CNO}\ . \tag{A.5.3}$$

In the case of envelope models whose structure is calculated down to a radius of $0.2R$, their stratification is not affected much by these expressions, since they only give non-zero values very close to the centre.

A.6 Numerical method

The method we use to solve the equations is a simple shooting method in the case of a full solar model or just an integration downwards if an envelope model is to be calculated. As described above the atmosphere is calculated by a shooting method between the photosphere (defined as $r{=}R$) and the atmosphere (where $m_r{=}M$). From such an integration we find the upper boundary conditions for the interior, namely $P{=}P_s$ and $m_r{=}m_{r,s}$. The temperature is the effective temperature. From there we can integrate down to some point, which for envelopes we normally take as $r{=}0.2R$. The boundary conditions and the value of α_c used define the base of the convection zone. If we require this to be at a specific point we then iterate on α_c in order to find the value that gives the base at the desired position.

In the case of full models the process is different. Here we also use a shooting method by integrating the equations from the centre and the surface. For doing so we need the values of the temperature and pressure at the centre and the Helium abundance, which

together with α_c (from the convection theory) provide the four parameters we must iterate until a solution is found. This corresponds to find four values for which we have continuous functions at the matching point of the two (inner and outer) integrations.

The numerical accuracy with which we solve the structure equations among others depend very strongly on the step used for integrating. Therefore we have implemented a varying step which is calculated at each point. The expressions used are

$$|\Delta x(x)| = \mathrm{Max}\left[\ 10^{-15} \quad ; \quad \mathrm{Min}\Big(h_{\mathrm{grid}}(x)\ ;\ h(x)\Big)\ \right]\ ,$$
$$h(x) = 0.005 \times \mathrm{Min}\left(\begin{array}{cc} 0.1 & ; \quad \dfrac{|z_i|}{\left|\dfrac{\mathrm{d}z_i}{\mathrm{d}x}\right| + 10^{-30}} \end{array}\right) \qquad \text{for i=1, 2, 3, 4 .} \tag{A.6.1}$$

Where h_{grid} represents the maximum allowed step as imposed by a specified mesh at which we want the output to be written. For our case this is included in order to force the integration to have more mesh points than it needs because they will be needed later in the calculation of the oscillations frequencies. However, for most of the model it is the value of h that imposes the value of Δx to be used. An expression as this guarantees that more mesh points are placed where the functions z to be integrated (as defined in (A.2.13)) vary more strongly.

Note that according to this expression the maximum step allowed is $\Delta x{=}5{\times}10^{-4}$ giving that at least the calculation will use 2000 mesh points to integrate the interior plus a few hundreds for the atmosphere. We also use this expression for the integration of the atmosphere where in that case x is the optical depth and the functions z are replaced by the functions f as defined in Eqs. (A.2.21).

The value of Δx giving by this expression is used to integrate the equations being the step in our fourth order Runge-Kutta integration rule. However, the output mesh includes only the points selected according to the spacing imposed by $h_{\mathrm{grid}}(x)$. Its values range from $10^{-3.5}$ in regions closer to the center down to 10^{-6} for the superadiabatic region and below where the eigenfunctions strongly vary with radius. These implies a relatively high density of points in the mesh near the surface, important in models used for the calculation of p-mode frequencies.

We also recall here that the code includes an iterative method which finds exactly where the boundaries of convective regions are located in order to force a mesh point to be used there and included in the output.

Finally, the solution is considered to be found if the relative difference of the two solutions (for all of the four dependent variables) at the matching point is below 10^{-7} in a full model. While for an envelope model the base of the convection zone must be within the required value by less than 10^{-9}. The iteration on the parameters in both cases is

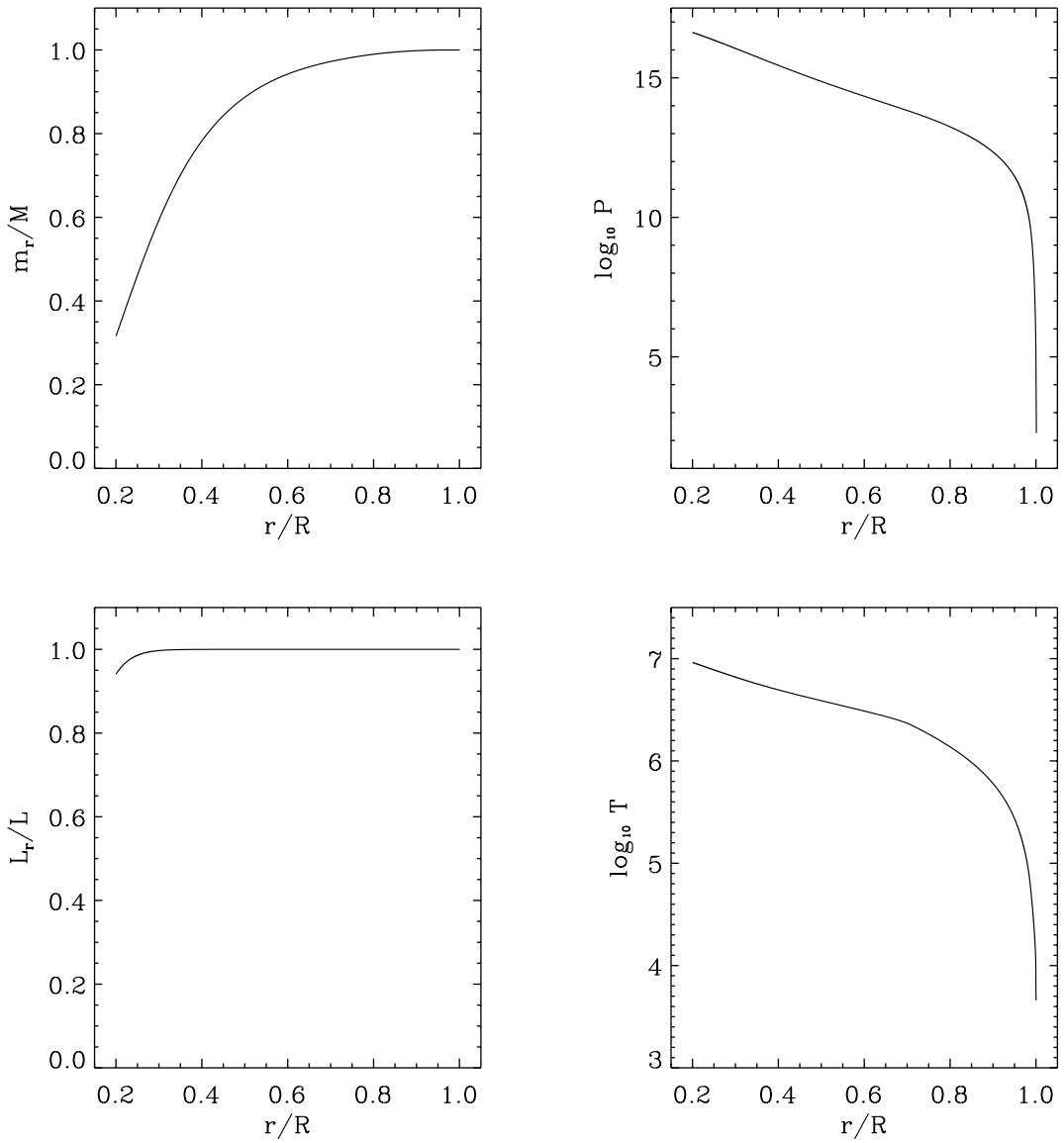

Fig. A.1: Plot of a solution of the four structure equations for the physics discussed in the text. Shown here are the four dependent variables; (a) mass, (b) pressure, (c) luminosity and (d) temperature, versus radius. It is an envelope model and so the integration only goes down to about 20% of the radius. The inner boundary condition has been replaced by a condition requiring the base of the convection zone to be located at $r_{\rm d}/R$=0.713. All quantities is CGS units.

done using a Newton-Rapson technique.

A.7 Example: Mixing Length Theory model

As an example we consider here an envelope model calculated using Mixing Length Theory, Cox & Tabor opacities, the CEFF equation of state and the base of the convection zone at r/R=0.713. The basic results that come out of the integration of the equations is of course our four dependent variables. These are shown in Fig. A.1 for our envelope model. Other variables, like density or adiabatic gradient come out of the equation of state and are therefore associated to the values of pressure and temperature at a given point. Some of these thermodynamic quantities relevant for the seismic properties of the models are shown in Chapter 1.

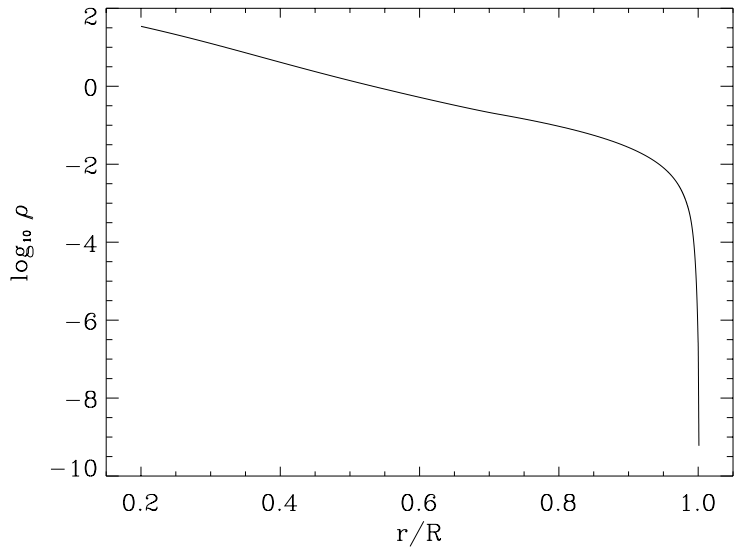

Fig. A.2: Plot of the density for the same model as in the previous figure. The units of density are grams.

One of the representative quantities is density, given by the equation of state. It is plotted in Fig. A.2, against radius. As for pressure and temperature, it varies very rapidly near the surface, where the behaviour can be closely described by an exponential.

The atmosphere of the model, also included in the previous figures, goes up to radius $1.001R$. It is shown separately in Fig. A.3, in terms of temperature versus pressure. Note the isothermal character of our solution for the upper layers of the atmosphere. This will be used as the boundary condition for modelling the oscillations.

Finally we provide here, for reasons that become clear in the next Appendix, the form of the output from the structure program for use in the calculation of its seismic properties. It is done in terms not of the dependent variables considered above but in a more convenient combination of these. The output is therefore written as the five a's,

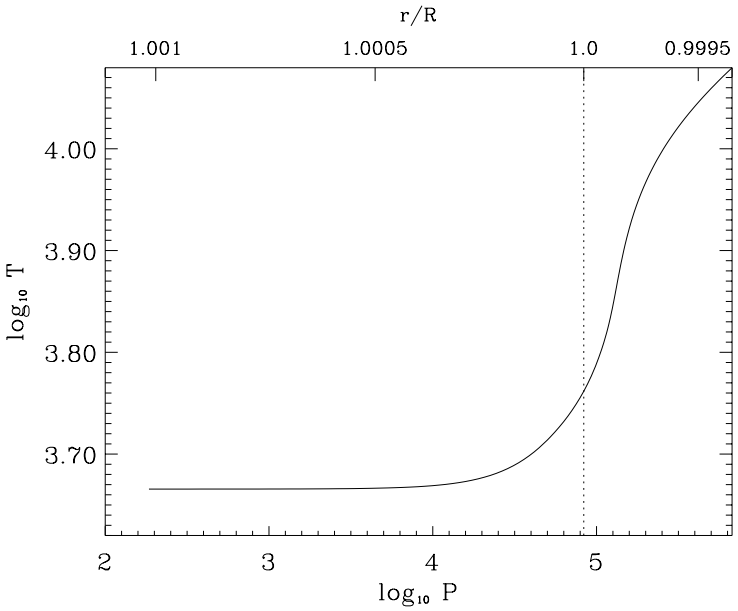

Fig. A.3: Atmosphere of the model, in terms of temperature versus pressure. The region shown corresponds to radius above $0.9993R$.

dimensionless functions of radius r, and defined as (cf the quantities considered by Unno et al. 1989)

$$
\begin{aligned}
r: \qquad a_1 &= \frac{m_r}{r^3}\,\frac{R^3}{M} \\
a_2 &= -\frac{1}{\Gamma_1}\,\frac{\mathrm{d}\log P}{\mathrm{d}\log r} \\
a_3 &= \Gamma_1 \\
a_4 &= \frac{1}{\Gamma_1}\,\frac{\mathrm{d}\log P}{\mathrm{d}\log r} - \frac{\mathrm{d}\log \rho}{\mathrm{d}\log r} \\
a_5 &= \frac{4\pi r^3 \rho}{m_r}\,.
\end{aligned}
\tag{A.7.1}
$$

These are all we need to construct the coefficients in the differential equations for linear oscillations (Appendix B).

B. Numerical Frequencies of Oscillation

The method used to calculate numerical frequencies of linear adiabatic oscillations for a solar model is presented in this Chapter. Starting from the hydrodynamic equations, the basic linear equations describing the oscillations are derived, in the form more adequate to calculate the numerical eigenfunctions and eigenvalues. The boundary conditions used and their implementation is also discussed. We also include a description of the numerical method and code developed to solve the set of four first order differential equations. The accuracy of the calculations is also discussed briefly.

B.1 Introduction

The objective of this Appendix is to present all the basic equations and results frequently referred to in the main text, concerning the frequencies of oscillation of solar models. Here only adiabatic non-radial oscillations in the linear regime are considered. Most of the frequencies used in several parts of the thesis have been calculated as described here.

We start by the mathematical formalism by beginning from the hydrodynamic equations in order to construct the differential equations describing the radial dependence of the amplitude of the eigenfunctions. We complete the equations by establishing the boundary conditions at the centre and at the surface. Because we also use solar envelope models an extra term for the expansion in the centre of the boundary condition has been included. We then briefly describe the numerical method implemented to integrate the differential equations and the procedure to find the eigenvalues of the system. The accuracy of the calculations is also discussed.

B.2 Equations

Our objective is to obtain the equations for non-radial adiabatic oscillations of spherically symmetric non-rotating stars. To do so, we start from the basic hydrodynamic equations. These are perturbed for small variations of the equilibrium quantities in order to write the linearized equations for the perturbations. The angular dependence can then be removed due to the assumption of spherical symmetry leaving the equations for the radial dependence of the amplitude of the eigenfunctions. We then rewrite these in the most convenient form for solving the system numerically. Finally the Section ends with the discussion of the boundary conditions necessary to solve the eigenvalue problem. Here a second order expansion in the centre for the boundary conditions has been considered due to the fact that in this work we have also used solar envelope models which go down to about two tenths of the radius. Therefore, the boundary condition for the centre has to be replaced by a boundary condition at the deepest mesh point of the model.

B.2.1 Hydrodynamic equations

Considering a fluid of density ρ, with a velocity field $\vec{v}$, pressure P and gravitational potential Φ, its state is described by the four basic hydrodynamic equations. These are;

$$\begin{aligned}
\text{Conservation of mass} \quad & \frac{\partial \rho}{\partial t} + \nabla \cdot (\rho \vec{v}) = 0 \\
\text{Conservation of momentum} \quad & \rho \, \frac{\partial \vec{v}}{\partial t} + \rho \, (\vec{v} \cdot \nabla) \vec{v} = -\nabla P + \rho \nabla \Phi \\
\text{Poisson's equation} \quad & \nabla^2 \Phi = -4\pi G \rho \\
\text{Thermodynamic relation} \quad & \frac{\delta \rho}{\rho} = \left(\frac{\partial \log \rho}{\partial \log P} \right)_S \frac{\delta P}{P} + \left(\frac{\partial \log \rho}{\partial \log S} \right)_P \frac{\delta S}{S} \, ,
\end{aligned} \tag{B.2.1}$$

where t and S are, respectively, time and entropy. In writing these we do not consider electric/magnetic fields or any type of energy dissipation. The last equation replaces the energy equation, describing the behaviour of the Lagrangian fluctuations $\delta\rho$, δP and δS for the fluid. The thermodynamic derivatives in the equation are respectively at constant entropy S and constant pressure P. The symbol G is for the gravitational constant.

We consider all quantities to be given in spherical coordinates (r, θ, ϕ) with, as usual, $r{=}|\vec{r}|$ being the radial distance, θ the latitude measured from the horizontal plane $z{=}0$ and ϕ the longitude measured in the horizontal plane from the axis ($x{\geq}0$, $y{=}0$). If we write the

components of the vector $\vec{v}$ as being (v_r, v_θ, v_ϕ), the operators used in these expressions are,

$$\begin{aligned}
\nabla \cdot \vec{v} &= \frac{1}{r^2}\,\frac{\partial}{\partial r}(r^2 v_r) + \frac{1}{r\sin\theta}\,\frac{\partial}{\partial\theta}(\sin\theta\; v_\theta) + \frac{1}{r\sin\theta}\,\frac{\partial v_\phi}{\partial\phi} \\
\nabla P &= \left(\frac{\partial P}{\partial r}, \frac{1}{r}\,\frac{\partial P}{\partial\theta}, \frac{1}{r\sin\theta}\,\frac{\partial P}{\partial\phi}\right) \\
\nabla^2 P &= \frac{1}{r^2}\,\frac{\partial}{\partial r}\left(r^2\frac{\partial P}{\partial r}\right) + \frac{1}{r^2\sin^2\theta}\,\left[\sin\theta\,\frac{\partial}{\partial\theta}\left(\sin\theta\,\frac{\partial P}{\partial\theta}\right) + \frac{\partial^2 P}{\partial\phi^2}\right] ,
\end{aligned} \tag{B.2.2}$$

and also having that $\nabla^2\vec{v} = \left(\nabla^2 v_r, \nabla^2 v_\theta, \nabla^2 v_\phi\right)$.

Since we are considering only adiabatic oscillations we may reduce the thermodynamic equation in (B.2.1) by using the fact that for an adiabatic change the entropy is conserved, therefore $\delta S \equiv 0$. Also, we introduce the definition of the adiabatic exponent Γ_1 given by the following thermodynamic derivative at constant entropy S,

$$\Gamma_1 = \left(\frac{\partial \log P}{\partial \log \rho}\right)_S . \tag{B.2.3}$$

The equations corresponding to the equilibrium configuration (subscript "0"), which here we considered as being a time independent spherically symmetric non-rotating star, are

$$\begin{aligned}
\vec{v}_0 &= 0 \\
\nabla P_0 &= \rho_0\,\nabla\Phi_0 \\
\nabla^2\Phi_0 &= -4\pi G\rho_0 .
\end{aligned} \tag{B.2.4}$$

In our notation, all equilibrium quantities depend only on the radial coordinate r being independent of time t and the horizontal spacial coordinates θ and ϕ. Note that this solution corresponds to the configuration we discuss in the previous Appendix.

B.2.2 Linear perturbation analysis

In order to linearize the equations we consider small fluctuations of all quantities around the equilibrium configuration. So, we perturb all quantities for small variations around the equilibrium values $(\rho_0, P_0, \vec{v}_0, \Phi_0)$, by writing the actual values as

$$\begin{aligned}
\rho &= \rho_0 + \rho' \\
P &= P_0 + P' \\
\vec{v} &= \vec{v}_0 + \vec{v}' \\
\Phi &= \Phi_0 + \Phi' .
\end{aligned} \tag{B.2.5}$$

The prime ($\prime$) corresponds to the Eulerian perturbation (at a given position) while a (δ) is reserved for the Lagrangian perturbation (for a given fluid element). If we consider a function $f=f(\vec{r},t)$ associated to the fluid, the two types of perturbation are related by

$$\delta f = f' + \vec{\xi}\cdot\nabla f \ , \tag{B.2.6}$$

with the displacement $\vec{\xi}$ being associated to the fluid velocity (to first order in $\vec{\xi}$) according to the relation

$$\vec{v} = \frac{\mathrm{d}\vec{\xi}}{\mathrm{d}t} \simeq \frac{\partial\vec{\xi}}{\partial t} + (\vec{v}_0\cdot\nabla)\,\vec{\xi}\,. \tag{B.2.7}$$

Now, after substituting expressions (B.2.5) in (B.2.1) we get, if terms of second or higher order in the small perturbations are neglected, that

$$\begin{aligned}
&\frac{\partial\rho'}{\partial t} + \nabla\cdot\left(\rho_0\frac{\partial\vec{\xi}}{\partial t}\right) = 0 \\
&\rho_0\,\frac{\partial^2\vec{\xi}}{\partial t^2} = -\nabla P' + \rho_0\nabla\Phi' + \rho'\nabla\Phi_0 \\
&\nabla^2\Phi' = -4\pi G\rho' \\
&\delta P = \frac{\Gamma_{1,0}P_0}{\rho_0}\,\delta\rho\ .
\end{aligned} \tag{B.2.8}$$

Where the displacement, since we have zero velocity for the equilibrium configuration, is related to $\vec{v}'$ simply by

$$\vec{v}' = \frac{\partial\vec{\xi}}{\partial t}\ . \tag{B.2.9}$$

The last equation in (B.2.8) can also be written as (by replacing Lagrangian fluctuations by Eulerian perturbations according to (B.2.6))

$$\frac{P'}{P_0} + \frac{\vec{\xi}\cdot\nabla P_0}{P_0} = \Gamma_{1,0}\,\left(\frac{\rho'}{\rho_0} + \frac{\vec{\xi}\cdot\nabla\rho_0}{\rho_0}\right)\ , \tag{B.2.10}$$

or

$$\frac{P'}{P_0} = \Gamma_{1,0}\,\frac{\rho'}{\rho_0} - \frac{\vec{r}\cdot\vec{\xi}}{r}\,\left(\frac{\mathrm{d}\log P_0}{\mathrm{d}r} - \Gamma_{1,0}\,\frac{\mathrm{d}\log\rho_0}{\mathrm{d}r}\right)\ . \tag{B.2.11}$$

Therefore, noting that since all coefficients in Eqs. (B.2.8) are time independent, we may separate the spacial dependence from the temporal dependence in the solution. Then the time dependence is written as a factor e(iωt), i.e.,

$$\begin{aligned}
P'(t,r,\theta,\phi) &= P'_s(r,\theta,\phi)\ \ \mathrm{e}^{\mathrm{i}\omega t} \\
\rho'(t,r,\theta,\phi) &= \rho'_s(r,\theta,\phi)\ \ \mathrm{e}^{\mathrm{i}\omega t} \\
\Phi'(t,r,\theta,\phi) &= \Phi'_s(r,\theta,\phi)\ \ \mathrm{e}^{\mathrm{i}\omega t} \\
\vec{\xi}(t,r,\theta,\phi) &= \vec{\xi}_s(r,\theta,\phi)\ \ \mathrm{e}^{\mathrm{i}\omega t} \\
&= \left[\xi_{r,s}(r,\theta,\phi), \xi_{\theta,s}(r,\theta,\phi), \xi_{\phi,s}(r,\theta,\phi)\right]\ \ \mathrm{e}^{\mathrm{i}\omega t}\ .
\end{aligned} \tag{B.2.12}$$

After substitution, it follows that

$$\begin{aligned}
&\rho_s' + \nabla \cdot \left(\rho_0 \vec{\xi}_s\right) = 0 \\
&\omega^2 \rho_0 \, \vec{\xi}_s - \nabla P_s' + \rho_0 \nabla \Phi_s' + \rho_s' \nabla \Phi_0 = 0 \\
&\nabla^2 \Phi_s' = -4\pi G \rho_s' \\
&\frac{P_s'}{P_0} = \Gamma_{1,0} \, \frac{\rho_s'}{\rho_0} - \xi_{r,s} \, \left(\frac{\mathrm{d} \log P_0}{\mathrm{d}r} - \Gamma_{1,0} \, \frac{\mathrm{d} \log \rho_0}{\mathrm{d}r} \right) \, .
\end{aligned} \tag{B.2.13}$$

Now, defining the operators

$$\begin{aligned}
&\nabla_\perp = \frac{1}{r} \, \left(0, \frac{\partial}{\partial \theta}, \frac{1}{\sin\theta} \, \frac{\partial}{\partial \phi} \right) \\
&\nabla_\perp^2 = \frac{1}{r^2 \sin^2\theta} \, \left[\sin\theta \, \frac{\partial}{\partial \theta} \left(\sin\theta \, \frac{\partial}{\partial \theta} \right) + \frac{\partial^2}{\partial \phi^2} \right] \, ,
\end{aligned} \tag{B.2.14}$$

and introducing $\vec{\xi}_{\perp,s}$=$(0, \xi_{\theta,s}, \xi_{\phi s})$, we may write (B.2.13) as

$$\begin{aligned}
&\frac{\rho_s'}{\rho_0} + \frac{\mathrm{d} \log \rho_0}{\mathrm{d}r} \, \xi_{r,s} + \frac{1}{r^2} \, \frac{\partial}{\partial r} (r^2 \xi_{r,s}) + \nabla_\perp \cdot \vec{\xi}_{\perp,s} = 0 \\
&\omega^2 \xi_{r,s} - \frac{1}{\rho_0} \, \frac{\partial P_s'}{\partial r} + \frac{\partial \Phi_s'}{\partial r} + \frac{\rho_s'}{\rho_0} \, \frac{\mathrm{d}\Phi_0}{\mathrm{d}r} = 0 \\
&\omega^2 \vec{\xi}_{\perp,s} - \nabla_\perp \left(\frac{P_s'}{\rho_0} - \Phi_s' \right) = 0 \\
&\frac{1}{r^2} \, \frac{\partial}{\partial r} \left(r^2 \frac{\partial \Phi_s'}{\partial r} \right) + \nabla_\perp^2 \Phi_s' + 4\pi G \rho_s' = 0 \\
&\frac{P_s'}{P_0} = \Gamma_{1,0} \, \frac{\rho_s'}{\rho_0} - \xi_{r,s} \, \left(\frac{\mathrm{d} \log P_0}{\mathrm{d}r} - \Gamma_{1,0} \, \frac{\mathrm{d} \log \rho_0}{\mathrm{d}r} \right) \, .
\end{aligned} \tag{B.2.15}$$

Now, using

$$\begin{aligned}
&\frac{\rho_s'}{\rho_0} = \frac{P_s'}{\Gamma_{1,0} \, P_0} + \xi_{r,s} \, \left(\frac{1}{\Gamma_{1,0}} \, \frac{\mathrm{d} \log P_0}{\mathrm{d}r} - \frac{\mathrm{d} \log \rho_0}{\mathrm{d}r} \right) = \frac{P_s'}{\Gamma_{1,0} \, P_0} + \frac{N_0^2}{g_0} \, \xi_{r,s} \\
&\vec{\xi}_{\perp,s} = \frac{1}{\omega^2} \, \nabla_\perp \left(\frac{P_s'}{\rho_0} - \Phi_s' \right) \, ,
\end{aligned} \tag{B.2.16}$$

where

$$g_0 = -\frac{\mathrm{d}\Phi_0}{\mathrm{d}r} = -\frac{1}{\rho_0}\,\frac{\mathrm{d}P_0}{\mathrm{d}r}$$

$$N_0^2 = g_0\left(\frac{1}{\Gamma_{1,0}}\,\frac{\mathrm{d}\log P_0}{\mathrm{d}r} - \frac{\mathrm{d}\log\rho_0}{\mathrm{d}r}\right) = -g_0\left(\frac{g_0\rho_0}{\Gamma_{1,0}\,P_0} + \frac{\mathrm{d}\log\rho_0}{\mathrm{d}r}\right)\,, \tag{B.2.17}$$

N_0^2 being the Brunt–Väisälä frequency (or Buoyancy frequency) and g_0 the gravitational acceleration, we eliminate ρ_s' and $\vec{\xi}_{\perp,s}$ from Eqs. (B.2.16). Obtaining

$$\left(\frac{\rho_0}{\Gamma_{1,0}\,P_0} + \frac{\nabla_\perp^2}{\omega^2}\right)\,\frac{P_s'}{\rho_0} + \frac{1}{r^2}\,\frac{\partial}{\partial r}(r^2\xi_{r,s}) + \frac{1}{\Gamma_{1,0}}\,\frac{\mathrm{d}\log P_0}{\mathrm{d}r}\,\xi_{r,s} - \frac{\nabla_\perp^2\Phi_s'}{\omega^2} = 0$$

$$\frac{1}{\rho_0}\,\left(\frac{\rho_0 g_0}{\Gamma_{1,0}\,P_0} + \frac{\partial}{\partial r}\right)\,P_s' - (\omega^2 - N_0^2)\,\xi_{r,s} - \frac{\partial\Phi_s'}{\partial r} = 0 \tag{B.2.18}$$

$$4\pi G\rho_0\,\left(\frac{P_s'}{\Gamma_{1,0}\,P_0} + \frac{N_0^2}{g_0}\,\xi_{r,s}\right) + \frac{1}{r^2}\,\frac{\partial}{\partial r}\left(r^2\frac{\partial\Phi_s'}{\partial r}\right) + \nabla_\perp^2\Phi_s' = 0\,.$$

Since all coefficients in these equations are independent of the horizontal coordinates, we can again separate the different dependences by writing

$$\begin{aligned} P'(r,\theta,\phi) &= \tilde{P}(r)\;\; f(\theta,\phi) \\ \rho'(r,\theta,\phi) &= \tilde{\rho}(r)\;\; f(\theta,\phi) \\ \Phi'(r,\theta,\phi) &= \tilde{\Phi}(r)\;\; f(\theta,\phi) \\ \xi_{r,s}(r,\theta,\phi) &= \xi_r(r)\;\; f(\theta,\phi)\,. \end{aligned} \tag{B.2.19}$$

After substitution we get that all equations can be written in the form

$$g_1(r)\;\; f(\theta,\phi) = g_2(r)\quad r^2\,\nabla_\perp^2 f(\theta,\phi)\,, \tag{B.2.20}$$

therefore we must have that

$$r^2\,\nabla_\perp^2 f = -\Lambda\,f\,, \tag{B.2.21}$$

where Λ is a constant. Or

$$\frac{1}{\sin^2\theta}\,\left[\sin\theta\,\frac{\partial}{\partial\theta}\left(\sin\theta\,\frac{\partial f}{\partial\theta}\right) + \frac{\partial^2 f}{\partial\phi^2}\right] = -\Lambda\,f\,. \tag{B.2.22}$$

Again this equation has coefficients which are independent of ϕ, and so we may also separate the dependence on ϕ by writing that

$$f(\theta,\phi) = f_1(\theta)\;\; f_2(\phi)\,, \tag{B.2.23}$$

which gives

$$\frac{1}{f_2}\,\frac{\mathrm{d}^2 f_2}{\mathrm{d}\phi^2} = C\,, \tag{B.2.24}$$

with C being a constant. The solution must then be $f_2(\phi) \propto e(\sqrt{C}\phi)$. Because the dependence on ϕ must be periodic as required by $f_2(\phi+2\pi)=f_2(\phi)$, it follows that $\sqrt{C}=im$, where m is an integer number.

Substituting back in (B.2.22) using (B.2.23), we get

$$\frac{1}{\sin\theta}\,\frac{\mathrm{d}}{\mathrm{d}\theta}\left(\sin\theta\,\frac{\mathrm{d}f_1}{\mathrm{d}\theta}\right)+\left(\Lambda-\frac{m^2}{\sin^2\theta}\right)\,f_1=0\,, \tag{B.2.25}$$

which becomes, if writing it for $\mu=\cos\theta$,

$$\frac{\mathrm{d}}{\mathrm{d}\mu}\left[(1-\mu^2)\,\frac{\mathrm{d}f_1}{\mathrm{d}\mu}\right]+\left(\Lambda-\frac{m^2}{1-\mu^2}\right)\,f_1=0\,. \tag{B.2.26}$$

It can be shown that this equation only has a regular solution for $\Lambda=l(l+1)$ (where l is non-negative integer), and with $|m|<l$, given by

$$f_1(\theta)=P_l^m(\cos\theta)\,, \tag{B.2.27}$$

with P_l^m being the Legendre polynomials. Therefore

$$f_{ml}(\theta,\phi)\propto P_l^m(\cos\theta)\,\mathrm{e}^{\mathrm{i}m\phi}\,. \tag{B.2.28}$$

The constant is determined by imposing the condition that

$$\int_0^{2\pi}\int_0^{\pi} f_{ml}(\theta,\phi)\;\;f_{m'l'}(\theta,\phi)\;\;\sin\theta\,\mathrm{d}\theta\,\mathrm{d}\phi=\delta_{ll'}\;\delta_{mm'}\,, \tag{B.2.29}$$

where δ_{ij} is the usual Kronecker delta (1 if $i=j$, and 0 otherwise). In this way we end up with

$$f(\theta,\phi)=Y_l^m(\theta,\phi)\equiv(-1)^{(m+|m|)/2}\;\left[\frac{2l+1}{2\pi}\,\frac{(l-|m|)!}{(l+|m|)!}\right]^{1/2}\,P_l^m(\cos\theta)\;\;\mathrm{e}^{\mathrm{i}m\phi}\,, \tag{B.2.30}$$

for $m=-l,\,-l+1,\ldots,l-1,l$. These form a complete set of normalized orthogonal functions Y_l^m, called spherical harmonics.

Now, using (B.2.30), (B.2.19) and (B.2.12) it can finally be written that

$$\begin{aligned}
P'(t,r,\theta,\phi)&=\tilde{P}(r)\;\;Y_l^m(\theta,\phi)\,\mathrm{e}^{\mathrm{i}\omega t}\\
\rho'(t,r,\theta,\phi)&=\tilde{\rho}(r)\;\;Y_l^m(\theta,\phi)\,\mathrm{e}^{\mathrm{i}\omega t}\\
\Phi'(t,r,\theta,\phi)&=\tilde{\Phi}(r)\;\;Y_l^m(\theta,\phi)\,\mathrm{e}^{\mathrm{i}\omega t}\\
\vec{\xi}(t,r,\theta,\phi)&=\left[\xi_r(r)\;\;Y_l^m(\theta,\phi),\;\xi_{\theta,s}(r,\theta,\phi),\;\xi_{\phi,s}(r,\theta,\phi)\right]\;\;\mathrm{e}^{\mathrm{i}\omega t}\,.
\end{aligned} \tag{B.2.31}$$

Using (B.2.16) we have

$$\xi_{\theta,s}=\xi_h\,\frac{\partial Y_l^m}{\partial\theta}\qquad\text{and}\qquad\xi_{\phi,s}=\frac{\xi_h}{\sin\theta}\,\frac{\partial Y_l^m}{\partial\phi}\,, \tag{B.2.32}$$

where we introduced, considering the second relation in (B.2.16),

$$\xi_h(r)=\frac{1}{r\omega^2}\,\left(\frac{\tilde{P}}{\rho_0}-\tilde{\Phi}\right)\,. \tag{B.2.33}$$

Giving finally that the displacement vector is

$$\vec{\xi}(t,r,\theta,\phi)=Real\left\{\mathrm{e}^{\mathrm{i}\omega t}\left[\xi_r(r)\,,\;\;\xi_h(r)\,\frac{\partial}{\partial\theta}\,,\;\;\frac{\xi_h(r)}{\sin\theta}\,\frac{\partial}{\partial\phi}\right]\;Y_l^m(\theta,\phi)\right\}\,. \tag{B.2.34}$$

The next step is to find the equations describing the radial dependence of the amplitude functions; $\tilde{P}$, $\tilde{\rho}$, $\tilde{\Phi}$, ξ_r and ξ_h.

B.2.3 Dependence of the eigenfunctions on radius

We start by substituting $\nabla_\perp^2 Y_l^m = -Y_l^m\, l(l+1)/r^2$ in (B.2.18) to obtain the three equations in the three variables $\tilde{P}$, ξ_r and $\tilde{\Phi}$ for adiabatic oscillations. If we define the adiabatic sound speed c_0 and the Lamb frequency S_l as

$$\begin{aligned} c_0^2 &= \frac{\Gamma_{1,0}\, P_0}{\rho_0} \\ S_l^2 &= l(l+1)\, \frac{c_0^2}{r^2}\,, \end{aligned} \tag{B.2.35}$$

the equations, after eliminating the factors in Y_l^m and t, are

$$\left(1 - \frac{S_l^2}{\omega^2}\right)\, \frac{\tilde{P}}{\rho_0} - \frac{1}{r^2}\, \left(g_0 - c_o^2\, \frac{\mathrm{d}}{\mathrm{d}r}\right)(r^2 \xi_r) + \frac{S_l^2}{\omega^2}\, \tilde{\Phi} = 0$$

$$\frac{1}{\rho_0}\left(\frac{g_0}{c_0^2} + \frac{\mathrm{d}}{\mathrm{d}r}\right)\, \tilde{P} - (\omega^2 - N_0^2)\, \xi_r - \frac{\mathrm{d}\tilde{\Phi}}{\mathrm{d}r} = 0 \tag{B.2.36}$$

$$\tilde{P} + \frac{\rho_0 c_0^2 N_0^2}{g_0}\, \xi_r - \frac{S_l^2}{4\pi G}\, \tilde{\Phi} + \frac{c_0^2}{4\pi G r^2}\, \frac{\mathrm{d}}{\mathrm{d}r}\left(r^2 \frac{\mathrm{d}\tilde{\Phi}}{\mathrm{d}r}\right) = 0\,.$$

Or, if we now consider the following variables

$$\begin{aligned} y_1 &= \frac{\xi_r}{r} \\ y_2 &= \frac{\omega^2}{g}\, \xi_h = \frac{1}{rg}\, \left(\frac{\tilde{P}}{\rho} - \tilde{\Phi}\right) \\ y_3 &= \frac{\tilde{\Phi}}{rg} \\ y_4 &= \frac{1}{g}\, \frac{\mathrm{d}\tilde{\Phi}}{\mathrm{d}r}\,, \end{aligned} \tag{B.2.37}$$

the equations can be written as

$$r\, \frac{\mathrm{d}y_1}{\mathrm{d}r} = \left(\frac{rg_0}{c_0^2} - 3\right) y_1 + \frac{rg_0}{c_0^2}\, \left(\frac{S_l^2}{\omega^2} - 1\right) y_2 - \frac{rg_0}{c_0^2}\, y_3$$

$$\begin{aligned} r\, \frac{\mathrm{d}y_2}{\mathrm{d}r} = &- \frac{r}{g_0}\, (N_0^2 - \omega^2) y_1 - \left(\frac{rg_0}{c_0^2} + \frac{\mathrm{d}\log\rho_0}{\mathrm{d}\log r} + 4\pi G\, \frac{r\rho_0}{g_0} - 1\right) y_2 - \\ &- \left(\frac{rg_0}{c_0^2} + \frac{\mathrm{d}\log\rho_0}{\mathrm{d}\log r}\right) y_3 \end{aligned} \tag{B.2.38}$$

$$r\, \frac{\mathrm{d}y_4}{\mathrm{d}r} = - \frac{4\pi G r^2 \rho_0}{c_0^2}\, \frac{c_0^2 N_0^2}{g_0^2}\, y_1 - \frac{4\pi G r^2 \rho_0}{c_0^2}\, y_2 + \left[l(l+1) - \frac{4\pi G r^2 \rho_0}{c_0^2}\right] y_3 -$$

$$- \frac{4\pi G r^2 \rho_0}{c_0^2}\, \frac{c_0^2}{r g_0}\, y_4\,.$$

From the two relations in (B.2.37) we also have that

$$r\,\frac{\mathrm{d}y_3}{\mathrm{d}r} = \left(1 - \frac{4\pi G r \rho_0}{g_0}\right) y_3 + y_4 \,. \tag{B.2.39}$$

We now introduce the following functions of the equilibrium structure (as in (A.7.1))

$$\begin{aligned}
a_1 &= \frac{m_{r,0}}{r^3}\,\frac{R^3}{M} \\
a_2 &= -\frac{1}{\Gamma_{1,0}}\,\frac{\mathrm{d}\log P_0}{\mathrm{d}\log r} = \frac{r g_0}{c_0^2} \\
a_3 &= \Gamma_{1,0} \\
a_4 &= \frac{1}{\Gamma_{1,0}}\,\frac{\mathrm{d}\log P_0}{\mathrm{d}\log r} - \frac{\mathrm{d}\log \rho_0}{\mathrm{d}\log r} = \frac{r}{g_0}\,N_0^2 \\
a_5 &= \frac{4\pi r^3 \rho_0}{m_{r,0}}\,,
\end{aligned} \tag{B.2.40}$$

where M and R are respectively the total mass and radius of the star. As used in Appendix A, m_r is the mass within a sphere of radius r.

The system can then be written simply as

$$\begin{aligned}
r\,\frac{\mathrm{d}y_1}{\mathrm{d}r} &= (a_2{-}3)y_1 + \left[\frac{l(l{+}1)}{\sigma^2}\,a_1 - a_2\right] y_2 + a_2 y_3 \\
r\,\frac{\mathrm{d}y_2}{\mathrm{d}r} &= \left(\frac{\sigma^2}{a_1} - a_4\right) y_1 + (1{+}a_4{-}a_5) y_2 - a_4 y_3 \\
r\,\frac{\mathrm{d}y_3}{\mathrm{d}r} &= (1{-}a_5) y_3 + y_4 \\
r\,\frac{\mathrm{d}y_4}{\mathrm{d}r} &= a_4 a_5 y_1 + a_2 a_5 y_2 + \left[l(l{+}1) - a_2 a_5\right] y_3 - a_5 y_4 \,,
\end{aligned} \tag{B.2.41}$$

where we have introduced the reduced frequency

$$\sigma^2 = \frac{R^3}{GM}\;\omega^2 \,. \tag{B.2.42}$$

In order to be used latter, we write these equations in a vectorial form by defining the matrix, with $L^2{=}l(l{+}1)$,

$$\mathcal{A} = \begin{bmatrix}
a_2{-}3 & \dfrac{L^2}{\sigma^2}\,a_1{-}a_2 & a_2 & 0 \\[2ex]
\dfrac{\sigma^2}{a_1}{-}a_4 & a_4{-}a_5{+}1 & -a_4 & 0 \\[2ex]
0 & 0 & 1{-}a_5 & 1 \\[2ex]
a_4 a_5 & a_2 a_5 & L^2{-}a_2 a_5 & -a_5
\end{bmatrix} . \tag{B.2.43}$$

The system is then simply written as

$$x \, \frac{\mathrm{d}\vec{y}}{\mathrm{d}x} = \mathcal{A} \cdot \vec{y} \, , \tag{B.2.44}$$

where the vector $\vec{y}$ has the components (y_1, y_2, y_3, y_4).

We now need to define four boundary conditions. The solution is to be found by integrating the equations between the centre of the star (r=0) and the top of the atmosphere. So, in fact we shall be establishing two boundary conditions at one point and other two at the other. The result is an eigenvalue problem with solutions existing for discrete values of σ, which are the eigenvalues associated to the corresponding eigenfunctions that satisfy the boundary conditions.

B.2.4 Boundary conditions at the centre

Since we have four dependent variables, the interior boundary conditions correspond to fix the values for two of the dependent variables. The other two are then related to these. These relations are what we are determining here.

Because the equations are integrated from r=0, the boundary conditions have to be such as to guarantee that the solutions are regular in the singular point, r=0, of the differential equations. So, we start by determining the limiting behaviour of the a_i's when $x \to 0$. Considering that for $x \equiv r/R \ll 1$ we can write

$$\rho \sim \rho_c (1 + f_2 \, x^2) \, , \tag{B.2.45}$$

where the subscript "c" stands for the value at x=0 and the constant f_2 is to be determined. Note that it has been assumed that the density has a maximum at x=0. Using the equation for the mass (see Appendix A) it follows that

$$m_r \sim \frac{4\pi R^3}{3} \, \rho_c \, x^3 \left(1 + \frac{3}{5} \, f_2 \, x^2 \right) \, . \tag{B.2.46}$$

While the hydrostatic equation gives

$$P \sim P_c \left(1 - f_0 \, x^2 \right) \, , \tag{B.2.47}$$

with

$$f_0 = \frac{4\pi G R^2}{6} \, \frac{\rho_c^2}{P_c} \, . \tag{B.2.48}$$

We also have a thermodynamic relation between density and pressure which is

$$\frac{\mathrm{d}\log\rho}{\mathrm{d}\log r} = \frac{1}{\chi_\rho} \, \frac{\mathrm{d}\log P}{\mathrm{d}\log r} \, (1 - \chi_T \, \nabla - \chi_\mu \, \nabla_\mu) \, , \tag{B.2.49}$$

with

$$\begin{aligned}\chi_\rho &= \left(\frac{\partial \log P}{\partial \log \rho}\right)_{T,\mu} \\ \chi_T &= \left(\frac{\partial \log P}{\partial \log T}\right)_{\rho,\mu} \\ \chi_\mu &= \left(\frac{\partial \log P}{\partial \log \mu}\right)_{\rho,T} ,\end{aligned} \tag{B.2.50}$$

and the gradients being

$$\begin{aligned}\nabla &= \frac{\mathrm{d}\log T}{\mathrm{d}\log P} \\ \nabla_\mu &= \frac{\mathrm{d}\log \mu}{\mathrm{d}\log P} .\end{aligned} \tag{B.2.51}$$

It is also common to use instead γ, the ratio of the specific heats C_P/C_V (C_P and C_V are the specific heats at constant pressure and constant volume, respectively), related to the above quantities according to

$$\begin{aligned}\chi_\rho &= \frac{\Gamma_1}{\gamma} \\ \chi_T &= \frac{\gamma-1}{\gamma}\,\frac{1}{\nabla_a} ,\end{aligned} \tag{B.2.52}$$

where ∇_a is the adiabatic gradient (see Appendix A). So, we finally find that

$$\frac{\mathrm{d}\rho}{\mathrm{d}r} = -\frac{g\rho^2}{\Gamma_1 P}\left[1-(\gamma-1)\,\frac{\nabla-\nabla_a}{\nabla_a} - \gamma\chi_\mu\nabla_\mu\right] . \tag{B.2.53}$$

Defining

$$\theta = 1-(\gamma-1)\,\frac{\nabla-\nabla_a}{\nabla_a} - \gamma\chi_\mu\nabla_\mu , \tag{B.2.54}$$

it follows from (B.2.53), when using (B.2.45)- (B.2.47), that near x=0

$$\frac{2\Gamma_{1c}}{R}\,\rho_c P_c\,\left(1-f_0x^2\right) f_2 x \sim \frac{4\pi GR}{3}\,\theta_c\rho_c^3 x\,\left(1+\frac{3}{5}f_2x^2\right)\left(1+f_2x^2\right)^2 . \tag{B.2.55}$$

Giving finally from the first order term in x that

$$f_2 = -f_0\,\frac{\theta_c}{\Gamma_{1c}} . \tag{B.2.56}$$

So we have that near the centre

$$\begin{aligned}\rho &\sim \rho_c\left(1-\frac{\theta_c}{\Gamma_{1c}}\,f_0x^2\right) \\ m_r &\sim \frac{4\pi R^3}{3}\,\rho_c\,x^3\left(1-\frac{3\theta_c}{5\Gamma_{1c}}\,f_0x^2\right) \\ P &\sim P_c\left(1-f_0x^2\right) .\end{aligned} \tag{B.2.57}$$

The next step is to use these expressions to determine the behaviour of the a_i's near the centre. From the definitions (B.2.40) and using the expansions given above, it follows

that

$$\begin{aligned} a_1 &\sim \frac{4\pi}{3}\,\bar\rho_c\,\left(1-\frac{3f_0\theta_c}{5\Gamma_{1c}}\,x^2\right)\\ a_2 &\sim \frac{2f_0}{\Gamma_{1c}}\,x^2\\ a_3 &\sim \Gamma_{1c}\\ a_4 &\sim \frac{2f_0}{\Gamma_{1c}}\,(\theta_c-1)\,x^2\\ a_5 &\sim 3\,\left(1-\frac{2f_0\theta_c}{5\Gamma_{1c}}\,x^2\right)\,, \end{aligned} \tag{B.2.58}$$

where $\bar\rho_c=R^3\rho_c/M$. Or, writing in vectorial form,

$$\begin{pmatrix} a_1\\ a_2\\ a_3\\ a_4\\ a_5 \end{pmatrix} \sim \begin{pmatrix} \frac{4\pi}{3}\,\bar\rho_c\\ 0\\ \Gamma_{1c}\\ 0\\ 3 \end{pmatrix} + \left(\frac{2f_0}{\Gamma_{1c}}\,x^2\right) \begin{pmatrix} -\frac{4\pi}{3}\,\bar\rho_c & \frac{3\theta_c}{10}\\ 1\\ 0\\ \theta_c-1\\ -\frac{3}{5}\,\theta_c \end{pmatrix}\,. \tag{B.2.59}$$

If we now substitute these in the definition (B.2.43) of the matrix $\mathcal{A}$, the problem is reduced to a simpler system of differential equations, valid near $x=0$. This is,

$$x\,\frac{\mathrm{d}\vec y}{\mathrm{d}x} \sim \mathcal{B}\cdot\vec y + \left(\frac{2f_0}{\Gamma_{1c}}\,x^2\right)\;\mathcal{C}\cdot\vec y\,, \tag{B.2.60}$$

with

$$\mathcal{B}=\begin{bmatrix} -3 & \frac{4\pi\bar\rho_c}{3}\,\frac{L^2}{\sigma^2} & 0 & 0\\ \frac{3}{4\pi\bar\rho_c}\,\sigma^2 & -2 & 0 & 0\\ 0 & 0 & -2 & 1\\ 0 & 0 & L^2 & -3 \end{bmatrix}\,, \tag{B.2.61}$$

and

$$\mathcal{C}=\begin{bmatrix} 1 & -\frac{4\pi\bar\rho_c}{3}\,\frac{3\theta_cL^2}{10\sigma^2}-1 & 1 & 0\\ \frac{3}{4\pi\bar\rho_c}\,\frac{3\theta_c\sigma^2}{10}+1-\theta_c & \frac{8\theta_c}{5}-1 & 1-\theta_c & 0\\ 0 & 0 & \frac{3\theta_c}{5} & 0\\ 3(\theta_c-1) & 3 & -3 & \frac{3\theta_c}{5} \end{bmatrix}\,. \tag{B.2.62}$$

This has general solutions for the y_i's given by series of powers of x, which we write as

$$y_j = x^t \sum_{i=0}^{\infty} \mathcal{Y}_{ij}\, x^{2i} \qquad ;\ j{=}1,2,3,4\ , \tag{B.2.63}$$

the value of t being defined as the first index of the general series that has a non-zero coefficient. After substitution in Eq. (B.2.60) we find an infinite set of equations determining all the coefficients of the four series, corresponding to the four dependent variables to be calculated. These are, with $j{=}1,2,3,4$,

$$\begin{aligned} &\sum_{k=1}^{4} (t\ \delta_{jk} - \mathcal{B}_{jk})\ \mathcal{Y}_{0k} = 0 \\ &\sum_{k=1}^{4} \left\{ \left[(t{+}2i)\ \delta_{jk} - \mathcal{B}_{jk} \right]\ \mathcal{Y}_{ik} - \frac{2f_0}{\Gamma_{1c}}\, \mathcal{C}_{jk}\ \mathcal{Y}_{i-1,k} \right\} = 0 \qquad \text{for } i{\geq}1\ , \end{aligned} \tag{B.2.64}$$

where δ_{jk} is 1 if $j{=}k$ and zero otherwise. From the first set of equations, we have that for non-zero $\mathcal{Y}_{0k}$ (as assumed),

$$t = \begin{cases} l{-}2 \\ \\ -(l{+}3)\ . \end{cases} \tag{B.2.65}$$

Since we must have a regular solution at $x{=}0$ the physical option has to be $t{=}l{-}2$. With this option we also have that

$$\begin{aligned} \mathcal{Y}_{01} &= \frac{4\pi\bar{\rho}_c}{3}\ \frac{l}{\sigma^2}\ \mathcal{Y}_{02} \\ \mathcal{Y}_{04} &= l\ \mathcal{Y}_{03}\ . \end{aligned} \tag{B.2.66}$$

The set of four equations corresponding to the second set of relations (i.e., for $i{=}1$) in (B.2.64) gives the following system

$$\left(l\,\mathcal{I} - \mathcal{B} \right)\ \cdot \left(\frac{\Gamma_{1c}}{2f_0} \right) \begin{pmatrix} \mathcal{Y}_{11} \\ \mathcal{Y}_{12} \\ \mathcal{Y}_{13} \\ \mathcal{Y}_{14} \end{pmatrix} = \mathcal{C} \cdot \begin{pmatrix} \frac{4\pi\bar{\rho}_c}{3}\ \frac{l}{\sigma^2}\ \mathcal{Y}_{02} \\ \mathcal{Y}_{02} \\ \mathcal{Y}_{03} \\ l\,\mathcal{Y}_{03} \end{pmatrix}\ , \tag{B.2.67}$$

where $\mathcal{I}_{jk}{=}\delta_{jk}$.

So, we finally have the boundary conditions. Giving $\mathcal{Y}_{02}$ and $\mathcal{Y}_{03}$, at $x{=}0$ we can determine $\mathcal{Y}_{01}$ and $\mathcal{Y}_{04}$ using (B.2.66). While at the second mesh point (or the first point if an envelope is considered instead of a full model)

$$x^{2-l}\ y_j(x) = \mathcal{Y}_{0j} + a_2(x)\ \ \bar{\mathcal{Y}}_{1j}\ , \tag{B.2.68}$$

where

$$\bar{\mathcal{Y}}_{1j} = \left(\frac{\Gamma_{1c}}{2f_0} \right)\ \mathcal{Y}_{1j}\ , \tag{B.2.69}$$

are determined by solving (B.2.67) with

$$\begin{aligned} \theta_c &= \frac{a_2+a_4}{a_2} \\ \frac{4\pi\bar{\rho}_c}{3} &= \frac{2a_1}{2-a_2-a_4} \; . \end{aligned} \tag{B.2.70}$$

The values of the a's used in these expressions are the ones at the deepest mesh point of the model (and so the centre for a full model).

B.2.5 Boundary conditions at the surface

Two boundary conditions have been used in the centre, so we now need to imposed more two boundary conditions at the top of the atmosphere.

In a similar fashion to what we have done for the centre, we also use now (the subscript "S" represents in the following the value at the top of the atmosphere, located at $r_S/R>1$) the following limiting ($x \to x_S$) behaviour for the a's,

$$\begin{aligned} a_1 &\sim 1 \\ a_2 &\sim a_{2S} \\ a_3 &\sim \Gamma_{1S} \\ a_4 &\sim a_{2S} \\ a_5 &\sim 0 \; . \end{aligned} \tag{B.2.71}$$

If an isothermal atmosphere is used then density decreases exponentially with radius. This has allowed us to approximate in the last relation the actual value of a_{5S} by zero. If we now substitute these values in matrix $\mathcal{A}$, given in (B.2.43), it follows that

$$\mathcal{A}_S = \begin{bmatrix} a_{2S}-3 & \frac{L^2}{\sigma^2}-a_{2S} & a_{2S} & 0 \\ \sigma^2-a_{4S} & 1+a_{4S} & -a_{4S} & 0 \\ 0 & 0 & 1 & 1 \\ 0 & 0 & L^2 & 0 \end{bmatrix} \; . \tag{B.2.72}$$

Redoing the analysis presented in the previous section, in particular using an expansion as (B.2.63), i.e.,

$$y_j = x^t \sum_{i=0}^{\infty} \mathcal{Y}_{S,ij} \, x^{2i} \qquad ; \; j=1,2,3,4 \; , \tag{B.2.73}$$

we find the following characteristic values for t;

$$t = \begin{cases} -l \\ l+1 \\ \frac{1}{2} \left[(a_{2S}+a_{4S}-2) \pm \gamma^{1/2} \right] \; , \end{cases} \tag{B.2.74}$$

where

$$\begin{aligned}\gamma &= (a_{2S}+a_{4S}-2)^2 + 4\left[(\sigma^2-a_{4S})\left(\frac{L^2}{\sigma^2}-a_{2S}\right) - (a_{2S}-3)(a_{4S}+1)\right] \\ &= (a_{2S}-a_{4S}-4)^2 + 4(\sigma^2-a_{4S})\left(\frac{L^2}{\sigma^2}-a_{2S}\right) \ .\end{aligned} \tag{B.2.75}$$

As before we have to discharge the value of $l+1$ because now $x \geq 1$, and so the solution would diverge for this case. However, for the last expression we must be more careful since the actual value for t can now be imaginary. If it happens the solution will have a propagating component at the boundary, which implies that the oscillations will be loosing energy at this boundary. This does not correspond to the type of solutions we are looking for. Therefore we only consider eigenvalues that are real corresponding to standing waves, i.e. solutions that are evanescent at the boundaries. For the same reason that led us to solution $l+1$ we also must drop the solution with the positive sign for $\gamma^{1/2}$. So, we are left with the two remaining expressions of t.

Note that the last relation in (B.2.74) imposes restrictions on the values the frequency σ can have for modes of oscillation. This point is discussed further in the main text of the Thesis. There it is presented as a reflecting condition at the surface, and therefore can only constraint waves whose frequency is below the value corresponding to the zero of γ. From here on we only consider solutions that do have a frequency below this value and are therefore waves exponentially damped in the atmosphere.

The relations equivalent to (B.2.66) come, in this case, from (for $j=1,2,3,4$)

$$\sum_{k=1}^{4} \left(t\ \delta_{jk} - \mathcal{A}_{S,jk}\right)\ \mathcal{Y}_{S,0k} = 0 \ , \tag{B.2.76}$$

giving that, after using the valid solutions in (B.2.74),

$$\begin{aligned}\mathcal{Y}_{S,01} &= 2\ \frac{\left(L^2/\sigma^2 - a_{2S}\right)\mathcal{Y}_{S,02} + a_{2S}\mathcal{Y}_{S,03}}{a_{4S}+4-\gamma^{1/2}} \\ \mathcal{Y}_{S,04} &= -(l+1)\ \mathcal{Y}_{S,03} \ .\end{aligned} \tag{B.2.77}$$

Once again we have the boundary conditions, i.e., given the values of $\mathcal{Y}_{S,02}$ and $\mathcal{Y}_{S,03}$ we can use these relations to find $\mathcal{Y}_{S,01}$ and $\mathcal{Y}_{S,04}$ in order to integrate the differential equations inwards.

B.3 Numerical calculation of the frequencies

The objective is to calculated the eigenvalues (frequencies of oscillation) of a solar model. We are now in conditions to do so since all the equations have been obtained, as written above. The information from the model is in the coefficients a, which are now use to solve the system of four first order linear differential equations using the above boundary conditions. In this Section we describe briefly how this is done.

Lets then rewrite all the expressions as they are used in the code. The basic differential equations to be solved are (B.2.41), which have been written as

$$x\,\frac{\mathrm{d}\vec{y}}{\mathrm{d}x} = \mathcal{A}\cdot\vec{y}\,, \tag{B.3.1}$$

where the matrix $\mathcal{A}$ is given by

$$\mathcal{A} = \begin{bmatrix} (a_2-3) & \left(\frac{L^2}{\sigma^2}\,a_1-a_2\right) & a_2 & 0 \\ \left(\frac{\sigma^2}{a_1}-a_4\right) & (a_4-a_5+1) & -a_4 & 0 \\ 0 & 0 & (1-a_5) & 1 \\ a_4a_5 & a_2a_5 & (L^2-a_2a_5) & -a_5 \end{bmatrix}. \tag{B.3.2}$$

The functions a_i are as listed in (B.2.40) and known on a mesh from the equilibrium model obtained from solving the stellar structure equations described in the previous Appendix. We have also defined a dimensionless frequency σ as

$$\sigma^2 = \frac{R^3}{GM}\omega^2\,, \tag{B.3.3}$$

where ω is the actual frequency of oscillation. As discussed above, under the boundary conditions, solutions exist only for discrete values of ω. These values and the corresponding solution $\vec{y}$ are what we are trying to find. The method we use consists in, given a value of the degree l, to determine the values(s) of σ that give a continuous solution at some meeting point (defined below as x_f). This point is where we stop the integration up from the centre, and the integration down from the atmosphere. In other words we find the value(s) of σ that have a global solution satisfying all our four boundary conditions. So what we do in fact is to iterate in σ in order to find the values that give the zeros of a function measuring the fitting of outer and inner solutions at x_f. These are our eigenvalues having the associated eigenfunctions as the solution $\vec{y}$ so found for each of them.

B.3.1 Numerical variables

Due to numerical control of errors and precision of the calculation we redefine the variables for different regions of the model. We do so by using some asymptotic results which allow us to estimate which regions of the star are evanescent for a given frequency. These boundaries are determined as the zero of an equation in terms of the characteristics frequencies (Section 1.3). The equation used in the code is given below.

For the inner evanescent region we redefine the variables according to

$$\vec{y}_{\rm in} = \left(\frac{x}{x_{\rm in}}\right)^{2-l} \vec{y} \; . \tag{B.3.4}$$

Here, $x_{\rm in}$ is the transition point separating this inner region from the zone where the usual variables, as given above, are used. Equation (B.2.1) becomes

$$x\frac{{\rm d}\vec{y}_{\rm in}}{{\rm d}x} = \mathcal{A}_{\rm in} \cdot \vec{y}_{\rm in} \; , \tag{B.3.5}$$

with

$$\mathcal{A}_{\rm in} = \begin{bmatrix} (a_2 - l - 1) & \left(\frac{L^2}{\sigma^2}\, a_1 - a_2\right) & a_2 & 0 \\ \left(\frac{\sigma^2}{a_1} - a_4\right) & (a_4 - a_5 - l + 3) & -a_4 & 0 \\ 0 & 0 & (3 - a_5 - l) & 1 \\ a_4 a_5 & a_2 a_5 & (L^2 - a_2 a_5) & (2 - a_5 - l) \end{bmatrix} . \tag{B.3.6}$$

For the outer evanescent region, above $x{=}x_{\rm out}$, we use instead

$$\vec{y}_{\rm out} = \left(\frac{x}{x_{\rm out}}\right)^{l} \vec{y} \; . \tag{B.3.7}$$

Which gives the equations in the form

$$x\frac{{\rm d}\vec{y}_{\rm out}}{{\rm d}x} = \mathcal{A}_{\rm out} \cdot \vec{y}_{\rm out} \; , \tag{B.3.8}$$

with

$$\mathcal{A}_{\rm out} = \begin{bmatrix} (a_2 + l - 3) & \left(\frac{L^2}{\sigma^2}\, a_1 - a_2\right) & a_2 & 0 \\ \left(\frac{\sigma^2}{a_1} - a_4\right) & (a_4 - a_5 + l + 1) & -a_4 & 0 \\ 0 & 0 & (1 - a_5 + l) & 1 \\ a_4 a_5 & a_2 a_5 & (L^2 - a_2 a_5) & (l - a_5) \end{bmatrix} . \tag{B.3.9}$$

The two points used here, $x_{\rm in}$ and $x_{\rm out}$, are the points corresponding to the roots of the following equation, depending on the model and the values of ω and degree l.

$$\omega^2 \, (\omega^2 - \omega_c^2) - S_l^2 \, (\omega^2 - N^2) = 0 \; . \tag{B.3.10}$$

See Chapter 1 for a discussion on where this equation comes from, and for the definition of the acoustic cutoff frequency ω_c.

So, recapitulating we integrate from x=0 to x=$x_{\rm in}$ determining $\vec{y}_{\rm in}$. From there to a fitting point x_f well within the oscillatory region (zone where the amplitudes of the eigenfunctions are larger) we integrate using the equations for $\vec{y}$. Note that the transition from one region to the other is quite natural considering our redefinitions ($\vec{y}_{\rm in}$ and $\vec{y}_{\rm out}$) of $\vec{y}$. On the other hand we integrate inward from x=x_S to x=$x_{\rm out}$ using instead the equations for $\vec{y}_{\rm out}$. From there, down to x_f we take again the equations for $\vec{y}$.

Resulting from these two integrations we have the two sets of values at x=x_f which are then continuous (after normalization), since the system of equations is linear, if and only if the value of σ is an eigenvalue. At this point what we actually do is to iterate on σ to find the zeros of the fitting determinant.

B.3.2 Method of integration

The method used to solve numerically the equations considered above is a shooting method using a second-order centered differences representation of the equations. It consists in writing the differential equations as

$$\vec{y}(n{+}1) = \vec{y}(n) + \frac{1}{2}\, h \left[\frac{{\rm d}\vec{y}}{{\rm d}x}(n) + \frac{{\rm d}\vec{y}}{{\rm d}x}(n{+}1) \right] \ , \tag{B.3.11}$$

where, $\vec{y}(n)$≡$\vec{y}(x_n)$ and $\mathcal{A}_n$≡$\mathcal{A}(x_n)$. After substituting the derivatives by

$$\begin{aligned} \frac{{\rm d}\vec{y}}{{\rm d}x}(n) &= \mathcal{A}_n \cdot \vec{y}(n) \\ \frac{{\rm d}\vec{y}}{{\rm d}x}(n{+}1) &= \mathcal{A}_{n+1} \cdot \vec{y}(n{+}1) \ , \end{aligned} \tag{B.3.12}$$

we get

$$\left(\mathcal{I} - \frac{1}{2}\, h_n\, \mathcal{A}_{n+1} \right) \cdot \vec{y}(n{+}1) = \left(\mathcal{I} + \frac{1}{2}\, h_n\, \mathcal{A}_n \right) \cdot \vec{y}(n) \ . \tag{B.3.13}$$

with h_n=x_{n+1}−x_n. Here $\mathcal{I}$ is again the identity matrix, having its elements given by $\mathcal{I}_{ij}$=δ_{ij}. So, the final relation giving the value of $\vec{y}$ at the next mesh point is

$$\vec{y}(n{+}1) = \left[\left(\mathcal{I} - \frac{1}{2}\, h_n\, \mathcal{A}_{n+1} \right)^{-1} \otimes \left(\mathcal{I} + \frac{1}{2}\, h_n\, \mathcal{A}_n \right) \right] \cdot \vec{y}(n) \ . \tag{B.3.14}$$

Equivalent sets of equations can of course be written for $\vec{y}_{\rm in}$ and $\vec{y}_{\rm out}$ in terms of $\mathcal{A}_{\rm in}$ and $\mathcal{A}_{\rm out}$, respectively.

We also have to implement the boundary conditions. It is done by setting the values of y_1 and y_3 at the boundaries (centre and surface) and to calculate the values of y_2 and y_4 (at both boundaries) from the relations constructed in the previous Section. Both linearly

independent solutions are found by setting the central/atmospheric values of y_1 equal to one and y_3 alternatively to one and to zero. The actual solution is a linear combination of these two (for the interior solution - up to x_f, as well as for the external solution - down to x_f).

Since we are using a shooting method, from the values of these two solutions ("in" and "out") at x_f, we construct the matching matrix whose determinant has to be zero if σ is an eigenvalue. So after finding an interval with a zero of the determinant we iterate in order to locate it, determining the eigenvalue. We maximize the efficiency of the search for the eigenvalues by using the fact that these are separated approximately by

$$\begin{aligned} \Delta\sigma_p^2 &\sim \left(\frac{GM}{R^3}\right)^{1/2} \frac{2\pi\sigma}{\int_0^R c^{-1}\mathrm{d}r} \qquad \text{for p-modes} \\ \Delta\sigma_g^2 &\sim \left(\frac{GM}{R^3}\right)^{1/2} \frac{2\pi\sigma^3}{\left(l+\frac{1}{2}\right)\int_0^R N^2 r^{-1}\mathrm{d}r} \qquad \text{for g-modes .} \end{aligned} \tag{B.3.15}$$

These expressions come from asymptotic analysis and give only estimates useful to find the next eigenvalue (i.e. the zero of the matching determinant) with a minimum of steps.

Finally we obtain the mode order of each eigenvalue using a method similar to the phase diagram as described by Unno et al. (1989). It consists in counting the crosses of the solution in the plane (y_1, y_2) over the line $y_1 \equiv 0$. If the cross is clockwise it counts as (-1) otherwise as (+1). To a total negative counting of the crosses corresponds a g-mode while p-modes have positive counting results, with the number corresponding to the mode order. The solutions corresponding to f-mode eigenvalues have a total of zero counts.

B.3.3 Accuracy of the results

The actual accuracy with which the final values of the frequencies are determined depend on several aspects of the calculation. As expected, it not only depends on the code to integrate the oscillations equations but also on the accuracy of the equilibrium model used. The accuracy of the equilibrium model has been discussed in the previous Appendix were the code for solving the stellar structure equations is described. However, another aspect associated to the equilibrium model also affecting the precision of the calculated eigenvalues is the mesh on which we use such a model. For the ones considered here we have about 3000 mesh points unequally spaced in radius. The density of points in regions where the eigenfunctions for p-modes change more rapidly (near the surface) is forced to be much higher than for the deep interior. Models including overshoot were also written on a mesh that has a high density of points around the base of the convection zone. In this way we minimize the errors caused by having too few points where the eigenfunctions vary more strongly.

Other aspects determining the accuracy of the eigenvalues is of course the numerical method used to integrate the four differential equations discussed above. In our case we have a second order rule of integration with the added help of using reduced dependent variables in the regions where the amplitudes of the eigenfunctions would be otherwise very small. We further consider an extrapolation to improve the accuracy with which each frequency is determined. It is a relation, known as Richardson Extrapolation, which uses the fact that our second order integration has an error which varies with the inverse of the squared number of mesh points. Using such a fact it can be written that the actual value of the eigenvalue is

$$\sigma^2 = \frac{\alpha}{\alpha-1}\ \sigma_N^2 - \frac{1}{\alpha-1}\ \sigma_{N'}^2 \qquad \text{with} \qquad \alpha = \left(\frac{N}{N'}\right)^2 , \tag{B.3.16}$$

where σ_N is the result found for a mesh of N points and $\sigma_{N'}$ for a mesh of N' points. In our code we use $N' \sim N/2$, giving $\alpha \sim 4$. This requires extra work but improves significantly the accuracy of the numerical frequencies (see for example Section V of Christensen-Dalsgaard & Berthomieu 1991).

From the behaviour of the errors when we increase the number of mesh points and after the comparison with results from another code we estimate that our frequencies of oscillation have a numerical error below 0.005μHz (using a model with a mesh of $\sim$3000 points). This is significantly below the current observational errors of solar frequencies.

References

Alongi M., Bertelli G., Bressans A., Chiosi C., 1991, A&A 244, 95

Antia H.M., Basu S., 1994, ApJ 426, 801

Antia H.M., Chitre S.M., 1993, ApJ 413, 778

Audard N., Provost J., 1993, A&A 282, 73

Audard N., Provost J., Christensen-Dalsgaard J., 1995, A&A 297, 427

Bachmann K.T., Brown T.M., 1993, ApJ 411, L45

Balmforth N.J., 1992a, MNRAS 255, 603

Balmforth N.J., 1992b, MNRAS 255, 632

Basu S., Antia H.M., 1994, JA&A 15, 143

Basu S., Antia H.M., 1995, in *GONG 1994: Helio and Asteroseismology from the Earth and Space*, (eds) R.K. Ulrich, E.J. Rhodes Jr and W. Däppen, A.S.P. Conf. Ser. Vol 76, 649

Basu S., Antia H.M., 1994, MNRAS 269, 1137

Basu S., Antia H.M., 1995, MNRAS 276, 1402

Basu S., Antia H.M., Narasimha D., 1993, MNRAS 267, 209

Baturin V.A., Mironova I.V., 1995, Astronomy Reports 39, No. 1, 105

Berthomieu G., Morel P., Provost J, Zahn J.-P., 1993, in *Inside the Stars*, (eds) A. Baglin and W.W. Weiss, A.S.P. Conf. Ser. Vol 40, 60

Böhm-Vitense E., 1958, Zs. Ap 46, 108

Canuto V.M., 1989, A&A 217, 333

Canuto V.M., 1996, in *Proc. "L. Gratton International Prize" Symposium on Stellar Convection, Frascati - Italy* (in Press)

Canuto V.M., Mazzitelli I., 1991, ApJ 370, 295

Canuto V.M., Mazzitelli I., 1992, ApJ 389, 724

Chan K.L., Nordlund A., Steffen M., Stein R.F., 1991, in *Solar Interior and Atmosphere*, (eds) A.N. Cox, W.C. Livingston, M.S. Matthews M.S., University of Arizona Press, 223

Chandrasekhar S., 1963, ApJ 138, 896

Chandrasekhar S., 1964, ApJ 139, 664

Christensen-Dalsgaard J., 1978, *Solar oscillations*, PhD Dissertation, University of Cambridge

Christensen-Dalsgaard J., 1982, MNRAS 199, 735

Christensen-Dalsgaard J., 1990, in *Proc. IAU Colloquium No 121, Inside the Sun*, (eds) G. Berthomieu G. & M. Cribier, Kluwer, Dordrecht, p. 305

Christensen-Dalsgaard J., 1996, in *The Structure of the Sun,* IV IAC *Winter School*, (ed) T. Roca Cortes, Cambridge University Press

Christensen-Dalsgaard J., Berthomieu G., 1991, in *Solar Interior and Atmosphere*, (eds) A.N. Cox, W.C. Livingston, M.S. Matthews M.S., University of Arizona Press, 401

Christensen-Dalsgaard J., Däppen W., 1992, A&AR 4, 267

Christensen-Dalsgaard J., Pérez Hernández F., 1991, in *Challenges to Theories of the Structure of Moderate-Mass Stars*, Lecture Notes in Physics Vol. 388, (eds) D.O. Gough, J. Toomre, Springer, Heidelberg, 43

Christensen-Dalsgaard J., Pérez Hernández F., 1992, MNRAS 257, 62

Christensen-Dalsgaard J., Thompson M.J., 1991, ApJ 367, 666

Christensen-Dalsgaard J., Thompson M.J., 1996, to be submitted to MNRAS

Christensen-Dalsgaard J., Bedding T.R., Kjeldsen H., 1995, ApJ 443, L29

Christensen-Dalsgaard J., Gough D.O., Thompson M.J., 1989, MNRAS 238, 481

Christensen-Dalsgaard J., Gough D.O., Thompson M.J., 1991, ApJ 378, 413

Christensen-Dalsgaard J., Proffitt C.R., Thompson M.J., 1993, ApJ 403, L75

Christensen-Dalsgaard J., Duvall Jr T.L., Gough D.O., Harvey J.W., Rhodes Jr E.J., 1985, Nature 315, 378

Cox A.N., Tabor J.E., 1976, ApJS 31, 271

Cox A.N., Guzik J.A., Kidman R.B., 1989, ApJ, 342, 1187

Cox J.P., Giuli R.T., 1968, *Principles of Stellar Structure. Vol. I. Physical Principles*, Gordon and Breach

Cowling T.G., 1941, MNRAS 101, 367

Däppen W., Gough D.O., 1986, in *Seismology of the Sun and the Distant Stars*, (ed) D.O. Gough, NATO ASI, D. Reidel, 275

Däppen W., Gough D.O., Thompson M.J., 1988, in *Seismology of the Sun and Sun-like Stars*, ESA SP–286, 505

Däppen W., Mihalas D., Hummer D.G., Mihalas B.W., 1988, ApJ 332, 261

Deubner F.-L., Gough D., 1984, Ann. Rev. Astron. Astrophys. 22, 593

Duvall Jr T.L., 1982, Nat 300, 242

Dziembowski W.A., Pamyatnykh A.A., Sienkiewicz R., 1991, MNRAS 249, 602

Eggleton P.P., Faulkner J., Flannery B.P., 1973, A&A 23, 325

Elsworth Y., Howe R., Isaak G.R., Mcleod C.P., Miller B.A., New R., Speake C.C., Wheeler S.J., 1994, ApJ 434, 801

Gingerich O., Noyes R.W., Kalkofen W., Cuny Y., 1971, Sol. Phys. 18, 347

Gough D.O., 1977, ApJ 214, 196

Gough D.O., 1985, Sol. Phys. 100, 65

Gough D.O., 1990, in *Progress of Seismology of the Sun and Stars*, Lecture Notes in Physics Vol 367, (eds) Y. Osaki and H. Shibahashi, Springer-Verlag, 283

Gough D.O., 1991, in *Astrophysical Fluid Dynamics*, (eds) J.-P. Zahn & J. Zinn-Justin, Elsevier Science Publishers

Gough D.O., Sekii T., 1993, in *Seismic Investigation of the Sun and Other Stars*, (ed) T.M. Brown, A.S.P. Conf. Ser. Vol 42, 177

Gough D.O., Thompson M.J., 1991, in *Solar Interior and Atmosphere*, (eds) A.N. Cox, W.C Livingston & M.S. Matthews, University of Arizona Press, 519

Gough D.O., Vorontsov S., 1995, MNRAS 273, 573

Gough D.O., Weiss N.O., 1976, MNRAS 176, 589

Grossman S.A., Narayan R., Arnett D., 1993, ApJ 407, 284

Guenther D.B., 1994, ApJ 422, 400

Guzik J.A., Cox A.N., 1992, ApJ 386, 729

Guzik J.A., Cox A.N., 1993, ApJ 411, 394

Houdek G., Balmforth N.J., Christensen-Dalsgaard J., 1996, in *Helioseismology, Proc. 4th* SOHO *Workshop*, (eds) V. Domingo et al., ESA SP-376, ESTEC, Noordwijk

Hummer D.G., Mihalas D., 1988, ApJ 331, 794

Hurlburt N.E., Toomre J., Massaguer J.M., 1986, ApJ 311, 563

Hurlburt N.E., Toomre J., Massaguer J.M., Zahn J.-P., 1994, ApJ 421, 245

Iglesias C.A., Rogers F.J., 1991, ApJ 371, 408

Iglesias C.A., Rogers F.J., Wilson B.G., 1992, ApJ 397, 717

Kim Y.-C., Fox P.A., Sofia S., Demarque P., 1995, ApJ 442, 422

Kippenhahn R., Weigert A., 1990, *Stellar Structure and Evolution*, Springer–Verlag

Kosovichev A.G., 1993, MNRAS 265, 1053

Kosovichev A.G., Christensen-Dalsgaard J., Däppen W., Dziembowski W.A., Gough D.O., Thompson M.J., 1992, MNRAS 259, 536

Krishna Swamy K.S., 1966, ApJ 145, 174

Lang K.R., 1980, *Astrophysical Formulae*, Springer–Verlag

Lattanzio J.C., Vallenari A., Bertelli G., Chiosi C., 1991, A&A 250, 340

Leibacher J.W., Stein R.F., 1971, Astrophys. Lett. 7, 191

Leighton R.B., Noyes R.W., Simon G.W., 1962, ApJ 135, 474

Libbrecht K.G., 1988, Space Sci. Rev. 47, 275

Libbrecht K.G., Woodard M.F., Kaufman J.M., 1990, ApJS 74, 1129

Lydon T.J., Fox P.A., Sofia S., 1992, ApJ 397, 701

Maeder A., 1975, A&A 40, 303

Maeder A., 1976, A&A 47, 389

Mihalas D., Däppen W., Hummer D.G., 1988, ApJ 331, 815

Moreno-Insertis F., Schüssler M., Ferriz-Mas A., 1992, A&A 264, 686

Nordlund A., Brandenburg A., Jennings R.L., Rientord M., Ruokolainen J., Stein R.F., Tuominen I., 1992, ApJ 392, 647

Paternó L., Ventura R., Canuto V.M., Mazzitelli I., 1993, ApJ 402, 733

Pecker J.-C., 1991, in *Solar Interior and Atmosphere*, (eds) A.N. Cox, W.C. Livingston & M.S. Matthews, University of Arizona Press, 1

Pérez Hernández F., Christensen-Dalsgaard J., 1994, MNRAS 269, 475

Petrovay K., 1991, in *The Sun and Cool Stars - Activity, Magnetism, Dynamos, IAU 130*, (eds) I. Tuominen, D. Moss & G. Rudiger, Springer, 67

Petrovay K., Marik M, 1995, in in *GONG 1994: Helio and Asteroseismology from the Earth and Space*, (eds) R.K. Ulrich, E.J. Rhodes Jr. and W. D"appen, A.S.P. Conf. Ser. Vol 76, 216

Pidatella R.M., Stix M., 1986, A&A 157, 338

Renzini A., 1987, A&A 188, 49

Rieutord M., Zahn J.-P., 1995, A&A 296, 127

Rogers F.J., Iglesias C.A., 1992, ApJ 401, 361

Roxburgh I.W., 1985, Sol. Phys. 100, 21

Roxburgh I.W., Simmons J., 1993, A&A 277, 93

Roxburgh I.W., Vorontsov S.V., 1993, in *Seismic Investigation of the Sun and Other Stars*, (ed) T. Brown, A.S.P. Conf. Ser. Vol 42, 169

Roxburgh I.W., Vorontsov S.V., 1994, MNRAS 268, 880

Rüdiger G., Brandenburg A., 1995, A&A 296, 557

Schmitt J.H.M.M., Rosner R., Bohn H.U., 1984, ApJ 282, 316

Schwarzschild M., 1958, *Structure and Evolution of the Stars*, Princeton University Press

Shaviv G., Salpeter E.E., 1973, ApJ 184, 191

Singh H.P., Roxburgh I.W., Chan K.L., 1995, A&A 295, 703

Skaley D., Stix M., 1991, A&A 241, 227

Stein R.F., Nordlund Å., 1989, ApJ 342, L95

Stothers R.B., Chin C.-W., 1992, ApJ 390, 136

Thompson M.J., 1988, in *Seismology of the Sun and Sun-like Stars*, (ed) E.J. Rolfe, ESA SP-286, ESTEC, Noordwijk, 321

Toutain T., Frohlich C., 1992, A&A 257, 287

Turck-Chièze S., Lopes I., 1993, ApJ 408, 347

Turck-Chièze S., Däppen W., Fossat E., Provost J., Schatzman E., Vignaud D., 1993, Phys. Rep. 230, 57

Ulrich R.K., 1970, ApJ 162, 993

Unno W., Osaki Y., Ando H., Saio H., Shibahashi H., 1989, *Nonradial Oscillations of Stars* ($2^{\rm nd}$ edition), University of Tokyo Press

van Ballegooijen A.A., 1982, A&A 113, 99

Vorontsov S.V., 1988, in *Proc. IAU Symp. 123, Advances in Helio- and Asteroseismology*, (eds) J. Christensen-Dalsgaard and S. Frandsen, Reidel, 151

Vorontsov S.V., Zharkov V.N., 1989, Sov. Sci. Rev. E. Astrophys. Space Phys. 7, 1

Vorontsov S.V., Baturin V.A., Pamyatnykh A.A., 1991, Nat 349, 49

Vorontsov S.V., Baturin V.A., Pamyatnykh A.A., 1992, MNRAS 257, 32

Xiong D.R., Chen Q.L., 1992, A&A 254, 362

Zahn J.-P., 1991, A&A 252, 179

References Associated to the Thesis

List of publications having the author of the thesis as a co-author and published during the PhD on subjects discussed in this thesis.

Christensen-Dalsgaard J., Monteiro M.J.P.F.G., Thompson M.J., 1995, "Helioseismic estimation of convective overshoot in the Sun", MNRAS 276, 283

Christensen-Dalsgaard J., Bedding T.R., Houdek G., Kjeldsen H., Rosenthal C., Trampedach R., Monteiro M.J.P.F.G., Nordlund A., 1996, "Near-surface effects in modelling oscillations of η Boo", in *Astrophysical Applications of Stellar Pulsation, IAU Coll. 155*, (eds) P.A. Whitelock and R.S. Stobie, A.S.P. Conf. Ser.

Monteiro M.J.P.F.G., Christensen-Dalsgaard J., Thompson M.J., 1993a, "Detecting convective overshoot in solar-type stars", in *Inside the Stars*, (eds) A. Baglin and W.W. Weiss, A.S.P. Conf. Ser. Vol 40, 557

Monteiro M.J.P.F.G., Christensen-Dalsgaard J., Thompson M.J., 1993b, "On detecting overshoot below the Sun's convective envelope", in *Seismic Investigation of the Sun and Other Stars*, (ed) T.M. Brown, A.S.P. Conf. Ser. Vol 42, 253

Monteiro M.J.P.F.G., Christensen-Dalsgaard J., Thompson M.J., 1994, "Seismic study of overshoot at the base of the solar convective envelope", A&A 283, 247

Monteiro M.J.P.F.G., Christensen-Dalsgaard J., Thompson M.J., 1995, "Helioseismic constraints on theories of convection", in *GONG 1994: Helio and Asteroseismology from the Earth and Space*, (eds) R.K. Ulrich, E.J. Rhodes Jr. and W. D"appen, A.S.P. Conf. Ser. Vol 76, 128

Monteiro M.J.P.F.G., Christensen-Dalsgaard J., Thompson M.J., 1996, "Seismic properties of the Sun's super-adiabatic layer. I. Theoretical modelling and parametrization of the uncertainties", A&A 307, 624

Rosenthal C.S., Christensen-Dalsgaard J., Houdek G., Monteiro M.J.P.F.G., Nordlund A., Trampedach R., 1996, "Seismology of the solar surface regions", in *Proc. 4th* SOHO *Workshop: Helioseismology*, (eds) V. Domingo et al., ESA SP-376, ESTEC.